

Universiteit  
Antwerpen

UNIVERSITEIT ANTWERPEN  
Faculteit Wetenschappen  
Departement Fysica

# **Identification of thin-film photovoltaic cell materials based on high-throughput first-principles calculations**

---

## **Identificatie van dunne-film fotonvoltaïsche materialen gebaseerd op high-throughput first-principles berekeningen**

Proefschrift voorgelegd tot het behalen van de graad van doctor in de wetenschappen aan  
de Universiteit Antwerpen te verdedigen door

**Nasrin Sarmadian**

### **Promotoren**

Prof. Dr. Dirk Lamoen  
Prof. Dr. Bart Partoens

Antwerpen  
June 2015

**Members of the Jury:****Chairman**

Prof. Dr. Milorad Milosevic, Universiteit Antwerpen, Belgium

**Supervisors**

Prof. Dr. Dirk Lamoen, Universiteit Antwerpen, Belgium

Prof. Dr. Bart Partoens, Universiteit Antwerpen, Belgium

**Members**

Prof. Dr. An Hardy, Universiteit Hasselt, Belgium

Dr. Guy Brammertz, IMEC, Belgium

Prof. Dr. Wouter Herrebout, Universiteit Antwerpen, Belgium

Prof. Dr. Erik Neyts, Universiteit Antwerpen, Belgium

**Contact Information**

Nasrin Sarmadian  
Department of Physics  
University of Antwerp (CGB)  
Groenenborgerlaan 171, U317  
B-2020 Antwerpen, Belgium  
nasrin.sarmadian@uantwerpen.be  
nasrin.sarmadian@gmail.com

# Acknowledgement

"If I have seen farther than others, it is because I was standing on the shoulders of giants."  
-Isaac Newton

I wish to thank everyone who contributed to the accomplishment of this work. Certainly, there are so many important people which always give me encouragement for my study whom I could not thank one by one here. I thank them very much for being part of my life and their contributions so that this thesis can be completed.

Firstly, I would like to sincerely thank and express my deepest gratitude to my promoters Dirk Lamoen and Bart Partoens for their constant guidance and motivation throughout my study. They have been very supportive and I am grateful to them for their continued encouragement and faith in my ideas. I would like to specially thank the members of my thesis committee: Milorad Milosevic, An Hardy, Guy Brammertz, Wouter Herrebout, and Erik Neyts who provided insightful suggestions and questions.

I sincerely thank Rolando Saniz, who has always been ready to help me by answering my questions. I also appreciate his advice for better understanding the results of the present work. I also thank all the members of CMT and EMAT group from 2010 to 2015 for being a very nice and helpful company.

I take this opportunity to thank Kalpana Voley, Guido Huyberegts, and Johan Paul in the flamac company for collaboration in the high-throughput bixbyite oxide project.

My gratitude is also addressed to Marnik Bercx for translating the summary of my thesis in Dutch. I must also thank Dmitry Batuk for providing me the ICSD data, and Stefan Becuwe in the Flemish Supercomputer Center (VSC) for his technical support.

I would like to thank Francois Peeters, head of CMT group, for his kind support and providing the atmosphere for the exchange of ideas in CMT group. I would also like to acknowledge Hilde Evans, the secretariat of the Department of Physics, for her administrative assistance.

I warmly thank many others I have not directly worked with, but with whom I have shared many interesting scientific (and non-scientific) conversations: Jia-Ji Justin Zhu, Arne Van Overloop, Edith Euan Diaz, Mozhgan Amini, Samira Dabbaghmanesh, Hemant Dixit, Massoud Ramezani Masir, Azam Karami, Kirsten Govaerts, and certainly many others.

Finally, I would like to thank my entire family for their love, support, and motivation over the years. My parents have always been amazingly supportive and encouraging. Words could not express my big thanks to them.

My heartfelt thanks go to my husband, Nima, who is proof that you should marry someone smarter than yourself. Without his never-ending love, support, and wisdom, this work never would have been possible, and for which I owe the biggest "thank-you" of all.

Nasrin Sarmadian  
Antwerpen - June 2015



# Contents

|  |           |
|--|-----------|
| <b>Contents</b>  | <b>v</b>  |
| <b>1 Introduction</b>  | <b>3</b>  |
| 1.1 Introduction to solar energy . . . . .                       | 3         |
| 1.2 Solar cell structure . . . . .                               | 4         |
| 1.2.1 Transparent conducting oxide (TCO) layer . . . . .         | 5         |
| 1.2.2 $n$ -layer . . . . .                                       | 6         |
| 1.2.3 Absorber layer . . . . .                                   | 7         |
| 1.2.4 Back contact . . . . .                                     | 8         |
| 1.3 Solar cell generations . . . . .                             | 8         |
| 1.3.1 Wafer based solar cells: First generation of PVs . . . . . | 8         |
| 1.3.2 Thin film solar cells: second generation of PVs . . . . .  | 8         |
| 1.3.3 Third generation of PVs . . . . .                          | 12        |
| 1.4 Purpose and content of this thesis . . . . .                 | 13        |
| <b>2 Density functional theory</b>                               | <b>15</b> |
| 2.1 Introduction . . . . .                                       | 15        |
| 2.2 Time-independent Schrödinger equation . . . . .              | 15        |
| 2.3 Born - Oppenheimer approximation . . . . .                   | 16        |
| 2.4 Hartree approximation . . . . .                              | 17        |
| 2.5 Hartree-Fock approximation . . . . .                         | 17        |
| 2.6 Density functional theory . . . . .                          | 18        |
| 2.6.1 The Hohenberg-Kohn theorems . . . . .                      | 19        |
| 2.6.2 The Kohn-Sham equations . . . . .                          | 20        |
| 2.6.3 The exchange-correlation energy . . . . .                  | 21        |
| 2.6.4 The hybrid functional approximation . . . . .              | 23        |

|          |   |           |
|----------|---|-----------|
| 2.7      | Band structure calculations . . . . .   | 24        |
| 2.7.1    | The Bloch theorem . . . . .   | 24        |
| 2.7.2    | Methods to calculate the electronic structure of solids . . . . .                         | 25        |
| 2.7.3    | Projected augmented wave method . . . . .   | 26        |
| <b>3</b> | <b>Optoelectronic properties of Al-doped MgO</b>  | <b>29</b> |
| 3.1      | Introduction . . . . .  | 29        |
| 3.2      | Optical properties within linear response . . . . .                                       | 30        |
| 3.3      | Computational Method . . . . .  | 36        |
| 3.4      | Results and discussion . . . . .  | 38        |
| 3.4.1    | Crystalline structures . . . . .  | 38        |
| 3.4.2    | Amorphous versus crystalline structure . . . . .  | 43        |
| 3.5      | Conclusions . . . . .   | 45        |
| <b>4</b> | <b>High-throughput screening approach based on density functional theory</b>              | <b>47</b> |
| 4.1      | Introduction . . . . .  | 47        |
| 4.2      | DFT based high-throughput screening procedure . . . . .                                   | 48        |
| 4.3      | Data generation . . . . .   | 48        |
| 4.4      | Convergence to the electronic ground state and problem handling . . . . .                 | 50        |
| 4.5      | Storing and analysing data . . . . .  | 51        |
| 4.6      | Numerical convergence . . . . .   | 52        |
| 4.7      | Role of scripting in high-throughput computations . . . . .                               | 53        |
| <b>5</b> | <b>Bixbyite Oxides for TCO Applications</b>   | <b>57</b> |
| 5.1      | Introduction . . . . .  | 57        |
| 5.2      | Computational Method . . . . .  | 58        |
| 5.2.1    | Generating candidates . . . . .   | 59        |
| 5.2.2    | Band gap screening . . . . .  | 60        |
| 5.2.3    | Band alignment screening . . . . .  | 61        |
| 5.2.4    | Phase stability screening . . . . .   | 62        |
| 5.3      | Results . . . . .   | 64        |
| 5.3.1    | Binary oxides . . . . .   | 64        |
| 5.3.2    | Ternary oxides . . . . .  | 69        |
| 5.4      | Conclusions . . . . .   | 76        |
| <b>6</b> | <b>Shallow acceptors in bixbyite <math>V_2O_3</math>, a novel <i>p</i>-type conductor</b> | <b>77</b> |
| 6.1      | Introduction . . . . .  | 77        |
| 6.2      | Defect calculations . . . . .   | 78        |
| 6.3      | Computational Method . . . . .  | 80        |

---

|          |  |            |
|----------|--|------------|
| 6.4      | Results . . . . .  | 81         |
| 6.5      | Conclusions . . . . .  | 89         |
| <b>7</b> | <b>Identification of <i>p</i>-type TCOs based on first-principles calculations</b> | <b>91</b>  |
| 7.1      | Introduction . . . . .   | 91         |
| 7.2      | Computational Method . . . . .   | 94         |
| 7.3      | Results . . . . .  | 95         |
| 7.4      | Conclusions . . . . .  | 106        |
| <b>8</b> | <b>Identification of stannite Cu-based absorber layers</b>                         | <b>107</b> |
| 8.1      | Introduction . . . . .   | 107        |
| 8.2      | Solar cell operation . . . . .   | 108        |
| 8.2.1    | Generation of charge carriers . . . . .  | 109        |
| 8.2.2    | Separation and collection of photo-generated carriers . . . . .                    | 109        |
| 8.2.3    | Efficiency and loss mechanism . . . . .  | 111        |
| 8.3      | Computational details . . . . .  | 114        |
| 8.4      | Results . . . . .  | 116        |
| 8.5      | Conclusions . . . . .  | 129        |
|          | <b>Appendices</b>  | <b>131</b> |
|          | <b>Summary and Outlook</b>   | <b>173</b> |
|          | <b>Samenvatting en Vooruitzicht</b>  | <b>179</b> |
|          | <b>Bibliography</b>  | <b>185</b> |
|          | <b>Curriculum Vitae</b>  | <b>205</b> |



# List of Abbreviations

|       |  |
|-------|--|
| PBE   | Branching Point Energy                   |
| BZ    | Brillouin zone                           |
| CBM   | Conduction Band Minimum                  |
| CIGS  | Copper Indium Gallium Selenide           |
| CIS   | Copper Indium Selenide                   |
| CGS   | Copper Gallium Selenide                  |
| CZTS  | Copper Zinc Tin Sulphide                 |
| DFT   | Density Functional Theory                |
| DOS   | Density Of States                        |
| FF    | Fill Factor                              |
| GGA   | Generalized Gradient Approximation       |
| HK    | Hohenberg-Kohn                           |
| HSE   | Heyd-Scuseria-Ernzerhof                  |
| HT    | High-Throughput                          |
| ICSD  | Inorganic Crystal Structure Database     |
| ITO   | Indium Tin Oxide                         |
| KS    | Kohn-Sham                                |
| LDA   | Local Density Approximation              |
| MP    | Monkhorst Pack                           |
| PAW   | Projector Augmented Wave Method          |
| PDOS  | Projected Density Of States              |
| PBE   | Perdew-Burke-Ernzerhof                   |
| PV    | Photovoltaic Cell                        |
| SLME  | Spectroscopic Limited Maximum Efficiency |
| SQ    | Shockley-Queisser                        |
| RPA   | Random Phase Approximation               |
| TCO   | Transparent Conducting Oxides            |
| TDDFT | Time Dependent Density Functional Theory |
| VASP  | Vienna Ab initio Simulation Package      |
| VBM   | Valence Band Maximum                     |
| XC    | Exchange-Correlation                     |



# Introduction

## 1.1 Introduction to solar energy

The world consumed about 164 PWh energy in 2011 and a 200 PWh global energy consumption is expected due to the worldwide increase in population and economy by 2020 [1]. Figure 1.1 compares the energy consumption for the years 1993, 2011, and gives a projection for the year 2020. A 22% increase in the global energy consumption in the next few years is expected. With this continual increase in energy demand, scientists are working to find ways to realize transition from fossil fuels to renewable energy sources which are more efficient and environmentally friendly. Figure 1.1 also shows a 33% increase in the share of renewable energy among all energy sources where solar energy after wind energy is the most used renewable energy source.

The energy which is delivered by the radiation of the sun to the earth's surface in one hour is more than the entire world energy consumption in one year. Realizing the full potential of solar power requires finding effective, inexpensive ways to utilize this vast energy source. The photovoltaic (PV) cell is the technology which enables us to harness solar energy. It generates direct current (DC) in semiconductors under solar irradiation. Although the produced energy accounts for a tiny fraction of the total energy used, the recent installation of worldwide PV has increased significantly. The global total produced power from solar PV was roughly 67 GW at the end of 2011. Over the past five years, solar PV has averaged an annual growth rate of over 50% [2].

Belgium represents about 2% of the cumulative global solar market and was the 11<sup>th</sup> largest solar market in 2013. Belgium had a national target of 1340 MW of Solar Capacity by 2020 which was reached in 2011. The country has the potential to reach 7000 MW of solar capacity by 2020. Over 60% of its PV capacity is in residential installations. 20% of the installations are commercial and a further 18% of solar capacity is in the industrial sector [1].

The commercial interest in PVs as a reliable source of energy will further increase if the price decreases and the applications increase. This requires modifications in the structure and operations of PV cells. Finding new cheap materials with specific properties for particular parts of the solar

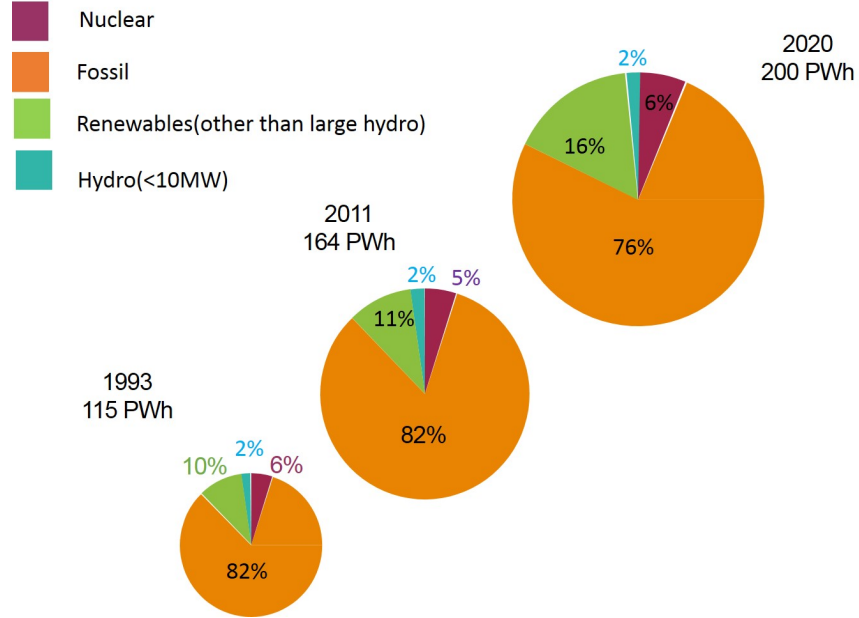


Figure 1.1: the global energy consumption and the shares of different energy sources over the years [1].

cell is one of the main goals. However, the high costs and time consuming synthesis procedures limit the experimental screening of hundreds or thousands of possible compounds to find new candidates. Fortunately, first principles computational methods are rapid, exact in results, and powerful in predictions. They can be used in high-throughput approaches to identify new possible materials for a particular part of the PV cell. The main aim of this thesis is to use an accurate computational high-throughput approach to investigate the optoelectronic properties of different materials and identify those that are appropriate for a specific part of the solar cell. Therefore, we first deal with the structure of the solar cell in this introduction, followed by a discussion of the role of each part of the solar cell in its operation.

## 1.2 Solar cell structure

The incident light passes through different layers in a solar cell. Each layer plays a certain role which is explained in this section. Figure 1.2 shows a typical stack of the active layers in a solar cell.



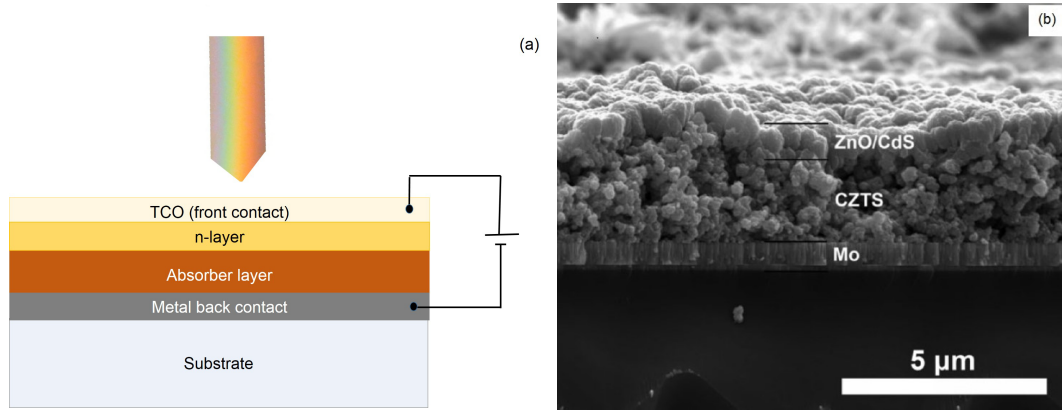


Figure 1.2: (a) A schematically drawing of the active layers in a typical solar cell, and (b) SEM image of a cross section of Copper Zinc Tin Sulphide (CZTS) solar cell [3].

### 1.2.1 Transparent conducting oxide (TCO) layer

The incident light first strikes the transparent conducting oxide. This element acts as a window layer for light to pass through it and the light can reach the active material beneath where carrier generation occurs. For good transmission of visible light, which has to be greater than 80%, the band gap has to be above 3.2 eV and the absorption coefficient should be low, requiring a low plasma frequency ( $\omega_p$ ).

This layer also acts as the front contact, thus it must have a high electrical conductivity ( $\sigma$ ). This can be achieved by high carrier concentration ( $n$ ) of the order of  $10^{20} \text{ cm}^{-3}$  and low resistivity of the order of  $10^{-4} \Omega \text{ cm}$ . High optical transparency and high electrical conductivity are two properties which normally exclude each other. Electrical conductivity is usually observed in metals, but they are not transparent. Highly doped semiconductors are transparent for light with an energy less than the band gap and in addition are conductive. Two key properties of a TCO are high electrical conductivity and low absorptivity of visible light. According to the Drude model in a crystal electrons move free between their collisions with the heavy positively charged ions. The equation of motion of these electrons can be explained with the second law of Newton

$$mv/\tau = eE \quad (1.1)$$

where  $E$  is the electrical field,  $m$  is the electron effective mass,  $e$  is the electric charge of an electron, and  $\tau$  is the average time between two successive collisions of electrons (relaxation time).  $v$  gives the average drift speed of electrons. In this model, the mobility ( $\mu$ ) and conductivity ( $\sigma$ ) of the electrons are related by the formula

$$\sigma = ne\mu \quad (1.2)$$

where the mobility of the electrons is given by  $\mu = e\tau/m$ . It is clear from Eq. (1.2) that the conductivity depends on the number of electrons  $n$  and the mobility of electrons, where the latter one depends on the effective mass, and the relaxation time. The number of electrons can be manipulated by the concentration of defects in the semiconductor. The effective mass of the carriers is given by the curvature of the energy band in the reciprocal space (in one dimension):

$$\frac{1}{m} = \frac{1}{\hbar^2} \frac{d^2 \epsilon_{nk}}{dk^2} \quad (1.3)$$

where  $\epsilon_{nk}$  is the energy of the carrier in the specific band  $n$  and  $k$  is the wave number. The effective mass of the each type of carriers (electron or hole) is in principle a  $3 \times 3$  symmetric matrix. For isotropic structures only one value can produce all the components of the effective mass matrix.

The low absorptivity of visible light depends on two properties of the material, the plasma frequency and the optical band gap. The plasma frequency puts a lower limit on the transparency window of a semiconductor. If the incident photon to the semiconductor has an energy lower than  $\omega_p$ , total reflection takes place. The Drude formula can be used to calculate this frequency

$$\omega_p^2 = \frac{4\pi N e^2}{m \epsilon_\infty} \quad (1.4)$$

where  $N$  is the number of free carriers,  $e$  is the charge of the electron,  $m$  is the electron effective mass, and  $\epsilon_\infty$  is the dielectric constant.

Another key property that plays an important role in the transparency of the compound is the optical band gap. It is the energy of first allowed transition from the valence band to the conduction band. It puts an upper limit on the transparency window of a semiconductor. As the visible light has an energy range between 1.65 to 3.23 eV, the ideal TCO has an optical band gap larger than 3.23 eV and a plasma frequency lower than 1.65 is ideal for the photovoltaic application of a TCO. However, the ideal value of the plasma frequency and the optical band gap can change depending on the application of the TCO.

### 1.2.2 $n$ -layer

The next layer that appears in the path of a photon in the solar cell is the  $n$ -layer, a vital part of the  $p$ - $n$  junction. Usually in most semiconductors the mobility is higher for electrons than holes [4], therefore it is intended to avoid absorption in the  $n$ -layer. As a result, the absorber is  $p$ -type, and also the  $n$ -layer should consist of a relatively wide band gap semiconductor compared to the absorber layer (see section 1.2.3) or one with low absorption. Cadmium sulfide is one of the mostly used semiconductors as  $n$ -layer. It has a 2.4 eV band gap and a low absorption coefficient. It absorbs 10% of the incident photons near the band edge, and this rate increases up to 80% for ultraviolet (UV) photons [5].

### 1.2.3 Absorber layer

After the light passes through the  $n$ -layer, it enters the  $p$ -layer. This layer is called the absorber layer because it is the layer where the absorption of photons and generation of carriers takes place. A direct band gap material is a good choice because it has a high absorption coefficient and allows a thin absorber layer and thus low material consumption. Indirect band gap absorbers like silicon require thick layers or light trapping techniques. The absorbed photons create electron-hole pairs, after which the electric field of the  $p$ - $n$  junction separates them and directs them to the electrical contacts. It is particularly important to ensure a reasonable transport of the photo-generated charge carriers because they dominate the electrical behavior of the  $p$ - $n$  junction. The intrinsic hole and electron concentration is the same in an intrinsic semiconductor. This concentration in Si, a typical semiconductor, is  $10^{10} \text{ cm}^{-3}$ . These carriers can be separated if they receive enough energy after which they will contribute to the conduction. The carrier concentration can be increased by doping the semiconductor with a proper dopant. Doping the semiconductor disturbs the balance between majority positively and minority negatively charged carriers. This results in an increase in the majority carrier concentration. The majority carrier concentration in a typical doped semiconductor is in the range of  $10^{17} \text{ cm}^{-3}$  to  $10^{19} \text{ cm}^{-3}$  while the minority carrier concentration is the intrinsic carrier concentration and stays as low as before doping,  $10^{10} \text{ cm}^{-3}$  [6]. Illuminating the absorber layer by photons increases the number of minority carriers compared to equilibrium. Recombination processes diminish the extra carriers, which decrease the output current density of the solar cell (Section. 8.2.3). The rate of the recombination ( $R$ ) depends on the number of excess minority carriers ( $\Delta n$ ) which can be formulated as

$$R = \tau \Delta n \quad (1.5)$$

Two parameters that affect this recombination rate are the minority carrier lifetime ( $\tau$ ) and diffusion length ( $L$ ). The lifetime of a carrier is the average time that a carrier has before the recombination happens. The diffusion length is the average distance that a carrier can move from the point of the generation until it recombines. In high quality silicon, the lifetime is 1 msec, and the diffusion length is typically 100-300  $\mu\text{m}$  [7]. Lifetime and diffusion length are interrelated by the diffusivity ( $D$ ) formula

$$L = \sqrt{D\tau} \quad (1.6)$$

Furthermore, the band gap energy and absorption coefficient characterize the ability of a semiconductor to absorb photons. The absorber layer should have a large absorption coefficient to absorb visible light efficiently. Furthermore, the band gap should be around 1.3 eV according to the Shockley-Queisser (SQ) limit in order to reach the maximal theoretical efficiency [8]. For photons which have an energy very close to the band gap, the absorption is relatively low since only electrons at the VBM can interact with the photons to cause absorption. As the photon energy increases, not only the electrons at the VBM but also some electrons that are at the bands below the

VBM can interact with such photons. This results in higher probability of absorption of photons by electrons. More absorbed photons results in a larger number of excited electrons.

### 1.2.4 Back contact

If the light has not been absorbed by the absorber layer and reaches the back contact, it should be reflected back into the absorber layer. Therefore, the back contact must be a good optical reflector. This element should also collect electrons and therefore it should be also a good electrical contact. These two essential properties can be provided by a metal like Molybdenum (Mo). The metal back contact is deposited on the substrate which is usually a glass plate.

## 1.3 Solar cell generations

Three generations of PVs can be distinguished. The wafer-based silicon solar cells form the first generation of PVs. All different thin-film solar cells are counted as the second generation whereas novel concepts are used to make the third generation of PVs as explained in Section 1.3.2, and 1.3.3, respectively. The main reason of existence of the second generation is to decrease the solar cell costs, while the third generation solar cells tries to increase the energy conversion efficiency while keeping the solar cell costs as low as the second generation [9].

Figure 1.3 shows the shares of different solar cells in today's solar energy market. The high share of silicon based solar cells is obvious from this figure.

### 1.3.1 Wafer based solar cells: First generation of PVs

About 91% of all installed solar cells in the world are silicon-based PVs [10]. This high share in the solar energy market is due to the well-developed fabrication techniques and relatively good energy conversion efficiencies of 20 to 25% [11].

In majority, mono-crystalline or multi-crystalline silicon is fabricated into bars and then wafers to be used in silicon (Si) solar cells. The high fabrication costs have motivated the PV community to search for new materials and technologies. Thin film technology offers a second generation of promising potential solar cell technology which has significant advantages in terms of material and fabrication.

### 1.3.2 Thin film solar cells: second generation of PVs

Thin film solar cells use Copper Indium Gallium Selenide (CIGS) and Copper Zinc Tin Sulphide (CZTS) which are materials with high absorptivity so the cells can be very thin (few hundred nanometers to tens of  $\mu\text{m}$ ), which reduces the amount of material by a factor of 10 and therefore also the solar cell price. The optical and electrical properties of thin films depend not only on the

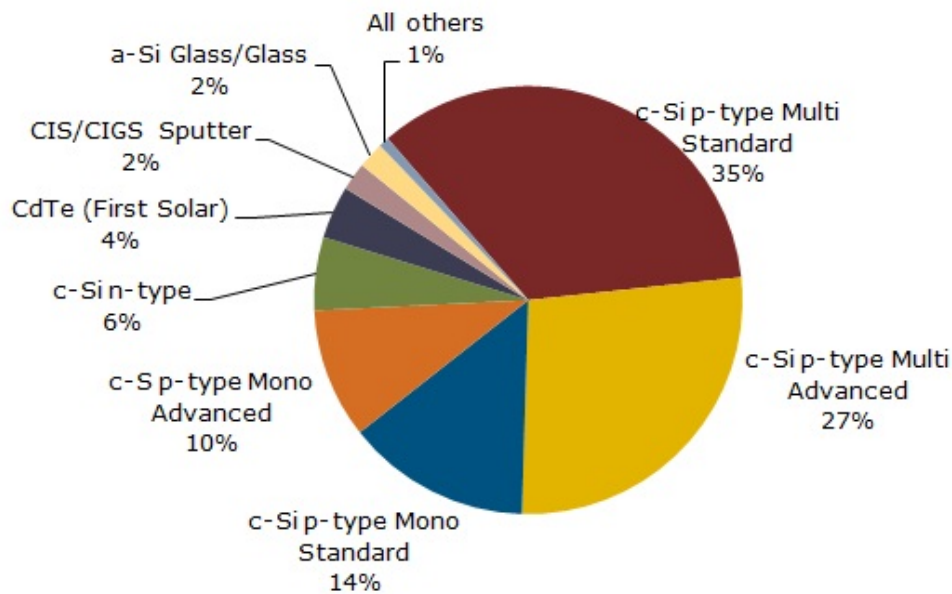


Figure 1.3: The shares of different solar cell technologies in today's solar energy market [10].

structure but also on the composition of the film. This means that by controlling the deposition parameters, the thin film properties can be controlled to benefit more from the solar spectrum. In addition, thin film solar cells are less sensitive to purity and crystallinity of the materials than wafer-based solar cells. The fabrication process of thin films can be done at low temperatures ( $200\text{ }^{\circ}\text{C} < T < 500\text{ }^{\circ}\text{C}$ ) comparing to the fabrication temperature for wafer-based Si solar cells which is relatively high at about  $800\text{ }^{\circ}\text{C}$ . This low temperature allows the use of cheap substrates like glass, plastic, and steel foil. Moreover, the thin film area in the solar cell module depends on the size of the equipment and can be as large as  $57000\text{ cm}^2$ , where the size of the wafer-based solar cell depends on the wafer size which is limited to  $225\text{ cm}^2$  in current technology. For wafer-based solar cells, it takes 2-3 years to deliver the equivalent energy as the energy of its production. A thin film solar cell has a shorter energy payback period of only 1 year. Recalling Fig. 1.3, thin film solar cells have approximately 6% of total solar energy market. However, this rate can increase because the use of abundant elements and relatively cheap and diverse fabrication techniques have led to an increased interest in the thin film technology.

The  $p$ - $n$  junction in a thin film solar cell is realized by connecting two semiconductors. Basically thin film solar cells can be made of every semiconductor but only a few of them provide reasonable efficiency for the conversion of light into electrical current. Figure 1.4 shows that one can substitute gradually Si by elements from lower and higher groups to make new semiconductors. Thus, on the basis of Si, at first the III-V semiconductors like GaAs and II-VI ones like CdTe can be deduced. Also, one can step further to substitute one half of the group II elements by a

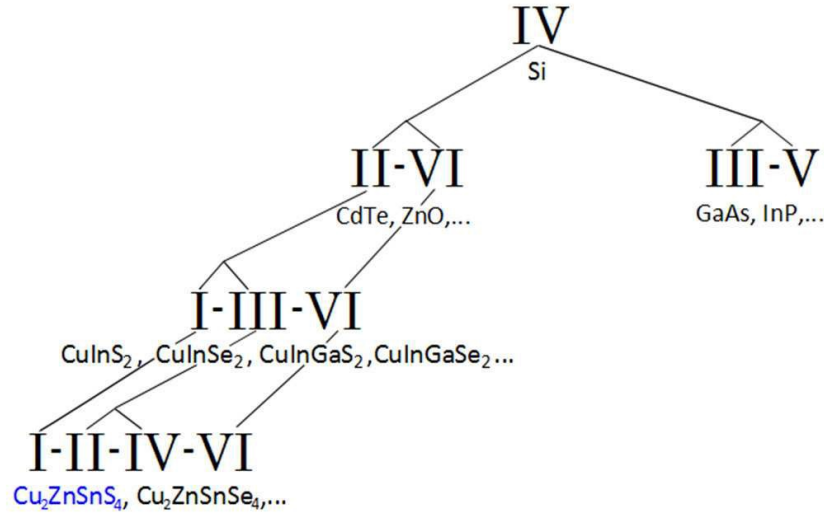


Figure 1.4: Possible semiconductors obtained by substituting elements by elements of groups from higher and lower group numbers [12].

group-I element and one half by a group-III element which results in a I-III-VI compound like  $\text{CuInSe}_2$  (CIS) or  $\text{CuGaSe}_2$  (CGS). Furthermore, one can replace half of the group-III elements by a group-II element and half by a group-IV element to make a new semiconductor. For example, substituting In/Ga by Zn and Sn in CIGS leads to Copper Zinc Tin Sulphide CZTS.

## Silicon (Si)

Although the crystalline phase of silicon is widely used in the first generation of PVs, two other phases of silicon, namely amorphous silicon (a-Si) and nano-crystalline silicon (nc-Si) are used for the second generation of PVs. a-Si has an extremely high defect density ( $> 10^{19} \text{ cm}^{-3}$ ) [13] which results in fast recombination of photo-generated carriers. But, hydrogenating a-Si leads to the passivation of most defects, and a decrease in the defect density to around  $10^{16} \text{ cm}^{-3}$  [14]. Thus, hydrogenated amorphous silicon (a-Si:H) is usable as PV material. Its band gap is about 1.7 eV and is direct (in contrast to crystalline Silicon (c-Si)). The first successful a-Si:H solar cell with an efficiency of 2.4% was reported by Carlson and Wronski in 1976 [15]. Nano-crystalline hydrogenated silicon (nc-Si:H) consists of many small crystals with sizes of several nanometers surrounded by an amorphous silicon tissue. Its structure is in between amorphous and crystalline silicon. Its band gap is 1.1 eV. It is a very interesting material for tandem (multi-junction) cells due to its relatively low band gap. The current record efficiency for both thin-film a-Si:H and nc-Si:H solar cells is 10.1% [16].

### Gallium arsenide (GaAs)

GaAs is a III-V semiconductor with a 1.42 eV direct band gap [17]. Its direct band gap provides a much more efficient absorption of light in comparison with Si. The high efficiency and high radiation tolerance of GaAs thin-film make it appropriate for PV applications in space. GaAs solar cells compared to Si solar cells have notable disadvantages such as its high cost (low abundance of Ga which is only about 19 ppm in the earth's crust [18]), heavy weight, and highly toxicity of Arsenic [19]. Thin-film GaAs solar cells are highly efficient with a current energy conversion efficiency of 28.8% [16]. Furthermore, crystalline GaAs solar cells can be produced, but they have lower efficiency than thin-film GaAs cells [16]. GaAs as an absorber layer can be used in high-efficiency multi-junction cells which consist of multiple thin films of GaAs, Ge, and GaInP<sub>2</sub> [20]. This solar cell reaches about 40.7% efficiency under solar radiation and laboratory conditions [21].

### Cadmium Telluride (CdTe)

CdTe is a II-VI semiconductor with a 1.45 eV direct band gap. CdTe can be easily deposited and is appropriate for large-scale production. A *p*-doped CdTe absorber with an *n*-doped CdS window layer forms a *p-n* junction [22]. The main layers in this solar cell are a transparent conductor as a top contact, CdS/CdTe hetero *p-n* junction, and a metallic back contact. Various supporting substrates from glass to metal or plastic can be used. The record efficiency has been reported as high as 17.3% [16]. Tellurium is one of the rarest stable solid elements in the earth's crust with an abundance of about 30 ppm [18, 23]. Although CdTe is toxic and its toxicity is derived from the toxicity of cadmium, many studies have shown that the release of cadmium to the atmosphere is lower with CdTe-based solar cells compared to the silicon PVs and other thin-film solar cell technologies [24].

### CIGS

CIGS is a I-III-VI<sub>2</sub> semiconductor material with the chemical formula CuIn<sub>1-x</sub>Ga<sub>x</sub>Se<sub>2</sub>, where by changing *x* between 0 and 1, the band gap varies between 1.0 eV for CIS to about 1.7 eV for CGS [25]. The *p-n* junction is formed between a *p*-doped CIGS absorber layer and an *n*-doped CdS transparent conductor [26, 27].

Usually glass of 1-3 mm thickness is used as a substrate for this semiconductor. First the glass is coated on one side with Mo that serves as a back contact, and then CIGS is deposited on top of the Mo. The hetero-junction is then completed by chemical bath deposition of CdS. Afterwards an intrinsic layer of undoped ZnO followed by a heavily-doped ZnO layer are deposited on top of CdS. The highest certified record efficiency is 21.7% [16].

### CZTS

Cu<sub>2</sub>ZnSnS<sub>4</sub> (CZTS) is a material for thin film solar cell applications. It contains earth-abundant non-toxic elements. CZTS is derived from the CIGS structure by the isoelectronic substitution of

In/Ga atoms by a Zn and Sn atom. As a consequence, some properties of CZTS are similar to those of CIGS. CZTS has a near-optimum direct band gap energy of about 1.5 eV and a large absorption coefficient ( $> 10^4 \text{ cm}^{-1}$ ) [28]. The highest achieved conversion efficiency for CZTS-based solar cells is as high as 12.6% [29]. The  $p$ - $n$  junction is built of a CdS  $n$ -layer and a CZTS  $p$ -type absorber layer. Mo as back contact is deposited on the glass substrate. ZnO acts as a window layer and front contact in this solar cell [3].

### 1.3.3 Third generation of PVs

According to the thermodynamics the highest conversion efficiency of sunlight into electricity is 85%. It opposes to the upper limit of 33% on the conversion efficiency of a single junction solar cell, which applies to the two first generations of solar cells. The gap between these two values relates to the design of solar cells. The performance of solar cells can be improved 2-3 times if different fundamental concepts are used in the solar cell design [30].

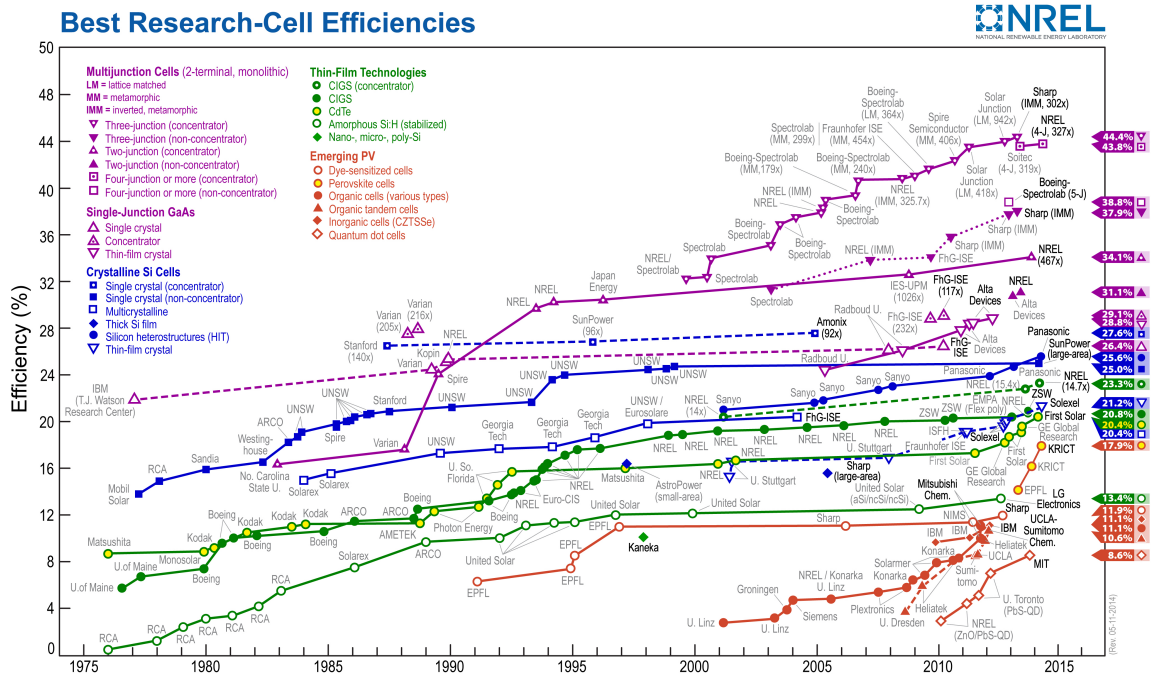


Figure 1.5: recent report of the NREL on the efficiency of the solar cell generations [31].

Figure 1.5 presents the world record efficiencies of various PV technologies [31]. This figure indicates 44% as highest conversion efficiency which is achieved by applying some fundamental changes in the traditional single junction solar cells.



Different approaches can be utilized to apply fundamental concepts on the solar cells in order to make new high efficient generations of solar cells.

1. Absorbing the photons from different parts of the solar spectrum using multiple materials as in a tandem solar cell, or by benefiting from the concept of the intermediate band (IB). There are different approaches to create the IB in solar cells. Impurity PVs use a high concentration of impurities in a large band gap semiconductor to create an IB. Quantum dot solar cells utilize the quantum confinement of electrons in low dimensional materials to form the IB.

2. Generating multiple electron-hole pairs by one photon which is based on Raman luminescence [9]. Raman scattering of a photon creates an electron-hole pair. The pair relaxes and emits a photon with lower energy. The newly created photon can generate another electron-hole pair.

3. Efficient use of the solar spectrum in the way that it suits for the solar cell material. This approach uses an extra layer as up-/down-converter of photons. The up-converter converts two low energy photons, that are transmitted by the absorber layer, to one high energy photon. The down-converter converts one high energy photon, that is inefficiently absorbed by the solar cell due to thermalisation losses, to two or more low energy photons. The converted photons are absorbed efficiently by the absorber layer.

4. Reducing thermalisation losses in hot carrier cells. The photons that have an energy much higher than the band gap of the absorber layer, excite the carriers to the bands far from the band edge of the material. Such carriers that are called hot carriers are likely to be thermalised and recombined. By applying special contacts into the PVs, it is possible to provide a situation for the hot carriers to traverse quickly through the material and to be collected before thermalisation.

## 1.4 Purpose and content of this thesis

This thesis deals with a wide group of materials that are part of solar cells, from insulators like MgAlO as a possible substrate to wide band gap TCOs as window layer and to relatively small band gap semiconductors as absorber layers. The aim of this thesis is to use an accurate high-throughput calculation approach based on the density functional theory (DFT) formalism to study the optical properties and electronic structure of these materials. The structure of the thesis is as follows:

**Chapter 2** gives a brief overview on the DFT formalism as an effective and accurate scheme which is used as the theoretical method throughout this thesis to calculate the properties of materials.

**Chapter 3** provides an introduction to the linear optical response in semiconductors and some important quantities like plasma frequency, absorption edge, and refractive index. Then, the results of our DFT calculations on the optoelectronic properties of Al-doped MgO are presented. We have studied the effect of the Al concentration on the structure, electronic and optical properties of Al-doped MgO. We have also compared the properties of the amorphous and crystalline phases for the highest considered Al concentration.

In **Chapter 4** our DFT based high-throughput approach to screen materials for a particular application is discussed. The approach is used throughout of **Chapter 5** and **Chapter 7** of this thesis.

**Chapter 5** contains the details of our high-throughput procedure to select potential TCOs from the pool of more than 1500 binary and ternary oxides. The content of this chapter covers discussion about the structure, generation of the materials, considered properties, and applied criteria. We have presented our results which include a list of the potential TCOs with a discussion on the results.

As we have found from the results of our high-throughput calculation in **Chapter 6**, bixbyite  $V_2O_3$  could be a potential *p*-type TCO candidate. Therefore, in **Chapter 5** we have studied the *p*-type dopability of bixbyite  $V_2O_3$  within the DFT formalism. First, we have discussed the magnetic state of bixbyite  $V_2O_3$  and then the site preference of dopants in the bixbyite structure is investigated. We have also explained briefly the formation energy and transition levels in defect systems. Finally, different extrinsic and intrinsic defects are considered, for which we have found that substitutional Mg and the V vacancy act as shallow acceptors.

**Chapter 7** deals with another high-throughput calculations on TCOs. In this chapter, we have shown the results of our screening of all binary, ternary, and quaternary oxides to identify potential low hole mass *p*-type TCOs. Details about the considered criteria to select the potential *p*-type candidates among a huge number of oxides are given. We have presented the results of our calculation including the list of low-mass *p*-type TCO candidates.

**Chapter 8** explains our approach to calculate the solar cell efficiency based on first-principles calculated properties. Then, the results of our study on stannite Cu-based solar cells are presented. With the aim of identifying possible absorber layers, we have studied the structure and optoelectronic properties of the Cu-based quaternary chalcogenides. Furthermore, we have used the SLME metric to estimate the conversion efficiency of the studied solar cells and a comparison with the theoretical efficiency limit of SQ is made. This thesis ends with conclusions and an outlook for future work.

# Density functional theory

## 2.1 Introduction

The computational modeling of the properties of existing materials and predicting the properties of new materials can be considered as the main steps in computational materials design. First-principles calculations based on density functional theory (DFT) is one of the most powerful approaches that provide a better understanding of the properties of materials. Also, DFT calculations can model and predict the properties of novel materials. The success of DFT in the description of the properties of large classes of materials and the wide predictive power of the DFT-based approaches make it the method of choice for modern electronic structure calculations [32]. The computational costs of DFT calculations scale very good with the system size.

We have used DFT as a powerful method to model the structural, electronic, and optical properties of a large class of materials with the aim of finding new materials for particular applications in the PVs. DFT is also used to calculate the electronic structure of the defects in TCO materials already introduced. This chapter gives an overview of DFT.

## 2.2 Time-independent Schrödinger equation

In condensed matter physics the main task is explaining the behavior of systems which consist of a large number of interacting particles. The relevant particles are sets of either electrons or nuclei. The fundamental equation that particles have to satisfy is the time independent Schrödinger equation

$$H\Psi(\mathbf{r}_1, \dots, \mathbf{r}_n; \mathbf{R}_1, \dots, \mathbf{R}_{n'}) = E\Psi(\mathbf{r}_1, \dots, \mathbf{r}_n; \mathbf{R}_1, \dots, \mathbf{R}_{n'}) \quad (2.1)$$

where  $\Psi$  is the many-body wave function,  $E$  is the energy of the system, and  $H$  is the Hamiltonian

which is defined as

$$H = - \sum_i \frac{\hbar^2 \nabla_i^2}{2m_e} - \sum_I \frac{\hbar^2 \nabla_I^2}{2M_I} + \frac{1}{4\pi\epsilon_0} \sum_{i \neq j} \frac{1}{2} \frac{e^2}{|\mathbf{r}_i - \mathbf{r}_j|} + \frac{1}{4\pi\epsilon_0} \sum_{I \neq J} \frac{1}{2} \frac{Z_I Z_J e^2}{|\mathbf{R}_I - \mathbf{R}_J|} - \frac{1}{4\pi\epsilon_0} \sum_{i,I} \frac{Z_I e^2}{|\mathbf{r}_i - \mathbf{R}_I|} \quad (2.2)$$

where  $\mathbf{r}_i$  and  $\mathbf{R}_I$  is the position of electrons and nuclei, respectively.  $m_e$  and  $M_I$  represents the electron and nucleus mass, respectively.  $Z_I$  is the atomic number, and  $e$  is the electron charge. For simplicity, hereafter atomic units ( $\hbar = m_e = e = 4\pi\epsilon_0 = 1$ ) will be used in the formulas. In Eq. (2.2), the first two terms correspond to the kinetic energy of the electrons ( $T_e$ ) and nuclei ( $T_N$ ), respectively. The third and fourth terms indicate the Coulomb interaction between electrons (internal potential energy,  $V_{ee}$ ) and between nuclei ( $V_{II}$ ), respectively. The last term corresponds to the electron-nucleus Coulomb interactions (external potential  $V_{ext}$ ). Then, the Hamiltonian can be written as

$$H = T_e + T_N + V_{ee} + V_{II} + V_{ext}. \quad (2.3)$$

Although the properties of a system can be calculated by knowing the particles, and interactions between them together with the Schrödinger equation, solving Eq. (2.1) is too complicated. Therefore, the central problem is solving Eq. (2.1) with  $H$  defined by Eq. (2.2) with accurate and practical approximations.

## 2.3 Born - Oppenheimer approximation

The first approximation arises from the fact that the mass of the nucleus is much larger than that of the electron ( $\frac{m_e}{M_I} \simeq 10^{-4}$ ), therefore the kinetic energy of the nucleus can be neglected and the electrons move in an external potential produced by the stationary nuclei. This approach is the Born-Oppenheimer approximation [33] that leads to the following Hamiltonian

$$H = H_e + V_{II} = (T_e + V_{ee} + V_{ext}) + V_{II}. \quad (2.4)$$

Then the total energy is the sum of the electronic and the nuclear repulsion energy ( $E_e$ , and  $E_I$ , respectively):

$$E = E_e + E_I. \quad (2.5)$$

By omitting the explicit dependence of  $\Psi_e$  on nuclei positions, the corresponding Schrödinger equation is given by

$$H_e \Psi_e(\mathbf{r}_1, \dots, \mathbf{r}_n) = E_e \Psi_e(\mathbf{r}_1, \dots, \mathbf{r}_n). \quad (2.6)$$

Even after the decoupling of the electronic from the nuclear degrees of freedom the problem is difficult to solve. Therefore, more approximations should be introduced to reduce the equation to a solvable problem.

## 2.4 Hartree approximation

The Hartree approximation introduces a simple way to solve the many-body equation [34–36]. In this approximation, each electron is considered as an independent particle moving in an average potential from all other electrons. Then, the total wave function becomes a product of all one-electron wave functions

$$\Psi_e(\mathbf{r}_1, \dots, \mathbf{r}_n) = \Phi_1(\mathbf{r}_1) \dots \Phi_n(\mathbf{r}_n). \quad (2.7)$$

According to the variational principle in quantum mechanics, if  $E_0$  is the ground state energy solution of the Schrödinger equation, for any wave function  $\phi$

$$\frac{\langle \phi | H | \phi \rangle}{\langle \phi | \phi \rangle} \geq E_0. \quad (2.8)$$

By using the variational principle with Eq. (2.6) the Hartree equation can be obtained as

$$\left[ -\frac{\nabla_i^2}{2} - \sum_I \frac{Z_I}{|\mathbf{r}_i - \mathbf{R}_I|} + \sum_j \int d\mathbf{r}_j \Phi_j^*(\mathbf{r}_j) \frac{1}{|\mathbf{r}_i - \mathbf{r}_j|} \Phi_j(\mathbf{r}_j) \right] \Phi_i(\mathbf{r}_i) = \epsilon_i \Phi_i(\mathbf{r}_i). \quad (2.9)$$

The effective potential on an independent electron is determined by an integration over the density of electrons. Therefore, the Hartree approximation replaces the many-body problem by  $n$  simpler problems in a mean-field potential. However, the wave function of each electron depends on the wave function of all other electrons, and the Hartree equation has to be solved self-consistently.

## 2.5 Hartree-Fock approximation

The Hartree approximation neglects an important fact about the electrons. According to the Pauli exclusion principle two electrons can have the same orbital wave function only if they have opposite spins. In other words, the electrons are fermions and the many-body wave function needs to be antisymmetric by exchange of the electrons

$$\Psi(\mathbf{r}_1, \mathbf{r}_2, \dots, \mathbf{r}_i, \dots, \mathbf{r}_j, \dots, \mathbf{r}_n) = -\Psi(\mathbf{r}_1, \mathbf{r}_2, \dots, \mathbf{r}_j, \dots, \mathbf{r}_i, \dots, \mathbf{r}_n). \quad (2.10)$$

The best solution for Eq. (2.10) based on single-particle wave functions can be obtained by using a Slater determinant [37] as wave function instead of Eq. (2.7)

$$\Psi(\mathbf{r}_1, \mathbf{r}_2, \dots, \mathbf{r}_n) = \frac{1}{\sqrt{n!}} \begin{vmatrix} \Phi_1(\mathbf{r}_1) & \Phi_2(\mathbf{r}_1) & \dots & \Phi_n(\mathbf{r}_1) \\ \Phi_1(\mathbf{r}_2) & \Phi_2(\mathbf{r}_2) & \dots & \Phi_n(\mathbf{r}_2) \\ \vdots & \vdots & \ddots & \vdots \\ \Phi_1(\mathbf{r}_n) & \Phi_2(\mathbf{r}_n) & \dots & \Phi_n(\mathbf{r}_n) \end{vmatrix} \quad (2.11)$$

The Hartree-Fock approximation adds an exchange potential to the Hartree approximation to correctly account for the fermion nature of the electrons

$$\begin{aligned} & \left[ -\frac{\nabla_i^2}{2} - \sum_I \frac{Z_I}{|\mathbf{r}_i - \mathbf{R}_I|} + \sum_j \int d\mathbf{r}_j \Phi_j^*(\mathbf{r}_j) \frac{1}{|\mathbf{r}_i - \mathbf{r}_j|} \Phi_j(\mathbf{r}_j) \right] \Phi_i(\mathbf{r}_i) \\ & - \sum_{j|i} \left[ \int d\mathbf{r}_j \Phi_j^*(\mathbf{r}_j) \frac{1}{|\mathbf{r}_i - \mathbf{r}_j|} \Phi_i(\mathbf{r}_j) \right] \Phi_j(\mathbf{r}_i) = \epsilon_i \Phi_i(\mathbf{r}_i) \end{aligned} \quad (2.12)$$

where the electrons are considered to have the parallel spin components. The Hartree-Fock approximation takes into account the classical Hartree interaction between electrons and the exchange interaction. The difference between the exact energy and Hartree-Fock energy defines the correlation energy

$$E_c = E_{exact} - E_{HF}. \quad (2.13)$$

## 2.6 Density functional theory

Several post-Hartree-Fock methods such as Møller-Plesset perturbation theory [38], configuration interaction (CI) [39], coupled cluster (CC) [40], and variational quantum Monte Carlo (QMC) [41] have been developed to include the correlation to the many-body wave function. Another alternative to the HF approximation is density functional theory, which treats both exchange and correlation energies. Modern Density functional is very popular in quantum chemistry and physics because the approximate functionals provide a useful balance between accuracy and computational cost. This theory makes it possible to calculate the electronic structure of much larger systems compared to the traditional ab initio methods, while retaining much of their accuracy. In the following sections, the fundamentals of DFT are explained and the approximations that are used in practical calculations are discussed.

### 2.6.1 The Hohenberg-Kohn theorems

Modern DFT is based on two theorems proposed and proven by Hohenberg and Kohn (HK) in 1964 [42].

- **Theorem I:** *For any system of interacting particles in an external potential  $V_{ext}(\mathbf{r})$  the potential  $V_{ext}(\mathbf{r})$  is determined uniquely, except for a constant, by the ground state density  $n_0(\mathbf{r})$ .*

This theorem states that the ground state electron density uniquely determines an external potential, the Hamiltonian, and thus all properties of the system.

**Proof I:**

Assume that there are two different potentials  $V_{ext}^1(\mathbf{r})$  and  $V_{ext}^2(\mathbf{r})$ , both give the same ground state density  $n_0(\mathbf{r})$ . Obviously, two different external potentials belong to two Hamiltonians  $H^1$  and  $H^2$  which give two distinct normalized wave functions  $\Psi^1$  and  $\Psi^2$ , and then two ground state energies  $E^1$  and  $E^2$ .

Corresponding to the variational principle, no wave function can give an energy that is less than the energy of  $\Psi^1$  for  $H^1$ :

$$\langle \Psi^1 | H^1 | \Psi^1 \rangle < \langle \Psi^2 | H^1 | \Psi^2 \rangle = \langle \Psi^2 | H^2 | \Psi^2 \rangle + \langle \Psi^2 | H^1 - H^2 | \Psi^2 \rangle \quad (2.14)$$

$$E^1 < E^2 + \int n_0(\mathbf{r}) [V_{ext}^1(\mathbf{r}) - V_{ext}^2(\mathbf{r})] d\mathbf{r}. \quad (2.15)$$

By exchanging the labels in Eq. (2.15), one obtains

$$E^2 < E^1 + \int n_0(\mathbf{r}) [V_{ext}^2(\mathbf{r}) - V_{ext}^1(\mathbf{r})] d\mathbf{r}. \quad (2.16)$$

Comparing Eq. (2.15) and Eq. (2.16) yields

$$E^1 + E^2 < E^2 + E^1 \quad (2.17)$$

which is clearly a contradiction, and so each potential corresponds to only one unique density for its ground state.

- **Theorem II :** *A universal functional for the energy  $E[n(\mathbf{r})]$  in terms of the density  $n(\mathbf{r})$  can be defined, independent of external potential  $V_{ext}(\mathbf{r})$ . The exact ground state energy of the system is the global minimum of this functional and the density that minimizes the functional is the exact ground state density  $n_0(\mathbf{r})$ .*

**Proof II:**

According to the theorem I, the external potential is uniquely determined by the density and the potential uniquely determines the ground state wave function. As a result, properties of the system such as kinetic energy are uniquely determined. Therefore one can write the energy as a functional of the density.

$$\begin{aligned} E_{HK}[n(\mathbf{r})] &= T_e[n(\mathbf{r})] + E_{ee}[n(\mathbf{r})] + \int n(\mathbf{r})V_{ext}[n(\mathbf{r})]d\mathbf{r} \\ &\equiv F_{HK}[n(\mathbf{r})] + \int n(\mathbf{r})V_{ext}[n(\mathbf{r})]d\mathbf{r} \end{aligned} \quad (2.18)$$

where  $F_{HK}[n]$  is a universal functional because the treatment of the kinetic and electron-electron interaction potential energies are the same for all systems. Levy and Lieb have independently provided a minimization principle which leads to the definition of the universal functional of HK [43, 44]. The unique ground state density defines the ground state energy, so a different density will necessarily give a higher energy.

$$E_0 \leq E_{HK}[n(\mathbf{r})] = F_{HK}[n(\mathbf{r})] + \int n(\mathbf{r})V_{ext}[n(\mathbf{r})]d\mathbf{r}. \quad (2.19)$$

It means that the ground state energy minimizes the Hohenberg and Kohn functional to give the ground state energy.

## 2.6.2 The Kohn-Sham equations

Although the HK theorems propose the density as fundamental quantity to solve the many-body problem, they do not say how the density can be obtained to perform the minimization. W. Kohn and L. J. Sham (KS) proposed to use a set of  $N$  non-interacting electron wave functions  $\Phi_i(\mathbf{r})$  as the main ingredients to obtain the same ground state density [45].

$$n(\mathbf{r}) = \sum_{i=1}^{occ.} |\Phi_i(\mathbf{r})|^2 \quad (2.20)$$

$\Phi_i(\mathbf{r})$  is an orbital of the non-interacting system which is called Kohn-Sham orbital. In the case of a non spin polarized system, each orbital contains two electrons.

This method considers a system of  $N$  non-interacting electrons with an effective potential instead of a system of interacting electrons with an external potential. Then, the exact kinetic energy of a non-interacting system can be written as

$$T_{KS}[n(\mathbf{r})] = -\frac{1}{2} \sum_{i=1}^N \langle \Phi_i | \nabla^2 | \Phi_i \rangle. \quad (2.21)$$



Therefore, the universal density functional in Eq. (2.19) can be separated as follows

$$F_{KS}[n(\mathbf{r})] = T_{KS}[n(\mathbf{r})] + E_H[n(\mathbf{r})] + E_{XC}[n(\mathbf{r})]. \quad (2.22)$$

Kohn-Sham kinetic energy, Hartree energy, and so-called exchange-correlation energy ( $V_{XC}[n(\mathbf{r})]$ ) contribute to  $F_{KS}[n(\mathbf{r})]$ . By comparing the KS and HK functional, Eqs. (2.22) and (2.18) respectively,  $V_{XC}[n(\mathbf{r})]$  is derived as follows

$$V_{XC}[n(\mathbf{r})] = T_e[n(\mathbf{r})] - T_{KS}[n(\mathbf{r})] + V_{ee}[n(\mathbf{r})] - V_H[n(\mathbf{r})]. \quad (2.23)$$

Now the Kohn-Sham Hamiltonian can be formulated as

$$H_{KS} = -\frac{1}{2}\nabla^2 + V_{KS} \quad (2.24)$$

where non-interacting electrons move in the effective potential  $V_{KS}$  which is given by

$$V_{KS} = -\sum_I \frac{Z_I}{|\mathbf{r}_i - \mathbf{R}_I|} + \int \frac{n(\mathbf{r}')d\mathbf{r}'}{|\mathbf{r} - \mathbf{r}'|} + \frac{\delta E_{XC}[n(\mathbf{r})]}{\delta n(\mathbf{r})} = V_{ext} + V_H + V_{XC}. \quad (2.25)$$

Using  $V_{KS}$  and  $H_{KS}$  the Kohn-Sham equation is given by

$$\left(-\frac{1}{2}\nabla^2 + V_{ext} + \int \frac{n(\mathbf{r}')d\mathbf{r}'}{|\mathbf{r} - \mathbf{r}'|} + \frac{\delta E_{XC}[n(\mathbf{r})]}{\delta n(\mathbf{r})}\right)\Phi_i(\mathbf{r}) = \epsilon_i\Phi_i(\mathbf{r}). \quad (2.26)$$

The wave function of the  $i^{th}$  electron depends on the wave functions of all other electrons, so this equation has to be solved self-consistently.

### 2.6.3 The exchange-correlation energy

#### Local density approximation (LDA)

LDA is a simple approximation to the exchange-correlation (XC) energy. In this approximation it is assumed that the local XC energy per particle depends on the local density, and is equal to the XC energy per particle of a homogeneous electron gas in a neutralizing positive background in which the homogeneous electron gas has the same density as the system. Thus, XC energy is written as the sum of each contribution of each point and is formulated in the following form

$$E_{XC}^{LDA}[n] = \int n(\mathbf{r})\epsilon_{XC}(n(\mathbf{r}))d\mathbf{r} \quad (2.27)$$

where  $\epsilon_{XC}(n(\mathbf{r}))$  is the XC energy per particle of the homogeneous electron gas of density  $n(\mathbf{r})$ . The quantity  $\epsilon_{XC}(n(\mathbf{r}))$  can be linearly split into exchange and correlation contributions

$$\epsilon_{XC}(n(\mathbf{r})) = \epsilon_X(n(\mathbf{r})) + \epsilon_C(n(\mathbf{r})) \quad (2.28)$$

where the exchange part  $\epsilon_X$  represents the exchange energy of an electron in a homogeneous electron gas of a particular density and is given by [46,47]

$$\epsilon_X = -\frac{3}{4} \left( \frac{3n(\mathbf{r})}{\pi} \right)^{1/3}. \quad (2.29)$$

There is no analytic expression for the correlation energy of the homogeneous electron gas except in the high and low density limits corresponding to infinitely weak and infinitely strong correlations. Therefore, various approaches using different analytic forms for  $\epsilon_C$  have generated several approximations for the correlation functional. One of the most used correlation energy functionals was proposed by Ceperly and Alder in 1980. They used quantum Monte-Carlo simulations for the homogeneous electron gas to find a numerical solution of  $\epsilon_C$  [48].  $\epsilon_C$  was parameterized differently by Perdew and Wang in 1992 [49]. As the LDA approximation considers a local dependence of the energy on the density, it leads to an almost correct estimation of properties for the systems with slowly varying densities [45]. However, this method usually underestimates bond lengths and overestimates binding energy [50]. Band gap underestimation by this approximation makes it inadequate for some applications.

### The generalized gradient approximation (GGA)

For systems for which the density varies in space, LDA should be improved to include the nonlocal dependence of the energy on the charge density. The natural improvement of the LDA approximation can be achieved by including the rate of change in the density functional. This approach was realized in the generalized gradient approximation (GGA) by Perdew and Wang [49]. The GGA is the approach that locally accounts for the inhomogeneity of the true electron density and expresses the XC energy as a functional of the density and its gradient,  $\nabla n(\mathbf{r})$ , as follows

$$E_{XC}^{GGA}[n] = \int n(\mathbf{r}) \epsilon_{XC}(n(\mathbf{r}), \nabla n(\mathbf{r})) d\mathbf{r} \quad (2.30)$$

whereas  $\epsilon_{XC}$  in the LDA is derived from the electron gas, there is no unique choice for it in the GGA. Over the years, a large number of GGA functionals have been proposed which are used in different calculations. Some GGA functionals are free of empirical parameters and start from physical principles, e.g. the Perdew-Burke-Ernzerhof (PBE) functional [51]. Also, there are other GGA functionals which use parameters that are fitted to experimental data, such as Becke exchange [52], and Lee-Yang-Parr (LYP) correlation [53] (BLYP). We used the PBE throughout this work. Our main reason to use this functional is that among the most frequently used GGA functionals, the PBE functional yields the most accurate and reliable results in most calculations [54,55]. A second reason is to stay consistent with the treatment of  $\epsilon_{XC}$  in the application of the hybrid functional

(HSE) [56, 57] calculations. (see also Section (2.6.4))

Although there is a good agreement between the predicted structural properties using LDA or GGA and experiment, some discrepancies can be observed for some systems. We recall some of them here:

- systematic underestimation of the band gap of semiconductors and insulators typically by 50% [58] This underestimation wrongly predicts some materials such as paramagnetic NiO and MnO to be metallic [59].
- disagreement with experiment in predicting the position of f-states, e.g. for Ce [60].
- discrepancy between calculated and experimental optical spectra, e.g. dielectric function of CIS [61, 62].

These discrepancies mostly originate from the underestimation of exchange and correlation effects in LDA and GGA, and the self-interaction error inherent to these approximations. The self-interaction error arises from a spurious interaction of an electron with itself.

### 2.6.4 The hybrid functional approximation

The hybrid functional method partly corrects the self-interaction error by mixing a fixed amount of the HF exchange to the GGA functional. This method gives better agreement with the experiment than GGA and LDA for some properties such as band gap and dielectric function. Heyd, Scuseria and Ernzerhof proposed a hybrid functional termed as HSE06 functional [56, 63].

The exchange energy used in HSE06 consists of short-range (SR) and long-range (LR) terms. In the short range term the HF exchange is mixed with PBE exchange, but in order to avoid the expensive calculations in the long-range term HF exchange is replaced by PBE exchange. The following equation shows all considered contributions in HSE06

$$E_{XC}^{HSE} = \alpha E_X^{HF,SR}(\omega) + (1 - \alpha) E_X^{PBE,SR}(\omega) + E_X^{PBE,LR}(\omega) + E_C^{PBE} \quad (2.31)$$

where  $\omega$  is the parameter that defines the range separation and indicates a distance for which the short range term can be neglected and which varies between 0.05 and 0.35 Å<sup>-1</sup>. The parameter  $\alpha$  represents the mixing of HF exchange energy. It is shown that 25% of HF exchange ( $\alpha = \frac{1}{4}$ ) leads to excellent results for many properties like the lattice parameters, bulk moduli, heats of formation, binding energies and band gaps for semiconductors and insulators [64]. Furthermore, HSE gives better optical spectra compared to GGA and LDA [61, 62]. Since there are adjustable parameters  $\omega$  and  $\alpha$  in the HSE06 approach, this cannot be treated as an ab initio method and one can adjust these two parameters to get the experiment band gap. For example, ZnO requires 37.5% of  $E_X^{HF,SR}$  to produce the experiment band gap [65].

## 2.7 Band structure calculations

Although the Kohn-Sham equations can be solved self-consistently to calculate the energy of the many-body system, solving this equation for a real crystalline solid with  $10^{24}$  electrons and ions per  $cm^{-3}$  from the point of view of computational cost is impossible. By benefitting from the periodicity of the crystalline structure of the solids, one has to solve the Kohn-Sham equations only for the electrons in the unit cell to calculate the eigenvalues of the considered solid.

### 2.7.1 The Bloch theorem

Periodic systems such as bulk crystals are defined by the atomic position within the unit cell and the lattice vectors  $\mathbf{T}_i$ ,  $i \in 1, 2, 3$ , to span the unit cell by periodicity. In such a system, the effective single electron potential has the periodicity of the lattice

$$V_{eff}(\mathbf{r}) = V_{eff}(\mathbf{r} + \mathbf{T}) \quad (2.32)$$

where  $\mathbf{T} = n_1\mathbf{T}_1 + n_2\mathbf{T}_2 + n_3\mathbf{T}_3$  is the lattice vector. The periodicity of the effective potential results in the same periodicity of the electron density. Therefore, the single electron states satisfy the equation

$$|\Phi_i(\mathbf{r} + \mathbf{T})|^2 = |\Phi_i(\mathbf{r})|^2. \quad (2.33)$$

The periodicity of the eigenstates is known as Bloch's theorem. According to the Bloch's theorem, the eigenstates of a one-electron Hamiltonian can be expressed as the product of a plane wave and a periodic function as follows

$$\Phi_{n\mathbf{k}}(\mathbf{r}) = e^{i\mathbf{k}\cdot\mathbf{r}} u_{n\mathbf{k}}(\mathbf{r}) \quad (2.34)$$

where the periodic function has the periodicity of the lattice and can be expanded in terms of plane waves as follows

$$u_{n\mathbf{k}}(\mathbf{r}) = \sum_{\mathbf{G}} c_{n\mathbf{k},\mathbf{G}} e^{i\mathbf{G}\cdot\mathbf{r}} \quad (2.35)$$

where  $\mathbf{k}$  is the wave vector which can be chosen in the first Brillouin zone.  $\mathbf{G}$  can be any vector of the reciprocal lattice.

Then by applying Eq. (2.35) to Eq. (2.34), the KS wave functions are expanded in terms of an infinite plane wave basis set

$$\Phi_{n\mathbf{k}}(\mathbf{r}) = \sum_{\mathbf{G}} c_{n\mathbf{k},\mathbf{G}} e^{i(\mathbf{k}+\mathbf{G})\cdot\mathbf{r}}. \quad (2.36)$$

One can restrict the number of the plane waves by applying an upper limit to the kinetic energy of the plane waves ( $\frac{|\mathbf{k} + \mathbf{G}|^2}{2}$ ). This limit is called the energy cut-off ( $E_{cut}$ ) and is given by

$$E_{cut} > \frac{|\mathbf{k} + \mathbf{G}|^2}{2}. \quad (2.37)$$

Because of the translational symmetry for a given  $\mathbf{k}$ , the KS equations give an eigenstate for each band labeled by  $n$ . As long as the KS potential has the periodicity of the lattice  $V(\mathbf{r}) = V(\mathbf{r} + \mathbf{T})$ , the energy eigenvalues are periodic in reciprocal space:

$$\epsilon_n(\mathbf{k}) = \epsilon_n(\mathbf{k} + \mathbf{G}). \quad (2.38)$$

Properties like band energy, electron density can be calculated by an integration over the first Brillouin zone. This integration is given by

$$\int_{\Omega_{BZ}} \Theta(\epsilon_{n\mathbf{k}} - \epsilon_F) d\mathbf{k} \quad (2.39)$$

where  $\Omega_{BZ}$  is the volume of the first Brillouin zone,  $\epsilon_F$  is the Fermi energy, and  $\epsilon_{n\mathbf{k}}$  is the energy of band  $n$  at  $\mathbf{k}$ -point  $\mathbf{k}$ .  $\Theta(\epsilon_{n\mathbf{k}} - \epsilon_F)$  is the step function which gives 1 for occupied bands and zero for unoccupied bands. Although for insulator and semiconductors, this function gives good results, some improvements in the integration method (e.g. tetrahedron method) can be made to give better results.

As there are some partially occupied bands in metals, a smooth function should be used to give the correct position of the Fermi level. For such materials, some alternative solutions to the step function can be used, e.g. Fermi-Dirac function, the Methfessel-Paxton method, and the Gaussian method.

Since the wave functions of nearby  $\mathbf{k}$ -points are almost identical, one needs to sample the first Brillouin zone only for a discrete number of  $\mathbf{k}$ -points. This sampling can be performed by using different schemes. The most used sampling method is the Monkhorst-Pack (MP) scheme which is also used in this thesis [66].

### 2.7.2 Methods to calculate the electronic structure of solids

In order to calculate the electronic band structure within the DFT formalism, the KS equations have to be solved. The very different behaviour of the wave function at different distances from the nuclei is an important issue. The electronic wave functions are eigenstates of the Kohn-Sham Hamiltonian, and therefore mutually orthogonal. Since the core states are localized around the nuclei, the valence states should oscillate rapidly in the core region to maintain the orthogonality. As a result, one needs to use a very large basis set, or a very fine mesh to describe the valence states accurately. On the other hand, the core electrons are very localized, and only the valence electrons contribute to the chemical behaviour. Then, it is numerically beneficial to treat core and valence electrons in a different way. One of such approaches is the pseudopotential method in which nuclei and core electrons are described by an effective and smooth potential which can reproduce

the correct effect on the valence electrons. By using the pseudopotential method the Kohn-Sham equations have to be solved only for the valence electrons which reduces the computational effort.

By using the pseudopotential method all information about the all-electron wave functions close to the nuclei is lost, making it hard to compute properties that rely on the core region like electric field gradients, and hyperfine parameters.

Another approach is provided by all-electron methods. The full information about the wave function can be derived by using these methods. One of these methods is Augmented-Plane-Wave (APW) [67]. In this method, the space is partitioned into two regions; a spherical region around each atom where the wave function is expanded into a local basis set in order to reproduce the variations, and an interstitial region where another basis set is chosen and connected to the first local basis set. Blöchl in 1994 proposed the Projector-Augmented-Wave method (PAW) as an extension of both augmented-wave and pseudopotential methods [68].

### 2.7.3 Projected augmented wave method

In this approach, the all-electron wave function can be derived by applying the linear transformation operator on the pseudo-wave function

$$|\Psi_n\rangle = \hat{T}|\tilde{\Psi}_n\rangle. \quad (2.40)$$

The transformation operator is given by

$$\hat{T} = 1 + \sum_i (|\Phi_i\rangle - |\tilde{\Phi}_i\rangle)\langle\tilde{p}_i|. \quad (2.41)$$

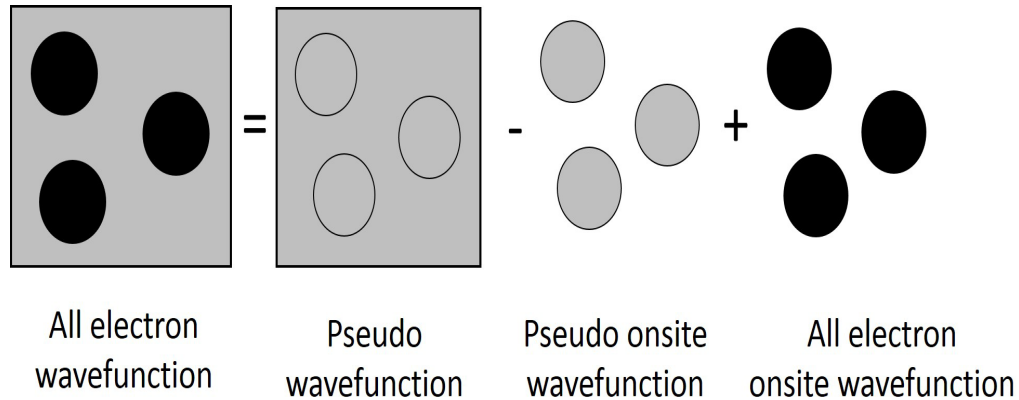


Figure 2.1: Schematic representation of PAW wave functions [69].

Then, the all-electron wave function is given by

$$|\Psi_n\rangle = |\tilde{\Psi}_n\rangle + \sum_i (|\Phi_i\rangle - |\tilde{\Phi}_i\rangle) \langle \tilde{p}_i | \tilde{\Psi}_n \rangle \quad (2.42)$$

where  $|\Phi_i\rangle$  and  $|\tilde{\Phi}_i\rangle$  are the all-electron and pseudo atomic orbitals, respectively. These two functions are equal outside the augmentation spheres where the projector function  $\tilde{p}_i$  is zero ( $\tilde{p}_i = 0$  for  $r > r_c$ ) because of the localization inside the augmentation spheres. The augmentation spheres ( $r < r_c$ ) are constructed around each atom. Figure 2.1 schematically represents the construction of PAW wave functions.

In Eq. (2.40),  $n$  is the band index and refers to the valence states. It is possible to calculate the eigenstates of all electrons or deal with the valence and core electrons separately. In other words, the all-electron atomic orbitals  $|\Phi_i\rangle$  can be obtained as solutions to the radial scalar relativistic Schrödinger equation for the spherical non-spin polarized atom

$$\left(-\frac{1}{2}\nabla^2 + V_{eff}\right)|\Phi_i\rangle = \epsilon_i|\Phi_i\rangle. \quad (2.43)$$

On the other hand the pseudo-atomic orbitals  $|\tilde{\Phi}_i\rangle$  obeys

$$\left(-\frac{1}{2}\nabla^2 + \tilde{V}_{eff}\right)|\tilde{\Phi}_i\rangle = \epsilon_i|\tilde{\Phi}_i\rangle \quad (2.44)$$

where  $\tilde{V}_{eff}$  is the spherical component of the effective pseudopotential, which can be chosen arbitrarily inside the augmentation sphere ( $r < r_c$ ) but must match  $V_{eff}$  for  $r > r_c$ .  $V_{eff}$  is the spherical component of the effective all electron potential. All calculations in this thesis are performed using the PAW approach which is implemented in a plane wave DFT code, the Vienna ab initio simulation package (VASP) developed by Kresse et al. [70]





# Optoelectronic properties of Al-doped MgO

## 3.1 Introduction

Understanding the response of a material to electromagnetic radiation and particularly to visible light is important for several applications. The knowledge about material's response to light is essential for predicting and even altering its optical properties. One can step further and benefit from such knowledge to design new materials with a particular optical behaviour for specific applications.

The interaction between light and materials can be studied through various optical techniques, e.g. absorption, transmission, reflection, scattering, or emission. The important point is that they are all frequency (i.e. energy) dependent. This dependence on the energy is related to the band structure of the material. In other words, information on energy eigenvalues and eigenfunctions is needed to calculate the energy dependent optical properties.

Light of sufficient energy excites electrons. A quantitative study of these transitions provides insight into the position of the initial and the final energy bands and the symmetry of their associated wave functions. The dielectric function which strongly depends on frequency and wave vector, provides significant features of the physical properties of solids. On the one hand, it describes the collective excitations of free carriers such as the volume plasmons. On the other hand, it explains the electron-electron, electron-lattice, and electron-impurity interactions in the crystal. It means that this quantity of solids provides an important tool for studying the energy band structure, and impurity energy levels of solids.

Moreover, from optical measurements, the dielectric function can be derived. As mentioned above,

---

The results of this chapter were published as: N. Sarmadian, R. Saniz, D. Lamoen, and B. Partoens, Physical Review B 86, 205129 (2012).

this quantity is directly related to the band structure and can therefore be obtained from ab-initio methods. We start to study the optical properties of solids in this thesis by calculating the dielectric function of Al-doped MgO.

Because of their very rich phenomenology [71], transition metal oxides, either stoichiometric or doped, are the subject of extensive research efforts worldwide and play a central role in present day technology. A simple compound such as MgO (magnesia), for example, was long used for its optical properties (being famously commercialized by Eastman-Kodak under the name Irtran-5) [72], and is currently a key element of plasma display devices because of its large secondary electron emission coefficient and its simultaneous role as an insulating layer [73]. Doped MgO has also attracted interest in different respects. Indeed, *p*-type doping has been investigated in Li-doped MgO [74], as well as magnetism in N-doped MgO [75], and cathodoluminescence in Cr-doped MgO [76], to name a few examples. Very recently, there has been theoretical and experimental interest in Al-doped MgO [77–80]. In these works, a magnetron sputtering technique was used to grow Al-doped MgO thin films, with Al substituting Mg, for a wide range of Al concentrations. An interesting finding is that both molecular dynamics simulations and experiment indicate that crystallinity is retained up to around 40 to 50% Al doping (depending on the substrate), beyond which level the system becomes amorphous [77, 79]. Measured properties such as hardness, refractive index, and other, were observed to vary correspondingly [78]. For a more complete characterization of experimentally grown films and for a better understanding of their properties, theoretical studies are of great assistance.

This chapter gives an overview to the concept of dielectric function as a tool to study the energy band structure deeply. Also the formalism used in this thesis to calculate this quantity and other optical properties calculated in the present work is explained. Then, the structural, electronic, and optical properties of Al-doped MgO calculated using DFT are explicitly discussed. The concentrations considered range from 6% to 56%. The qualitative changes in the electronic properties of the crystalline phases with Al concentration is discussed. Moreover, in the latter case of Al concentration, we also compare the optical properties of the amorphous and crystalline phases to shed light on how the crystalline to amorphous transition with Al doping level can be characterized.

## 3.2 Optical properties within linear response

As DFT maps the static Schrödinger equation onto a one-electron problem (cf. Section 2.2), the time dependent density functional theory (TDDFT) does the same for the time dependent Schrödinger equation

$$i\frac{\partial\Psi(t)}{\partial t} = H'\Psi(t) \quad (3.1)$$

where the time dependent Hamiltonian ( $H'$ ) defines the time-dependent many-body problem as the problem of interacting electrons moving in a time dependent effective potential  $v_{eff}$

$$H' = -\frac{\hbar^2}{2m}\nabla^2 + v_{eff}[n(\mathbf{r}, t)]. \quad (3.2)$$

The effective potential consists of an external potential caused by an external electric field, the Hartree potential, and the exchange-correlation potential:

$$v_{eff}[n(\mathbf{r}, t)] = v_{ext}[n(\mathbf{r}, t)] + v_H[n(\mathbf{r}, t)] + v_{xc}[n(\mathbf{r}, t)]. \quad (3.3)$$

The Runge-Gross theorem [81] is the basis of TDDFT just as the Hohenberg-Kohn theorems form the basis of DFT [42]. This theorem states that for a given initial state, a one-to-one correspondence exists between the time dependent charge density  $n(\mathbf{r}, t)$  and the time dependent external potential  $v_{ext}(\mathbf{r}, t)$ .

In spectroscopic experiments the external electric field is weaker than the internal electric field caused by the interaction between ions. This regime is known as linear response i.e. the external field applied on the material can be considered as a perturbation. In that case, perturbation theory can be used in first order to calculate the time dependent wave function and then the time dependent charge density.

The key quantity is the response function to the electric field. The response function ( $\chi$ ) of the interacting system which describes the response of the system to the external potential is given by

$$\chi(\mathbf{r}, \mathbf{r}', \omega) = \frac{\delta n(\mathbf{r}, \omega)}{\delta v_{ext}(\mathbf{r}', \omega)} \quad (3.4)$$

where the response function is written in frequency space ( $\omega$ ). The response function, charge density, and potential are interrelated and they are not known for a general system. A simplification can be made by replacing the total response function of the interacting system to the external potential with the KS response function ( $\chi^{KS}$ ) of the non-interacting system to the effective potential ( $v_{eff}$ ). In other words, the relation between  $\chi$  and  $v_{ext}$  is the same as the relation between  $\chi^{KS}$  and  $v_{eff}$ . The requirement for this link is that the change of the density is the same in both descriptions.

$$\chi^{KS}(\mathbf{r}, \mathbf{r}', \omega) = \frac{\delta n(\mathbf{r}, \omega)}{\delta v_{eff}(\mathbf{r}', \omega)}. \quad (3.5)$$

Now an approximation should be applied to calculate the KS response function. The simplest approximation is the random phase approximation (RPA) which neglects the effect of the external field (i.e. perturbation) on  $v_{XC}$  [82] and the effect of the exchange-correlation potential is only partially included.

The matrix of the dielectric function couples the total electric field applied on a material to the external electric field  $\mathbf{E}_{ext}$

$$\mathbf{E}_{tot} = \varepsilon^{-1} \mathbf{E}_{ext}. \quad (3.6)$$

The electric field can be expressed as a composition of longitudinal and transverse components ( $E_L$ , and  $E_T$ ) which are parallel and perpendicular to the wave vector  $\mathbf{q}$ , respectively. For

slowly varying fields (long wave length regime,  $\mathbf{q} \rightarrow 0$ ) both longitudinal and transverse dielectric functions become equal [83]. Moreover, it is stated by Gajdoš et al. that the longitudinal dielectric function is more accurate than the transverse one for the PAW method [84]. In this thesis we use the PAW method implemented in the VASP code, thus we calculate the longitudinal dielectric function in the long wave length regime.

Slowly varying electric fields only result from slowly moving charges. Such electric fields can be described by  $\mathbf{E} = -\nabla v$ . The relation between the potential ( $v$ ) and the charge density of the system is given by the Poisson equation  $\nabla^2 v = -4\pi n$ . For such electric fields, the charge density and potential are related via  $\nu$  ( $v = \nu n$ ) where  $\nu$  is the Coulomb kernel in the reciprocal space ( $\nu = 4\pi e^2/q^2$ ). Moreover, the longitudinal electric field contributes to the Hamiltonian via  $v_{ext}$  and Eq. (3.6) can be rewritten as

$$v_{tot} = \epsilon^{-1} v_{ext} \quad (3.7)$$

where  $v_{tot} = v_{ext} + v_{ind}$  consists of the external and induced potential which is caused by the external and induced charge density ( $n_{ind} = \chi v_{ext}$ ), respectively. Therefore, the inverse of the dielectric function ( $\epsilon^{-1}$ ) can be expressed as

$$\epsilon^{-1} = \frac{v_{tot}}{v_{ext}} = \frac{v_{ext} + v_{ind}}{v_{ext}} = 1 + \nu \frac{n_{ind}}{v_{ext}} = 1 + \nu \chi. \quad (3.8)$$

According to Eq. (3.8), the dielectric function can be calculated if the response function is known. The  $3 \times 3$  dielectric function matrix consists of the real and imaginary parts  $\epsilon = \epsilon^r + i\epsilon^i$  where the imaginary component  $\epsilon^i$  is given by [84]

$$\epsilon_{\alpha\beta}^i(\omega) = \frac{4\pi^2 e^2}{\Omega} \lim_{q \rightarrow 0} \frac{1}{q^2} \sum_{c,v,\mathbf{k}} 2w_k \delta(\epsilon_{c\mathbf{k}} - \epsilon_{v\mathbf{k}} - \omega) \langle u_{c\mathbf{k}+\mathbf{e}_\alpha q} | u_{v\mathbf{k}} \rangle \langle u_{c\mathbf{k}+\mathbf{e}_\beta q} | u_{v\mathbf{k}} \rangle^* \quad (3.9)$$

where  $\Omega$  is the volume of the primitive cell,  $w_k$  is the  $\mathbf{k}$ -point weight, and  $u_{n\mathbf{k}}$  is the cell periodic part of the wave function. Vectors  $\mathbf{e}_\alpha$  are unit vectors for the three Cartesian directions.  $n$  in  $u_{n\mathbf{k}}$  refers to  $c$  and  $v$  in Eq. (3.9) which represents the conduction band and valence band, respectively. The factor 2 before the weights refers to the fact that we consider a spin degenerate system. Note that frequency ( $\omega$ ) has the dimension of an energy.

In metals, an electron can be excited from a state below the Fermi level to one above the Fermi level both belonging to the same band. Such transitions are called intraband transitions ( $c = v$  in Eq. (3.9)). In semiconductors and insulators the transitions occur between fully occupied bands ( $w_k = 1$ ) and empty bands ( $w_k = 0$ ). The energy difference between such two states ( $c \neq v$  in Eq. (3.9)) is given by  $\epsilon_{c\mathbf{k}} - \epsilon_{v\mathbf{k}}$ . This energy indicates the energy of the interband transition. Moreover, the probability of each transition is calculated by  $\langle u_{c\mathbf{k}+\mathbf{e}_\alpha q} | u_{v\mathbf{k}} \rangle \langle u_{c\mathbf{k}+\mathbf{e}_\beta q} | u_{v\mathbf{k}} \rangle^*$ . A transition with high probability is reflected as a peak with high intensity in the spectrum.

The real part of the dielectric function  $\epsilon^r(\omega)$  is obtained by the Kramers-Kronig transformation [85]

$$\varepsilon_{\alpha\beta}^r(\omega) = 1 + \frac{2}{\pi} P \int_0^\infty \frac{\varepsilon_{\alpha\beta}^i(\omega') \omega'}{\omega'^2 - \omega^2} d\omega' \quad (3.10)$$

where  $P$  denotes the principle value.

When we calculate the real part and imaginary part of the dielectric function, other optical properties such as energy reflectivity ( $R(\omega)$ ), power loss ( $L(\omega)$ ), refractive index ( $n$ ), extinction coefficient ( $k$ ), and absorption coefficient ( $\alpha$ ) can be derived using the following formulas

$$L(\omega) = -Im(\varepsilon^{-1}) = \frac{\varepsilon^i(\omega)}{\varepsilon^{r^2}(\omega) + \varepsilon^{i^2}(\omega)} \quad (3.11)$$

$$R(\omega) = \left| \frac{\sqrt{\varepsilon^i(\omega)} - 1}{\sqrt{\varepsilon^i(\omega)} + 1} \right|^2 \quad (3.12)$$

$$n = \sqrt{\frac{\sqrt{\varepsilon^{r^2} + \varepsilon^{i^2}} + \varepsilon^r}{2}} \quad (3.13)$$

$$k = \sqrt{\frac{\sqrt{\varepsilon^{r^2} + \varepsilon^{i^2}} - \varepsilon^r}{2}} \quad (3.14)$$

$$\alpha = \frac{2\omega k}{c} \quad (3.15)$$

where  $c$  is the speed of light.

The dielectric function is correlated with the band structure and density of states of the material, therefore electronic properties such as optical band gap, fundamental band gap, and plasma frequency can be deduced from dielectric function spectra. Figure 3.1(a) shows a schematic representation of the density of states of a semiconductor. Both localized and extended states are shown in this plot. Extended states refer to the continuous CB and VB that can be found in both crystalline and amorphous semiconductors. Localized states are mainly caused by impurities and are present in amorphous and doped semiconductors. Figure 3.1(b) represents a schematic plot of the optical spectra, dielectric function, power loss, and reflectivity. Three regions in the dielectric function spectra can be considered that correspond to possible optical transitions between different states of VB and CB. All three regions and the corresponding transitions are labeled consistently in Fig. 3.1.

Region 1 or Tauc region contains the optical transitions between extended states. This region is the high absorption region ( $\alpha > 10^4 \text{ cm}^{-1}$ ) and includes high intensity peaks of the dielectric function and significant opto-electronic properties that are correlated to the electronic structure of the material. The density of such extended states can be considered as a parabolic function of the energy. Tauc stated that for these states the product of the absorption coefficient and energy of photons is given by [87]

$$E\alpha = C(E - E_{\text{optical}})^n \quad (3.16)$$

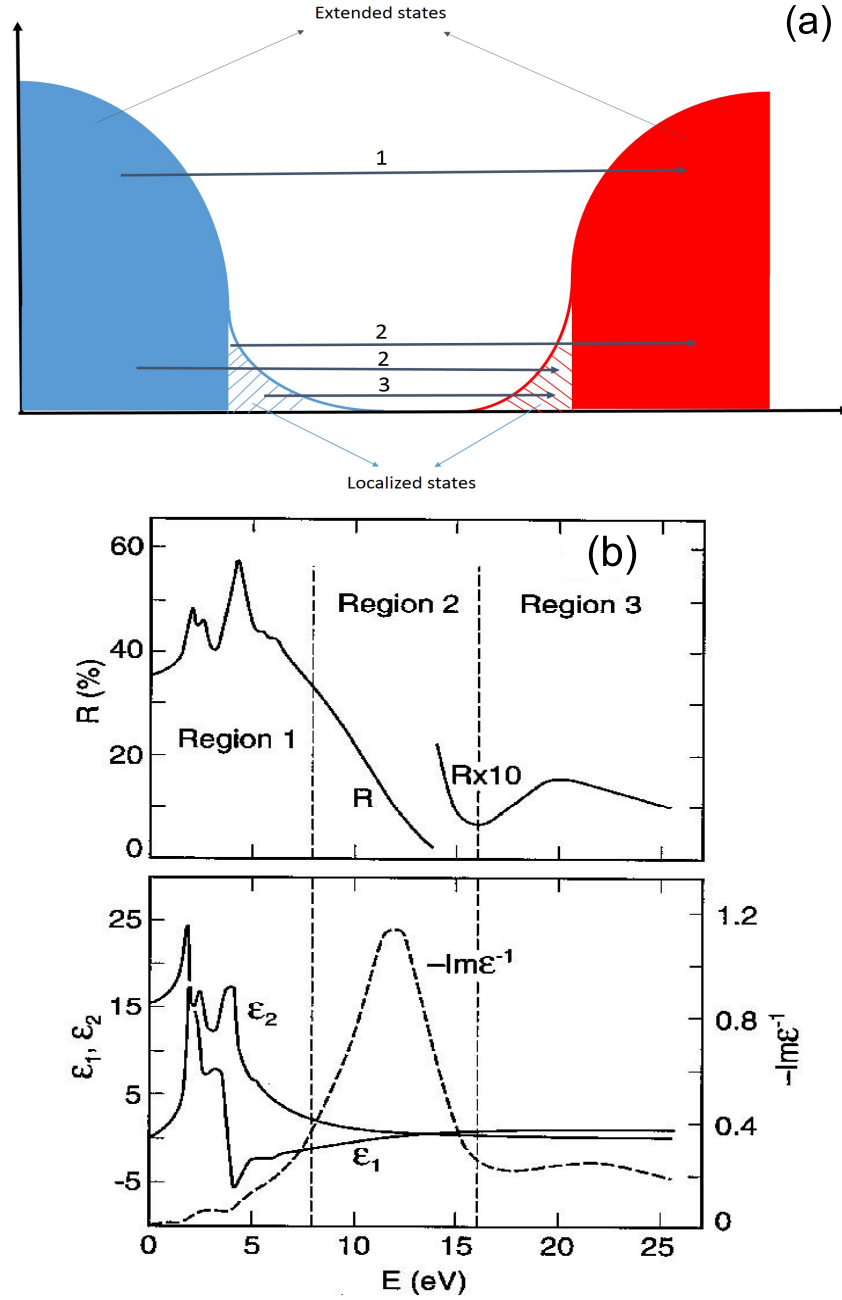


Figure 3.1: Schematic representation of (a) density of states, and (b) dielectric function and reflectivity of a semiconductor [86]. Note that  $\epsilon_1$ , and  $\epsilon_2$  in the figure corresponds to  $\epsilon^r$  and  $\epsilon^i$ , respectively.

where  $C$  is a constant,  $E$  is the absorption energy of photons, and  $n$  is 0.5 and 2 for direct and indirect band gap materials, respectively. The Tauc equation can be used to calculate the optical band gap ( $E_{\text{optical}}$ ) of a semiconductor. One plots  $(E\alpha)^n$  as a function of  $E$ , then extrapolating the linear regime in the plot to the abscissa yields the optical band gap. Moreover, as the optical band gap is the energy of the first allowed transition, then it corresponds to the first peak of the imaginary part of the dielectric function and the edge of the absorption coefficient spectrum.

In addition, the fundamental band gap appears as a shoulder next to the optical band gap peak and as expected it has a lower energy than the optical band gap. In the corresponding density of states, the fundamental band gap is indicated by the energy difference between the VBM and CBM which can occur at the same k-point in the direct band gap materials or at the different k-point in the indirect band gap materials.

The structure of region 2 or the Urbach region is mainly a result of the optical transitions from the localized states in the VB to the extended states in the CB and vice versa. The density of the localized states depends exponentially on the energy, and the absorption coefficient is given by the Urbach equation [88]

$$\alpha = C \exp\left(\frac{\hbar\omega}{E_U}\right) \quad (3.17)$$

where  $C$  is a constant, and  $E_U$  is the Urbach energy. This low absorption region ( $10^{-1} < \alpha < 10^4 \text{ cm}^{-1}$ ) shows a rapid decrease of the reflectivity due to the collective plasma oscillations of the valence electrons. In this region, valence electrons being unbound can perform collective oscillations. A sharp peak in the power loss ( $L(\omega)$ ) describes the energy loss of the valence electrons moving through the material. The change in the behaviour of a semiconductor from insulator-like to metal-like has been usually associated with the plasma frequency. This plasma frequency describes the high frequency plasma oscillations and is called valence-band-edge electrons plasma frequency. The sum rule for the dielectric function [89, 90] can be used to calculate this plasma frequency

$$\int_0^\infty d\omega \omega \varepsilon^i(\omega) = \frac{\pi}{2} \tilde{\omega}_p^2. \quad (3.18)$$

At this frequency,  $\varepsilon^i$  drops to zero and  $\varepsilon^r$  changes the sign from negative to positive.

One can also consider another plasma frequency which is called free carrier plasma frequency ( $\omega_p$ ) which falls in the low frequency region. This plasma frequency is already introduced in Sec. 1.2.1.

Region 3 is known as the weak absorption tail (WAT) where the optical transitions mainly occur between localized states in VB and CB. Such transitions are weak because of the transition matrix elements are integrals over all space and over the products of two functions (initial and final states) which are separated in space and exhibit no overlap for localized states. In this region  $\alpha < 10^{-1} \text{ cm}^{-1}$  and the rise of the reflectivity is a good indicator of this region.

### 3.3 Computational Method

We perform first-principles calculations using DFT [42, 45] as implemented in the VASP code [70, 91]. We use LDA with the Ceperley-Alder parametrization [48] and PAW potentials [68, 92]. The Mg  $2p$   $3s$ , O  $2s$   $2p$ , and Al  $3s$   $2p$  orbitals are treated as valence. An energy cutoff of 450 eV is used for the plane-wave basis set. For structure relaxation and total energy calculations the Brillouin Zone is sampled using a  $3 \times 3 \times 3$  MP grid [66].

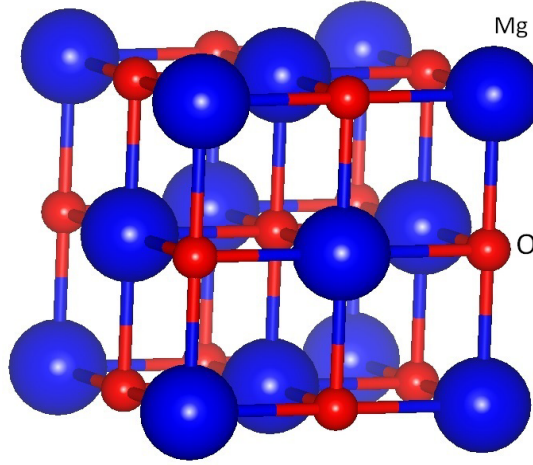


Figure 3.2: Crystal structure of MgO-Rocksalt (space group  $Fm\bar{3}m$ , No. 225).

We study different doping concentrations of Al in MgO. MgO is an ionic solid that crystallizes in the rocksalt structure. The rocksalt primitive cell (space group  $Fm\bar{3}m$ , No. 225) contains 2 atoms, one Mg and one O atom. The Mg atom occupies 4a Wyckoff position (site symmetry  $O_h$ ), and the O atom sits on 4b (site symmetry  $O_h$ ). In this structure, there is an ionic bond between Mg and O atom. The length of this bond is 2.08 Å, calculated with PBE functional. The conventional unit cell of the rocksalt crystal structure of MgO is shown in Fig. 3.2. The conventional cubic unit cell contains 4 formula units of MgO.

We study the doping of Al using a 64-atom conventional cubic cell of MgO. To keep the cation-anion charge balance, doping obeys to  $Mg_{1-3x/2}Al_xO$ . Thus, for every two Al atoms introduced, there is one Mg vacancy with respect to the original rocksalt structure. For each Al concentration,  $x$ , we consider three different possible (not exhaustive) configurations. The Al atom distribution was uniform, but random. As an example we present the atomic geometries of three considered configurations for the case of 6% Al doped MgO in Fig. 3.3.



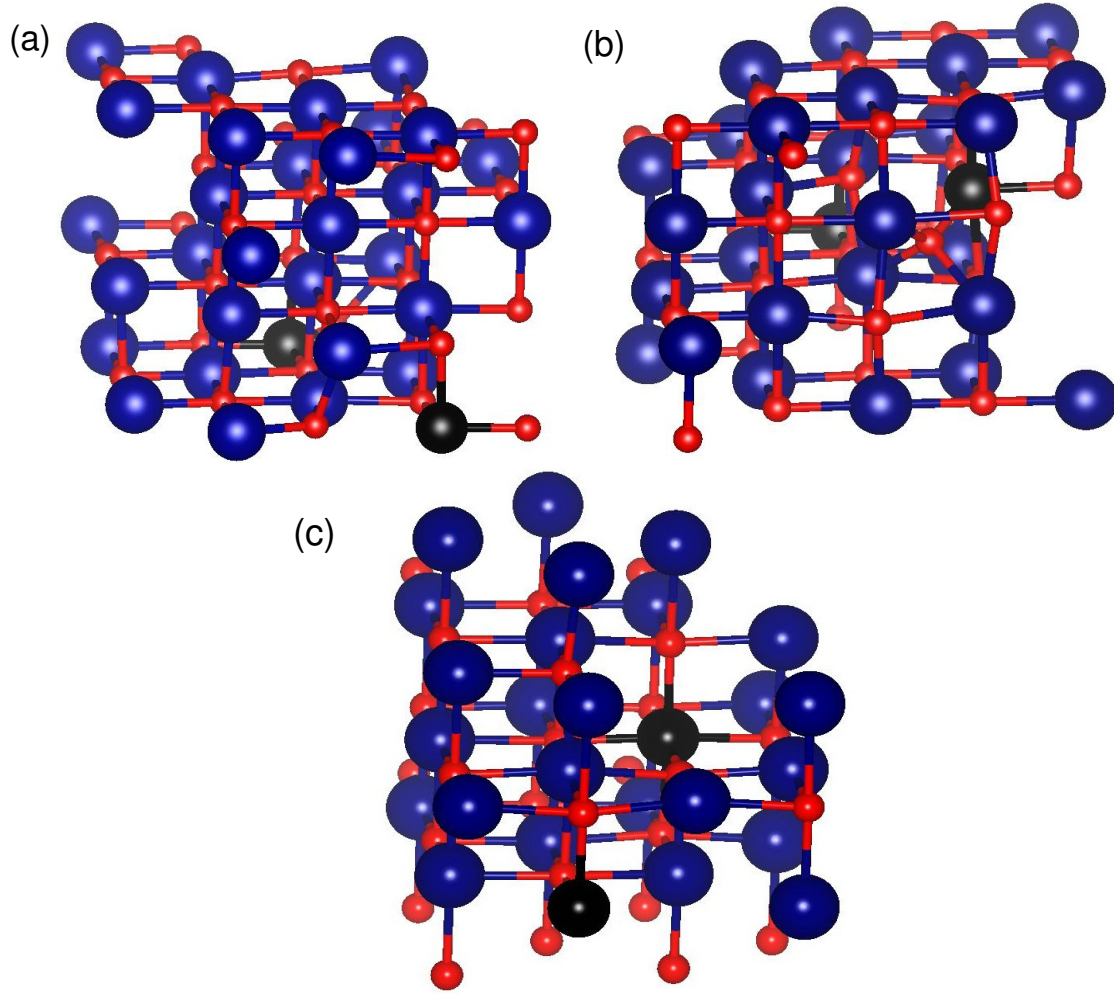


Figure 3.3: Atomic geometries of three considered configurations for the case of 6% Al doped MgO.

In all cases, the calculations are made at the equilibrium lattice constants. Atomic relaxations are made until residual forces on the atoms are less than  $0.01 \text{ eV/\AA}$  and total energies are converged within 1 meV. For each doping concentration, we average the dielectric function over all considered configurations. The results are also averaged with respect to the direction of polarization. We found that it is enough to sample the Brillouin zone using a  $6 \times 6 \times 6$  MP grid for our supercell to obtain a converged  $\epsilon(\omega)$  matrix. We increase the number of bands up to 320 in order to guarantee a converged dielectric function in the 0–45 eV energy range.

## 3.4 Results and discussion

### 3.4.1 Crystalline structures

We model first crystalline structures, and study the lattice parameters dependence on Al concentration. Here the concentration is given by ratio of the number of Al atoms over the number of Al plus Mg atoms in the supercell. The Al concentrations considered are 6%, 13%, 21%, 29%, 37%, and 56%.

Figure 3.4(a) shows the dependence of the supercell primitive vector lengths ( $a$ ,  $b$  and  $c$ ) on Al concentration. This dependence is shown for three different possible configurations considered, for each Al content level. The solid lines indicate the averages over the three configurations. These can be expected to be closer to what is found in experiment. Figure 3.4(b) shows a similar plot for the angles ( $\alpha$ ,  $\beta$  and  $\gamma$ ) between the supercell primitive vectors. As one can see in the figures, the averages indicate that the crystal structure remains approximately cubic up to an Al content of 30 to 37%. Above that value, there is a very clear departure from a cubic structure. This is interesting, because in experiment there is a transition from the crystalline to an amorphous phase for an Al concentration between 40 and 50% (depending on whether the films are deposited on an amorphous or crystalline substrate) [77, 79].

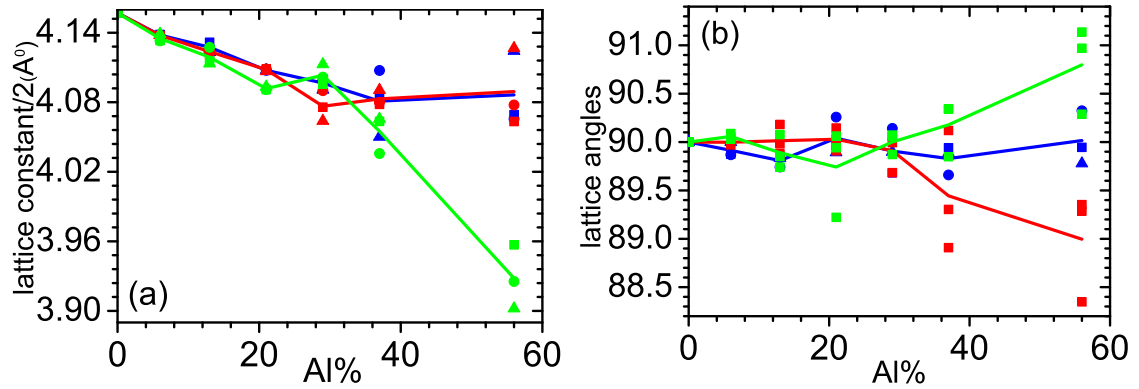


Figure 3.4: Lattice constants (a) and angles between the lattice vectors (b) as a function of Al concentration. The blue, red and green colors correspond to the lattice constants  $a$ ,  $b$  and  $c$  in (a) and the angles  $\alpha$ ,  $\beta$  and  $\gamma$  in (b). For every concentration, three configurations are considered. The lines correspond to the average value.

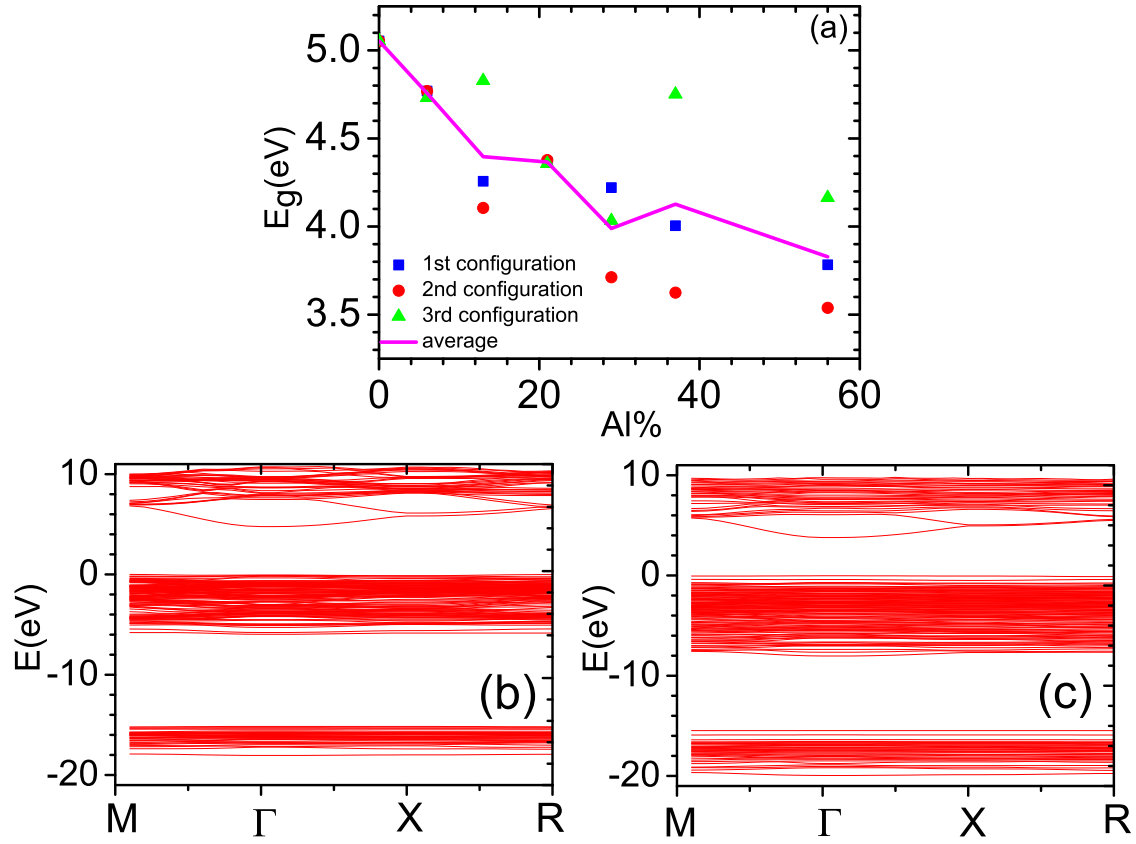


Figure 3.5: (a) Band gap dependence on the Al concentration. (b) Band structure for 6% Al-doped MgO, and similar in (c) for 56% Al-doped MgO. There is a notable increase in band widths at higher doping level.

We think that both the above observations are related to an increasing instability of the rocksalt structure with increasing Al concentration. In this respect, we note the following. First, the x-ray diffraction measurements in Ref. [79] indicate a crystallinity fraction with respect to the rocksalt structure (space group  $Fm\bar{3}m$ ) that decreases with Al concentration. Second, the molecular dynamics calculated radial distribution functions for the different bonds are not completely consistent with the MgO crystal structure, with the Al-O radial distribution function deviating from it [77].

The thermodynamic ground state of the doped system is expected to present phase segregation into MgO and  $MgAl_2O_4$ . However, according to Saraiva and co-workers the experimental structures are kinetically determined, and not thermodynamically, because of a too low adatom mobility during deposition [79]. Kinetic barriers also trap our ab initio structures in local energy minima, away from the thermodynamic ground state. Hence, we can expect the theoretical structures to be

reasonably close to the experimental ones. Thus, in Fig. 3.4 one can see that the average lattice constant (average of the three primitive vector lengths) decreases approximately linearly with increasing Al content. This is in agreement with experiment, where it is concluded that the lattice parameter dependence on Al concentration follows Vegard's law [79]. This can be understood as due to the smaller Al radius compared to Mg and to the increasing number of vacancies in the supercells with increasing Al content.

We turn now to the dependence of the electronic properties on the Al doping level. We found that the system is insulating for all the doping concentrations considered.

In Fig. 3.5(a) we show the band gap as a function of Al concentration. The different configurations can show very different gaps, but in films that are several hundred nm to 1  $\mu\text{m}$  thick, only an average can be observed experimentally.

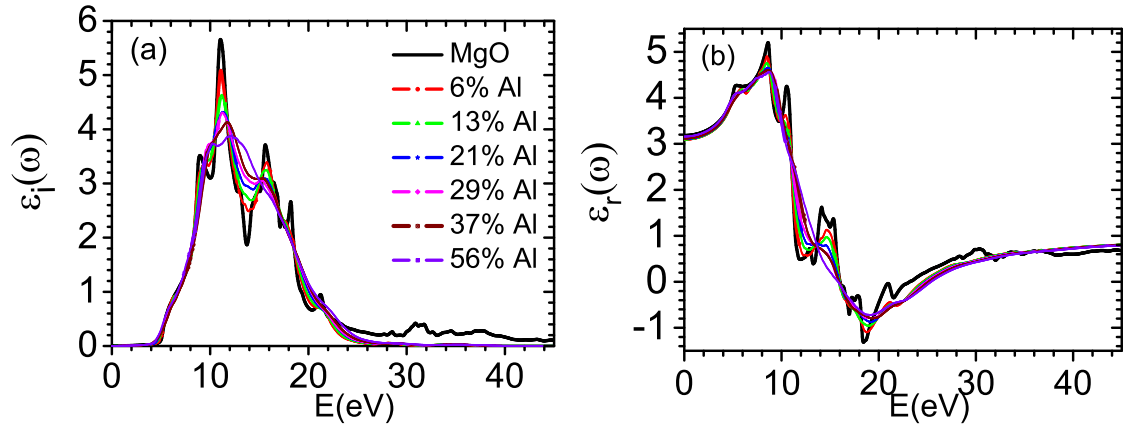


Figure 3.6: Influence of Al concentration on (a) imaginary part and (b) real part, of the dielectric function of Al-doped MgO.

The average over the different configurations considered here is given by the solid line. The band gaps show a clear tendency to decrease with increasing Al concentration, and this leads to an almost monotonic decrease of the average band gap. The average band gap falls by near 25% from the calculated MgO value, roughly 5 eV, to the  $\sim 3.8$  eV value at 56% doping. At this point we recall that the LDA can severely underestimate band gaps. In the case of MgO, the calculated band gap is to be compared with the experimental value of 7.8 eV [93]. However, the trends in the dependence of the band gap on lattice parameters are considered to be described quite reliably by the LDA scheme used here [94, 95]. The fact that the band gap has a tendency to decrease with Al concentration obeys two facts. First, both valence and conduction band widths increase with Al content because of the lattice constant reduction. To show this, we plot the band structure for Al concentrations of 6% and 56% (for one of the possible configurations) in Figs. 3.5(b) and (c), respectively. Second, doping with Al creates O-like acceptor states, just above the valence band

maximum. They are created by the Mg vacancies and passivated by the Al electrons. These states tend to detach more from the valence band continuum with increasing doping concentration, thus contributing further to the band gap narrowing.

This is also illustrated in Figs. 3.5(b) and (c). Furthermore, as can be seen in these figures, for higher Al content, the eigenvalue distribution as a function of  $\mathbf{k}$  point and band tends to be more homogeneous than for lower Al content, reflecting the lower symmetry of the former case. The band widths are also larger in the former case. This has an influence on the optical spectra peak structure, as discussed below.

Of interest in experiment has been the refractive index [78]. Therefore, we consider dependence on Al concentration of the average dielectric function. Figures 3.6(a) and (b) show the imaginary ( $\epsilon''$ ) and real ( $\epsilon'$ ) parts, respectively, for the different Al concentrations we are studying here. For reference, the dielectric function for MgO is also plotted. In both figures one can clearly see that the rather sharp structure in the spectrum for low Al content gradually disappears as Al concentration increases. This can be understood by considering the evolution of the density of states (DOS) with Al concentration. Indeed, due to a more homogeneous eigenvalue distribution (within each band manifold) among  $\mathbf{k}$  points in the Brillouin zone [cf. Figs. 3.5(b) and (c)], the structure in the DOS itself tends to disappear as the Al content increases. This is shown in Figs. 3.7(a) and (b), where we plot the total DOS corresponding to Figs. 3.5(b) and (c). The joint density of states will show a similar behavior and will result in the trends seen in Fig. 3.6. The broader band widths for higher Al content, also reflected in the DOS, will contribute further to a smoother dielectric function as a function of energy. Consider now the low frequency behavior of the dielectric function. There are two aspects that are relevant to experiment. One is the absorption edge, essentially determined by onset of the imaginary part of the dielectric function. The other is the zero frequency limit of the real part of the dielectric function, i.e. the optical dielectric constant.

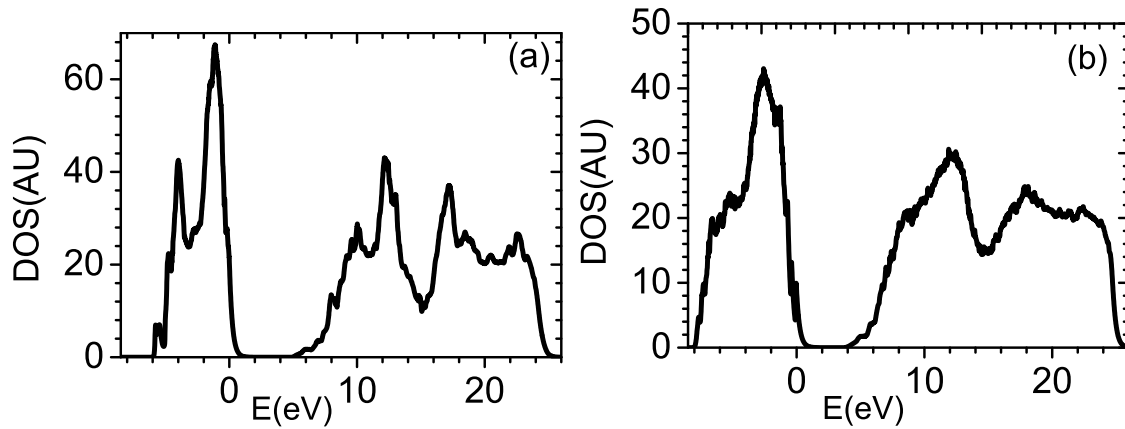


Figure 3.7: DOS plots for (a) 6% and (b) 56% Al-doped MgO. At higher doping level, the fine structure in the density of states tends to disappear.

In Fig. 3.8(a), we consider the evolution of the absorption edge with Al concentration. Comparing with Fig. 3.5(a), one can see that the absorption edge is correlated directly with the band gap, as can be expected. The absorption edge width gradually increases with Al concentration can be attributed to the corresponding decrease of crystalline order. Figure 3.8(b) shows the low frequency behavior of the real part of the dielectric function as a function of Al doping level. One can see that  $\varepsilon_\infty$  drops as soon as Al replaces some of the Mg atoms. This indicates that the polarizability of the system tends to be reduced with respect to MgO. However, the drop is rather small compared to the absolute value of the dielectric constants. Note that our result  $\varepsilon_\infty \simeq 3.18$  is reasonably close to the experimental value of 3 [96]. The slight overestimation can be mainly attributed to the underestimation of the band gap.

The low frequency limit of the refractive index is given by  $n = \sqrt{\varepsilon^r(0)}$ . This is plotted in Fig. 3.8(c), where one can see a tendency to increase with Al concentration.

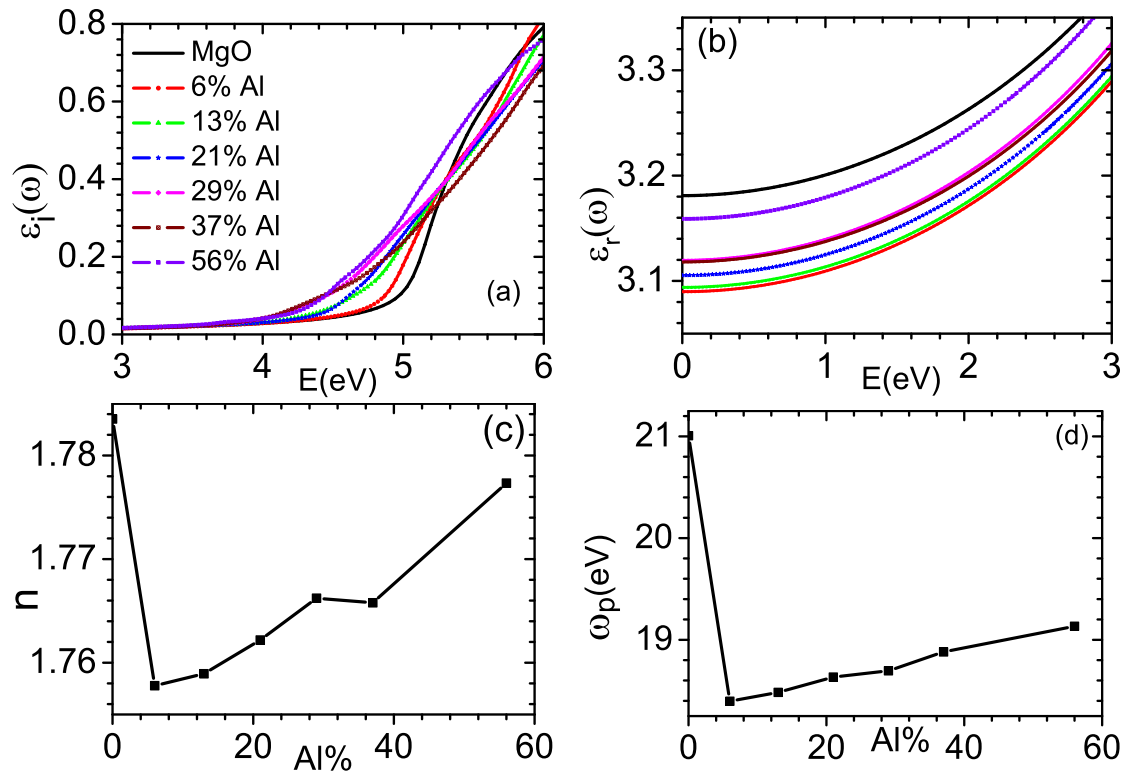


Figure 3.8: (a) Change in the imaginary part of the dielectric function of Al-doped MgO around the absorption edge varying Al concentration. (b) Low frequency dependence of the real part of the dielectric function for the different Al concentrations considered in this work. (c) and (d) dependence of the refractive index and plasma frequency, respectively, on Al concentration.

The same tendency is observed in experiment up to 40% Al doping, although our values are between 7 and 11% higher than the measured values [78]. For an Al concentration higher than 40%, our results cannot be directly compared with experiment. In the latter, the phase is amorphous, while in our calculations it is not. On the other hand, it should be noted that the accuracy of the experimental values is not completely clear. For instance, for a pure MgO crystal, the optical dielectric constant value is 3 [96]. We find a value of 3.18, as mentioned above, against a value of around 3.5 in experiment [78]. To conclude this subsection, we consider another quantity that can be used to characterize a system, namely, the plasma frequency,  $\omega_p$ . It can be readily calculated from the dielectric function using the well known sum rule (Eq. (3.18)). Here we study the dependence on Al concentration of the plasma frequency averaged also over the three spatial directions. The results are plotted in Fig. 3.8(d). One can clearly see that  $\omega_p$  increases with Al content. Given that the number of valence electrons is independent of Al content, the increase of  $\omega_p$  can be understood as a consequence of the reduction of the lattice constant with increasing Al concentration. We verified that the valence electron density gives plasma frequencies very close to those determined with the sum rule above.

### 3.4.2 Amorphous versus crystalline structure

As indicated above, experiment and molecular dynamics simulations show that an Al doping concentration larger than 40 to 50% leads to an amorphous system [77, 79]. Snapshots of the molecular dynamics simulations are found in Ref. [77]. We note that these show no indication of phase segregation as the Al content increases. In this last subsection, we consider 56% Al-doped MgO in the amorphous and crystalline structures, and compare their structural and optical properties. To model the amorphous structure we proceed as follows. Data from molecular dynamics simulations for a supercell containing 11 Mg, 13 Al, and 32 O atoms are obtained [80]. In our calculations, one Al atom was added to that structure in order to obtain a charge balanced system. We then constructed two additional configurations by completely randomly changing the positions of Al and Mg atoms in the charge balanced system. The supercell size and atomic positions of the pseudo-amorphous structures corresponding to these three configurations are fully optimized. In the following, we consider the averaged properties of these three structures as representative of an amorphous structure.

The amorphous supercell size thus obtained is 8.279 Å, compared to 8.066 Å for the crystalline structure. The larger supercell size in the former case (larger by 2.6%) is due to the increased disorder in this structure.

The optical gap of the amorphous structure can be determined by means of a Tauc plot [87], which is commonly used to determine the optical gap of amorphous materials [97]. One plots  $(E\alpha)^{1/2}$ , where  $E$  is the absorption energy and  $\alpha$  is the optical absorption, versus  $E$  (cf. Fig. 3.9). Extrapolating the linear regime in the plot to the abscissa yields the optical gap. Thus, we obtain an optical gap of 3.56 eV. For reference, we note that the band gap of the crystalline structure is 3.85 eV.

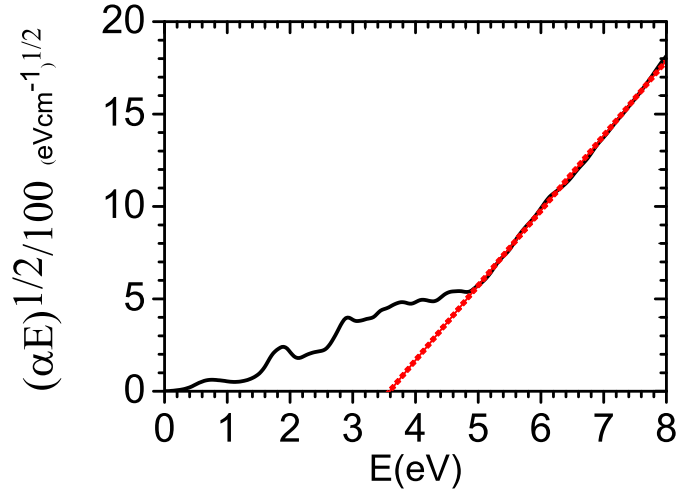


Figure 3.9: Tauc plot for pseudo-amorphous 56% Al-doped MgO.

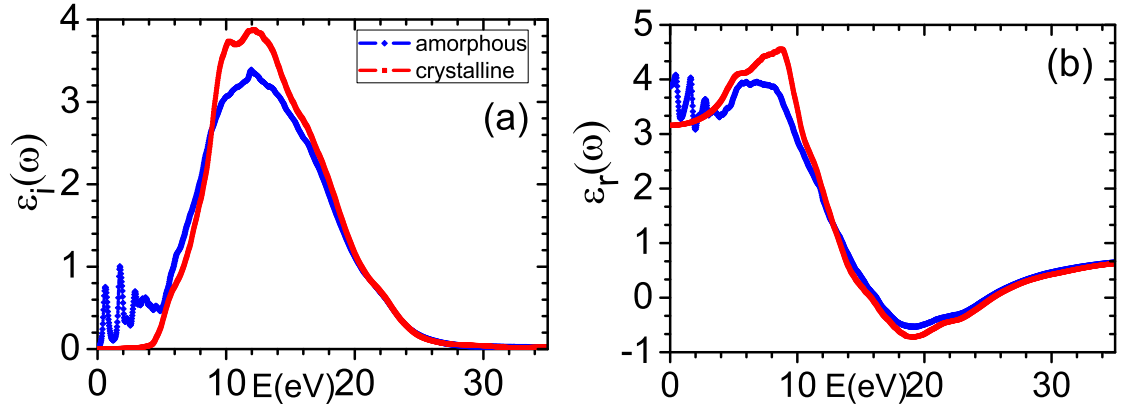


Figure 3.10: Frequency dependence of the calculated dielectric function (a)  $\varepsilon''(\omega)$  and (b)  $\varepsilon'(\omega)$ , comparing the crystalline and amorphous cases in 56% Al-doped MgO.

For further comparison, in Figs. 3.10(a) and (b), we plot the imaginary and real parts of the dielectric function, respectively, for both structures. The plots reflect immediately a fundamental difference in the electronic structure of two systems, namely, the disorder-induced states in the band gap in the amorphous case. The latter produce the absorption peaks below 5 eV in  $\varepsilon''$  in Fig. 3.10(a). To discuss this further, we plot the corresponding density of states in Figs. 3.11(a) and (b). We note that the states in the gap are robust, i.e., averaging over different disordered configurations tends to



broaden their overall energy spread, but does not really weaken their effect.

Figure 3.11(a) clearly shows two localized states in the gap in the amorphous phase just above the Fermi level (0 eV). Finally, we comment that we find the optical dielectric constant for the amorphous system is 3.87, to compare with 3.16 for the crystalline system. Using the Clausius-Mossotti relation [96], one can readily deduce that the polarizability of the amorphous phase is 26% higher than in the crystalline phase.

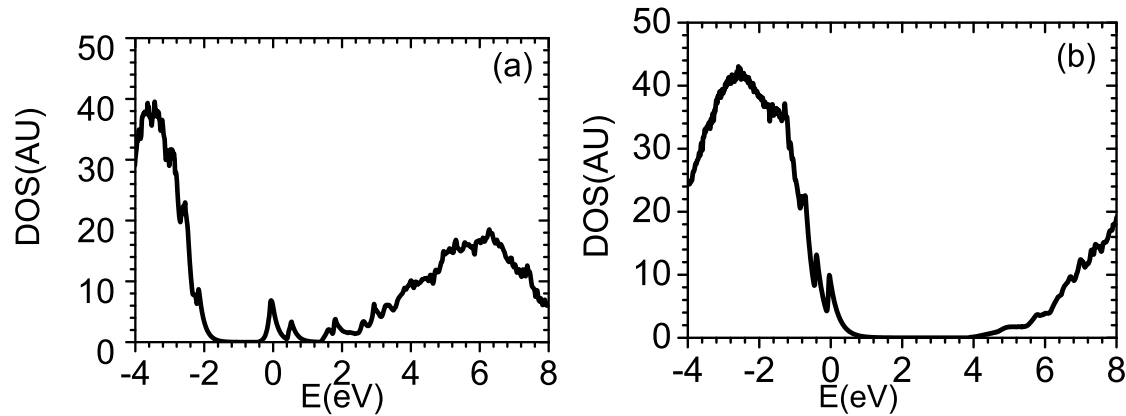


Figure 3.11: density of states (DOS) for (a) amorphous and (b) crystalline 56% Al-doped MgO.

The higher polarizability in the amorphous phase may be due to the weakening of the bond strength in the amorphous phase. This is in line with our finding above, that the band gap in the amorphous phase is smaller than in the crystalline phase [98].

We also calculated the plasma frequency in the amorphous phase. We find it is 18.10 eV, which is smaller than the 19.13 eV value for the crystalline system [cf. Fig. 3.10]. Given that the valence charge in both systems is the same, this can be understood as due to the larger supercell size in the amorphous case (i.e., lower electron density). This is similar to what is observed in other amorphous systems, such as amorphous carbon [99].

## 3.5 Conclusions

It is interesting that the results in the previous Section show that the electronic properties of crystalline Al-doped MgO are rather robust against doping level. Indeed, although the band gap, dielectric function, and related properties show quantitative changes upon changing the Al concentration, the changes are nearly monotonic. This implies that the electronic properties do not change qualitatively in a really significant way. It is only when one considers the amorphous phase that one finds a more significant change in the electronic properties. The most important effect is the appearance of impurity levels deep in the band gap. There are several observable consequences of

this. We mention, in particular, the important red shift of the optical absorption edge, due to these levels, and the related sudden drop of the band gap. A further consequence is an equally sudden jump upward of  $\varepsilon_\infty$  and of the refractive index. Thus, these effects can be considered as a further signature of the transition from the crystalline to the amorphous phase in these systems. As such, they provide additional criteria for the experimental characterization of the crystalline/amorphous transition.

# High-throughput screening approach based on density functional theory

## 4.1 Introduction

The growing demand for improved materials in the PV field (both absorber layers and TCOs) has led to an intense research activity both in academia and industry [100, 101]. It takes approximately 20 years between the initial discovery of a new material and its commercialization [102]. The major part of this time is invested in overcoming the optimization problems of the mechanical properties, thermal stability, cost, large-scale fabrication, and other factors. Shortening the discovery and optimization time is achievable by screening the properties of a large class of materials for specific applications. More than one hundred years ago Thomas Edison screened about 6000 materials experimentally for light bulb filaments [103]. However, the experimental screening of materials is limited by high costs and time-consuming synthesis procedures. Therefore, benefiting from another screening approach which is rapid, exact in results, and powerful in predictions plays a crucial role in materials design. Ab initio computational methods based on DFT solve the quantum mechanical equations for a system with high accuracy [32, 104]. They calculate the properties of a wide range of the materials without any need of pre-existing experimental knowledge [105, 106]. Moreover, improvement in ab initio computational methods and development in computing power have made it possible to perform a very larger number of calculations in a fixed time compared to the past [107, 108]. The combination of computational ab initio methods with a database construction and data mining provides a high-throughput ab initio approach [109]. The approach includes automatizing the large number of ab initio calculations to create a database of the calculated properties of existing and new possible materials and then search for the materials with particular properties [110–112]. If the approach reproduces the properties of the existing materials correctly, it is reliable in predicting the properties of the possible new materials.

Now it is more than one decade that the research community benefits from high-throughput DFT approaches for designing new materials in order to develop the properties of the existing ones for different applications [108, 110–126]

In this thesis, we use a high-throughput approach based on DFT to generate data for (i) bixbyite oxides, and (ii) Cu-based stannite quaternary chalcogenides. We search our generated database for new materials for TCO applications, and for new absorber layers for PV applications. Moreover, we use the AFLOWLIB electronic structure database [127] to identify new materials for *p*-type TCO applications.

This chapter first provides details about the DFT-based high-throughput approach used in this thesis. Then, we discuss the steps of building our high-throughput infrastructure. Finally, the details are given about the roles of scripting in each step of the high-throughput procedure.

## 4.2 DFT based high-throughput screening procedure

Since a high-throughput computational screening deals with a large number of calculations, the challenging part of such a procedure is designing the infrastructure to generate data for all calculations, run the computations, store the output data, and finally analyse the results with respect to the desired application. In the present thesis, we implemented Python scripts to build this infrastructure. In section 4.7 we provide the details on how the scripts form the infrastructure and deal with a large number of data. Figure 4.1 shows the general schematic plot of the important steps in our high-throughput approach. In the next three sections, we give the details of the steps represented in Fig. 4.1.

## 4.3 Data generation

Data generation for computational high-throughput screening has two steps, selecting materials and generating the input data of the selected materials to compute their properties. Material selection depends on the specific details of the application of the materials, so it is different from one research project to another. One efficient approach is to select compounds from those tabulated in external databases such as the inorganic crystal structure database (ICSD) [128, 129]. The compounds presented in such databases are in general characterized experimentally, therefore one can be confident that they can be synthesized. This is the main advantage of this approach. Computations can further be expanded to predict the existence of new materials [112, 130, 131]. In this thesis, we use both external crystal databases and compound prediction to create our database for the particular applications. We will explain the data selection and data generation approach for all performed high-throughput work in this thesis separately (see section 5.2.1, section 7.1, and section 8.3).

After selecting the materials for the application of interest, we proceed by computing the properties of each compound. We calculate the properties of the materials using the DFT formalism. Since

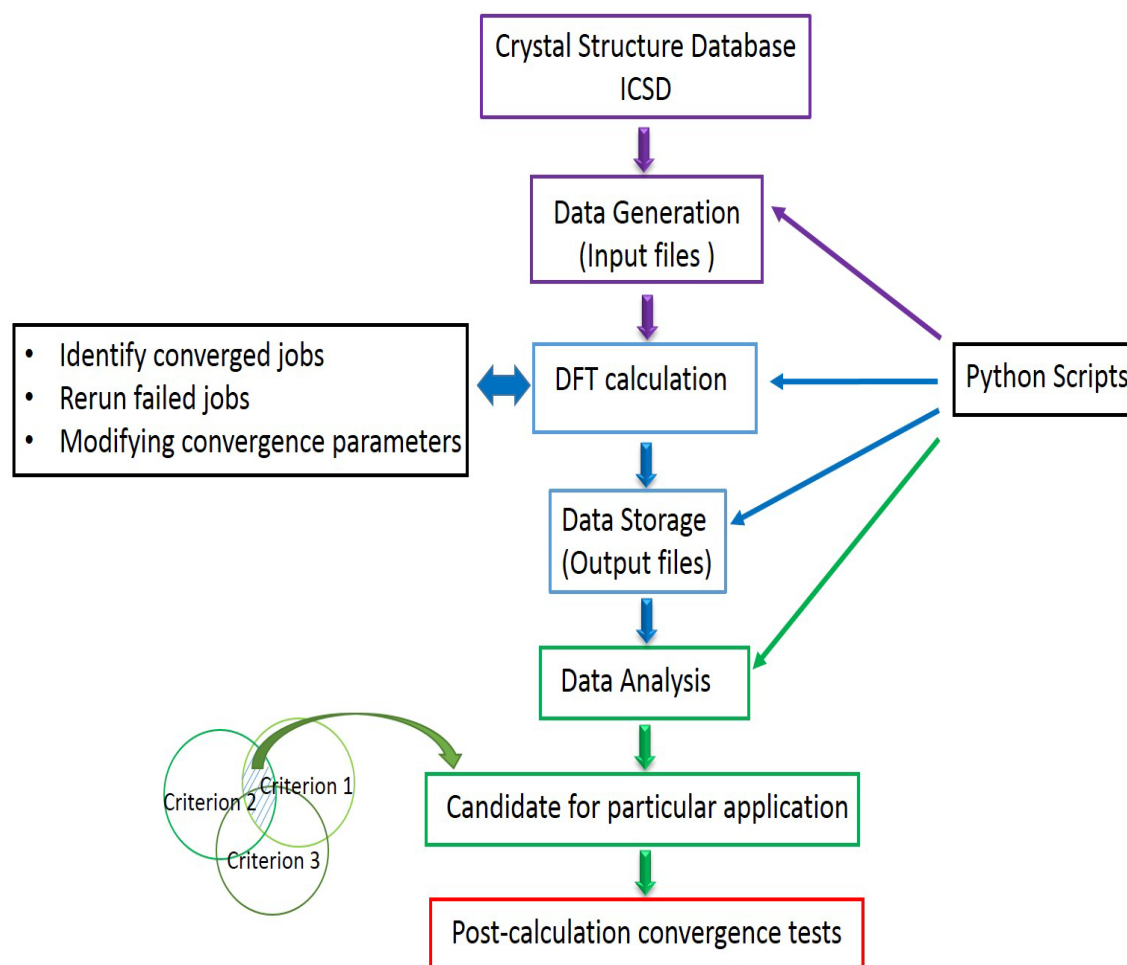


Figure 4.1: Diagram of important steps in our high-throughput computational screening procedure.

DFT calculations have a relatively small number of control parameters, the calculations are well-established for a high-throughput approach. However, automating DFT calculations is not trivial because the calculations need a set of parameters (such as k-point mesh, energy cut-off) which controls the convergence of the calculations. Furthermore, this set of parameters depends on the compound. In addition, we have to define a "stopping" criterion which controls the convergence of the self consistent field cycle and that of the structural relaxation. Our Python script produces input files for all calculations with reasonable values for the control parameters and stopping criteria. In Section (4.6) we will give details on the default values for all parameters mentioned above, followed by a discussion on the convergence of the calculation results with respect to these parameters.

## 4.4 Convergence to the electronic ground state and problem handling

Our Python script initiates the parallel calculations after the required input data are generated. It also identifies which calculation is converged. If the calculation is not converged after 150 electronic steps, it should be returned for some modifications that will lead the calculation to convergence. For such an improvement, we should first know the possible reasons of the convergence failure and also the possible solutions.

In DFT calculations, the main task is to solve the KS equations to get the ground state energy. Kresse and Furthmüller have implemented algorithms in VASP code to solve these equations iteratively [70]. There are different algorithm choices and the convergence to the ground state depends on them. These algorithms (the corresponding VASP variables are given in the parentheses) include the matrix diagonalization scheme used to solve for the wave functions (ALGO), the charge mixing strategy (IMIX), and the method of performing numerical integration of the energy over a finite k-point grid (ISMEAR). Although most of the systems converge rapidly using preset minimization algorithms and parameters found in modern electronic structure codes such as VASP, there are difficult systems which often require improvement in such parameters to converge in a reasonable time. The main issue with the DFT high-throughput calculations is to choose the algorithms that efficiently and rapidly yield a converged ground state energy because it is not possible to tune the parameters manually for each of the thousands of computations. Therefore, we need a good choice of algorithms as a default for all calculations and a script to find and handle the convergence problems. We use a default algorithm for each of the three main schemes that are already mentioned. If the default algorithm fails to converge the calculations, we use the alternative algorithm. Here we give the default and alternative algorithms used in our calculations for three main schemes:

- We use a built-in routine in VASP for our default Hamiltonian matrix diagonalization algorithm (ALGO = Fast). This approach uses a mixture of two methods, the blocked Davidson approach [132] for the first few iterations, and then the residual minimization method-direct inversion in the iterative subspace (RMM-DIIS) method [133, 134]. This approach is efficient and rapid because the RMM-DIIS is quite fast, but requires good initial wave functions to converge to the correct ground state [70, 135]. The blocked Davidson method can generate a reliable wave function to be used in the RMM-DIIS method. In the cases that this approach fails to converge after 150 electronic iterations, we switch to the pure blocked Davidson approach (ALGO = Normal) as recommended in this situation by the VASP developers [135].
- We employ the Pulay mixer as suggested in the VASP manual as a default for charge density mixing [134]. This method combines the charge densities from all previous iterations in a manner that minimizes their residual vectors while conserving the number of electrons in the system. However, if there is a convergence problem even after using blocked Davidson, the mixing parameters may need to be tuned [70, 136].

- Among the several existing strategies for integration of the band structure over the reciprocal space, we use the tetrahedron method with Blöchl's corrections (ISMEAR = -5) [137]. This method linearly interpolates energies between k-points and corrects quadratic errors and converges rapidly with respect to the number of k-points [68, 70]. This efficient method fails to converge for the systems with a number of k-points smaller than 4. Also, in metals and very small band gap materials, where the Fermi level separates the occupied and unoccupied states discontinuously, this method is not able to determine the Fermi level correctly. As an alternative method, we use the Gaussian smearing method (ISMEAR = 0) which is known to smooth the discontinuity in the Fermi level at zero temperature and to lead to accurate values for the Fermi level [70].

## 4.5 Storing and analysing data

After each single calculation is finished and identified as a converged one, the result can be stored in the library which can vary from text files to complicated huge online databases. Regarding to the large amount of data in a high-throughput work, only a well-designed data storage allows researchers to explore the data intuitively in order to discover scientific trends in the data and possibly find new compounds as candidates for the desired application. One can manage data through a relational database management system (RDBMS) as implemented in commercial database systems such as Sybase [138] and Oracle [139]. Relational databases can store data compactly and efficiently which makes them a good option for data storage in high-throughput work.

As an alternative solution to the commercial database systems, we store our generated results in files which are created by using Python scripts. We simply apply the idea of the relational model [140] to construct our database. The generated data are tabulated on the basis of their relations.

Table 4.1: part of the generated data based on the relational model.

| compound | band gap type | band gap1 | band gap2 | CBM       | VBM       | BPE       |
|----------|---------------|-----------|-----------|-----------|-----------|-----------|
| K2Pb2O3  | indirect      | 2.283444  | 0.594713  | 1.470302  | -0.813142 | -0.328580 |
| Pr2SeO2  | indirect      | 3.125732  | 2.456973  | 2.355799  | -0.769933 | -0.792933 |
| NaNbO2   | indirect      | 2.315698  | 0.273189  | 3.150475  | 0.834777  | -1.992626 |
| Ca4As2O  | indirect      | 1.966102  | 0.614237  | -0.828373 | -2.794475 | 1.811424  |
| YZnPO    | indirect      | 2.016872  | 0.600527  | 2.709097  | 0.692224  | -1.700661 |
| DyZnPO   | indirect      | 1.948139  | 0.697085  | 1.976760  | 0.028621  | -1.002691 |

Table 4.1 represents a part of our generated data (data will be analysed and discussed in Chapter 6). As table 4.1 shows each table has a header and body. The header is simply the list of columns in the relation. The body is the set of data that actually populates the relation organized into rows.

In this aspect, all the results which should be analysed for a considered application, are stored as tables. The subsequent analysis are performed by using Python scripts. First we define the criteria for all quantities that are considered in the particular application. If a calculated value of the compound satisfies the criterion, the corresponding compound can stay in the list of the qualified compounds, otherwise the compound is screened from the list. The same procedure is used for all considered properties. The compound is identified as a qualified material when it satisfies all criteria (i.e. it simply belongs to the intersection of the three circles in Fig. 4.1).

## 4.6 Numerical convergence

The DFT calculations lead to the total energy and then to other properties of the studied system via iterative methods. The calculations should be converged with respect to the following parameters

- An energy cutoff of the plane wave basis set for representing the wave function.
- A k-point mesh which determines the integration over the first Brillouin zone.
- A criterion for stopping the iterative optimization of the electronic structure and also the structural relaxation. This can be specified by setting the thresholds for energy and force differences in the iterative optimizations.

Among these parameters the last one relates to the self-consistency of the methods used in the calculations. In small calculations, it is possible to converge the properties of the studied system with respect to the three parameters. In other words, one can alter the criteria (increase the number of k-points and energy cutoff, and decrease the stopping criterion) until there is no significant change in the results. Although this convergence procedure is a good way to get reasonable parameters for converged results, this is practically not possible in a high-throughput work. The main reason is that such tests in a high-throughput work result in a large number of additional calculations that should be performed for thousands of systems.

In our high-throughput work we apply the following procedure to keep the computational expenses for the convergence tests to a minimum. We set the energy cutoff to be 30% higher than the maximum energy cutoff recommended by the PAW datasets [135]. We tested this setting for a large number of different materials from metallic phases of the elements to semiconducting oxides and we found that this setting gives accurate and converged results for the vast majority of the calculations.

We sample the Brillouin zone (BZ) with at least  $500/N$  k-points in the irreducible BZ where  $N$  is the number of atoms in the unit cell. This k-point mesh is dense enough to get converged results. However, we perform post-calculation convergence tests for the total energy and some other properties of interest (i.e. position of the charge neutrality level) with respect to the k-mesh density. In this approach, first we use a relatively dense k-mesh to sample the Brillouin zone for all the compounds. We perform the calculations to investigate the desired properties and identify the



potential candidates for a particular application. Then, for the qualified compounds, we perform additional convergence tests.

Atomic relaxations are made until residual forces on the atoms are less than 0.01 eV/Å and total energies are converged to within 0.1 meV.

Altogether, it is possible to generate high-throughput data sets of total energy and other properties without performing explicit convergence test for each compound. However, post-calculation convergence tests for potential candidates (for a particular application) ensure reliable converged results (see also the last step in Fig. 4.1)

## 4.7 Role of scripting in high-throughput computations

A high-throughput project deals with a large number of input and output data. Therefore, the classification of data is an important task that can be performed efficiently using scripts. We consider six libraries, including INPUT, SCRIPT, CALCULATION, RESULT, ERROR, and OUTPUT to classify the data of our high-throughput work as represented in Fig. 4.2. Figure 4.2 and the following discussion give insight into the role of the scripts in each step that is already shown in Fig. 4.1.

In the libraries there are files, and directories. The path to the file and directory are referred by "/DIRECTORY/SUBDIRECTORY/file", and "/DIRECTORY/SUBDIRECTORY/DIRECTORY-OF-INTRUST/", respectively. We refer to the files with lowercase letters in *italic*, and to the directories with uppercase letters.

The first library is INPUT and includes all required input data to start a DFT calculation. There is a directory in the INPUT library for each type of the calculations. Each directory includes five files. Four of them provide input data for the calculation and the last one is the job submission script. In this library, there is also a list of the compounds for a particular calculation. Input files for the calculations include the position of the atoms, variables for the DFT calculations (e.g. stopping criteria in atomic relaxation, and energy cutoff), k-point mesh, and atomic potentials.

The second library is SCRIPT. There are one bash script *multijob*, two Python scripts *makedir* and *analysis*, and one directory GETRESULT in this library. The script *makedir* uses data from the INPUT library to make a directory for each compound and adopts the input data for it.

The bash script *multijob* allows us to submit multiple jobs in one submission. By running the *multijob* from a directory that has some subdirectories, one job for each subdirectory is submitted if the subdirectory has a job submission script. The directory of each compound in the CALCULATION library has one bash script for job submission, *job-submit*. By running the *multijob* script, it calls the *job-submit* to submit a job for that compound.

There is a Python script for each type of the calculations, including relaxation, band structure, effective mass, and optical spectrum in the GETRESULT directory. Each of these scripts first collects the output data and then performs the required "post-DFT calculations" on them. The post-DFT calculations refer to the calculations on the output data resulted from the DFT calculations in order to calculate the properties of interest. A large number of properties are not written as the output data in the output file of the VASP calculations, but they can be extracted out of the DFT

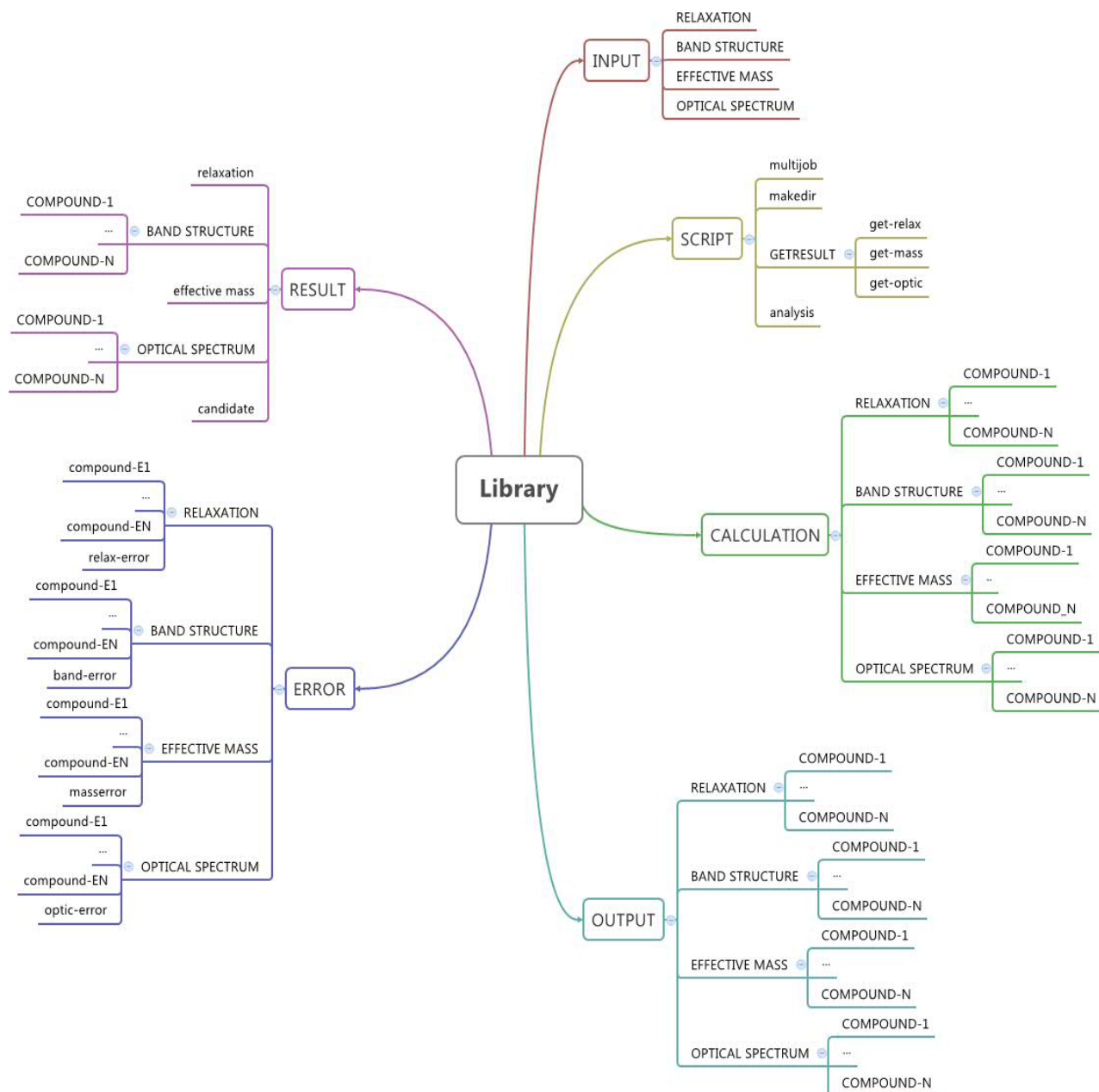


Figure 4.2: The libraries for a high-throughput computational project. Uppercase letters show the directories and lowercase letters correspond to the files.

results with some calculations. We call such calculations the post-DFT calculations. Total energy, lattice parameters, plasma frequency, and dielectric constant are some of the direct outputs of the DFT calculations by VASP while the formation energy, stability triangle, branching point energy, band gaps (including fundamental band gap, optical band gap, second gap in the conduction band, and second gap in the valence band), hole and electron effective mass, and refractive index are some of the properties that result from the post-DFT calculations. The output data after the calculations are collected from the CALCULATION Library and they are appended to the corresponding files in the RESULT library. Finally the directory of the compound is compressed as a zipped file and is moved to the OUTPUT library.

Let us consider an example, the result of the relaxation of compound-x. The *get-relax* script collects the lattice parameter, total energy, Fermi level, and calculates the branching point energy from the DFT data that are written in /CALCULATION/RELAXATION/COMPOUND-X/out and appends them as raw data to the /RESULT/relaxation.

As a final task of the *get-relax* script for the compound-x, it makes compound-x.zip and moves it to the /OUTPUT/RELAXATION/compound-x.zip. The *analysis* script applies certain criteria on the considered properties that are collected and stored in the RESULT library for all studied compounds. If a compound fulfills all the applied criteria, the full list of its properties is appended to the file /RESULT/candidate. As it is already mentioned, the directory of each calculation includes a script (*job-submit* script) that is used to submit a job of the calculation. The *job-submit* script has some lines that allow to copy the errors and warnings from the output file of each compound and write it to the corresponding file. An error file is created for each type of calculations. If there is an error or a warning in the particular calculation for a compound, the script writes the name of the compound and the type of calculation to the corresponding error file. For example, if there is an error or a warning in the relaxation of compound-x, the error or what caused the problem is copied from the file /CALCULATION/RELAXATION/COMPOUND-X/out and is written into the file /ERROR/RELAXATION/compound-Ex. Also "relaxation:compound-x" is written to the file /ERROR/RELAXATION/relax-error. A calculation job for the compound is considered for resubmission after the problem that caused the error or warning is solved.



# Bixbyite Oxides for TCO Applications

## 5.1 Introduction

Transparent conductors oxides (TCOs) have long been ubiquitous in electronic devices, and the desire of finding the optimum material for each type of application is at the heart of research efforts in the field for decades now [141]. Indium tin oxide,  $\text{In}_2\text{O}_3:\text{Sn}$  (ITO) [141, 142] is one of the most widely used *n*-type TCOs for various optoelectronic applications. However, it does not present the optimum properties in some respects. For instance, its transparency is not as high as that of fluorine-doped ZnO [141]. Furthermore, because of the scarcity and high price of In, it is not cost effective, and for the past several years finding an alternative to ITO in different applications has been an important research goal for many groups. Possible routes for this include studying oxides with different structure, or substituting In partially, or replacing In altogether but still keeping the  $\text{In}_2\text{O}_3$  bixbyite structure. Of course, the number of conceivable compounds within these bounds can run into the hundreds or even thousands. Clearly, it is not possible to experimentally study all of them in order to determine whether there are other TCOs in this class of materials and whether their properties are competitive. On the other hand, high-throughput *ab initio* computations can be currently used to screen large classes of materials, searching for those compounds that exhibit a predetermined basic set of properties qualifying them as potential competitive candidates for a certain application [108, 143, 144]. This approach has recently been used with success in the search for novel materials for applications ranging from field-effect transistors [145] to piezoelectrics [146] to thermoelectrics [118] to TCOs [147].

In this chapter, we present the high-throughput approach schematically represented in Fig. 5.1, to search for candidates suitable for TCO applications. The screening criteria chosen are geared toward (i) a minimum band gap guaranteeing a reasonable transparency in the visible, (ii) a min-

---

The results of this chapter were published as: N. Sarmadian, R. Saniz, B. Partoens, D. Lamoen, K. Vollety, G. Huyberechts, and J. Paul, Journal of Physical Chemistry Chemical Physics 16, 17724(2014).

imum thermodynamic phase stability, and (iii) a positioning of the charge neutrality level in the band gap indicating easy *n*- or *p*-type dopability. We show that this set of criteria can be efficiently used to screen the compounds in a large class of materials and that it has a good predictive power. As an application, we aim at replacing In, partially or completely, in  $\text{In}_2\text{O}_3$ . For this we screen all the binary oxides that can be found in the bixbyite structure, as well as ternaries arising from their alloying. This narrows the search to one structure, and, at the same time, increases the likelihood of finding stable compounds. We consider ternaries with cation-cation alloying ratios of 25%, 50%, and 75%.

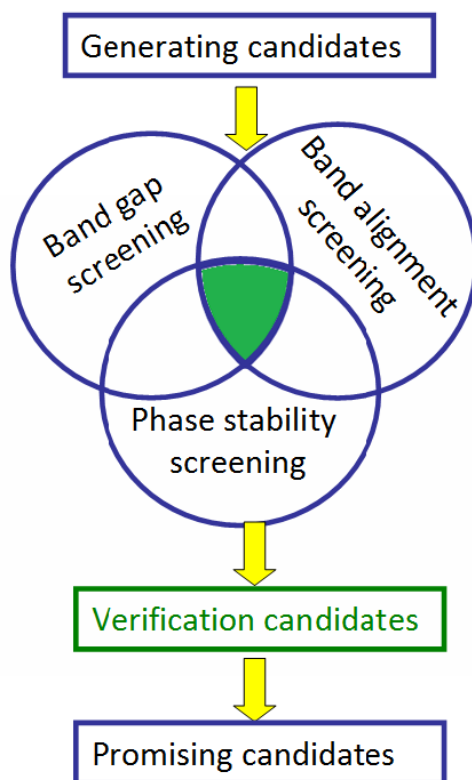


Figure 5.1: The high throughput screening procedure to identify new promising TCO candidates among bixbyite oxides.

## 5.2 Computational Method

Our *ab initio* computations are based on DFT [42, 45], and are carried out using the VASP [70, 91, 136, 148]. We use PAW [68, 92] potentials to describe the electron-ion interaction. We use

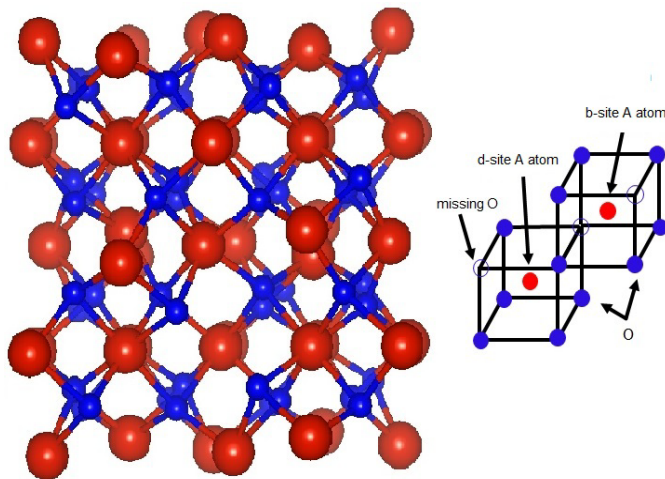


Figure 5.2: *Left*: Example of  $A_2O_3$  bixbyite unit cell. The blue color indicates oxygen atoms. *Right*: Schematic illustration of the atomic arrangement around cation A in Wyckoff sites  $b$  and  $d$ . The oxygen atoms are denoted by solid blue circles, the A atoms by red circles, and the missing oxygen atoms (with respect to the fluorite structure) by open circles.

the PBE [51] GGA to the exchange-correlation potential to perform all structural calculations. Formation energies and electronic structure are calculated using either the PBE functional, or the HSE hybrid functional [56, 57]. In general the HSE functional improves the band gap compared to PBE for bulk semiconductors [149]. It is, however, much more costly from a computational point of view, and cannot be used systematically in a high-throughput approach. We use it, thus, selectively, as explained in more detail further down, to calculate the properties of all the binary oxides, and to confirm the properties of several of the more promising ternary oxides. We modify the value of the exact exchange potential in HSE06 calculations to 0.325 compared with the standard value which is 0.25 in order to reproduce the experiment fundamental band gap of well known TCO material,  $In_2O_3$  [150].

The bixbyite structure is a cubic structure. Its primitive cell (space group  $Ia\bar{3}$ , No. 206) contains 8 formula units, i.e., 40 atoms (cf. Fig. 5.2). An energy cutoff of 520 eV is used for the plane-wave basis set. Total energies are converged to within 1 meV. This is achieved using  $3 \times 3 \times 3$  MP grid to sample the Brillouin Zone [66]. Atomic relaxations are made until residual forces on the atoms are less than 0.01 eV/Å.

### 5.2.1 Generating candidates

As seen in Fig. 5.1, we first generate the candidates to be screened. To begin, we consider all the binary bixbyite oxides reported to exist in the literature. These have the formula  $A_2O_3$ , with A belonging to the set  $\mathcal{S} = \{Sc, V, Mn, Fe, Ga, Y, In, La, Ce, Pr, Pm, Sm, Eu, Gd, Tb, Dy, Ho, Er,$

Tm, Yb, Lu, Tl, Bi}. We then combine two such oxides to construct ternary oxides. These are bixbyite oxides with general formula  $(A_{1-x}B_x)_2O_3$ , with A and B belonging to  $\mathcal{S}$ . In the present study,  $x$  takes the values 0, 0.25, 0.50, and 0.75. This should be sufficient to observe trends in the properties of interest as a function of alloying concentration. The bixbyite structure can be seen as the  $MnO_2$  fluorite structure, with one fourth of the O atoms removed. As shown in Fig. 5.2, the A atoms in  $A_2O_3$  occupy two inequivalent Wyckoff sites,  $b$  (site symmetry  $S_6$ ) and  $d$  (site symmetry  $C_2$ ), with a distorted octahedral coordination of O atoms. Four of the A atoms in the bixbyite structure sit in  $b$  sites, and 12 occupy  $d$  sites. As a result, there are different possible configurations for every alloying concentration. Again, to detect trends we choose randomly some of the possible configurations. We verify that different possible configurations lead essentially to the same conclusions in the case of 50% alloying, i.e.,  $x = 0.5$ , in which case we consider four possible configurations. For the 25% and 75% alloying compounds we consider at random one possible configuration. Thus, in this study we screen the electronic properties of a total of 1541 bixbyite oxides (23 binary and 1518 ternary oxides).

### 5.2.2 Band gap screening

One of the most important properties of a TCO is its band gap value. A good TCO needs a large enough band gap (of the order of 3 eV) to be transparent in the visible light range [151]. To screen the generated compounds according to this property, we calculate *ab initio* their band gaps. In this regard, it is known that standard DFT calculations, using local or semi-local exchange-correlation functionals such as the LDA or PBE, seriously underestimate the band gap of the semiconductors [152, 153], while the hybrid functional HSE06 has proven to be capable of giving close-to-experiment predictions for a large range of compounds [154]. Because of its computational cost, however, we rely on the HSE06 functional to calculate the band gap of only the binary oxides, which constitute a relatively small subset of all the oxides we consider. We choose to screen out the binaries with a band gap smaller than 2.5 eV. For the ternary oxides, we follow two approaches. In the first approach, we use the PBE functional, screening out the ternaries with a band gap energy lower than 1 eV. This is because a material predicted to have a band gap of 1 eV with the PBE functional might in fact have an experimental band gap closer to the requirement for a good TCO. We verify this with the HSE06 functional for candidate oxides that have successfully passed the three screening criteria in our procedure. In the second approach, we interpolate the HSE06 band gaps of the binary oxides to obtain an estimate of the band gaps of the ternaries. Again, we screen out those with a band gap energy below 2.5 eV. We note that, to be consistent, we follow the same two approaches in the band alignment and phase stability screening steps discussed below. That is, on one hand we calculate the relevant quantities using the PBE functional, and on the other, we interpolate the HSE06 results for the binaries.



### 5.2.3 Band alignment screening

In this step, we screen the candidate materials searching for those that can be expected to be easily *n*- or *p*-type dopable. A good predictor for this purpose is to see the alignment of the conduction band minimum (CBM) and valence band maximum (VBM) of a material with respect to the branch-point energy (BPE) [155]. Indeed, if the BPE falls high up in the band gap, or above the CBM in a material, it is a good indication that the material will be easily doped *n*-type. Conversely, if the BPE falls low in the band gap, or below the VBM, then the material is probably easily *p*-type dopable. The BPE can be calculated as a weighted average of the midgap energies over the Brillouin zone [156, 157],

$$E_{BP} = \frac{1}{2N_k} \sum \left[ \frac{1}{N_{CB}} \sum_i^{N_{CB}} \varepsilon_{c_i}(k) + \frac{1}{N_{VB}} \sum_i^{N_{VB}} \varepsilon_{v_j}(k) \right]. \quad (5.1)$$

Here,  $N_k$  is the number of points in the *k*-point mesh,  $N_{CB}$  and  $N_{VB}$  are the number of conduction and valence bands considered, with  $\varepsilon_c$  and  $\varepsilon_v$  their corresponding energies. The number of valence and conduction bands used is determined by scaling them according to the number of valence electrons in the primitive cell (excluding *d* electrons), as in the work of Schleife *et al.* [155] We checked that a  $3 \times 3 \times 3$  *k*point mesh is sufficient to give a converged BPE value.

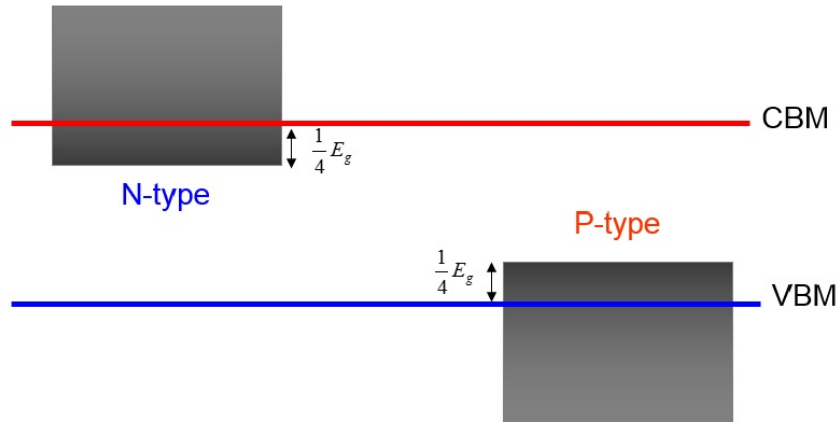


Figure 5.3: Schematic band alignment. The gray shaded area represents the accepted BPE position with respect to the CBM (*n*-type) or VBM (*p*-type) in our screening procedure.

Figure 5.3 illustrates our screening criterion regarding dopability. The oxides for which the BPE falls in the conduction band or in the upper part of the band gap, within at least one-fourth of  $E_g$  below the CBM (cf. shaded area at the left in Fig. 5.3), are considered as *n*-type oxides. Conversely, the oxides for which the BPE falls in the valence band, or maximum one-fourth of  $E_g$  above the VBM are considered as *p*-type oxides (cf. shaded area on the right side in Fig. 5.3).

### 5.2.4 Phase stability screening

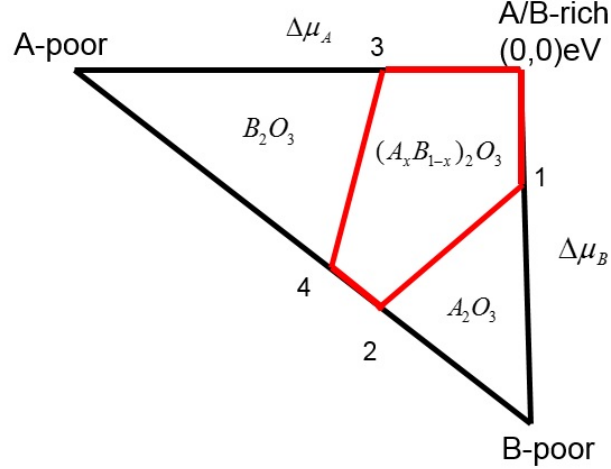


Figure 5.4: Schematic stability triangle. The area inside the red contour indicates the range of chemical potentials for which the bixbyite ternary oxide is stable against the formation of the competing phases indicated.

A new candidate should be thermodynamically stable. Thus, one of our screening criteria is the phase stability of the candidates. Since all the binary oxides considered here have been synthesized, we focus on the ternary oxides. The formation energies of ternary oxides depend on the chemical potentials of the different constituent elements ( $\mu_A$ ,  $\mu_B$ , and  $\mu_O$ ). The chemical potentials depend on the experimental growth conditions of the compound which can vary from X-poor to X-rich, where X could be either of A, B or O.

One of the main quantities in the study of the phase stability is the Gibbs free energy. The change in the Gibbs free energy of the system is given by

$$\Delta G = \Delta E + P\Delta V - T\Delta S \quad (5.2)$$

where  $\Delta E$  is the change in the total energy,  $P$  is the pressure,  $\Delta V$  is the change in the volume of the cell, and  $\Delta S$  is the change in the entropy of the system. As our calculations are performed at  $T = 0\text{K}$ , the change in the Gibbs free energy of the system is equal to the formation energy of the system ( $\Delta G \equiv \Delta H_f$ ).

For a considered ternary oxide  $(A_xB_{1-x})_2O_3$  the formation energy is given by:

$$\Delta H_f^{(A_xB_{1-x})_2O_3} = 2x\Delta\mu_A + 2(1-x)\Delta\mu_B + 3\Delta\mu_O \quad (5.3)$$

where  $\Delta\mu_{A/B} = \mu_{A/B} - \mu_{A/B}^{(A/B)bulk}$ , and  $\Delta\mu_O = \mu_O - \mu_O^{O_2molecule}$ . There should be a minimum range of possible values for these chemical potentials ensuring a stable oxide against the formation

of the binary phases or precipitation of the constituent elements:

$$\Delta\mu_A \leq 0, \Delta\mu_B \leq 0, \Delta\mu_O \leq 0. \quad (5.4)$$

The range of the chemical potentials determined by the heat of formation of the oxide and the limitation imposed by avoiding the precipitation of the constituent elements can be plotted in a two-dimensional graph, resulting in what is known as the stability triangle in the literature [158, 159]. This is schematically shown in a two-dimensional  $(\mu_A, \mu_B)$  plane in Fig. 5.4. The vertices of the stability triangle are given by the host condition Eq. (5.3) giving the limits of A/B rich, A-poor, and B-poor environments, respectively. The A-rich condition ( $\Delta\mu_A = 0$ ) leads to the maximum possible variation of the B chemical potential  $\Delta\mu_B = \frac{1}{2(1-x)}\Delta H_f^{(A_xB_{1-x})_2O_3}$  ( $\Delta\mu_O = 0$ ). On the other hand, the B-rich condition ( $\Delta\mu_B = 0$ ) leads to  $\Delta\mu_A = \frac{1}{2x}\Delta H_f^{(A_xB_{1-x})_2O_3}$ . The line joining the A-poor and B-poor vertex refers to  $\Delta\mu_O = 0$  and mimics the oxygen rich condition. Thus within this triangle the ternary oxide can exist, but the binary structures might have a lower formation energy. Therefore, the constraints are also imposed by the formation of competing binary oxides  $A_2O_3$ , and  $B_2O_3$  which are

$$2\Delta\mu_{A/B} + 3\Delta\mu_O \leq \Delta H_f^{(A/B)_2O_3}. \quad (5.5)$$

These constraints limit the possible accessible range of chemical potentials ( $\Delta\mu_{A/B}$ ) for  $(A_xB_{1-x})_2O_3$ . The vertices of this stable region are labeled as (1, 2, 3, 4) and the coordinates of the vertices are given by  $(\Delta\mu_A, \Delta\mu_B, \Delta\mu_O)$  which can be determined as follows. The first vertex, (1), refers to A-rich conditions ( $\Delta\mu_A = 0$ ) which leads to  $\Delta\mu_O = \frac{1}{3}\Delta H_f^{A_2O_3}$  and  $\Delta\mu_B = \frac{1}{2(1-x)}(\Delta H_f^{(A_xB_{1-x})_2O_3} - \Delta H_f^{A_2O_3})$  by using Eqs. (5.5) and (5.3) respectively. Second and fourth vertices, (2), and (4), refer to O-rich conditions ( $\Delta\mu_O = 0$ ). For vertex (2) the O-rich condition should be applied in Eq. (5.4) under the condition that  $A_2O_3$  is formed, which leads to  $\Delta\mu_A = \frac{1}{2}\Delta H_f^{A_2O_3}$ . Inserting this value into Eq. (5.3) yields  $\Delta\mu_B = \frac{1}{2(1-x)}(\Delta H_f^{(A_xB_{1-x})_2O_3} - x\Delta H_f^{A_2O_3})$ . For vertex (4) a similar analysis can be made but now with the formation of  $B_2O_3$ , which results in  $\Delta\mu_B = \frac{1}{2}\Delta H_f^{B_2O_3}$  and  $\Delta\mu_A = \frac{1}{2x}(\Delta H_f^{(A_xB_{1-x})_2O_3} - (1-x)\Delta H_f^{B_2O_3})$ . Vertex (3) refers to B-rich conditions ( $\Delta\mu_B = 0$ ) which yields  $\Delta\mu_O = \frac{1}{3}\Delta H_f^{B_2O_3}$  and  $\Delta\mu_A = \frac{1}{2x}(\Delta H_f^{(A_xB_{1-x})_2O_3} - \Delta H_f^{B_2O_3})$  on applying Eqs. (5.5) and (5.3) respectively. The relative size of the stable region with respect to the total area of the triangle shows how easy or how difficult it is to realize the thermodynamic conditions under which  $(A_xB_{1-x})_2O_3$  formation can take place and the precipitation of the parent binary compounds can be avoided. In order to limit the list of potential TCOs we impose a minimum ratio of 10% between the area of the stability region and that of the whole triangle.

## 5.3 Results

### 5.3.1 Binary oxides

We consider first the binary oxides,  $A_2O_3$ . For these materials, we calculate lattice parameters, band gaps, and formation energies using both the PBE and HSE06 functionals. In addition, we calculate the electron or hole effective masses, according to whether the band alignment indicates good electron or hole dopability. This is of particular interest to TCOs because mobility, a key quantity for the efficiency of many electronic devices, is inversely proportional to the electron effective mass. The effective mass is calculated along the  $\Gamma$ -X direction. This is sufficient because the bixbyite are cubic systems, so the effective mass is isotropic. In the first instance, we use the PBE functional for this calculation because it is known to give good values for the effective mass of semiconductors compared to experiment. However, when the PBE wrongly predicts a binary to be a metal, we use the HSE06 functional to estimate the effective mass.

Table 5.1 shows our results for the lattice constant, band gap (determined with the HSE06 hybrid functional), and effective mass of the binary oxides. For comparison, experimental data and/or other theoretical results are shown where available. The theoretical method is also indicated when available.

Table 5.1: Comparing our calculated lattice constant, band gap, and effective mass (in units of the free electron mass  $m_0$ ) for the binary oxides with experiment and other theoretical results.

| Binary oxide | a(Å)   | $E_g^{\ddagger}$ (eV) | $m^*$              | $\Delta H_f$ (eV) | reference                               |
|--------------|--------|-----------------------|--------------------|-------------------|---|
| $Sc_2O_3$    | 9.915  | 6.205                 | 1.143              | -17.80            | this work                               |
|              | 9.50   | $6^b$                 |                    |                   | Y. Bréard et al. [160]                  |
|              |        |                       |                    |                   | H. H. Tippins [161] <sup>†</sup>        |
|              | 9.911  |                       |                    |                   | J. R. Rustad [162] <sup>†</sup>         |
| $V_2O_3$     |        |                       |                    | -19.78            | CRC [163]                               |
|              | 9.263  | 2.388                 | 6.807 <sup>a</sup> | -10.43            | this work                               |
|              | 9.3947 | 1.29 <sup>b</sup>     |                    |                   | D. Weber et al. [164]                   |
|              |        |                       |                    |                   | A. Bergerud et al. [165] <sup>†</sup>   |
| $Mn_2O_3$    | 9.034  | 2.422                 | 2.422              | -7.00             | this work                               |
|              | 9.41   |                       |                    |                   | C.M. Julien et al. [166]                |
| $Fe_2O_3$    | 8.977  | 0.026                 |                    | -5.28             | this work                               |
|              | 9.5    |                       |                    |                   | Y. Bréard et al. [160]                  |
|              | 9.393  |                       |                    |                   | L. Ben-Dor et al. [167]                 |
| $Ga_2O_3$    | 9.409  | 4.455                 | 0.225              | -13.26            | this work                               |
|              | 9.401  | 2.3                   |                    |                   | S. Yoshioka et al. [168] <sup>†</sup>   |
| $Y_2O_3$     | 10.705 | 5.999                 | 0.516              | -17.88            | this work                               |
|              | 10.637 | 6                     |                    |                   | Ž. Antić et al. [169]                   |
|              |        |                       |                    |                   | P. W. Peacock et al. [170] <sup>#</sup> |

Table 5.1 Continued

| Binary Oxide                   | a(Å)                                    | E <sub>g</sub> <sup>‡</sup> (eV)      | m <sup>*</sup>                     | ΔH <sub>f</sub> (eV)                | reference                             |                                 |
|--------------------------------|---|---------------------------------------|------------------------------------|-------------------------------------|---------------------------------------|---------------------------------|
|                                | 10.701                                  | 6.2                                   | 0.166                              | -19.74                              | G. Wilk et al. [171]                  |                                 |
|                                |   | 4                                     |                                    |                                     | J. R. Rustad [162] <sup>†</sup>       |                                 |
|                                |   |                                       |                                    |                                     | L. Marsella et al. [172] <sup>†</sup> |                                 |
|                                | In <sub>2</sub> O <sub>3</sub>          | 10.305                                |                                    | 2.849                               | -9.05                                 | CRC [163]                       |
|                                |   | 10.10                                 |                                    | 2.9 <sup>c</sup>                    | this work                             |                                 |
| 10.33                          |   | 2.93 <sup>c</sup>                     | A. Bourlange et al. [173]          |                                     |                                       |                                 |
|                                |   | 2.67                                  | A. Walsh et al. [150] <sup>‡</sup> |                                     |                                       |                                 |
|                                | P. D. C. King et al. [174] <sup>‡</sup> |                                       |                                    |                                     |                                       |                                 |
|                                | 10.33                                   | 2.93 <sup>c</sup>                     | -9.59                              | I. Tanaka et al. [175] <sup>†</sup> |                                       |                                 |
|                                |   |                                       |                                    | S. Lany et al. [176] <sup>θ</sup>   |                                       |                                 |
|                                |   | CRC [163]                             |                                    |                                     |                                       |                                 |
|                                | La <sub>2</sub> O <sub>3</sub>          | 11.375                                |                                    | 5.451                               | -18.63                                | this work                       |
|                                |   | 11.136                                |                                    | 4                                   | G.-Y. Adachi [177]                    |                                 |
| 11.387                         |   | L. Marsella et al. [172] <sup>†</sup> |                                    |                                     |                                       |                                 |
| Ce <sub>2</sub> O <sub>3</sub> |   | 11.405                                | 5.454                              | -19.74                              | J. R. Rustad [162] <sup>†</sup>       |                                 |
|                                | 11.16                                   | 5.7                                   | G. Wilk et al. [171]               |                                     |                                       |                                 |
|                                | 11.414                                  | CRC [163]                             |                                    |                                     |                                       |                                 |
| Pr <sub>2</sub> O <sub>3</sub> | 11.180                                  | 5.632                                 | 1.136                              | -18.59                              | this work                             |                                 |
|                                | 11.52                                   | 0.528                                 | -16.74                             | G.-Y. Adachi [177]                  |                                       |                                 |
|                                | 11.290                                  |                                       | J. R. Rustad [162] <sup>†</sup>    |                                     |                                       |                                 |
| Pm <sub>2</sub> O <sub>3</sub> | 11.071                                  | 5.673                                 | 0.508                              | -30.05                              | this work                             |                                 |
|                                | 10.99                                   |                                       | G.-Y. Adachi [177]                 |                                     |                                       |                                 |
| Sm <sub>2</sub> O <sub>3</sub> | 11.000                                  | 5.697                                 | 0.495                              | -17.34                              | this work                             |                                 |
|                                | 10.93                                   | 5.04                                  | G.-Y. Adachi [177]                 |                                     |                                       |                                 |
|                                | 10.998                                  |                                       | A. F. Andreeva et al. [178]        |                                     |                                       |                                 |
|                                | Eu <sub>2</sub> O <sub>3</sub>          | 10.805                                | 5.851                              | 0.488                               | -26.36                                | J. R. Rustad [162] <sup>†</sup> |
|                                |   | 10.866                                | 4.6                                | -18.89                              | H. Jiang et al. [179] <sup>‡</sup>    |                                 |
|                                | 11.02                                   | 2.5                                   | -17.12                             | CRC [163]                           |                                       |                                 |
|                                |   |                                       |                                    | G. Concas et al. [181] <sup>◇</sup> |                                       |                                 |
|                                |   | H. Jiang et al. [179] <sup>‡</sup>    |                                    |                                     |                                       |                                 |
|                                | Gd <sub>2</sub> O <sub>3</sub>          | 10.814                                |                                    | 6.179                               | 0.479                                 | -18.80                          |

Table 5.1 Continued

| Binary Oxide                   | a(Å)                               | $E_g^{\dagger}$ (eV) | $m^*$     | $\Delta H_f$ (eV) | reference                               |
|--------------------------------|------------------------------------|----------------------|-----------|-------------------|---|
|                                | 10.813                             | $5.9^b$              |           | -18.86            | G.-Y. Adachi [177]                      |
|                                |                                    |                      |           |                   | M. Badylevich et al. [182] <sup>‡</sup> |
|                                | 10.819                             | 4.8                  |           |                   | J. R. Rustad [162] <sup>†</sup>         |
|                                |                                    |                      |           |                   | H. Jiang et al. [179] <sup>‡</sup>      |
|                                |                                    |                      | CRC [163] |                   |   |
| Tb <sub>2</sub> O <sub>3</sub> | 10.741                             | 5.860                | 0.470     | -22.67            | this work                               |
|                                | 10.730                             | 4.77                 |           | -19.33            | G.-Y. Adachi [177]                      |
|                                |                                    |                      |           |                   | A. F. Andreeva et al. [178]             |
|                                | 10.744                             | 4                    |           |                   | J. R. Rustad [162] <sup>†</sup>         |
|                                | H. Jiang et al. [179] <sup>‡</sup> |                      |           |                   |   |
|                                |                                    |                      | CRC [163] |                   |   |
| Dy <sub>2</sub> O <sub>3</sub> | 10.676                             | 5.895                | 0.432     | -18.07            | this work                               |
|                                | 10.667                             | 4.9                  |           | -19.31            | G.-Y. Adachi [177]                      |
|                                |                                    |                      |           |                   | A. I. Shelykh et al. [183]              |
|                                | 10.675                             | 4.6                  |           |                   | J. R. Rustad. [162] <sup>†</sup>        |
|                                | H. Jiang et al. [179] <sup>‡</sup> |                      |           |                   |   |
|                                |                                    |                      | CRC [163] |                   |   |
| Ho <sub>2</sub> O <sub>3</sub> | 10.605                             | 5.952                | 0.451     | -18.30            | this work                               |
|                                | 10.607                             | 5.3                  |           | -19.67            | G.-Y. Adachi [177]                      |
|                                |                                    |                      |           |                   | A. I. Shelykh et al. [183]              |
|                                | 10.609                             | 4.6                  |           |                   | J. R. Rustad [162] <sup>†</sup>         |
|                                | H. Jiang et al. [179] <sup>‡</sup> |                      |           |                   |   |
|                                |                                    |                      | CRC [163] |                   |   |
| Er <sub>2</sub> O <sub>3</sub> | 10.533                             | 5.980                | 0.444     | -18.29            | this work                               |
|                                | 10.547                             | 5.3                  |           | -19.58            | G.-Y. Adachi [177]                      |
|                                |                                    |                      |           |                   | A. I. Shelykh et al. [183]              |
|                                | 10.544                             | 4.7                  |           |                   | J. R. Rustad [162] <sup>†</sup>         |
|                                | H. Jiang et al. [179] <sup>‡</sup> |                      |           |                   |   |
|                                |                                    |                      | CRC [163] |                   |   |
| Tm <sub>2</sub> O <sub>3</sub> | 10.472                             | 6.011                | 0.431     | -18.46            | this work                               |
|                                | 10.488                             | 5.4                  |           | -18.81            | A. W. Carbonari et al. [184]            |
|                                |                                    |                      |           |                   | A. I. Shelykh et al. [183]              |
|                                | 10.472                             | 4.7                  |           |                   | J. R. Rustad [162] <sup>†</sup>         |
|                                | H. Jiang et al. [179] <sup>‡</sup> |                      |           |                   |   |
|                                |                                    |                      | CRC [163] |                   |   |
| Yb <sub>2</sub> O <sub>3</sub> | 10.682                             | 6.038                | 0.474     | -11.19            | this work                               |
|                                | 10.439                             | 5.3                  |           |                   | G.-Y. Adachi [177]                      |
|                                |                                    |                      |           |                   | A. F. Andreeva et al. [178]             |
|                                |                                    |                      |           |                   | CRC [163]                               |

Table 5.1 Continued

| Binary Oxide                   | a(Å)   | $E_g^{\ddagger}$ (eV) | $m^*$              | $\Delta H_f$ (eV) | reference                                 |
|--------------------------------|--------|-----------------------|--------------------|-------------------|---|
| Lu <sub>2</sub> O <sub>3</sub> | 10.360 | 6.066                 | 0.419              | -18.63            | this work                                 |
|                                | 10.438 |                       |                    |                   | Ž. Antić et al. [169]                     |
|                                | 10.391 |                       |                    |                   | G.-Y. Adachi [177]                        |
|                                |        | 5.5                   |                    |                   | A. I. Shelykh et al. [183]                |
|                                |        | 4.5                   |                    |                   | H. Jiang et al. [179] <sup>‡</sup>        |
| Tl <sub>2</sub> O <sub>3</sub> |        |                       |                    | -19.46            | CRC [163]                                 |
|                                | 10.766 | 0.431                 | 0.119 <sup>a</sup> | -3.57             | this work                                 |
|                                | 10.541 |                       |                    |                   | A. W. Carbonari et al. [184] <sup>†</sup> |
|                                | 10.56  | 0.33                  |                    |                   | A. B. Kehoe et al. [185] <sup>∅</sup>     |
| Bi <sub>2</sub> O <sub>3</sub> | 11.217 | 3.169                 | 36.776             | -10.18            | this work                                 |
|                                | 11.21  |                       |                    |                   | A. Matsumoto et al. [186] <sup>†</sup>    |

<sup>a</sup>  $m^*$  is the calculated effective mass of the hole.

<sup>b</sup> optical band gap

<sup>c</sup> fundamental band gap

<sup>†</sup> GGA

<sup>‡</sup> LDA + scissors correction

<sup>∅</sup> LDA+U

<sup>‡</sup> G<sub>0</sub>W<sub>0</sub> @ LDA+U

(Fundamental band gaps are estimated from Figure 3 in Ref. 52)

<sup>∅</sup> HSE06

<sup>‡</sup> The theoretical gap values refer to the fundamental band gap.

Note that for the transition metal oxides, such as Y<sub>2</sub>O<sub>3</sub> and Sc<sub>2</sub>O<sub>3</sub>, the calculated band gaps are in very good agreement with experiment. On the other hand, the band gap of the lanthanides is systematically overestimated. This does not affect the outcome of our screening procedure, since it only involves a lower limit for the band gap and not an upper limit. We calculate, furthermore, the standard enthalpy of formation energy of all the studied binary oxides (A<sub>2</sub>O<sub>3</sub>), i.e., taking as reference the energies of the constituent elements in their standard states (oxygen molecule for O and crystalline solid for A). The results, also presented in Table 5.1, show that all studied binary oxides are stable, as expected. For comparison, where available, the experimental values are also shown.

Figure 5.5 shows the band alignment for the studied binary oxides, where the positions of CBM and VBM with respect to their BPEs are indicated. The results using both the PBE and HSE06 functionals are shown. For In<sub>2</sub>O<sub>3</sub>, the calculated band gap and the positions of CBM and VBM are in good agreement with experimental and other theoretical results [174]. The position of the BPE in In<sub>2</sub>O<sub>3</sub>, above the CBM, indicates that it should be readily doped *n*-type, while doping it *p*-type should be more difficult, which is indeed a well known experimental fact [187]. Figure 5.5 also shows that Ga<sub>2</sub>O<sub>3</sub> in its bixbyite structure is a good *n*-type TCO candidate. It is interesting

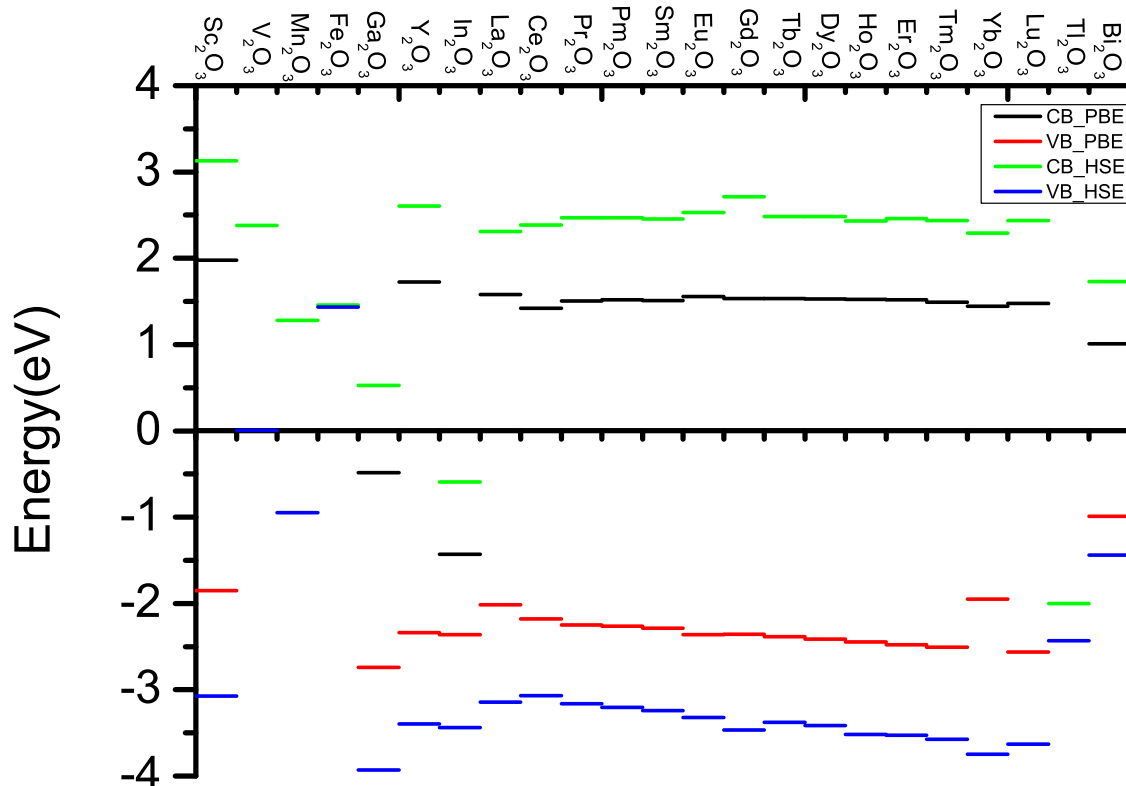


Figure 5.5: The band alignment of binary oxides, comparing the positions of the CBM and VBM calculated using the PBE and HSE06 functionals. The band edges are aligned with respect to the BPE. For the materials that PBE describes as metallic, only HSE results are shown. These materials include  $V_2O_3$ ,  $Mn_2O_3$ ,  $Fe_2O_3$ , and  $Tl_2O_3$ .

to note that  $Ga_2O_3$  in its monoclinic phase ( $\beta$ - $Ga_2O_3$ ) has a band gap of 4.9 eV and exhibits *n*-type conductivity [188]. Furthermore, one can see in Fig. 5.5 that bixbyite  $V_2O_3$ , with a band gap of 2.4 eV, is an interesting candidate material for a *p*-type TCO. In its corundum ground state structure  $V_2O_3$  is a metal. The structural phase transition from corundum to monoclinic occurs at 170 K [189]. In its monoclinic phase  $V_2O_3$  is an antiferromagnetic insulator with a band gap of 0.6 eV [190]. The study of  $V_2O_3$  is mostly limited to its metal-insulator transition. However, vanadium sesquioxide was recently synthesized in the bixbyite structure [164], and several of its basic properties have now been reported [165, 191].



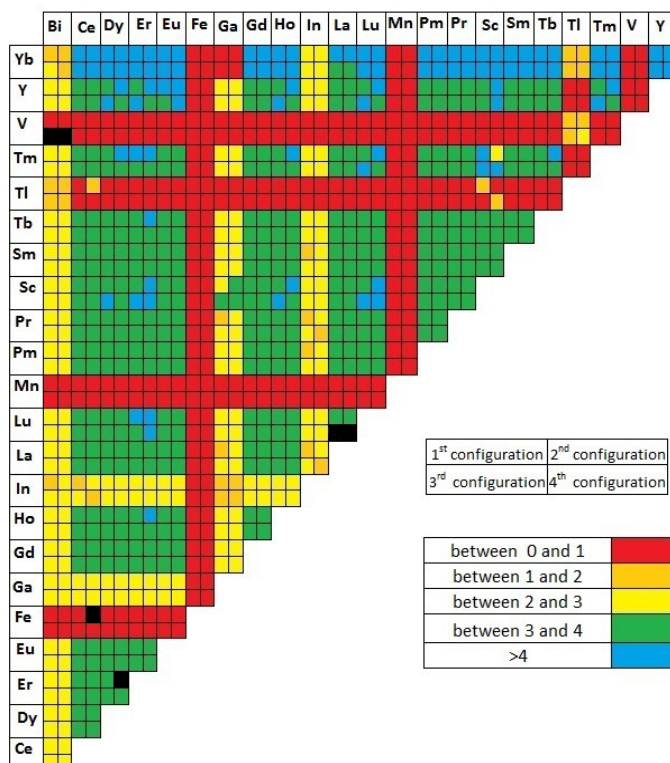


Figure 5.6: PBE band gap for the 50% ternary compounds. The cells for each pair of cations are subdivided in four subcells, corresponding to the four possible configurations considered.

### 5.3.2 Ternary oxides

We calculate the formation energy, lattice parameter, band gap, and positions of the band edges of the ternary compounds generated as indicated above. The calculations are done with the PBE functional in our first approach (cf. Section 5.2.2). As mentioned, there are several possible configurations for a given alloying percentage. To see the effect of configuration on the properties of interest, we study the  $(A_{0.5}B_{0.5})_2O_3$  compounds. An analysis of the formation energies shows that 9%, 45%, 31%, and 13% of these oxides prefer the 1st, 2nd, 3rd, and 4th configurations considered, respectively. The difference between the lattice parameter of two comparing configurations is smaller than 5%. More importantly, the difference in the formation energies between two different configurations of more than 91% of the 50% ternaries, is smaller than 5%. This indicates that the configuration has a small effect on the stability triangle. Also, we find that for more than 95% of the 50% ternary oxides, the difference between the band gap of two different configurations is smaller than 10%. The configuration has a similarly weak effect on band alignment. Thus, we consider

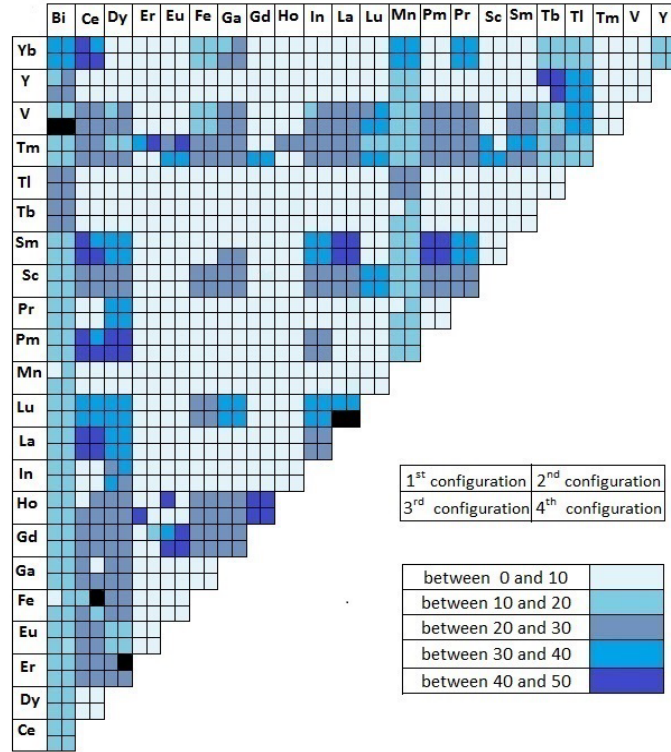


Figure 5.7: PBE calculated percent of the stability area of the 50% ternary compounds with respect to the total area of the stability triangle. The cells are subdivided as in Figure 5.6.

that including all possible configurations in this study would not alter significantly our conclusions. Figs 5.6 and 5.7 illustrate the capability of high-throughput calculations, where band gap (Fig. 5.6) and stability triangle (Fig. 5.7) of the 50% alloys (253 oxides) are screened. The different colors indicate how close or far the different oxides are to fulfill the screening criteria. There are four boxes for each oxide, representing the four different configurations considered. Black boxes indicate the very few cases in which the calculations failed to converge.

To analyse the effect of alloying concentration on the band gap and lattice constant, we compare the calculated values with those obtained using Vegard's law [192]. For the lattice constant, the latter predicts

$$a_{A_xB_{1-x}} = xa_A + (1 - x)a_B. \quad (5.6)$$

The analysis of the results shows that the Vegard's law is satisfied by most of the ternary oxides considered. Indeed, for more than 91% of all four configurations of the 50% alloys the difference

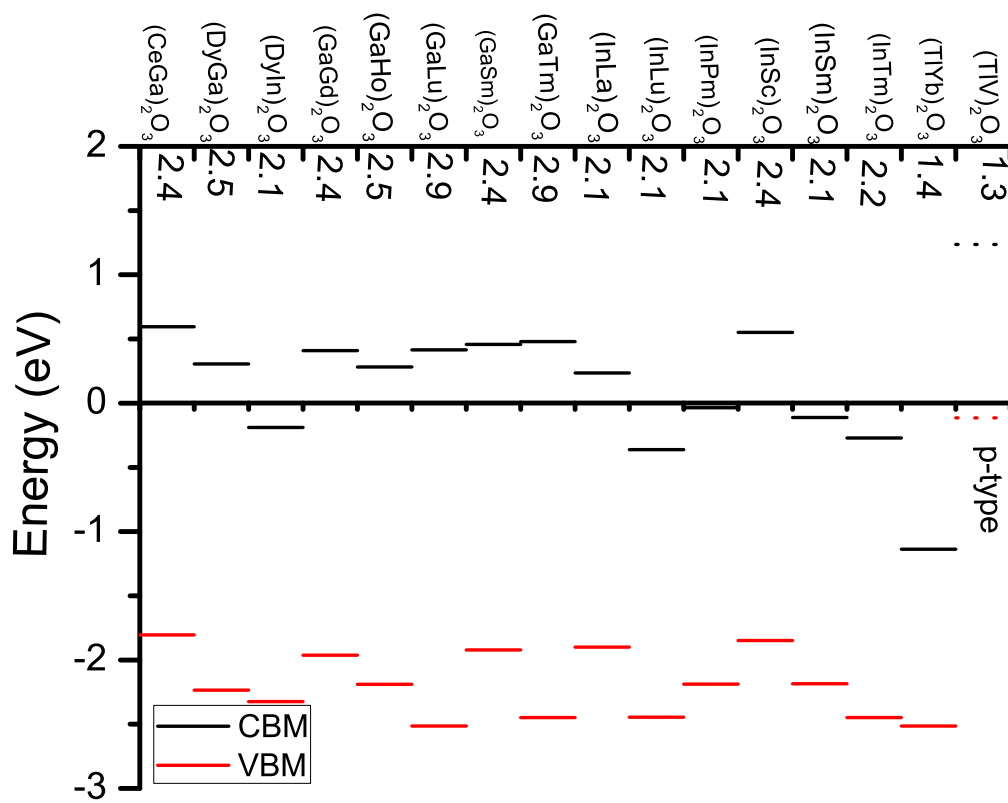


Figure 5.8: PBE band alignment of the most stable configuration of the 50% ternary compounds.<sup>1</sup>

between the calculated lattice parameter and the interpolated value using Vegard's law is smaller than 5%. This is also the case for 98% of the 25%  $[(A_{0.25}B_{0.75})_2O_3]$  and 75%  $[(A_{0.75}B_{0.25})_2O_3]$  alloys. A similar comparison for the band gaps shows that for most of the studied ternary compounds, the deviation of the calculated band gap from Vegard's law is smaller than 10%. The difference is large only in the cases in which one of the binary oxides is wrongly predicted to be a metal by the PBE functional (namely,  $A=Fe, Mn, Tl$ , and  $V$ ). But, of course, in such cases Vegard's law cannot be applied to the band gap.

As indicated in the section devoted to computational aspects, in addition to the calculations based on the PBE functional, we estimate the band gaps, band alignment, and phase stability area for the ternaries by interpolating the HSE06 results for the binaries. The relatively good compliance with Vegard's law of the lattice parameter and band gap as a function of alloying concentration, already mentioned above, supports this approach.

By screening properties of the 1518 ternary oxides we generated and by discarding the oxides

<sup>1</sup>All calculated data are available in table. A.1 of the Appendix A.

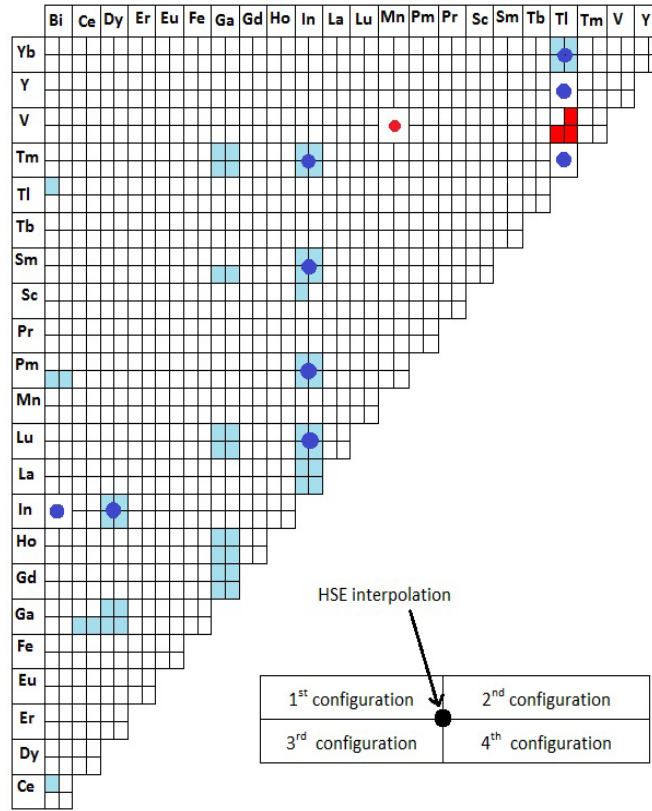


Figure 5.9: Identified 50% ternary oxide TCO candidates  $(A_{0.5}B_{0.5})_2O_3$ . Cell subdivision as in Fig. 5.6. A filled circle in the center indicates that the three screening criteria are fulfilled within the HSE06 interpolation scheme as well. Blue and red correspond to *n*-type and *p*-type TCOs, respectively.

which do not fulfill the three criteria we impose, we find a list of candidate TCOs. Thus, for instance,  $(Bi_{0.5}Ce_{0.5})_2O_3$  is a *n*-type TCO candidate in its 1st configuration, but that is not its most stable one among the four considered configurations, so it is not included in Fig. 5.8. In the case of  $(Tl_{0.5}V_{0.5})_2O_3$ , a *p*-type TCO candidate, the 3rd configuration is the most stable one. The calculations predict these to have band gap larger than 1 eV, *n*- or *p*-type band alignment, and a stability region in the stability triangle larger than 10%, and a band gap larger than 1 eV (2.5 eV) in the case of PBE (HSE06 interpolation) calculations.

Figure 5.8 illustrates the PBE band alignment of the 50% ternary oxides. For simplicity, in this plot we only consider the oxides for which the most stable (lowest energy) configuration fulfills the three screening criteria. As indicated before, for the 25% and 75% compounds, one of the possible configurations is chosen at random.

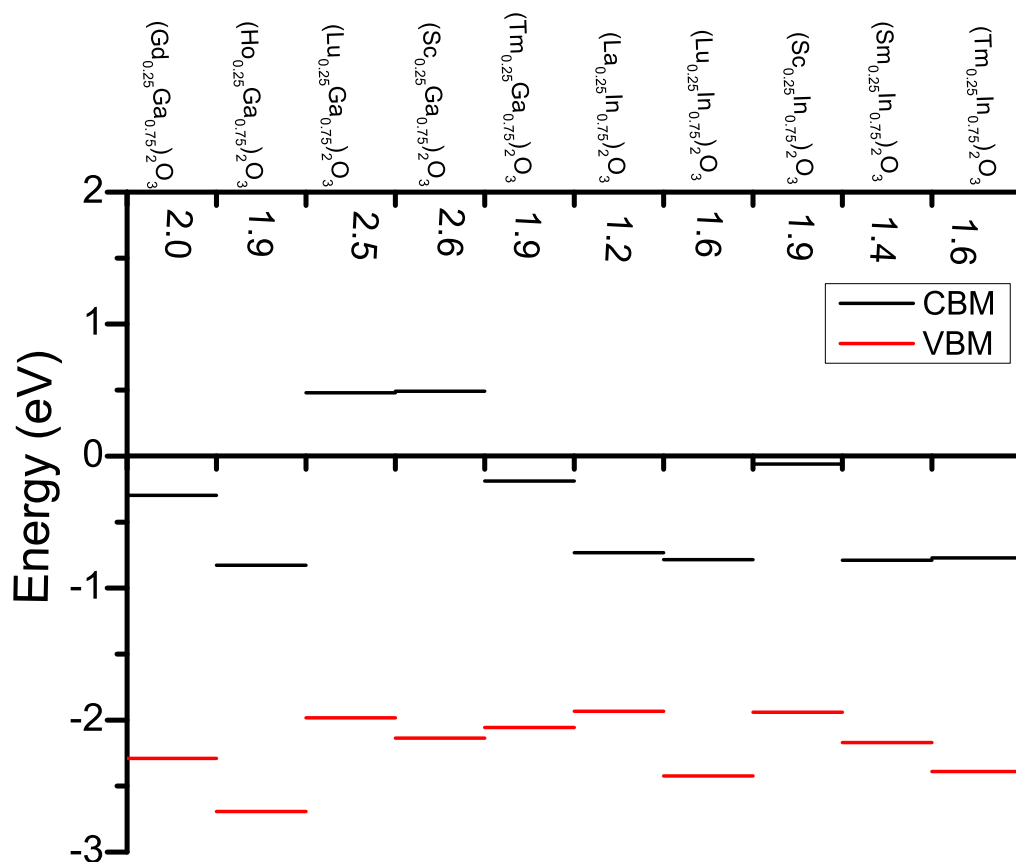


Figure 5.10: The band alignment of the *n*-type 25% ternary compounds from calculations based on the PBE functional. One possible configuration was considered for the calculations.

In Fig. 5.9, all the *n*-type and *p*-type 50% ternary oxides identified are presented, a colored box indicating that a given configuration fulfills all three criteria within the PBE approach. Thus, in some cases all configurations fulfill the required conditions, while in others only some do so. There is a full circle in the center when the HSE06 interpolation identifies an oxide as a good TCO (there is a single result because the configuration degree of freedom is absent in the interpolation approach). Blue and red indicate *n*- and *p*-type oxides, respectively.

Similarly, Fig. 5.10 shows the PBE band alignment of the 25% and 75% alloying *n*-type TCO candidates. As mentioned above, one random configuration was considered for these calculations. Figure 5.11 shows the all the identified 25% and 75% *n*- and *p*-type TCO candidates, both for the PBE and HSE06 interpolation calculations. Again, blue and red indicate *n*- and *p*-type oxides, respectively.

Examination of Figs. 5.9 and 5.11 shows the following. First, considering *n*-type TCOs, none

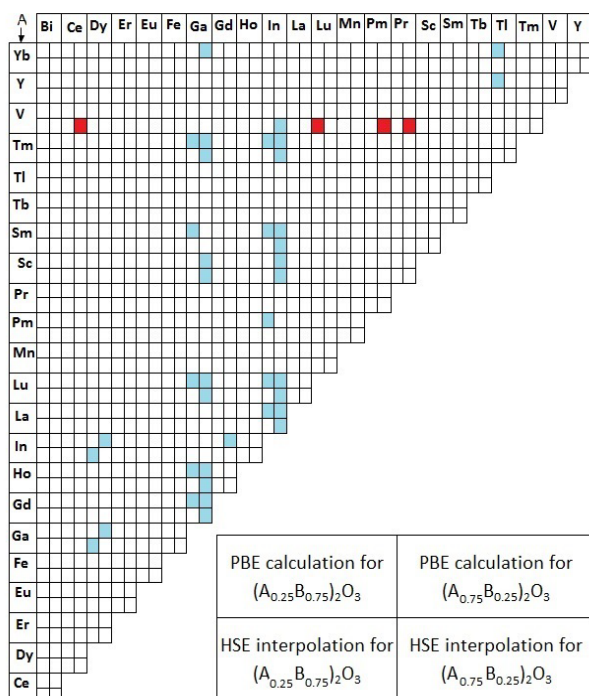


Figure 5.11: Identified potential 25%( $x=0.75$ ) and 75%( $x=0.25$ ) ternary oxide TCO candidates ( $A_xB_{1-x}$ ) $_2O_3$  (one random configuration). Color as in Fig. 5.9.

of the oxides containing Er, Eu, Fe, Pr, Mn, or Tb, fulfill all of the three selected criteria, in neither PBE or HSE06 interpolation approaches. On the other hand, there are a few elements that appear repeatedly in the  $n$ -type TCO ternary candidates. Indeed, it is striking that most of the  $n$ -type ternary oxides contain Ga and In, independently of the approach (PBE or HSE06 interpolation). Note that the approach based on the PBE functional produces noticeably more 50% alloying TCO candidates than HSE06 interpolation approach. This is not the case for the 25% of 75% alloys.

Turning to the  $p$ -type ternary oxides, it is interesting that the ternary  $p$ -type TCO candidates all contain V (cf. Figs. 5.9 and 5.11). There are far less candidates than for  $n$ -type TCOs, whether in the 50% or in the 25% and 75% alloying cases. In the 50% alloying case, the PBE approach produces a single candidate [(Tl<sub>0.5</sub>V<sub>0.5</sub>) $_2O_3$ ], while the HSE06 interpolation approach produces another single candidate [(Mn<sub>0.5</sub>V<sub>0.5</sub>) $_2O_3$ ] (cf. Fig. 5.9). In the 25% alloying case, the PBE approach results in no candidate, while the HSE06 interpolation results four candidates in the 25% ternaries (cf. Fig. 5.11). Interestingly, the latter also all contain V.

In order to examine whether the two procedures followed to obtain candidate TCO materials are reliable, we focus on the 50% alloying  $n$ -type ternaries and proceed as follows. We select those ternaries for which the most stable configuration is indeed a  $n$ -type TCO candidate according to

the PBE procedure, and which at the same time are found to be  $n$ -type candidates with the HSE06 interpolation procedure (cf. Table 5.2). The reliability of the HSE06 interpolation procedure is, of course, not limited to the 50% alloying cases. We illustrate this by comparing the interpolated band gaps to the HSE06 band gaps for two families of compounds, namely  $(\text{Dy}_x\text{In}_{1-x})_2\text{O}_3$  and  $(\text{Tl}_x\text{Yb}_{1-x})_2\text{O}_3$ , for  $x=0, 0.25, 0.5, 0.75$ , and 1. In Table 5.3 we compare three methods for calculating the band gap: PBE, HSE06, and HSE06 interpolated values of ternary materials. These results indeed show that the interpolated values are very close to those obtained directly from a HSE06 calculation for all values of  $x$ . Moreover, all three methods yield the same trend for the band gap value on changing the composition  $x$ .

Table 5.2: Comparing band gap and position of the band edges of the most stable configuration of 50% ternary oxides with PBE calculation, HSE calculation, and HSE interpolation results.<sup>†</sup>

| AB   | band gap(eV) | CBM   | VBM   |
|------|--------------|-------|-------|
| DyIn | 2.14         | -0.19 | -2.32 |
|      | 3.98         | 0.69  | -3.29 |
|      | 4.37         | 0.95  | -3.43 |
| InLu | 2.08         | -0.36 | -2.45 |
|      | 3.97         | 0.50  | -3.47 |
|      | 4.46         | 0.92  | -3.53 |
| InPm | 2.15         | -0.04 | -2.19 |
|      | 3.98         | 0.86  | -3.12 |
|      | 4.26         | 0.94  | -3.32 |
| InSm | 2.07         | -0.11 | -2.19 |
|      | 3.89         | 0.75  | -3.15 |
|      | 4.27         | 0.93  | -3.34 |
| InTm | 2.18         | -0.27 | -2.45 |
|      | 4.07         | 0.63  | -3.44 |
|      | 4.43         | 0.92  | -3.51 |
| TlYb | 1.38         | -1.14 | -2.51 |
|      | 2.24         | -0.40 | -3.44 |
|      | 3.24         | 0.14  | -3.09 |

<sup>†</sup> For each oxide, 1<sup>st</sup>, 2<sup>nd</sup>, and 3<sup>rd</sup> row of data refer to PBE calculation, HSE calculation, and HSE interpolation results.

The natural step following this study is to search for suitable dopants, i.e. dopants that act as shallow donors or acceptors in the identified oxides. Furthermore, one must make sure that the doping energy levels are stable against the formation of native defects [193]. Thus, further work is required to identify the impurities that will indeed convert these oxides in good  $n$ - or  $p$ -type TCOs. In the next chapter we study in details different defects in bixbyite  $\text{V}_2\text{O}_3$  in order to find shallow

Table 5.3: Comparing band gap of  $(\text{Dy}_x\text{In}_{1-x})_2\text{O}_3$ , and  $(\text{Tl}_x\text{Yb}_{1-x})_2\text{O}_3$  with PBE calculation, HSE calculation, and HSE interpolation results.

| compound   | $E_{g,PBE}$ | $E_{g,HSE}$ | $E_{g,HSEinterp.}$ |
|--|-------------|-------------|--------------------|
| $\text{In}_2\text{O}_3$                          | 0.93        | 2.85        | 2.85               |
| $(\text{Dy}_{0.25}\text{In}_{0.75})_2\text{O}_3$ | 1.57        | 3.44        | 3.61               |
| $(\text{Dy}_{0.5}\text{In}_{0.5})_2\text{O}_3$   | 2.14        | 3.98        | 4.37               |
| $(\text{Dy}_{0.75}\text{In}_{0.25})_2\text{O}_3$ | 2.27        | 4.26        | 5.13               |
| $\text{Dy}_2\text{O}_3$                          | 3.94        | 5.90        | 5.90               |
| $\text{Tl}_2\text{O}_3$                          | 0.01        | 0.44        | 0.44               |
| $(\text{Tl}_{0.75}\text{Yb}_{0.25})_2\text{O}_3$ | 0.46        | 1.67        | 1.83               |
| $(\text{Tl}_{0.5}\text{Yb}_{0.5})_2\text{O}_3$   | 1.38        | 2.24        | 3.23               |
| $(\text{Tl}_{0.25}\text{Yb}_{0.75})_2\text{O}_3$ | 2.25        | 3.09        | 4.63               |
| $\text{Yb}_2\text{O}_3$                          | 3.4         | 6.04        | 6.04               |

acceptor for this  $p$ -type oxide.

## 5.4 Conclusions

We present a density-functional based computational high-throughput scheme to screen a class of oxides in order to find new candidate TCO materials. The high-throughput method presented here can be easily applied to different classes of materials. Here, we screen the electronic properties of 1541 bixbyite oxides: 23 binaries and 1518 ternaries. The oxides are screened to ensure (i) a minimum band gap, guaranteeing a reasonable transparency in the visible, (ii) a minimum thermodynamic phase stability, and (iii) a positioning of the charge neutrality level in the band gap indicating easy  $n$ - or  $p$ -type dopability. Among the binaries, our calculations yield  $\text{V}_2\text{O}_3$ , a relatively simple system with a band gap of 2.4 eV, as an interesting possible  $p$ -type TCO. Our results indicate  $\text{Ga}_2\text{O}_3$  as a  $n$ -type candidate, besides  $\text{In}_2\text{O}_3$ . Among the ternaries, it is remarkable that most of the  $n$ -type candidates contain either Ga or In, while the  $p$ -type candidates all contain V. Focusing on the 50% alloys, a more robust short list of  $n$ -type candidates is produced by comparing the results of our two screening approaches (PBE calculation, and HSE interpolation) with full HSE06 calculations. The promising candidates thus identified, most of them with a band gap larger than 3 eV, are given by  $(\text{A}_{0.5}\text{B}_{0.5})_2\text{O}_3$  with  $\text{AB}=(\text{DyIn}, \text{InLu}, \text{InSm}, \text{InTm})$ . Although  $(\text{In}_{0.5}\text{Pm}_{0.5})_2\text{O}_3$ , and  $(\text{Tl}_{0.5}\text{Yb}_{0.5})_2\text{O}_3$  are in Table 5.2, we do not include them in the final list because Pm is radioactive, and Tl is toxic. Further research should identify the type of dopants that can effectively bring about these systems as TCOs.



# Shallow acceptors in bixbyite $V_2O_3$ , a novel $p$ -type conductor

## 6.1 Introduction

There is continued interest in the semiconductor research community in novel  $p$ -type conductors. This is motivated by the desire of improving the properties of the materials currently used in electronic components such as light emitting diodes, transistors, or photovoltaic cells, or by the need of finding alternative materials to those already used, for reasons of cost or ease of synthesis.

The  $p$ -type conductivity of a semiconductor depends on the specifics of the hole generation mechanism. Introducing a very small amount of impurities can improve the electronic properties of a semiconductor and make it conducting. Therefore, it is essential to understand the fundamental processes that determine the properties of impurities in order to control the hole generation and conductivity in semiconductors. This process starts by selecting a dopable semiconductor and then a proper defect that can possibly provide extra holes to contribute to the conductivity. How the defect might improve the conductivity of the host semiconductor can be calculated or measured experimentally. First-principles calculations make it possible to understand the behavior of the defects in semiconductors. It means that the stable position for a particular impurity in a semiconductor, total energies and then formation energies and transition levels can be calculated from first-principles. The first step of the investigation of the conductivity in a material, selecting a convenient semiconductor, is already performed in **Chapter 5**. The results of the DFT-based high-throughput screening of the properties of oxides with the bixbyite structure show that  $V_2O_3$  presents very promising  $p$ -type dopability [194]. Therefore, bixbyite  $V_2O_3$  can be an interesting semiconductor for  $p$ -type defect investigations.

---

The results of this chapter were published as: N. Sarmadian, R. Saniz, B. Partoens, and D. Lamoen, *Journal of Applied Physics* (2014)

Because of its unique properties, such as an intriguing metal-insulator transition [195], and its different applications in catalysts, and chemical sensors,  $V_2O_3$  has been the subject of numerous investigations [196, 197]. The study of  $V_2O_3$ , however, has been mostly limited to its rhombohedral (corundum) and monoclinic structures. Vanadium sesquioxide was only recently synthesized in the bixbyite structure [164], and although several of its basic properties have now been reported [165, 191], a more complete characterization requires further investigation.

The second step to realize a good conductivity in a material is to find a proper defect that can improve the conductivity in the host semiconductor. This is the main goal of this chapter. In this chapter, we first explain the defect calculation approach for a semiconductor and specifically  $p$ -type oxides, where we introduce related terms such as  $p$ -type defects, shallow and deep acceptor. The chapter continues by explaining some important properties in defect calculations like formation energies and transition levels. Finally we address specifically the prediction of  $V_2O_3$  in the bixbyite structure as a novel  $p$ -type conductor by calculating the formation energies and charge transition levels of V and O vacancies as native defects, and of elements Mg, Y, and Sc substituting V as impurities.

## 6.2 Defect calculations

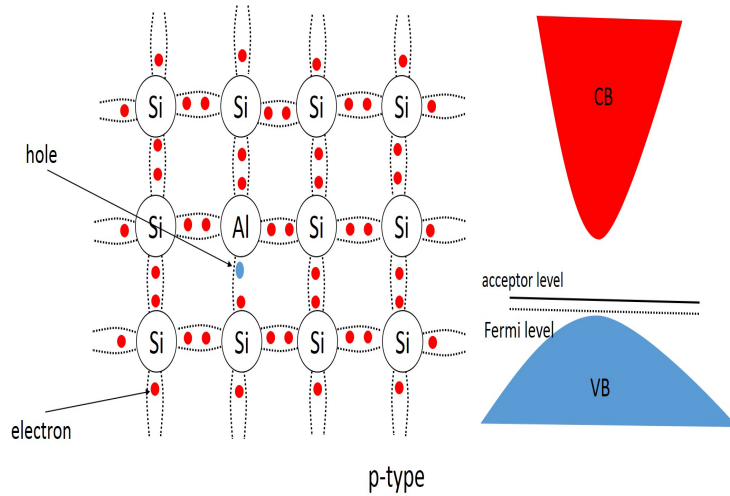


Figure 6.1: Schematic representation of (a) the crystal structure and (b) band structure of  $p$ -doped Si.

The mechanism of hole generation in semiconductors can be performed by introducing a low concentration (e.g. one impurity atom per million host atoms) of an acceptor defect in a semiconductor. The defects that increase the number of holes by reducing the number of free electrons in

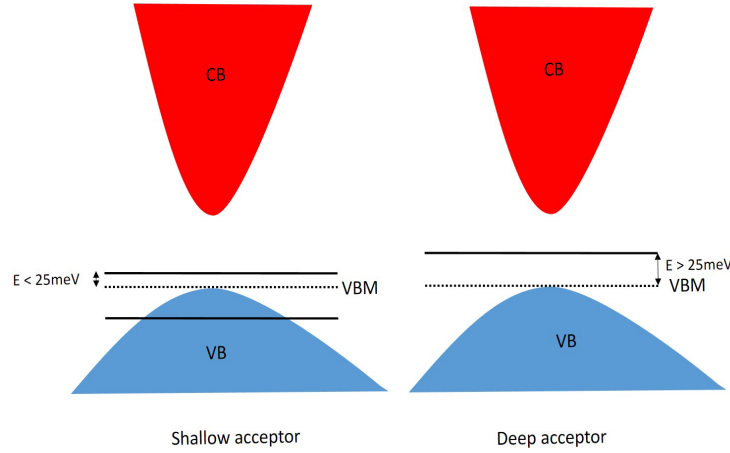


Figure 6.2: Schematic representation of shallow and deep acceptor level in a *p*-type semiconductor.

a semiconductor are referred to as acceptors. One can think about making a *p*-type oxide by substituting one silicon (Si) atom by an element that has at least one less valence electron than Si. Si has four valence electrons and each Si shares these four electrons in four covalent bonds with other four neighbor Si atoms. Substituting one Si by Al that has three valence electrons results in one less electron compared to the pure Si crystal. Generally speaking, the electron deficiency results in creating the dangling bond between defect and host atom close to the defect (i.e. between Al and Si atom) that would like to accept an electron. The acceptor alters the electronic band structure of the host and leads to a nonrigid shift of the Fermi level towards the valence band maximum. Fig. 6.1 shows the schematic representation of the *p*-type doping of crystalline Si.

This process of *p*-type doping leads to the creation of acceptor levels in the band structure of the host semiconductor. In the case that the acceptor level is located in the valence band or in the band gap but very close to the top of the valence band, the defect can be considered as a shallow acceptor. If the ionization energy of a shallow acceptor is comparable to the  $k_B T = 25$  meV, then the holes can be ionized and contribute to the conductivity at room temperature. If the acceptor level is located in the band gap and not close to the VBM, the acceptor is called deep and such an acceptor does not contribute to the conductivity. Fig. 6.2 shows schematically shallow and deep acceptor levels in a *p*-type semiconductor.

The position of the transition level between different charge states (i.e.  $q_1$  and  $q_2$ ) of a defect determines its shallow or deep character. The defect calculation investigates the position of such transition levels. The transition level  $\epsilon(q_1, q_2)$  can be calculated by using the formation energy of a defect in each charge state because it is just the Fermi energy for which the formation energy of charge states  $q_1$  and  $q_2$  are equal:

$$E_f[D^{q_1}] = E_f[D^{q_2}]. \quad (6.1)$$

The formation energy of a specific charge state  $q$  of a considered defect  $D$  is defined as

$$E_f(D^q) = E_{tot}(D^q) - E_{tot}(bulk) - \sum_i n_i \mu_i + q(E_F + E_v + \Delta V) \quad (6.2)$$

where  $E_{tot}(D^q)$  is the total energy of the cell containing the defect and  $E_{tot}(bulk)$  is the total energy of the pure crystal (i.e.  $V_2O_3$  in this chapter).  $n_i$  is the number of atoms of type  $i$  added or removed from the cell ( $n_i < 0$  if the atom is removed, and  $n_i > 0$  if the atom is added).  $\mu_i$  is the corresponding chemical potential. The calculation of the chemical potentials will be explained at the end of this section.  $E_F$  refers to the Fermi energy and represents the chemical potential of the electron. It is measured with respect to the VBM of the pure crystal ( $E_v$ ) and varies between zero and the band gap value.

The defect containing and pure cells have different reference energies. In order to use the same reference energy level and align the potentials in the defect containing and pure cells,  $\Delta V$  has to be added to the formation energy of charged defects. To calculate  $\Delta V$ , first the potential of the defect containing cell in some point far from the defect has to be calculated. Then, it should be aligned with respect to the the potential of the pure cell. The potential difference resulted from this alignment is  $\Delta V$  [198]. It was shown by Lyons and co-workers that the potential alignment can also correct the finite cell size effects on the formation energies of a charged defect, with an accuracy comparable to that of other methods [199].

As Eq. (6.2) shows the formation energies depend on the chemical potentials, which in turn depend on the experimental growth conditions. It means that in the case of the binary oxides like bixbyite  $V_2O_3$ , the limits of the chemical potential for V and O are imposed by the formation of  $V_2O_3$  in the bixbyite phase. The V and O chemical potentials,  $\mu_V$  and  $\mu_O$  respectively, are mutually dependent through

$$E_{tot}(bulk) = 2\mu_V + 3\mu_O. \quad (6.3)$$

The upper limit of the V chemical potential, representing extreme V-rich conditions, is given by its elemental bulk phase,  $\mu_V = \mu_{V(bulk)}$ . Likewise, the upper limit for the O chemical potential, representing extreme O-rich conditions, is given by molecular oxygen,  $\mu_O = \mu_{O(O_2)}$ . Moreover, the chemical potential of dopants is limited by the formation of the corresponding oxides. Thus, for instance, the chemical potential of Mg in bixbyite  $V_2O_3$  is determined by  $E_{tot}(MgO \text{ bulk}) = \mu_{Mg} + \mu_O$ .

### 6.3 Computational Method

We perform first-principles computations based on DFT [42, 45], using VASP code [70, 91]. The PAW [68, 92] potentials are used to describe the electron-ion interactions. We use the HSE06 hybrid functional [56, 57] approximation to the exchange-correlation potential, both for structural relaxation and formation energy calculations. This is of particular importance in the present study,

because the HSE06 functional is free of the band gap underestimation problem faced by other commonly used functionals, and is capable of a reliable description of defect levels in semiconductors [200]. Because of the computational cost of the HSE06 functional, we first perform our calculations on the primitive cell of the bixbyite structure, a body-centered cubic lattice (space group  $Ia\bar{3}$ , No. 206) with a basis containing 8 formula units, i.e., 40 atoms. Defects behaving as acceptors are then studied using the bixbyite conventional cell, containing 16 formula units, i.e., 80 atoms. An energy cutoff of 400 eV is used for the plane-wave basis set. For structure relaxation and total energy calculations the Brillouin zone of the primitive and conventional cells are sampled using a  $3 \times 3 \times 3$ , and a  $2 \times 2 \times 2$  MP grid, respectively [66]. Atomic relaxations are made until residual forces on the atoms are less than 0.01 eV/Å and total energies are converged to within 1 meV.

As already mentioned in section 5.2.1, V atoms occupy two inequivalent Wyckoff sites (*b*-site and *d*-site). This means that there are two possible inequivalent positions to substitute a V atom with a dopant atom. Note that a previous study showed that in the case of rare earth oxides with the bixbyite structure, if the substituting cation is larger than the host cation the dopant prefers the *b*-site, while the *d*-site is preferred if the substituting cation is instead smaller [201]. We will also look into this question in section 6.4.

## 6.4 Results

By performing full optimization of the lattice constant and atomic positions using the HSE06 hybrid functional, we obtain a calculated lattice parameter of 9.287 Å. This is in very good agreement with the experimental value of 9.395 Å [164]. First-principles calculations are reported in Refs. [164] and [191], but the calculated lattice parameters are not indicated, so a comparison is not possible. We find  $-10.43$  eV for the enthalpy of formation of  $V_2O_3$  in its bixbyite structure, which is 0.07 eV per formula unit higher than the enthalpy of formation we obtain for  $V_2O_3$  in the corundum structure. This is in line with the findings in the first studies reporting bixbyite- $V_2O_3$  as a metastable polymorph of vanadium sesquioxide. In those studies it is found that the bixbyite phase is about 0.09 eV per formula unit less stable than the corundum phase [164, 191]. It is also shown through quasiharmonic phonon calculations that the bixbyite phase is dynamically stable [164]. Our HSE06 calculations indicate that bixbyite  $V_2O_3$  is an indirect gap semiconductor, with the valence band maximum (VBM) at the  $\Gamma$  point and the conduction band minimum (CBM) at the H point, and a fundamental gap of 1.61 eV. The optical gap has a value of 1.98 eV and is located at the H point, although the optical gap at other  $\mathbf{k}$ -points is almost the same. Thus, the onset of optical absorption in this material should be rather clear in experiment. For some applications, such as light absorber layers, it is the optical gap that is relevant.

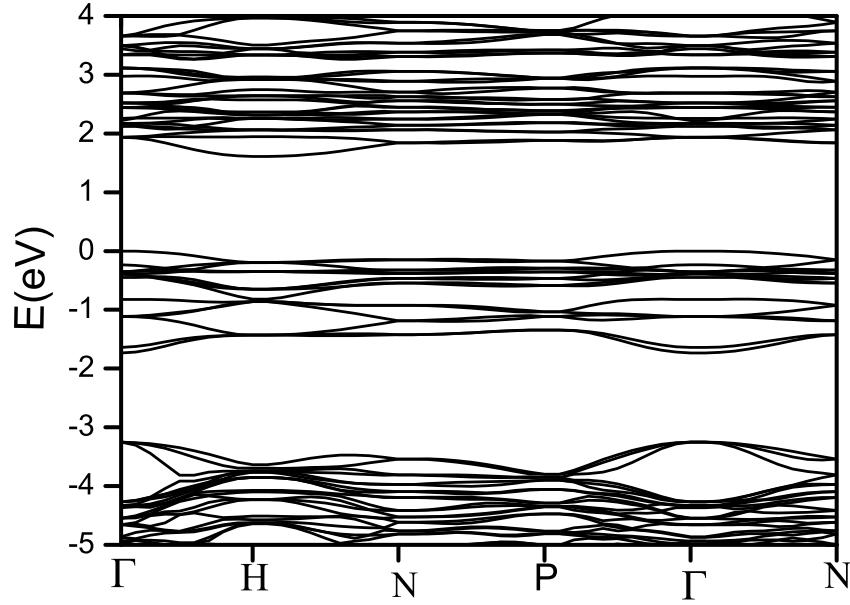


Figure 6.3: HSE06 calculated Band structure of bixbyite  $V_2O_3$ .

Figure 6.3 shows the band structure of bixbyite  $V_2O_3$  along high symmetry lines. Experimentally, the optical gap of bixbyite  $V_2O_3$  colloidal nanocrystals has been reported in Ref. 165, where UV-vis spectroscopy absorbance indicates a direct gap of 1.29 eV. There can be several reasons for the discrepancy between our result and experiment. In Ref. 165, it is indicated that the nanocrystals have a structure that is closer to the fluorite structure, due to the filling of the oxygen vacancies in the original bixbyite structure, and present a uniform lattice expansion with respect to the latter. Hence, the observed gap in the nanocrystals may not be directly comparable to our calculated results because a lattice expansion usually results in a gap reduction, and the oxygen interstitials may give rise to impurity states in the gap, resulting again in an apparently smaller gap compared to the bulk bixbyite gap. On the other hand, it appears that the HSE06 functional tends to overestimate the band gap of vanadium oxides. This is the case for  $VO_2$  and  $V_2O_5$ , [202, 203] and it might also be the case for  $V_2O_3$ , further contributing to the mismatch between our result and the reported value. However, it is important to recognize that the exact value of the band gap has very little bearing on the energy levels of the acceptor impurities we study in this work.

We note that the ground state structure of the bixbyite phase of  $V_2O_3$  is found to be canted antiferromagnetic, with a phase transition to a paramagnetic phase around 50 K [164]. Focusing on applications at room temperature, or at temperatures slightly above that, we can safely ignore magnetic effects in our calculations and consider bixbyite  $V_2O_3$  as paramagnetic.

The mobility of the holes in a  $p$ -type material depends on the hole effective mass matrix. The bixbyite structure is cubic, so the corresponding matrix at the VBM is isotropic and it suffices to calculate the hole effective mass along one direction. We find a value of 6.807 along the  $\Gamma$ -X

direction. This value is somewhat high, but the high doping concentrations considered here can nevertheless lead to reasonably good conductivities.

As discussed in section 5.2.3 the position of the CBM and VBM of a material with respect to its branch-point energy (BPE) can indicate whether it is *n*- and/or *p*-type dopable [155]. If the BPE falls low in the band gap, or below the VBM, then the material will be easily doped *p*-type. The BPE can be calculated as a weighted average of the midgap energies over the Brillouin zone using the Eq. (5.1).

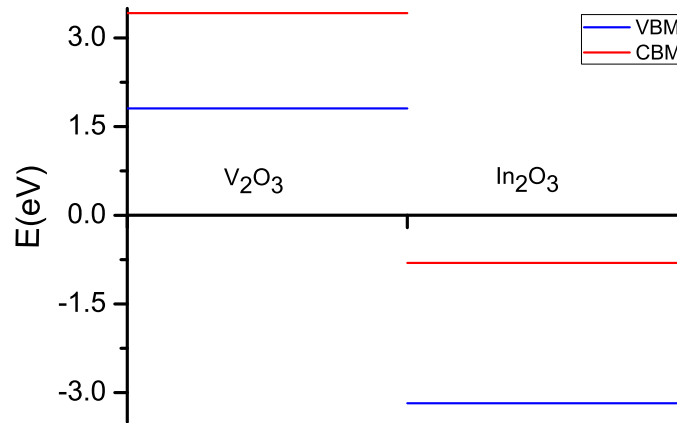


Figure 6.4: Band alignment of  $V_2O_3$  besides  $In_2O_3$ .

In Fig. 6.4, on the left side we plot the band edges of  $V_2O_3$  with respect to the BPE, setting the latter to 0 eV. One can readily see that it can be considered as a *p*-type dopable oxide. Hence, it should be possible to find dopants leading to shallow, or near shallow, acceptor levels in this oxide. For comparison, on the right side of Fig. 6.4 we present the alignment of the band edges of  $In_2O_3$  with respect to the BPE, showing its well known *n*-type dopability character.

In general, *p*-type behavior may result from an intrinsic defect, such as a cation vacancy, or from an extrinsic defect, such as cation substitution with a foreign atom with less valence electrons. Indeed, this may result in a net electron deficiency and might give rise to acceptor levels. Thus, we consider first a vanadium vacancy, which we denote  $V_V$ . As extrinsic defect we consider  $Mg_V$ , because the typical valence of Mg is 2+, whereas V in  $V_2O_3$  has in principle a valence 3+. One can also consider substituting V with group 3 elements. Although the typical valence of the latter is also 3+, the resulting isovalent center might behave as an acceptor, a donor, or remain electrically neutral [204]. Hence, we consider the  $Sc_V$  and  $Y_V$  substitutional defects in this study. Finally, it is important to consider  $V_O$ , i.e., oxygen vacancy defects. Indeed, the latter may give rise to donor levels that could compensate the potential acceptor levels created by the previous defects, precluding any *p*-type behavior.

As indicated above, there are two inequivalent V positions in the bixbyite structure, and it is necessary to determine the preferred substitutional site. Table 6.1 compares the total energy of atoms A ( $A = Mg, Sc, \text{ and } Y$ ) replacing V on the inequivalent *b*- and *d*-sites. It shows that all

three dopants prefer the  $b$ -site. Therefore, all formation energy calculations are performed with the substitutional dopants residing on this site. Table 6.1 also compares atomic radii for the three dopants and shows that Mg has a better lattice match than the other two.

Table 6.1: Comparison of atomic radii $\S$  and total energy for A-doped  $V_2O_3$  (A= Sc, Y, and Mg) with A substituting V in the two possible inequivalent positions.

| A  | $\Delta R_{A,V}^\dagger(\text{\AA})$ | $\Delta E_{b,d}^\ddagger(\text{eV})$ |
|----|--------------------------------------|--------------------------------------|
| Sc | 0.25                                 | -0.18                                |
| Y  | 0.45                                 | -0.16                                |
| Mg | 0.15                                 | -0.15                                |

$^\dagger\Delta R_{A,V} = R_A - R_V$  where  $R_A$ , and  $R_V$  are the atomic radius of substitutional impurity, and V atom, respectively.

$^\ddagger\Delta E_{b,d} = E_b - E_d$  where  $E_b$  and  $E_d$  are the total energy of the defect system when the substitutional atom sits on the b-, and d-site, respectively.

$\S$  values from Ref. [205]

We use Eq. (6.2) to calculate the formation energy of different charge states of various considered defects in  $V_2O_3$ . We take into account that the chemical potential of dopants, i.e., Mg, Sc, or Y is limited by the formation of the corresponding oxide, i.e., MgO,  $Sc_2O_3$ , or  $Y_2O_3$ , respectively. Thus, for instance, the chemical potential of Mg is determined by  $E_{\text{tot}}(\text{MgO bulk}) = \mu_{\text{Mg}} + \mu_{\text{O}}$ . A corresponding expression applies to Sc and Y.

Fig. 6.5 plots the formation energy of the most stable charge states of the intrinsic and extrinsic defects considered in  $V_2O_3$  as a function of the Fermi energy  $E_F$  for both V-rich (Fig. 6.5(a)) and O-rich (Fig. 6.5(b)) conditions. One can see immediately that  $Y_V$  and  $Sc_V$  are very deep donors, with a transition level from charge state  $+$  to 0,  $\epsilon(+/0)$ , lying low in the band gap. Thus, in both cases isovalent doping results in an essentially electrically neutral impurity. Note that the oxygen vacancy ( $V_O$ ), which is a potential compensating native defect, has a high formation energy and occurs in its neutral state. Hence, it does not pose a problem to any possible  $p$ -type behavior.

The defects of interest to our study are  $V_V$  and  $Mg_V$ , which present transition levels  $\epsilon(0/-2) = 0.19$  eV and  $\epsilon(0/-) = 0.17$  eV, respectively, above the VBM, and thus act as acceptors. The question is whether these acceptors are shallow enough to give rise to  $p$ -type conductivity at, e.g., room temperature. For this we study these defects in the bixbyite conventional 80-atom cell. This represents an impurity concentration of 1.25 at.%, which corresponds to the typical concentrations in  $n$ - and  $p$ -type conducting oxides [206, 207]. In Fig. 6.6 we compare the transition levels of these two defects in the primitive and conventional bixbyite cells, both in V-rich [Fig. 6.6(a)] and O-rich [Fig. 6.6(b)] conditions. We immediately see that  $Mg_V$  becomes a shallow acceptor at this concentration, with the  $\epsilon(0/-)$  lying below the VBM. Furthermore, its formation energies remain low, while those of  $V_O$  (not shown) remain high. Thus, we predict Mg-doped  $V_2O_3$  to be a stable  $p$ -type conductor. The behavior of the  $V_V$  defect is somewhat different. In the bixbyite primitive



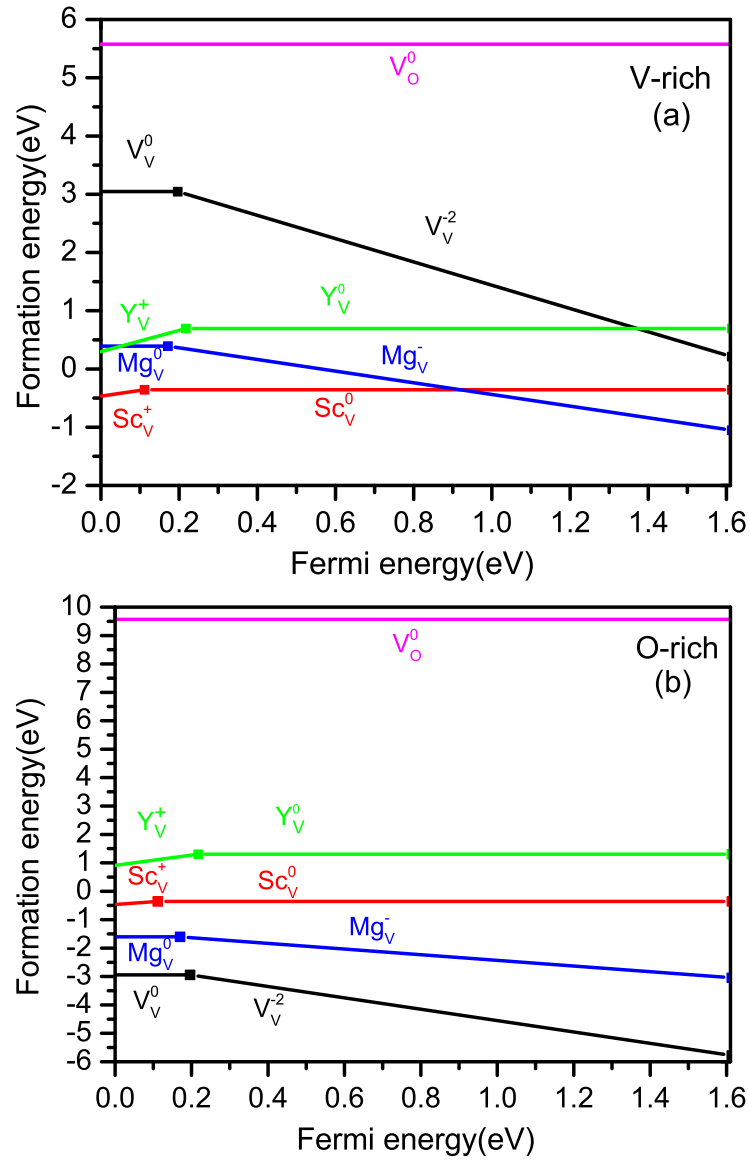


Figure 6.5: Calculated intrinsic defect and impurity formation energies as a function of the Fermi energy under (a) V-rich, and (b) O-rich conditions. The calculations are performed for the primitive cell of  $V_2O_3$  using the HSE06 functional.

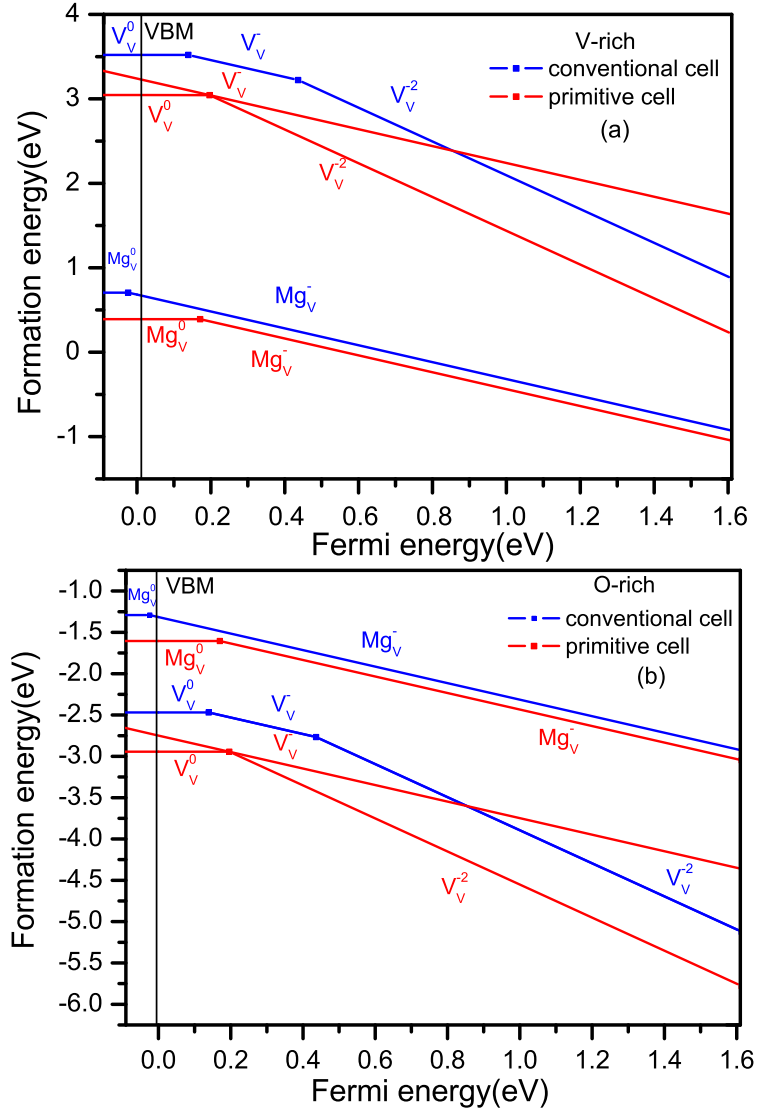


Figure 6.6: The effect of diluting the defect concentration on the position of the transition level. The calculated formation energies of  $Mg_V$  and  $V_V$  as a function of the Fermi energy under (a) V-rich, and (b) O-rich conditions with HSE06.

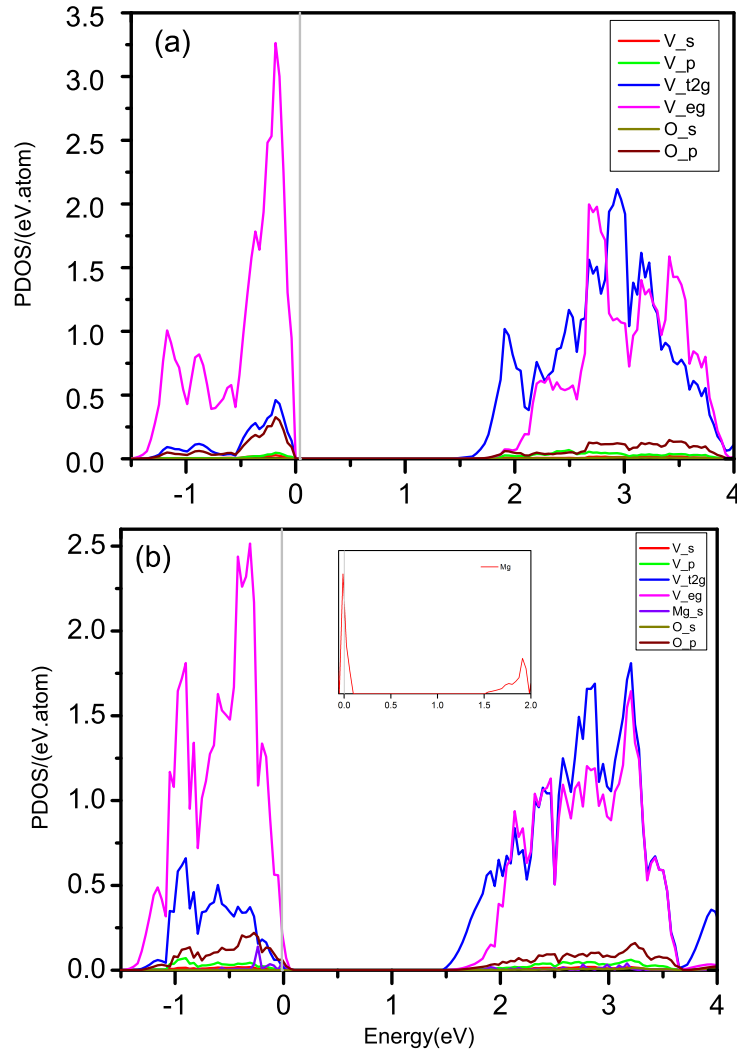


Figure 6.7: HSE06 calculated PDOS of (a) pure  $\text{V}_2\text{O}_3$ , and (b) Mg doped  $\text{V}_2\text{O}_3$  for primitive bixbyite cell.

cell, the  $\epsilon(0/-)$  transition level of this defect (not seen in Fig. 6.5, shown in Fig. 6.6) is slightly above the  $\epsilon(0/-2)$  transition level, with both transition levels almost touching. As shown in Fig. 6.6, in the conventional cell  $\epsilon(0/-)$  lies clearly below  $\epsilon(0/-2)$ , at a energy 0.14 eV above the VBM. Thus, as an acceptor,  $V_V$  is shallower in the conventional cell by 0.05 eV compared to the primitive cell.

For a more complete description of the system studied, Fig. 6.7 plots the projected density of states (PDOS) for  $V_2O_3$  and Mg-doped  $V_2O_3$ . From Fig. 6.7(a) it can be seen that the character of the VBM and CBM of  $V_2O_3$  is  $V_{eg}$ , and  $V_{t_{2g}}$ , respectively. Note that the fact that the VBM and CBM consists of V 3d states appears to be typical of  $V_2O_3$ , occurring also in its other phases. This is thought to be linked to its Mott-Hubbard insulator behavior at low temperature [208]. In Mg-doped  $V_2O_3$ , the Fermi level lies below the VBM, as expected. This leads to the empty states seen as a small shoulder with partial Mg character just above the Fermi level.

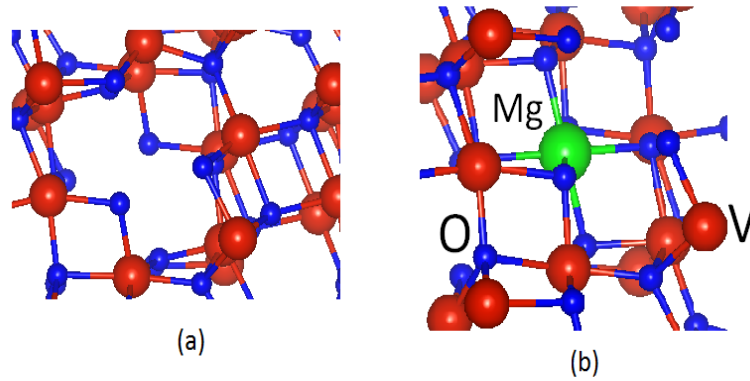


Figure 6.8: Relaxed atomic geometries for (a) V vacancy, and (b) substitutional Mg in bixbyite  $V_2O_3$ . Red, blue, and green spheres show V, O, and Mg atoms, respectively.

Table 6.2: Cation-O bond lengths ( $\text{\AA}$ ) for nearest neighbors in case of defective  $V_2O_3$  compared with the 2.00  $\text{\AA}$  bond length between b-site V and O.

| Site   | bond length |
|--------|-------------|
| $Sc_V$ | 2.07        |
| $Y_V$  | 2.21        |
| $Mg_V$ | 2.05        |
| $V_V$  | 2.21        |

Finally, table 6.2 summarizes the cation-O bond lengths in each defect system before and after optimization. Fig. 6.8 shows the relaxed positions of the  $V_V$  and  $Mg_V$  in  $V_2O_3$ . All substitutional

atoms prefer to sit at the b-site (cf. Table 6.1), where, because of symmetry, the A-O bond lengths of all six nearest neighbors are the same. Hence, there is only one bond length parameter for the nearest neighbors of each dopant. In the unrelaxed structure the bond length is 2.00 Å. After optimization of the atomic positions, the bond length changes. Comparing table 6.2 and table 6.1 we can see that by increasing the atomic radius of atom A (from Mg to Sc and then to Y), the A-O bond length increases.

## 6.5 Conclusions

We reported on the electronic structure and defect properties of  $V_2O_3$  as a novel *p*-type conductor. We studied Mg, Y, and Sc as impurities substituting V, as well as oxygen and vanadium vacancies as native defects. Our DFT calculations show that, as in other bixbyite oxides, dopants with an atomic radius larger than the one of V prefer to substitute it on the b-site, rather than the d-site. We represented that  $Mg_V$  acts as a shallow acceptor, with a low formation energy. Furthermore, we found that oxygen vacancies are electrically neutral, and hence do not behave as hole-killing defects. Thus, we predict Mg-doped  $V_2O_3$  to be a *p*-type conductor. We also showed that  $V_V$  acts as a relatively shallow acceptor, with an activation energy of 0.14 eV. Thus, it may also lead to *p*-type conductivity. On the other hand, we found that substitutional Sc and Y ( $Sc_V$  and  $Y_V$ ) behave as deep donors.



# Identification of *p*-type TCOs based on first-principles calculations

## 7.1 Introduction

*P*-type transparent conducting oxides (TCOs) have multiple uses in optoelectronic devices such as light emitting diodes (LEDs), transparent thin film transistors, and solar cells [209–211]. Current *p*-type TCOs have limitations in stability, present difficulties during synthesis, or are unable to match the conductivities of *n*-type TCOs. This has fueled the search for new *p*-type TCOs, capable of improving device performance or enabling new devices. Two of the most important properties of a host TCO are the (direct) band gap and the effective mass. The former should prevent the absorption of visible light and the latter should bolster the mobility of the charge carriers. The hole effective mass of the well-known Cu based delafossite *p*-type TCOs (e.g. SrCu<sub>2</sub>O<sub>2</sub>, CuCrO<sub>2</sub>, and CuAlO<sub>2</sub>), is around 4–7  $m_e$ , with a band gap generally  $> 3$  eV [212]. ZnO, which doped with Al is a leading *n*-type TCO, has a band gap of 3.4 eV, and a hole effective mass between 0.29 and 2.55  $m_e$ , depending on the direction [213]. For this reason, there have been concerted efforts to obtain *p*-type doped ZnO. In spite of this, to date no stable *p*-type doping of ZnO has been achieved. Thus, a wide enough band gap and low effective mass do not promise a stable *p*-type TCO. A property indicating easy *n*- or *p*-type dopability is the position of the branch-point energy (BPE) [155]. In ZnO the BPE lies just above the conduction band minimum (CBM) [155], which is why it proves hard to dope *p*-type. To be easily *p*-type dopable a material should have its BPE low in the band gap or below the valence band maximum (VBM). For practical purposes, moreover, a new TCO should be relatively simple to synthesise. In view of very large number of existing oxides that can be studied for possible TCO applications, a systematic experimental study is not possible. High-throughput *ab initio* computations, on the other hand, can be used to screen large classes of materials, searching for those that exhibit a predetermined basic set of properties, qualifying them

as potential candidates for a specific application [108, 143]. This approach has recently been used successfully in the search for novel materials for various applications [118, 146, 147, 214].

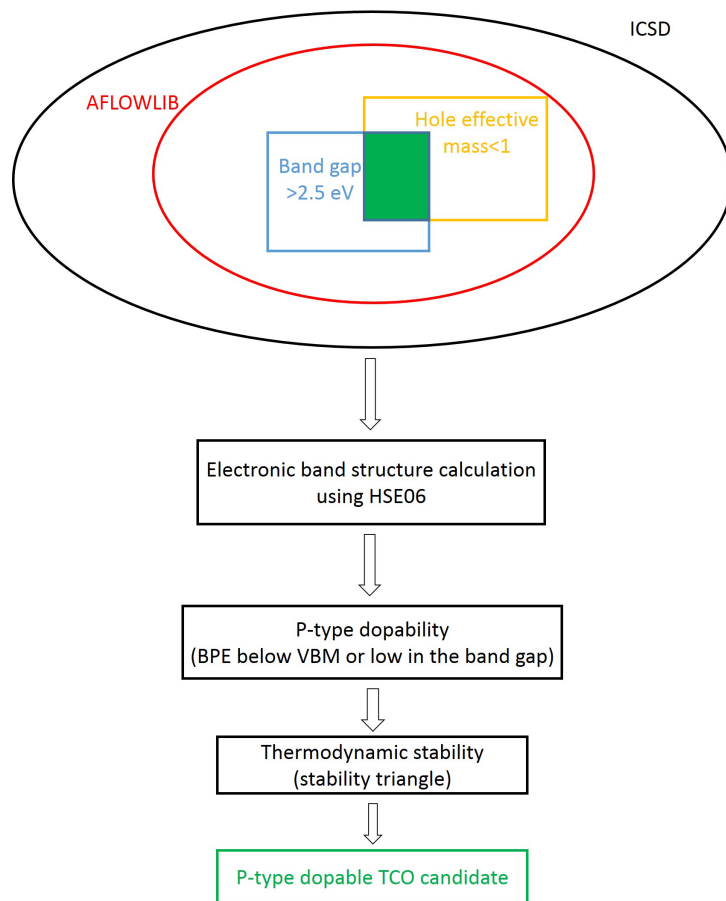


Figure 7.1: The high-throughput screening procedure to identify new *p*-type TCO candidates starting from the binary, ternary, and quaternary oxides in the AFLOWLIB database.

In **Chapter 5** we have introduced a DFT-based high-throughput screening approach to identify new compounds for TCO applications. We applied our approach to binary and ternary bixbyite oxides, which resulted in a list of new compounds as candidate TCOs [194]. In this chapter, we present the results of applying a similar approach to identify specifically *p*-type TCO candidates with competing properties regarding band gap and hole effective mass, and which at the same time are easily *p*-type dopable and thermodynamically stable. We follow the high-throughput approach schematically represented in Fig. 7.1. We first screen all the binary, ternary, and quaternary oxides in the AFLOWLIB computational database [215, 216], all of them existing oxides from the Inorganic Crystal Structure Database (ICSD) [217]. The screening criteria are (i) a minimum band gap of 2.5



eV guaranteeing a reasonable transparency in the visible light energy range, and (ii) a maximum effective mass of  $1 m_e$ , contributing to a high mobility. Figure 7.2 shows the hole effective mass versus the band gap of such compounds. As it is clear from Fig. 7.2, there are a lot of compounds that have large band gap and low hole effective mass. However, not all of them are *p*-type dopable. Therefore, at this stage the main goal is to identify *p*-type dopable compounds among those that are presented in Fig. 7.2.

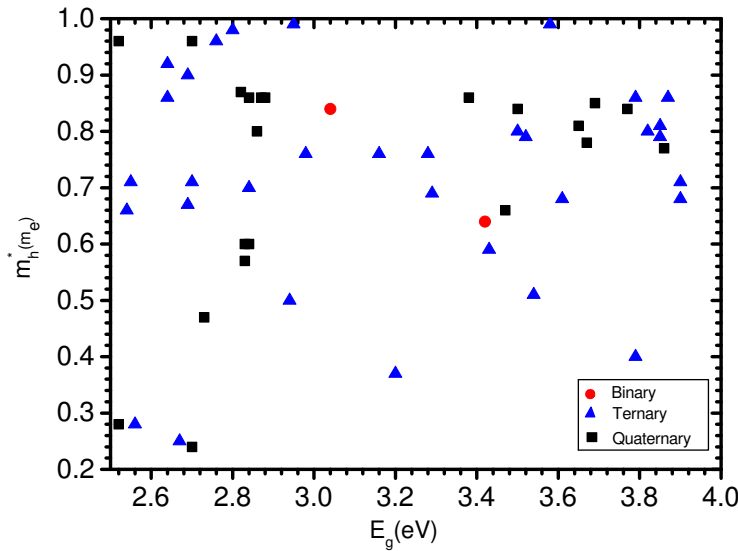


Figure 7.2: Effective mass versus band gap for the compounds that have effective mass lower than  $1 m_e$  and band gap larger than 2.5 eV (based on the data from the AFLOWLIB database) [215].

We calculate the electronic structure of all the oxides that meet two mentioned conditions. By applying the approach that is already discussed in section 5.2.3, we calculate the position of the BPE and align the band edges with respect to the BPE. Then a screening of the compounds based on their BPE position is performed. The oxides for which the BPE level falls in the valence band or low in the band gap, within one-fourth of  $E_g$  above the VBM are considered as *p*-type dopable oxides. (cf. Fig. 5.3) Before proceeding, since the AFLOWLIB database does not provide theoretically accurate band gaps (cf. further down for details), to avoid investing resources on candidates that in fact have a low gap, it is convenient to try to verify whether the band gaps of the materials found to be *p*-type dopable are indeed at least 2.5 eV wide. We determine the BPE by performing the electronic structure calculations. The candidates that present a minimum thermodynamic stability against phase segregation (a quantitative criterion is given in the next section) make our final list of potential *p*-type TCOs.

We note that a high-throughput search of *p*-type TCO candidates was performed previously by other authors in Ref. 147. Our working scheme differs from theirs in two important respects. First, the selecting criteria in Ref. 147 were a calculated band gap of at least 1 eV (DFT calculations

performed with the PBE exchange-correlation functional) and a hole effective mass  $< 1.5 m_e$ . Second, and more importantly, *p*-type dopability and thermodynamic stability are not included as screening criteria in that study. The difference in the resulting lists are discussed in Section 3. In this chapter, we first present the computational methodology used, discussing the different steps of our approach in more details. It continues with a discussion of the results. Finally, we conclude this chapter by summarizing our main findings.

## 7.2 Computational Method

We carry out the *ab initio* computations based on DFT [42, 45] using the VASP code [70, 91, 136, 148]. We use the HSE06 hybrid functional for the exchange-correlation potential [56, 57] to calculate the lattice parameters and to relax the atomic positions, as well as to determine the electronic structure. The HSE06 hybrid functional is currently the functional of choice when it comes to describe the electronic structure of semiconductors, accounting very well for their band gaps [149]. To calculate effective masses and formation energies, we use instead the PBE functional, because it is sufficiently accurate for those properties and is computationally inexpensive. As we discussed in section 4.6 in a high-throughput approach, it is impractical to perform rigorous energy cutoff and  $\mathbf{k}$ -point convergence studies during the screening procedure. Thus, we use an energy cutoff of 400 eV for the plane-wave basis set, which is sufficiently high to ensure convergence. To sample the Brillouin zone, we use a MP grid [66], making sure that the  $\Gamma$  point is included in the mesh. For the number of  $\mathbf{k}$ -points in the mesh, we follow Ref. 218, sampling the first Brillouin Zone using a grid of at least  $500/n$   $\mathbf{k}$ -points, where  $n$  is the number of atoms in the unit cell. The convergence tests are performed for the candidates selected at the end of the screening procedure, focusing on the BPE and formation energy. Finally, we note that atomic relaxations are made until residual forces on the atoms are less than 0.01 eV/Å and total energies are converged to within 1 meV.

The AFLOWLIB database provides theoretical data on the different materials that exist in the ICSD. All values in this database are based on calculations with the PBE functional, using the VASP code. The band gap reported is estimated from the PBE-calculated value via an energy dependent curve given by a least-squares fit to the experimental gaps of a set of 100 selected compounds. The root-mean-square of the percentage error of the fit is reported to be 24% [219]. This is reasonable for an initial high-throughput screening. Furthermore, for each material an average hole effective mass is reported, taking into account symmetry considerations and contributions from bands falling within 26 meV of the band edges (similarly for the effective electron mass) [215, 219]. For these calculations the PBE functional is used, which is known to give good effective mass values compared to experiment. Scanning all the binary, ternary, and quaternary oxides in the database, searching for those with a band gap larger than 2.5 eV, and a hole effective mass smaller than  $1 m_e$ , results in a list of 70 oxides, including 2 binary, 41 ternary, and 27 quaternary oxides. For the compounds for which the AFLOWLIB database reports a non-zero total magnetic moment, we performed spin-polarized calculations. For such compounds the *f*-electrons are treated as valence electrons. However, we screen out the numerous oxides that have a non-zero

total magnetic moment and at the same time contain toxic elements (As, Cd, Hg, Tl, and Pb).

Consequently, the list of oxides considered for the HSE06 calculations includes 2 binary, 37 ternary, and 21 quaternary oxides. (cf. Fig. 7.3).

The smallest unit cell of the oxides considered contains 5 atoms (e.g.  $\text{Er}_2\text{SeO}_2$ ), and the largest unit cell corresponds to  $\text{Bi}_{12}\text{PbO}_{20}$ , with 40 atoms. We perform a full optimization of the lattice constants and atomic positions, then we calculate the electronic structure. With this we proceed to calculate the BPE, which can be calculated as a weighted average of the midgap energies over the Brillouin zone [156, 157]. The method is already explained in details in Section. 5.2.3.

As already indicated, for the materials that qualify as easily *p*-type dopable and have a HSE06 band gap not less than 2.5 eV, the enthalpy of formation is calculated and the stability is analyzed. For this purpose, the chemical potentials of the different constituents have to be considered. The details about how to determine the stability area is already explained in Section. 5.2.4.

## 7.3 Results

Table 7.1 presents the list of oxides in the AFLOWLIB database that comply to the band gap and hole effective mass requirements indicated above. The table consists of two parts. In Part I, compounds with similar chemical formula and crystal symmetry, differing only by one atom type, are grouped together, with the crystal structure indicated. The rest of the compounds are presented in Part II. The first three columns present the lattice parameters. The next three columns give band gap, the hole and the electron effective masses reported in the AFLOWLIB database. For completeness, the reported electron effective mass is also given. The upper values for the lattice parameters are the experimental values, from the ICSD database, and the lower values are our calculated HSE06 results.

Table 7.1: lattice parameters ( $a$ ,  $b$ , and  $c$ ) in Å, fundamental band gap ( $E_g$ )(eV), and electron and hole effective mass ( $m_e^*$ , and  $m_h^*$  respectively) in units of the free electron mass  $m_e$ . The lattice parameters in the first row are from the ICSD database. The band gap and effective mass values in the first row are from the AFLOWLIB database. Second row of data presents HSE06 calculated values.

| oxide  | structure <sup>††</sup> | a    | b    | c     | $E_g$ | $m_e^*$ | $m_h^*$ |
|--|-------------------------|------|------|-------|-------|---------|---------|
| <b>part I</b>                                |                         |      |      |       |       |         |         |
| LiNbO <sub>2</sub>                           | HEX                     | 2.90 | 2.90 | 10.46 | 3.16  | 2.39    | 0.76    |
|  |                         | 2.90 | 2.90 | 10.32 | 2.39  |         |         |
| NaNbO <sub>2</sub>                           | HEX                     | 2.95 | 2.95 | 11.58 | 2.84  | 0.90    | 0.70    |
|  |                         | 2.95 | 2.95 | 11.46 | 2.32  |         |         |
| Pr <sub>2</sub> SO <sub>2</sub> <sup>†</sup> |                         | 3.93 | 3.93 | 6.75  | 4.03  | 1.11    | 0.84    |
|  |                         | 3.94 | 3.94 | 6.79  | 2.61  |         |         |

Table 7.1 Continued

| oxide  | structure <sup>††</sup> | a    | b    | c     | E <sub>g</sub> | m <sub>e</sub> <sup>*</sup> | m <sub>h</sub> <sup>*</sup> |
|--|-------------------------|------|------|-------|----------------|-----------------------------|-----------------------------|
| Pr <sub>2</sub> SeO <sub>2</sub> <sup>†</sup>  | HEX                     | 4.01 | 4.01 | 7.05  | 3.29           | 0.88                        | 0.69                        |
|  |                         | 3.97 | 3.97 | 7.00  | 3.26           |                             |                             |
| Ba <sub>2</sub> InFO <sub>3</sub>              |                         | 4.16 | 4.16 | 13.94 | 3.67           | 0.34                        | 0.78                        |
|  |                         | 4.14 | 4.14 | 13.87 | 3.73           |                             |                             |
| Ba <sub>2</sub> InClO <sub>3</sub>             | TET                     | 4.22 | 4.22 | 15.03 | 3.50           | 0.33                        | 0.84                        |
|  |                         | 4.21 | 4.21 | 14.95 | 3.50           |                             |                             |
| Ba <sub>2</sub> InBrO <sub>3</sub>             |                         | 4.24 | 4.24 | 15.48 | 3.38           | 0.31                        | 0.86                        |
|  |                         | 4.24 | 4.24 | 15.54 | 3.33           |                             |                             |
| K <sub>2</sub> Sn <sub>2</sub> O <sub>3</sub>  |                         | 7.28 | 7.28 | 7.28  | 2.67           | 0.84                        | 0.27                        |
|  |                         | 7.14 | 7.14 | 7.14  | 2.15           |                             |                             |
| K <sub>2</sub> Pb <sub>2</sub> O <sub>3</sub>  | BCC                     | 7.29 | 7.29 | 7.29  | 3.20           | 1.24                        | 0.37                        |
|  |                         | 7.22 | 7.22 | 7.22  | 2.66           |                             |                             |
| Sb <sub>4</sub> Cl <sub>2</sub> O <sub>5</sub> |                         | 5.11 | 6.24 | 13.54 | 4.47           | 3.77                        | 0.69                        |
|  |                         | 5.16 | 6.40 | 13.38 | 3.43           |                             |                             |
| Sb <sub>4</sub> Br <sub>2</sub> O <sub>5</sub> | MCL                     | 5.13 | 6.59 | 13.43 | 4.11           | 1.73                        | 0.70                        |
|  |                         | 5.16 | 6.46 | 13.39 | 3.47           |                             |                             |
| Part II  |                         |      |      |       |                |                             |                             |
| La <sub>2</sub> O <sub>3</sub>                 | HEX                     | 6.12 | 6.12 | 3.93  | 3.04           | 0.56                        | 0.84                        |
|  |                         | 6.27 | 6.27 | 3.26  | 2.68           |                             |                             |
| B <sub>6</sub> O                               | RHL                     | 5.15 | 5.15 | 5.15  | 3.42           | 0.37                        | 0.67                        |
|  |                         | 5.12 | 5.12 | 5.12  | 2.85           |                             |                             |
| SrNiO <sub>2</sub> <sup>†</sup>                | ORCC                    | 3.58 | 3.92 | 8.38  | 2.55           | 8.19                        | 0.71                        |
|  |                         | 3.53 | 3.87 | 8.35  | 1.64           |                             |                             |
| AgNbO <sub>3</sub>                             | ORCC                    | 6.63 | 6.63 | 6.23  | 3.39           | 4.91                        | 0.86                        |
|  |                         | 6.69 | 6.69 | 6.12  | 1.94           |                             |                             |
| Rb <sub>2</sub> Sn <sub>2</sub> O <sub>3</sub> | RHL                     | 6.14 | 6.14 | 6.14  | 2.56           | 0.44                        | 0.28                        |
|  |                         | 6.05 | 6.05 | 6.05  | 1.96           |                             |                             |
| BTl <sub>3</sub> O <sub>3</sub>                | HEX                     | 9.27 | 9.27 | 3.78  | 2.76           | 0.44                        | 0.96                        |
|  |                         | 9.21 | 9.21 | 3.66  | 1.96           |                             |                             |

Table 7.1 Continued

| oxide   | structure <sup>††</sup> | a            | b            | c              | $E_g$        | $m_e^*$ | $m_h^*$ |
|---|-------------------------|--------------|--------------|----------------|--------------|---------|---------|
| MnWO <sub>4</sub> <sup>†</sup>                | MCL                     | 4.81<br>4.78 | 5.04<br>4.96 | 5.83<br>5.70   | 3.90<br>2.11 | 28.91   | 0.68    |
| CaNb <sub>2</sub> O <sub>4</sub>              | ORC                     | 5.05<br>5.04 | 5.84<br>5.82 | 11.90<br>11.83 | 2.70<br>2.12 | 0.99    | 0.71    |
| VAg <sub>3</sub> O <sub>4</sub>               | MCLC                    | 5.09<br>4.96 | 5.83<br>5.61 | 9.58<br>9.53   | 2.80<br>2.14 | 2.14    | 0.98    |
| Tl <sub>6</sub> TeO <sub>6</sub>              | RHL                     | 6.35<br>6.59 | 6.35<br>6.59 | 6.35<br>6.59   | 2.69<br>2.33 | 0.40    | 0.90    |
| TiPbO <sub>3</sub>                            | CUB                     | 3.88<br>3.91 | 4.00<br>3.91 | 4.21<br>3.91   | 4.08<br>2.65 | 38.34   | 0.79    |
| Na <sub>3</sub> AgO <sub>2</sub>              | ORCI                    | 5.46<br>5.40 | 5.93<br>5.85 | 6.79<br>6.70   | 2.64<br>2.71 | 0.56    | 0.92    |
| BiIO  | TET                     | 3.98<br>4.01 | 3.98<br>4.01 | 9.13<br>9.47   | 2.94<br>2.72 | 0.23    | 0.50    |
| Nd <sub>2</sub> SeO <sub>2</sub> <sup>†</sup> | HEX                     | 3.97<br>3.95 | 3.97<br>3.96 | 6.98<br>6.97   | 3.52<br>2.76 | 0.94    | 0.79    |
| Ca <sub>4</sub> As <sub>2</sub> O             | BCT                     | 4.54<br>4.53 | 4.54<br>4.53 | 8.36<br>8.33   | 2.54<br>2.91 | 0.29    | 0.66    |
| Bi <sub>12</sub> PbO <sub>20</sub>            | BCC                     | 8.91<br>8.76 | 8.91<br>8.76 | 8.91<br>8.76   | 2.97<br>3.04 | 1.68    | 0.89    |
| Gd <sub>2</sub> OSe <sub>2</sub> <sup>†</sup> | ORC                     | 3.87<br>3.87 | 3.87<br>3.87 | 6.85<br>6.86   | 2.98<br>3.07 | 1.19    | 0.76    |
| Tl <sub>4</sub> V <sub>2</sub> O <sub>7</sub> | HEX                     | 5.94<br>5.88 | 5.94<br>5.88 | 7.73<br>7.59   | 4.41<br>3.10 | 1.93    | 0.75    |
| Hg <sub>2</sub> SeO <sub>3</sub>              | ORCI                    | 7.83<br>7.71 | 8.81<br>8.77 | 8.81<br>8.77   | 4.06<br>3.10 | 2.53    | 0.58    |

Table 7.1 Continued

| oxide   | structure <sup>††</sup> | a    | b    | c     | $E_g$ | $m_e^*$ | $m_h^*$ |
|---|-------------------------|------|------|-------|-------|---------|---------|
| SbTiO <sub>3</sub>  | HEX                     | 5.31 | 5.31 | 14.25 | 3.79  | 0.61    | 0.86    |
|   |                         | 5.29 | 5.29 | 13.69 | 3.12  |         |         |
| Si <sub>2</sub> O <sub>6</sub>                                | MCLC                    | 4.69 | 7.94 | 8.58  | 3.48  | 0.87    | 0.59    |
|   |                         | 4.63 | 7.83 | 8.28  | 3.18  |         |         |
| Er <sub>2</sub> SeO <sub>2</sub>                              | HEX                     | 3.79 | 3.79 | 6.74  | 3.85  | 0.61    | 0.81    |
|   |                         | 3.79 | 3.79 | 6.74  | 3.19  |         |         |
| Ho <sub>2</sub> SeO <sub>2</sub>                              | HEX                     | 3.81 | 3.81 | 6.77  | 3.82  | 0.65    | 0.80    |
|   |                         | 3.78 | 3.78 | 6.73  | 3.19  |         |         |
| PbSb <sub>2</sub> O <sub>6</sub>                              | HEX                     | 5.30 | 5.30 | 5.38  | 3.54  | 0.39    | 0.51    |
|   |                         | 5.34 | 5.34 | 5.35  | 3.26  |         |         |
| La <sub>2</sub> SeO <sub>2</sub>                              | HEX                     | 4.07 | 4.07 | 7.12  | 4.06  | 0.73    | 0.92    |
|   |                         | 4.06 | 4.06 | 7.12  | 3.49  |         |         |
| CaTe <sub>3</sub> O <sub>8</sub>                              | MCLC                    | 5.66 | 6.90 | 9.65  | 3.61  | 0.54    | 0.68    |
|   |                         | 5.34 | 5.97 | 9.54  | 3.54  |         |         |
| PbAs <sub>2</sub> O <sub>6</sub>                              | HEX                     | 4.87 | 4.87 | 5.48  | 3.79  | 0.36    | 0.40    |
|   |                         | 4.94 | 4.94 | 5.47  | 3.66  |         |         |
| Hg <sub>2</sub> SO <sub>4</sub>                               | MCL                     | 4.43 | 6.28 | 8.37  | 3.50  | 0.55    | 0.80    |
|   |                         | 4.36 | 6.28 | 8.37  | 3.17  |         |         |
| HfPbO <sub>3</sub>  | ORC                     | 5.84 | 5.17 | 11.71 | 3.58  | 0.38    | 0.99    |
|   |                         | 5.81 | 8.09 | 11.63 | 3.58  |         |         |
| LaHO  | TET                     | 5.74 | 8.07 | 8.07  | 3.87  | 0.55    | 0.86    |
|   |                         | 5.66 | 8.00 | 8.00  | 3.82  |         |         |
| BiAsO <sub>4</sub>  | MCL                     | 6.73 | 6.88 | 7.16  | 3.28  | 3.00    | 0.76    |
|   |                         | 6.55 | 6.69 | 7.07  | 4.88  |         |         |
| Tb <sub>2</sub> Ti <sub>2</sub> S <sub>2</sub> O <sub>5</sub> | BCT                     | 3.79 | 3.79 | 11.74 | 2.73  | 0.71    | 0.47    |
|   |                         | 3.74 | 3.74 | 11.66 | 1.81  |         |         |

Table 7.1 Continued

| oxide  | structure <sup>††</sup> | a     | b     | c     | $E_g$ | $m_e^*$ | $m_h^*$ |
|--|-------------------------|-------|-------|-------|-------|---------|---------|
| DyZnPO   | RHL                     | 10.35 | 10.35 | 10.27 | 2.83  | 0.49    | 0.57    |
|  |                         | 10.27 | 10.27 | 10.27 | 1.95  |         |         |
| YZnPO  | RHL                     | 10.35 | 10.35 | 10.35 | 2.84  | 0.51    | 0.60    |
|  |                         | 10.30 | 10.30 | 10.30 | 2.02  |         |         |
| NdBi <sub>2</sub> ClO <sub>4</sub> <sup>†</sup>  | TET                     | 3.91  | 3.91  | 8.99  | 2.62  | 0.28    | 0.96    |
|  |                         | 3.89  | 3.89  | 8.88  | 2.19  |         |         |
| KNdPdO <sub>3</sub> <sup>†</sup>                 | MCLC                    | 3.94  | 6.89  | 7.37  | 2.66  | 0.75    | 0.28    |
|  |                         | 3.92  | 6.82  | 7.24  | 2.24  |         |         |
| NaVS <sub>2</sub> O <sub>8</sub> <sup>†</sup>    | MCLC                    | 4.85  | 4.85  | 7.19  | 2.69  | 2.93    | 0.67    |
|  |                         | 4.68  | 4.68  | 6.79  | 2.75  |         |         |
| TbBi <sub>2</sub> ClO <sub>4</sub>               | TET                     | 3.86  | 3.86  | 8.91  | 2.82  | 0.27    | 0.87    |
|  |                         | 3.84  | 3.84  | 8.82  | 2.82  |         |         |
| DyBi <sub>2</sub> ClO <sub>4</sub>               | TET                     | 3.86  | 3.86  | 8.89  | 2.84  | 0.27    | 0.86    |
|  |                         | 3.83  | 3.83  | 8.82  | 2.85  |         |         |
| Hg <sub>2</sub> PFO <sub>3</sub>                 | ORCI                    | 8.57  | 8.79  | 8.79  | 2.86  | 0.45    | 0.80    |
|  |                         | 8.47  | 8.75  | 8.75  | 2.86  |         |         |
| HoBi <sub>2</sub> ClO <sub>4</sub>               | TET                     | 3.85  | 3.85  | 3.89  | 2.87  | 0.27    | 0.86    |
|  |                         | 3.82  | 3.82  | 8.81  | 2.88  |         |         |
| ErBi <sub>2</sub> ClO <sub>4</sub>               | TET                     | 3.84  | 3.84  | 8.88  | 2.88  | 0.27    | 0.86    |
|  |                         | 3.82  | 3.82  | 8.81  | 2.90  |         |         |
| ZnTiBi <sub>2</sub> O <sub>6</sub>               | TET                     | 4.99  | 5.31  | 5.31  | 2.52  | 0.41    | 0.96    |
|  |                         | 4.82  | 5.20  | 5.20  | 3.08  |         |         |
| Ba <sub>3</sub> Bi <sub>2</sub> TeO <sub>9</sub> | HEX                     | 6.18  | 6.18  | 14.86 | 3.99  | 0.56    | 0.84    |
|  |                         | 6.16  | 6.16  | 14.69 | 3.09  |         |         |
| MoNiO <sub>6</sub> Sr <sub>2</sub> <sup>†</sup>  | BCT                     | 5.58  | 5.58  | 5.62  | 3.65  | 1.53    | 0.81    |
|  |                         | 5.47  | 5.47  | 5.51  | 3.10  |         |         |

Table 7.1 Continued

| oxide                              | structure <sup>††</sup> | a    | b    | c     | $E_g$ | $m_e^*$ | $m_h^*$ |
|------------------------------------|-------------------------|------|------|-------|-------|---------|---------|
| FeTeFO <sub>3</sub> <sup>†</sup>   | MCL                     | 5.05 | 5.07 | 12.40 | 3.86  | 3.88    | 0.77    |
|                                    |                         | 4.88 | 4.92 | 12.41 | 3.11  |         |         |
| Ba <sub>2</sub> AlInO <sub>5</sub> | HEX                     | 5.78 | 5.78 | 19.63 | 3.69  | 0.38    | 0.85    |
|                                    |                         | 5.81 | 5.81 | 19.63 | 3.39  |         |         |
| NaVF <sub>2</sub> O <sub>2</sub>   | MCL                     | 3.59 | 6.40 | 7.22  | 3.90  | 32.30   | 0.71    |
|                                    |                         | 3.46 | 6.17 | 6.88  | 3.63  |         |         |
| KGdPdO <sub>3</sub> <sup>†</sup>   | MCLC                    | 3.91 | 6.80 | 7.32  | 3.14  | 0.75    | 0.24    |
|                                    |                         | 3.89 | 6.75 | 7.21  | 2.32  |         |         |

<sup>††</sup> The structure ( and its acronym): Monoclinic (MCL), Base Centered Monoclinic (MCLC), Base Centered Orthorhombic (ORCC), Body Centered Orthorhombic (ORCI), Tetragonal (TET), Body Centered Tetragonal (BCT), Rhombohedral (RHL), Hexagonal (HEX), Cubic (CUB), Body Centered Cubic (BCC).

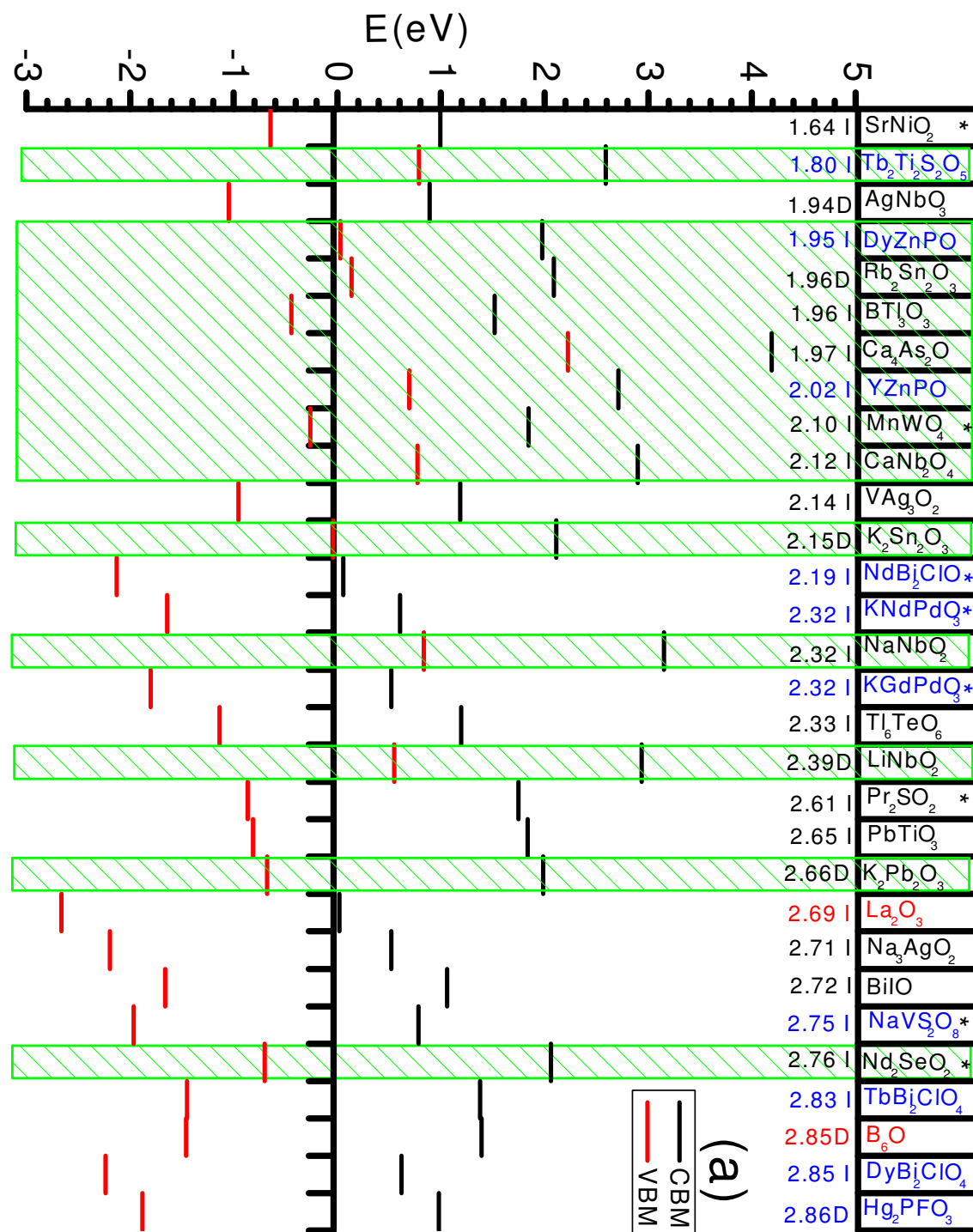
<sup>†</sup> The HSE06 calculated magnetic moment of the compounds that have a non-zero total magnetic moment are available in table B.2 of Appendix B.

The results of the compounds that are found metallic with HSE06 (Sn<sub>2</sub>F<sub>5</sub>O, and MnMoO<sub>4</sub>) are not included in the table.

In Fig. 7.3 we present the band alignment of all the oxides in Table 7.1, with the BPE as the energy reference. Figure 7.3 shows the band alignment of the studied oxides, with the compounds sorted in ascending order of the band gap. The CBM and VBM positions are indicated by horizontal segments for each compound. The values of the HSE06 band gaps are also given, with “D”/“I” indicating the direct/indirect nature of the fundamental gap. Notice that this shows an interesting feature, i.e., that few of the oxides that qualified so far have a direct band gap. Indeed, this is the case for only 9 of the 45 oxides considered (7 ternaries out of 37, one quaternary out of 21, and one of the binaries).

The alignment allows us to classify the studied oxides in three classes. In the first class we have the oxides that we consider easily *p*-type dopable, i.e., those for which the BPE lies at most  $\frac{1}{4}E_g$  above the VBM. The compounds in this first class are highlighted in Fig. 7.3. One can see that there are fourteen ternary and four quaternary oxides in this class. On the other hand, the only two binaries in Fig. 7.3 are not easily doped *p*-type. We note that the differences between the AFLOWLIB band gaps and our calculated HSE06 band gaps can be considerable. For instance, the ternary LiNbO<sub>2</sub>, and the quaternaries DyZnPO and YZnPO have AFLOWLIB (HSE06) band gaps of 3.16 (2.39), 2.83 (1.95), and 2.84 (2.02) eV, respectively. At the same time, the optically determined gaps turn out to be around 2 eV for all three materials [220, 221], so the HSE06 gaps are clearly closer to





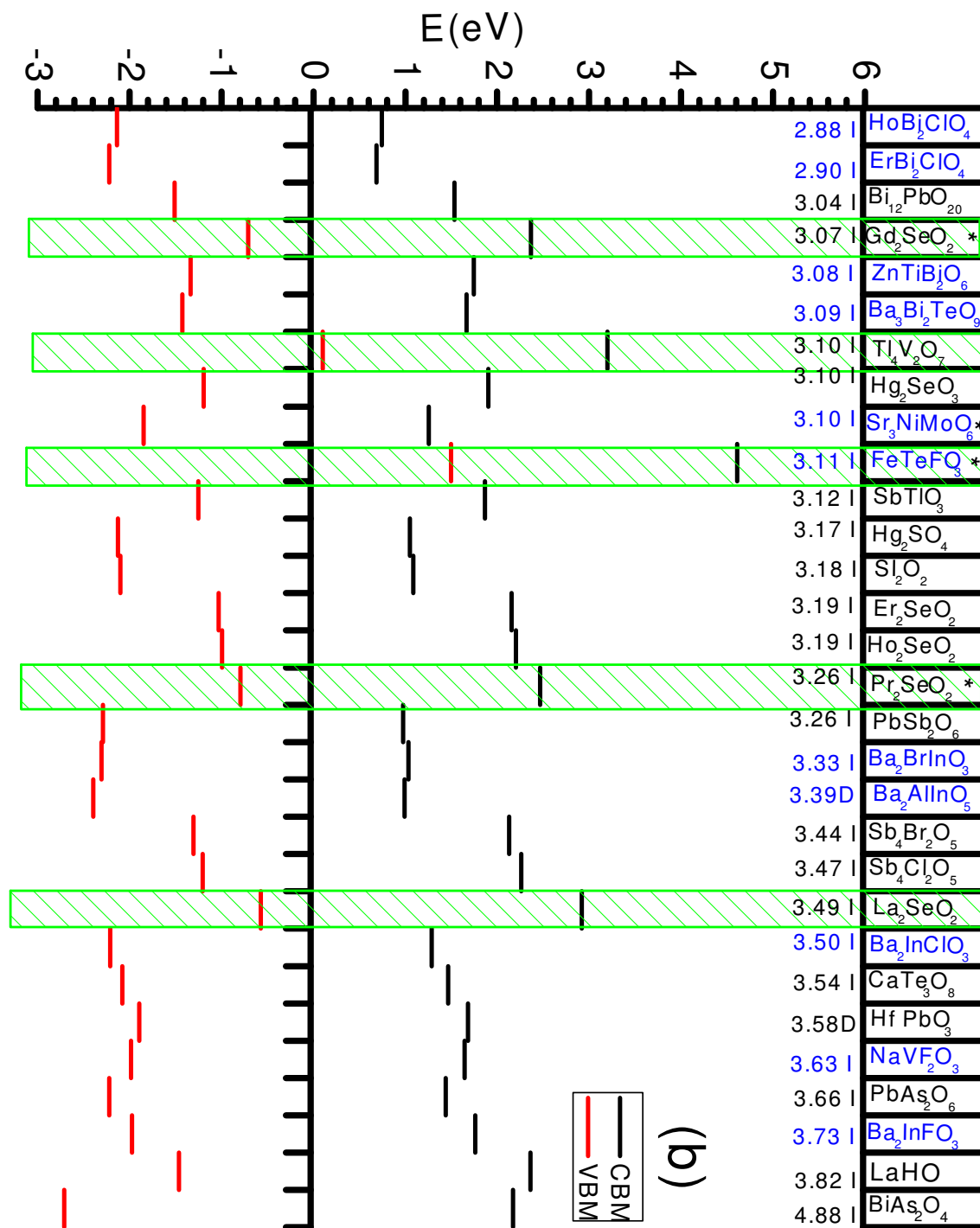


Figure 7.3: The band alignment of the studied oxides, with the compounds sorted in ascending order of the band gap. "D"/"I" beside the band gap value refers to its direct/indirect nature. The *p*-type dopable compounds are highlighted. \* For the compounds that have a non-zero total magnetic moment the BPE is the average of the BPE of two spin components.

experiment. We address the thermodynamic stability of these compounds further down.

We classify in the second class the oxides for which the BPE lies above the CBM, or at most  $\frac{1}{4}E_g$  below the CBM. These oxides are easily doped *n*-type. We do not focus on *n*-type TCOs in this work, so we just mention that  $\text{La}_2\text{O}_3$ ,  $\text{Na}_3\text{AgO}_2$  and the quaternaries  $\text{KGdPdO}_3$ ,  $\text{Bi}_2\text{ClXO}_4$ , where  $\text{X}=\text{Dy, Ho, Nd, or Er}$ , belong to this class. The third class consists of the rest of the oxides. Oxides for which the BPE is closer to the center of the band gap than to the band edges do not show any obvious trend. Some may still be *n*- or *p*-type dopable, and some may be both (ambipolar). However, for oxides with a band gap of 2.5 eV or larger, as those considered here, this is probably difficult. Indeed, for wide band gap materials doping becomes increasingly challenging the further the BPE falls away from the band edges. Ambipolar doping can be feasible in the case of compounds with a band gap of around 1 eV or lower, but is difficult for larger gaps. Well known examples of the two cases are  $\text{CuInSe}_2$  (gap of 1 eV) and  $\text{CuGaSe}_2$  (gap of 1.7 eV), respectively [222]. Given the lack of a clear trend, we avoid any strong statements about the dopability of this third class of compounds.

Fig. 7.4 shows the stability triangle of the ternary oxides in the first class that have a HSE06 gap larger than 2.5 eV. The area in which the ternary is stable is delimited by the areas in which competing binary phases can form. In all six cases the stability area is larger than 10%. Hence, our final list of *p*-type TCO candidates consists of these oxides, and is presented in Table 7.2. The stability triangle and all calculated data for the compounds that are found *p*-type dopable (highlighted in Fig. 7.3) and have a HSE06 band gap smaller than 2.5 eV are available in Appendix B.

For completeness, for these compounds we report our calculated values for the fundamental gap, the direct gap, the so-called second gap, the average hole effective mass, and the enthalpy of formation. The second gap in a TCO, defined as the energy difference between VBM and the next eigenvalue below it, is of interest because at high carrier concentration a low second band gap will tend to limit the transparency through the absorption of photons by the carriers [223]. Thus, at high carrier concentration, the wider the second gap, the better. Of the seven candidates in Table 7.2, five have not been identified before, namely  $\text{X}_2\text{SeO}_2$ , with  $\text{X} = \text{La, Pr, Nd, and Gd}$ , and  $\text{FeTeFO}_3$ . With a direct band gap larger than 3.1 eV, these candidates ensure an excellent transparency, and present very low hole effective masses. With their good dopability and thermodynamic stability, these are perhaps the best *p*-type candidates identified in this study. Note that because of the magnetic order in the last four compounds predicted by DFT-based calculations, these are in fact *p*-type ferromagnetic TCO candidates, adding greatly to their interest. Indeed, this type of materials are long sought because of their remarkable potential applications [224,225]. The other two candidates,  $\text{Tl}_4\text{V}_2\text{O}_7$  and  $\text{K}_2\text{Pb}_2\text{O}_3$  were already identified as *p*-type TCO candidate materials in Ref. 147. The good *p*-type dopability we find for these materials confirms this. However, as remarked in the later work, toxicity concerns might hinder the industrial interest of Tl and Pb containing compounds. A few further comments regarding our findings are in order. First, it is interesting to note that the hole effective masses of the *p*-type dopable oxides in Fig. 7.3 tend to be lower than the corresponding electron effective masses (cf. Table 7.1). Indeed, this is the case in 73% of the cases. The fact that only 30% of all the oxides in Table 7.1 has an electron effective mass higher than  $1 m_e$  makes

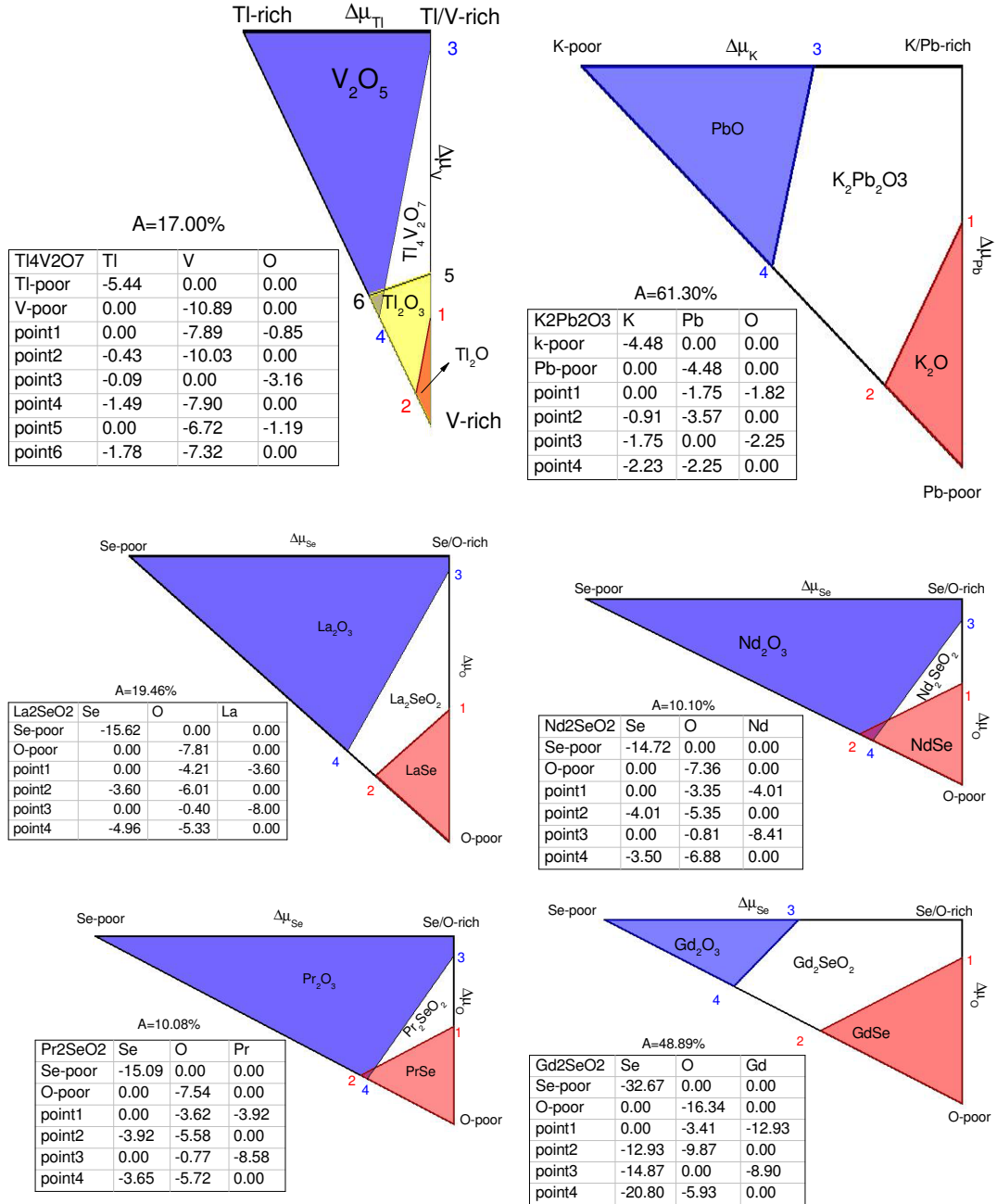


Figure 7.4: Stability triangle of the ternary TCO candidates. Each plot indicates the range of the chemical potentials for which the ternary oxide is stable against the formation of the competing phases<sup>a,b,c</sup>. For each compound, the chemical potential values (in eV) at the points delimiting the different stability areas are shown in the table next to the triangle. The value for 'A' above each table indicates the ratio of the ternary stability area to the total area of the triangle (in %).

<sup>a</sup> All the binaries that may contribute in synthesis of a ternary are considered as competing phases.

<sup>b</sup> We ensure that the most common phase of each binary is considered as a competing phase.(e.g.  $\text{Ti}_2\text{O}_3$  compared to  $\text{Ti}_2\text{O}$  for  $\text{Ti}_4\text{V}_2\text{O}_7$ ) is considered as a competing phase.

<sup>c</sup> For clarity, we only show the binary oxide for which the stability area is not completely covered by that of other considered binary oxides. (e.g. the stability area of  $\text{Ti}_2\text{O}$  is completely covered by that of  $\text{Ti}_2\text{O}_3$  in the case of  $\text{Ti}_4\text{V}_2\text{O}_7$ .)

Table 7.2: The HSE06 calculated band gaps (fundamental band gap  $E_g$ , first direct band gap  $E_g^d$ , second gap in the valence band  $E_{g,VB}^2$ ) in comparison with other available results (second row for each compound), PBE calculated hole effective mass along symmetry directions ( $m_h^*$ ), average hole effective mass ( $m_h^{*avg}$ ), and enthalpy of formation  $\Delta H_f$  for the  $p$ -type TCOs. (All energies are in eV, and all effective masses are in units of  $m_e$ )

| oxide        | $E_g$                          | $E_g^d$ | $E_{g,VB}^2$ * | $m_h^*$ †  | $m_h^{*avg}\dagger\dagger$ | $\Delta H_f^\ddagger$ |
|--------------|--------------------------------|---------|----------------|--|----------------------------|-----------------------|
| $K_2Pb_2O_3$ | 2.66<br>2.6 <sup>b</sup> [147] | 2.66    | 1.55           | 0.30   | 0.30                       | -8.94                 |
| $Nd_2SeO_2$  | 2.76                           | 3.12    | 1.76           | 0.98 <sup>[100]</sup> , 0.18 <sup>[001]</sup>                            | 0.71                       | -14.72                |
| $Gd_2SeO_2$  | 3.07                           | 3.95    | 2.28           | 0.49 <sup>[100]</sup> , 1.18 <sup>[001]</sup>                            | 0.72                       | -32.67                |
| $Tl_4V_2O_7$ | 3.10<br>4.5 <sup>b</sup> [147] | 3.13    | 1.49           | 0.53 <sup>[100]</sup> , 0.97 <sup>[001]</sup>                            | 0.65                       | -21.78                |
| $FeTeFO_3$   | 3.11                           | 3.12    | 0.41           | 0.27 <sup>[100]</sup> , 1.50 <sup>[010]</sup> ,<br>0.23 <sup>[001]</sup> | 0.67                       | -8.87                 |
| $Pr_2SeO_2$  | 3.26                           | 4.09    | 1.99           | 1.03 <sup>[100]</sup> , 0.22 <sup>[001]</sup>                            | 0.76                       | -15.09                |
| $La_2SeO_2$  | 3.49                           | 4.02    | 1.55           | 0.28 <sup>[100]</sup> , 2.63 <sup>[001]</sup>                            | 0.59                       | -15.62                |

†† Average hole effective mass is calculated using  $m^{*avg} = (m_1 m_2 m_3)^{1/3}$  where  $m_1$ ,  $m_2$ , and  $m_3$  is the hole effective mass along [100], [010], and [001], respectively.

‡  $\Delta H_f$  is the formation energy (per formula unit) of the compound with respect to the metal phase of the elements and oxygen molecules.

\* For the compounds that have a non-zero total magnetic moment  $E_{g,VB}^2$  is considered as the energy difference between the two highest occupied bands with the same spin component. However, for the compounds  $Nd_2SeO_2$ ,  $Pr_2SeO_2$ , and  $Gd_2SeO_2$  the two highest occupied bands have different spin components. The energy difference between two highest occupied bands is 0.10, 0.11, and 0.20 eV for  $Nd_2SeO_2$ ,  $Pr_2SeO_2$ , and  $Gd_2SeO_2$ , respectively.

<sup>b</sup> Other theoretical results

this all the more remarkable. The reason is of course that a  $m_h/m_e < 1$  implies that the electron-momentum dispersion is higher at the VBM than at the CBM, which tends to push the BPE lower in the gap. However, all the  $\mathbf{k}$ -points in the Brillouin zone contribute to the BPE, which is why its position in the band gap does not correlate exactly with the  $m_h/m_e$  ratio.

We mentioned in the Introduction that in Ref. 147 a high-throughput search of *p*-type candidate oxides is also performed. The overlap of good *p*-type TCO candidates in the two studies is only partial because, as already indicated, the screening criteria are different. Of the candidates presented in Ref. 147, ZrOS is not in our list in Table 7.2 because of its hole effective mass is higher than  $1 m_e$ . PbTiO<sub>3</sub> and B<sub>6</sub>O do not make it into our list because they are not easily *p*-type dopable according to our criterion. This is in line with a recent first-principles report, which indicates that the reported *p*-type conductivity of PbTiO<sub>3</sub> is unstable [226]. With respect to B<sub>6</sub>O, which falls in the third class of oxides, a recent study on its possible ambipolarity has shown that it indeed will not be easy to dope it either *p*- or *n*-type [227]. The only possible *p*-type dopant identified for B<sub>6</sub>O with low enough formation energy near the VBM is a (CH)<sub>O</sub> complex but it requires at the same time substitutional Carbon in Boron position (C<sub>B</sub> defects) are avoided. Furthermore, the possible *n*-type dopant identified, Si<sub>i</sub>, has a very high formation energy. Thus, our predictions regarding dopability appear to be reliable. Finally, K<sub>2</sub>Sn<sub>2</sub>O<sub>3</sub> is excluded from our final list because its HSE06 calculated band gap is 2.15 eV, i.e., too low (the corresponding *GW* band gap in Ref. 147, at 2.4 eV, is still lower than 2.5 eV).

## 7.4 Conclusions

We carried out a DFT based high-throughput search for new *p*-type TCO candidates. Our procedure consists of the following steps. We first screen all the binary, ternary and quaternary oxides in the AFLOWLIB database to identify those compounds that are reported to have a band gap larger than 2.5 eV, and a hole effective mass lower than  $1 m_e$ . We calculate the electronic structure of the thus identified compounds in order to determine their *p*-type dopability via the position of their BPE with respect to the band edges. We then determine the thermodynamic stability of the oxides that are *p*-type dopable and that are confirmed by our calculations to have a band gap of at least 2.5 eV. We identify the compounds La<sub>2</sub>SeO<sub>2</sub>, Pr<sub>2</sub>SeO<sub>2</sub>, Nd<sub>2</sub>SeO<sub>2</sub>, Gd<sub>2</sub>SeO<sub>2</sub>, and FeTeFO<sub>3</sub> as very good new *p*-type TCO candidates. These compounds have not been identified as such previously in the literature. With a direct band gap larger than 3.1 eV and an average hole effective mass lower than  $0.76 m_e$ , these materials have the potential of outperforming any of the currently used *p*-type TCO materials. In addition, the last four compounds are candidates with a quite unusual combination of *p*-type dopability, transparency, and magnetic order.

# Identification of stannite Cu-based absorber layers

## 8.1 Introduction

The operation of solar cells involves several processes that lead to the conversion of sunlight energy into electricity. There is an extensive research activity for improving solar cell performance by enhancing the efficiency of this conversion [228–234]. To search for new materials as absorber layers is one of the main steps in designing highly efficient solar cells.

The potential applications of the multinary chalcogenide semiconductors in optoelectronics bring an intensive interest in their design and synthesis that dates back to the 1950s. [235–241] As it is already explained in Section 1.3.2 ternary I-III-VI<sub>2</sub> compounds can be generated from binary II-VI chalcogenides through substituting the group II atoms by pairs of group I and III atoms. Because of the increased chemical and structural flexibility in ternary compounds, they exhibit more flexible optoelectronic properties than binary ones [232, 242]. For example, CuGaSe<sub>2</sub> has a band gap of 1.68 eV that is lower than that of ZnSe (2.82 eV) [243]. This is one of the characteristics of CuGaSe<sub>2</sub> that makes it convenient for application in thin-film solar cells. By following the same method, it is natural to further increase the chemical and structural flexibilities by making quaternary chalcogenides. The enhanced flexibilities allow to engineer the functional properties to satisfy a certain application, e.g. high-efficiency photovoltaic absorber layers or light emitting diodes.

There are two approaches to substitute the cations in ternary I-III-VI<sub>2</sub> to design quaternary compounds. One is to replace two III atoms by one II and one IV atom, forming a I<sub>2</sub>-II-IV-VI<sub>4</sub> compound. The other one is to replace one I atom and one III atom by two II atoms, forming II<sub>2</sub>-I-III-VI<sub>4</sub> compounds. Such quaternary chalcogenides with I = {Cu, Ag}, II = {Zn, Cd}, III = {Ga, In}, IV = {Ge, Sn}, and VI = {S, Se, Te} have been synthesized by different groups [239, 240, 244]. In particular, Cu-based chalcogenides Cu<sub>2</sub>-II-IV-VI<sub>4</sub> can be found at the center of various technolog-

ical innovations. Among these compounds,  $\text{Cu}_2\text{ZnSnS}_4$  (CZTS) and  $\text{Cu}_2\text{ZnSnSe}_4$  (CZTSe) combine promising characteristics for optoelectronic applications (e.g. direct band gap of 1.0-1.4 eV, a high optical absorption coefficient up to  $10^5 \text{ cm}^{-1}$ , low toxicity and a relatively high abundance of the elements [241, 245–247]). Such characteristics make them the low-cost and environmentally friendly alternative to the conventional photovoltaic materials like Si, CdTe and  $\text{CuIn}_{1-x}\text{Ga}_x\text{Se}_2$  [245–247]. The obtained results for CZTS, and CZTSe increase the interest in other members of the  $\text{Cu}_2\text{-II-IV-VI}_4$  family that could be considered as possible materials for photovoltaic applications. While a significant attention has been paid to CZTS and CZTSe [231, 238, 248], most of the other compounds in this family remain relatively unexplored. Limited theoretical attention has been paid to these chalcogenides, so their electronic structures and optical properties remain unclear, which limits their usage in semiconductor devices. A deeper knowledge of their optoelectronic properties might bring further improvements in their applications [249].

On the one hand, extensive measurements have been performed to study the change of the power conversion efficiency of the photovoltaic solar cells with respect to the characteristics of the absorber layers. On the other hand, the conversion efficiency of the solar cells are investigated theoretically, but very few of such studies calculate the efficiency of the solar cells using first-principles methods. Some successful first-principles studies have identified new materials with high conversion efficiency for PV applications. L. Yu et al. introduced the "spectroscopic limited maximum efficiency (SLME)" (see section 8.2.3 for details) which is the theoretical power efficiency that can be investigated using first-principles calculated quantities. They used the SLME parameter as a selection metric to identify new absorber materials [250].

The main goal of the present chapter is to use the SLME parameter to investigate how the efficiency of the  $\text{Cu}_2\text{-II-IV-VI}_4$  compounds change by changing the material composition. The underlying principle of solar cells is discussed first to enable understanding of the rest of this chapter. The basics of the operation of solar cells and some of the characteristics of their performance are presented. Some good textbooks on semiconductor and photovoltaic physics can be referred to for more details, such as reference [251]. Then, we discuss the mechanisms that affect the conversion efficiency of solar cells. Next, the theoretical conversion efficiency based on the Shockley-Queisser (SQ) limit [8], and the SLME selection metric are introduced. Finally, we study the case of the quaternary Cu-based chalcogenides. We investigate the electronic and optical properties of  $\text{Cu}_2\text{-II-IV-VI}_4$  with  $\text{II} = \{\text{Cd, Hg, and Zn}\}$ ,  $\text{IV} = \{\text{Sn, and Ge}\}$ , and  $\text{VI} = \{\text{S, Se, and Te}\}$ . We also estimate the maximum photovoltaic conversion efficiency for the studied solar cells.

## 8.2 Solar cell operation

The solar cell working principles are based on the photovoltaic effect [252] which can be explained as the production of a voltage (potential difference) in a junction of two different materials ( $n$ -type and  $p$ -type) in response to the electromagnetic field of the photon radiation. The basic processes behind this effect are explained in this section.



### 8.2.1 Generation of charge carriers

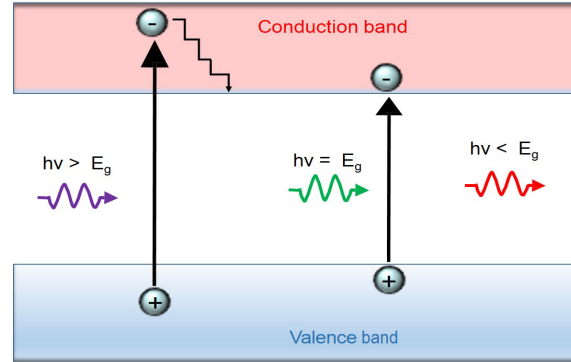


Figure 8.1: The relation between the absorption of the incident photon by a material and the difference between its energy and the band gap of the material.

Figure 8.1 shows that how the absorption of the incident photon by the material is related to the difference between energy of the photon and band gap of the material. The incident solar radiation can only be absorbed by the material if its energy is larger than or equal to the optical band gap of the material ( $h\nu \geq E_g$ ). The absorbed photon excites an electron from the VB to the CB. The excitation of the negatively charged electron to the CB creates its positively charged counterpart, a hole in the VB. If the energy of the incident photon is smaller than the band gap ( $h\nu < E_g$ ), it transmits through the material without any interaction. On the other hand, if the photon energy is much larger than the band gap, it will be absorbed strongly by the material and the electron will be excited not to the conduction band minimum (CBM) but to a state higher in energy in the CB. This cannot be exploited in the solar cells because electrons thermalise back to the CBM. The optical band gap is the shortest possible direct transition between the state in the VB and the state in the CB with the same  $k$  vector. In an indirect band gap material like silicon, the band gap does not occur between two states with the same  $k$  vector. A photon only excites an electron from the valence band maximum (VBM) to the intermediate state with the same  $k$  vector as initial state. The transition of the electron from the intermediate state to the CBM which is the final state is performed by a phonon. Therefore, the absorption coefficient ( $\alpha$ ) in a direct band gap material is much higher than one with indirect band gap. Then, to have the same energy conversion a layer with a direct band gap material can be thinner than one with an indirect band gap material [17].

### 8.2.2 Separation and collection of photo-generated carriers

A solar cell in the dark works as a large diode which is constructed from a  $p$ - $n$  junction. The majority of the carriers that are electrons in  $n$ -type and holes in  $p$ -type diffuse to the other part of the junction because of the difference in the carrier concentration between the  $n$  and  $p$  regions.

Therefore, the region close to the junction becomes depleted of the charge carriers and the left ions build up an intrinsic electric field. Under illumination, the photo-generated carriers are separated by the intrinsic electric field. The minority carriers (holes in  $n$ -type and electrons in  $p$ -type) can be swept through the junction, where they are now the majority carriers. If two electrodes of the solar cell are connected together the solar cell is short-circuited, then the photo-generated carriers flow through the external circuit.

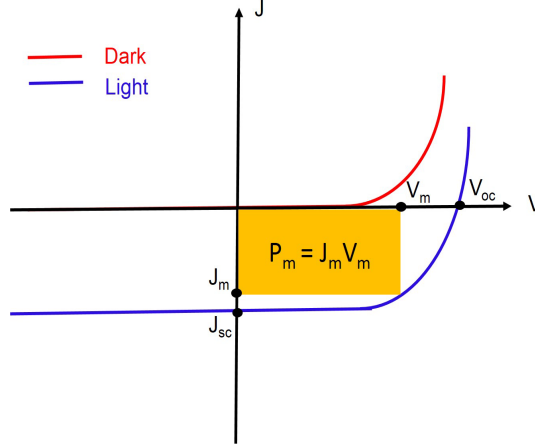


Figure 8.2: Schematic J-V curves for a solar cell in dark and light.

Figure 8.2 shows the current-voltage (J-V) curves in dark and light. The dark J-V curve is the diode J-V curve which corresponds to the situation in which there is no incident radiation on the cell to generate charge carriers. The light J-V curve is the superposition of the dark J-V curve with a short circuit current density  $J_{sc}$ .  $J_{sc}$  is the current through the solar cell when the solar cell is short circuited and the voltage across the solar cell is zero. The open circuit voltage ( $V_{oc}$ ) is the voltage at zero current. In this voltage the photo-generated current cancels out the recombination current [253]. The recombination current will be discussed in detail in Section. 8.2.3. The short circuit current density can be formulated as

$$J_{sc} = e \int_0^{\infty} a(E) I_{sun}(E) dE \quad (8.1)$$

where  $e$  is the charge of the electron,  $I_{sun}(E)$  is the solar radiation flux, and  $a(E)$  is the absorptivity of the material as function of the energy  $E$  of the photon. In order to be able to compare solar cells, standard conditions such as spectrum, intensity and temperature have been considered. The standard solar spectrum is prefixed "AM" which stands for Air Mass and followed by a number which refers to the length of the light path through the atmosphere in relation to the shortest length. This number can be formulated roughly as  $AM = \frac{1}{\cos(\theta)}$  where  $\theta$  is the Zenith angle.

Three standardized solar spectra are defined as AM0, AM1, and AM1.5 [31]. Outside the atmosphere the spectrum is AM0. AM1 is the spectrum on the earth's surface for normal incidence. The spectrum AM1.5 corresponds to  $48^\circ$  as angle of incident solar radiation relative to the surface normal [21]. We use AM1.5 as solar spectrum in this thesis which is shown in the upper part of Fig. 8.4.

The produced current density depends not only on the solar radiation at the location of the solar cell, but also on the optoelectronic properties of the solar cell material such as the band gap and absorptivity  $a(E)$ . The latter is given by

$$a(E) = (1 - R)(1 - e^{-2\alpha(E)L}) \quad (8.2)$$

where  $\alpha(E)$  is the absorption spectrum of the material,  $L$  its thickness, and  $R$  its reflectivity. In the ideal case, it is assumed that the reflectivity of the front surface of the absorber layer is zero and the reflectivity of its back surface is one. It means that no incident photon is reflected. Moreover, all the photons that go through the material and reach the back surface of the layer are reflected back into the material. As a result  $R = 0$  and  $a(E) = 1 - e^{-2\alpha(E)L}$ .

### 8.2.3 Efficiency and loss mechanism

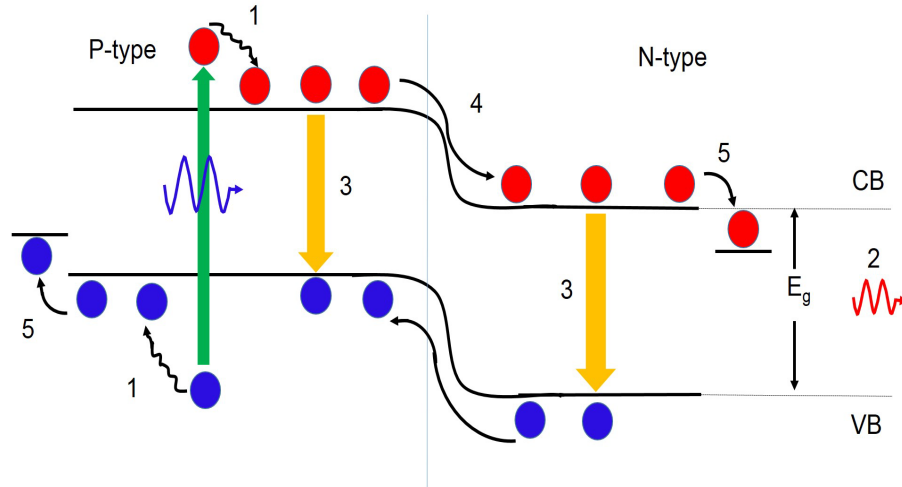


Figure 8.3: Loss mechanisms in a single-junction solar cell: (1) lattice thermalisation losses (2) transparency loss (3) recombination loss (4) junction loss (5) contact voltage loss [254].

The loss mechanisms limit the output voltage and thus the efficiency of the solar cell in converting electromagnetic radiation to a voltage. Figure 8.3 shows the loss mechanisms in the standard solar cells. Process 1 and 2 in Fig. 8.3 explain the most significant loss mechanisms which are non-radiative losses. Process 1 is due to the relaxation of hot charge carriers that are created by

the absorption of a high energy photon. The excess energy of a high energy photon is rapidly dissipated as heat by the thermalisation of the electron and the hole to the edges of the CB and VB, respectively. This loss mechanism plays a more important role when the solar cell is based on a semiconductor with a small band gap. This transmission of photons with energies below the band gap of the semiconductor material is shown by process 2. The transmission loss mechanism contributes more for wide band gap solar cells, because a large part of the solar spectrum cannot be absorbed [254]. Process 3 shows the radiative recombination of electron-hole pairs. In this process one electron meets a hole at the VBM and they recombine and generate a photon. If the carriers have a longer lifetime, then they have more time to be collected by the contacts and participate in the voltage production. Therefore, this loss process can be minimized by control the mobility of the minority carriers in the semiconductor materials. The radiative recombination is more important in direct band gap materials than in indirect band gap ones because in an indirect band gap material, the radiative recombination process needs to be accompanied by emitting or absorbing a phonon in order to conserve the momentum of the electron. The electron should have very long lifetime to meet a phonon with the right momentum before any undesired non-radiative recombination happens, thus this radiative recombination does not occur frequently [255]. The only unavoidable loss mechanism is the emission of photons produced by non-radiative recombination that includes voltage drops across the contacts and junction. These two mechanisms are denoted by processes 4 and 5 in Fig. 8.3.

By considering both radiative and non-radiative recombination processes, the loss current density can be calculated as

$$J_{loss} = J_0(1 - e^{\frac{eV}{k_B T}}) \quad (8.3)$$

where  $V$  is the voltage,  $k_B$  is the Boltzmann constant, and  $T$  is the temperature.  $J_0$  corresponds to the total electron-hole recombination current in dark and can be expressed as a fraction of the radiative recombination current density ( $f_r$ )

$$J_0 = J_0^r / f_r \quad (8.4)$$

$f_r$  depends on the difference between fundamental band gap ( $E_g$ ) and optical band gap which determines the direct allowed transitions ( $E_g^{da}$ ).

$$f_r = e^{-\Delta / k_B T} \quad (8.5)$$

$$\Delta = E_g^{da} - E_g. \quad (8.6)$$

The radiative recombination process results in a current in the opposite direction of the short circuit current and can be formulated as

$$J_0^r = e\pi \int_0^\infty a(E) I_{bb}(E, T) dE. \quad (8.7)$$

The blackbody radiation ( $I_{bb}$ ) is given by

$$I_{bb}(E, T) = \frac{2E^2}{h^3 c^2 (e^{\frac{E}{k_B T}} - 1)} \quad (8.8)$$

where  $c$  is the speed of light, and  $h$  is Planck's constant.

In the detailed balance model developed by Shockley and Queisser (SQ), the symmetry between photon absorption and emission can be used to derive the fundamental limits on the achievable solar cell conversion efficiency [8]. This model results in the output current density which is the summation over loss current density and short circuit current density:

$$J = J_{sc} - J_{loss}. \quad (8.9)$$

Conversion efficiency of a solar cell is defined as  $\eta = P_m/P_{in}$ , where  $P_m$  is the maximum output power density and  $P_{in}$  is the total incident solar power density.  $P_m$  can be obtained by numerically maximizing  $P = J \times V$ .  $P_m$  is the area of the rectangular that is represented in Fig. 8.2.

Another power efficiency that can be defined for the solar cell is the nominal power,  $P_{nominal}$ . It is simply the product of the highest value of the voltage and current density of the solar cell. It means that  $P_{nominal}$  is calculated using the formula

$$P_{nominal} = J_{sc} \times V_{oc} \quad (8.10)$$

where  $V_{oc}$  is the open circuit voltage and corresponds to the voltage of the solar cell under  $J = 0$ . Applying this condition on Eq. (8.9) results in the following formula for  $V_{oc}$

$$V_{oc} = \frac{k_B T}{e} \ln(1 + \frac{J_{sc}}{J_0}). \quad (8.11)$$

At  $J_{sc}$  the voltage is zero and at  $V_{oc}$  there is no current. Therefore, at these two points, the power is zero. However, the definition of  $P_{nominal}$  is useful because it is used to calculate the Fill Factor (FF) of the solar cell. FF is the ratio between  $P_m$  and  $P_{nominal}$  and presents the fraction of the maximum power that can be obtained from the cell.

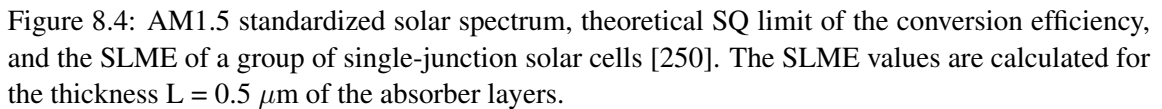
The highest theoretical efficiency according to the SQ limit only depends on the band gap value of the semiconductor which means that in Eq. (8.2)  $a(E)$  is assumed to be step function

$$a(E) = \begin{cases} 1 & E \geq E_g \\ 0 & E < E_g \end{cases} \quad (8.12)$$

Applying this step function to Eq. (8.1), and Eq. (8.7) gives respectively

$$J_{sc} = e \int_{E_g}^{\infty} I_{sun}(E) dE \quad (8.13)$$

Eq. (8.13) and Eq. (8.14) can be plugged into Eq. (8.3), and then Eq. (8.9) to finally obtain the conversion efficiency. As Fig. 8.4 shows the highest possible theoretical efficiency using the SQ limit is 33% for a single-junction solar cell with  $E_g$  equal to 1.3 eV.



Considering the absorptivity of the material with a finite thickness  $L$  results in a lower conversion efficiency than that provided by the SQ limit. The SLME is a convenient selection metric for the absorber layer. This metric takes into accounts the band gap and absorptivity of a material to give a value for the conversion efficiency. Figure 8.4 represents the SLME of a group of solar cells that can be compared with the values given by the SQ limit.

### 8.3 Computational details

The distribution of the cations within the unit cell of  $\text{Cu}_2\text{-II-IV-VI}_4$  depends on the nature of the group II and IV atoms. For example the kesterite structure is the most stable phase for

Figure. 8.5 show the atoms II, IV, and VI in the periodic table. Stannite  $\text{Cu}_2\text{-II-IV-VI}_4$  compounds are quaternary complexes with a crystal structure similar to the zinc-blende structure of  $\text{ZnS}$  and the kesterite structure of  $\text{CuInS}_2$ . The stannite primitive cell (space group  $\text{Ia}\bar{4}2\text{m}$ , No. 121) contains 8 atoms.

|           |           |    |           |    |           |
|-----------|-----------|----|-----------|----|-----------|
|           |           |    | IV        |    | VI        |
|           | II        |    | ↓         |    | ↓         |
|           |           | B  | C         | N  | O         |
|           |           | Al | Si        | P  | <b>S</b>  |
| <b>Cu</b> | <b>Zn</b> | Ga | <b>Ge</b> | As | <b>Se</b> |
| Ag        | <b>Cd</b> | In | <b>Sn</b> | Sb | <b>Te</b> |
| Au        | <b>Hg</b> | Tl | Pb        | Bi | Po        |

Figure. 8.6 presents the schematic stannite structure. Such structure contains Cu as a monovalent cation. There are alternating cation layers of mixed II and IV atoms, which are separated from each other by layers of Cu atoms. Each anion is tetrahedrally coordinated by four cations. Two equivalent Cu atoms occupy the 4d Wyckoff position (site symmetry  $S_4$ ), one II atoms on 2a, one IV atoms on 2b (both II and IV with  $D_{2d}$  symmetry) and four VI atoms on 8i position (site symmetry  $C_s$ ). In this structure, each anion has thereby three inequivalent bonds(VI-A) with the cations  $A = \{\text{Cu, Zn, and Sn}\}$ . The ideal stannite structures when all bond lengths are equal as in a binary zinc-blende structure are obtained for a ratio  $c/a = 2$  of the lattice constants, and with an anion atom positioned at  $(3/4, 3/4, 7/8)$ .

Our *ab initio* computations are based on DFT [42, 45], and are carried out using the VASP code [70, 91, 136, 148]. We use PAW [68, 92] potentials to describe the electron-ion interaction. We use the GGA to the exchange-correlation potential, in the parametrization by PBE [51] to perform all structural calculations. Electronic structure and optical properties are calculated using the HSE06 hybrid functional [153]. An energy cutoff of 350 eV is used for the plane-wave basis set. For structure relaxation and total energy calculations the Brillouin Zone was sampled using a

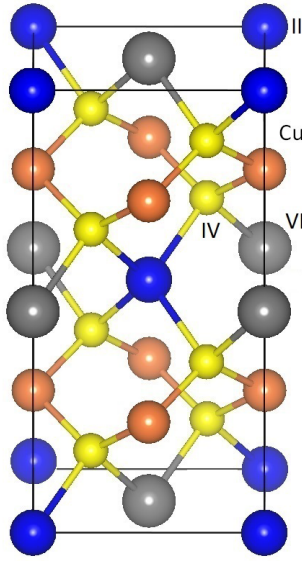


Figure 8.6: Crystal structure of  $\text{Cu}_2\text{-II-IV-VI}_4\text{-stannite}$  (space group  $\bar{I}4_2m$ , No. 122).

$4 \times 4 \times 4$  MP grid [66]. Atomic relaxations were made until residual forces on the atoms were less than  $0.01 \text{ eV/\AA}$  and total energies were converged to within 1 meV.

In order to calculate the absorption spectra, the imaginary part of the dielectric function tensor is obtained using the random phase approximation, as implemented in the VASP code [84, 259]. The real part of the dielectric function is obtained from the imaginary part through the Kramers-Kronig relation. We found that it is enough to sample the Brillouin zone using a  $10 \times 10 \times 10$  MP grid to obtain a converged  $\varepsilon(\omega)$  tensor. The number of unoccupied bands used here is 4 times the number of occupied bands.

Since the photovoltaic conversion efficiency strongly depends on the band gap, it is important to get an accurate value from our first-principles calculations. As it is discussed in section 2.6.4 it is known that standard DFT calculations, using local or semi-local exchange-correlation functionals such as the LDA or PBE, seriously underestimate the band gap of semiconductors [152, 153], while the hybrid functional HSE06 has proven to be capable of giving close-to-experiment predictions for a large range of compounds including Cu-based compounds [154, 250]. Moreover, for series of compounds, HSE gives the dielectric function spectrum that has better agreement compared to the one calculated using PBE or LDA functionals [61, 62].

## 8.4 Results



Table 8.1: HSE06 calculated lattice constants ( $a$  and  $c$  in Å), band gap ( $E_g$  in eV), enthalpy of formation ( $\Delta H_f^{\dagger\dagger}$  in eV), plasma frequency ( $\omega_p^{\dagger}$  in eV), refractive index ( $n$ )<sup>†</sup>, and dielectric constant ( $\epsilon_\infty$ )<sup>†</sup> for the studied Cu-based chalcogenides. The calculated data are compared with other available results in the literature.

| Compound                            | a                       | c/a                     | $E_g$                   | $\Delta H_f$ | $\omega_p$ | $\epsilon_\infty$          |
|-------------------------------------|-------------------------|-------------------------|-------------------------|--------------|------------|----------------------------|
| Cu <sub>2</sub> ZnGeS <sub>4</sub>  | 5.30                    | 2.02                    | 1.76                    | -2.99        | 19.62      | 6.09                       |
|                                     | 5.34 <sup>a</sup> [240] | 1.97 <sup>a</sup> [240] | 2.06 <sup>a</sup> [240] |              |            |                            |
|                                     | 5.33 <sup>b</sup> [260] | 2.02 <sup>b</sup> [260] | 2.14 <sup>b</sup> [260] |              |            | 6.8 <sup>b</sup> [260]     |
| Cu <sub>2</sub> ZnGeSe <sub>4</sub> | 5.60                    | 2.01                    | 0.90                    | -2.31        | 18.16      | 7.56                       |
|                                     | 5.63 <sup>a</sup> [261] | 1.96 <sup>a</sup> [261] | 1.63 <sup>a</sup> [261] |              |            |                            |
|                                     | 5.38 <sup>b</sup> [260] | 2.02 <sup>b</sup> [260] | 1.32 <sup>b</sup> [260] |              |            | 9.01 <sup>b</sup> [260]    |
| Cu <sub>2</sub> ZnGeTe <sub>4</sub> | 6.04                    | 1.99                    | 0.49                    | -3.21        | 16.53      | 10.17                      |
|                                     | 5.60 <sup>a</sup> [240] | 1.99 <sup>a</sup> [240] |                         |              |            |                            |
|                                     | 6.09 <sup>b</sup> [260] | 2.00 <sup>b</sup> [260] | 0.5 <sup>b</sup> [260]  |              |            | 17.93 <sup>b</sup> [260]   |
| Cu <sub>2</sub> ZnSnS <sub>4</sub>  | 5.42                    | 2.01                    | 1.30                    | -3.15        | 19.00      | 6.25                       |
|                                     | 5.44 <sup>a</sup> [234] | 2.01 <sup>a</sup> [234] | 1.29 <sup>a</sup> [234] |              |            |                            |
|                                     | 5.34 <sup>c</sup> [262] | 2.01 <sup>c</sup> [262] | 1.27 <sup>c</sup> [262] |              |            | 6.48 <sup>a</sup> [234]    |
|                                     |                         |                         |                         |              |            | 6.99 <sup>c(z)</sup> [262] |
| Cu <sub>2</sub> ZnSnSe <sub>4</sub> | 5.71                    | 2.00                    | 0.71                    | -4.23        | 16.37      | 9.74                       |
|                                     | 5.61 <sup>a</sup> [263] | 1.99 <sup>a</sup> [263] | 1.41 <sup>a</sup> [264] |              |            |                            |
|                                     | 5.61 <sup>c</sup> [262] | 1.99 <sup>c</sup> [262] | 0.69 <sup>c</sup> [262] |              |            | 8.19(x) <sup>c</sup> [262] |
|                                     |                         |                         |                         |              |            | 8.27(z) <sup>c</sup> [262] |
| Cu <sub>2</sub> ZnSnTe <sub>4</sub> | 6.13                    | 2.00                    | 0.58                    | -2.24        | 16.38      | 9.74                       |
|                                     | 6.20 <sup>a</sup> [263] | 1.99 <sup>a</sup> [263] | 0.5 <sup>a</sup> [263]  |              |            |                            |
|                                     | 6.20 <sup>b</sup> [263] | 1.99 <sup>b</sup> [263] |                         |              |            | 14 <sup>a</sup> [263]      |
| Cu <sub>2</sub> CdGeS <sub>4</sub>  | 5.52                    | 1.91                    | 1.71                    | -3.97        | 19.02      | 6.06                       |
|                                     | 5.34 <sup>a</sup> [265] | 1.97 <sup>a</sup> [265] |                         |              |            |                            |
| Cu <sub>2</sub> CdGeSe <sub>4</sub> | 5.79                    | 1.92                    | 0.95                    | -3.08        | 18.46      | 7.51                       |
|                                     | 5.75 <sup>a</sup> [266] | 1.92 <sup>a</sup> [266] | 1.30 <sup>a</sup> [266] |              |            |                            |
| Cu <sub>2</sub> CdGeTe <sub>4</sub> | 6.20                    | 1.93                    | 0.71                    | -2.24        | 16.36      | 9.78                       |
|                                     | 6.13 <sup>a</sup> [257] | 1.94 <sup>a</sup> [257] |                         |              |            |                            |

Table 8.1 Continued

| Compound                     | a  | c/a  | $E_g$                           | $\Delta H_f$ | $\omega_p$ | $\varepsilon_\infty$             |
|------------------------------|--|--|---------------------------------|--------------|------------|----------------------------------|
| $\text{Cu}_2\text{CdSnS}_4$  | 5.617<br>5.59 <sup>a</sup> [267]                           | 1.940<br>1.94 <sup>a</sup> [267]                           | 1.22<br>1.45 <sup>a</sup> [268] | -3.74        | 18.68      | 6.25                             |
| $\text{Cu}_2\text{CdSnSe}_4$ | 5.88   | 1.95   | 0.70<br>0.96 <sup>a</sup> [269] | -4.01        | 17.74      | 7.72                             |
| $\text{Cu}_2\text{CdSnTe}_4$ | 6.27<br>6.20 <sup>a</sup> [270]                            | 1.97<br>1.98 <sup>a</sup> [270]                            | 0.70                            | -2.28        | 16.19      | 9.44                             |
| $\text{Cu}_2\text{HgGeS}_4$  | 5.52   | 1.92   | 1.21                            | -3.05        | 19.43      | 6.80                             |
| $\text{Cu}_2\text{HgGeSe}_4$ | 5.79   | 1.92   | 0.54                            | -3.14        | 18.40      | 8.90                             |
| $\text{Cu}_2\text{HgGeTe}_4$ | 6.19<br>6.11 <sup>a</sup> [257]                            | 1.94<br>1.95 <sup>a</sup> [257]                            | 0.38                            | -1.74        | 17.06      | 11.93                            |
| $\text{Cu}_2\text{HgSnS}_4$  | 5.61<br>5.57 <sup>a</sup> [271]                            | 1.95<br>1.95 <sup>a</sup> [271]                            | 0.83                            | -2.78        | 19.10      | 7.08                             |
| $\text{Cu}_2\text{HgSnSe}_4$ | 5.88<br>5.83 <sup>a</sup> [257]<br>5.84 <sup>b</sup> [273] | 1.95<br>1.96 <sup>a</sup> [257]<br>1.97 <sup>b</sup> [273] | 0.36<br>1.2 <sup>a</sup> [272]  | -2.28        | 18.12      | 9.58<br>13.78 <sup>b</sup> [273] |
| $\text{Cu}_2\text{HgSnTe}_4$ | 6.20<br>6.19 <sup>a</sup> [257]                            | 1.97<br>1.98 <sup>a</sup> [257]                            | 0.39                            | -1.71        | 16.15      | 11.38                            |

<sup>a</sup> Experimental results.

<sup>b</sup> Theoretical results using GGA functional.

<sup>c</sup> Theoretical results using HSE functional.

† The value is an average with respect to the direction of polarization.

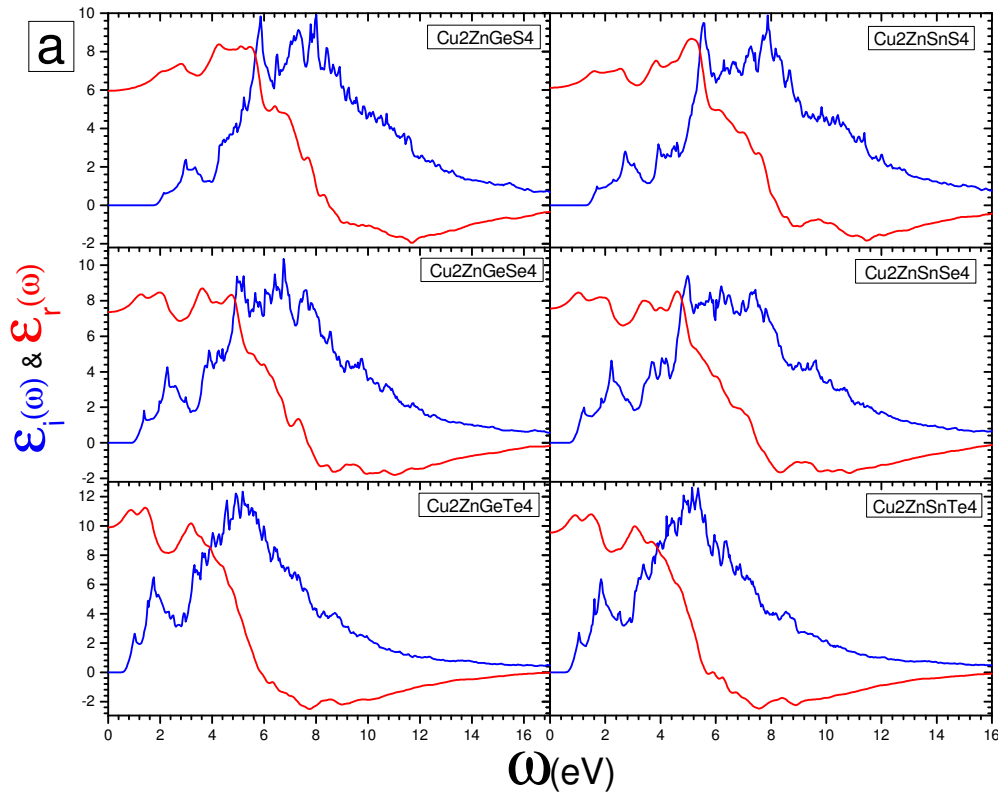
†† The PBE functional is used for the calculation of the formation energy.

(x), and (z) refer to  $\varepsilon_\infty$  in x, and z direction respectively.

Table 8.1 presents the list of studied stannite Cu-based chalcogenides.  $\text{Cu}_2\text{Zn}$ -based is followed by  $\text{Cu}_2\text{Cd}$ -based, and then  $\text{Cu}_2\text{Hg}$ -based compounds. For each compound, the first row presents the calculated HSE06 results, and the following rows contain the available experimental and theoretical data. For materials for which both HSE06 and GGA calculated results are available, we compare our results with the corresponding HSE06 values. For some materials such as

$\text{Cu}_2\text{ZnGeTe}_4$ , there is a discrepancy between our HSE06 calculated results and other theoretical data for  $\epsilon_\infty$  calculated using GGA/LDA functionals. The origin of this discrepancy is that the GGA/LDA calculated optical spectra are different from the HSE06 ones. Furthermore, the HSE06 spectra are comparable with the experimental ones and the GGA/LDA calculated spectra do not agree with the experimental ones. Table 8.1 shows that in each family of chalcogenides, e. g.  $\text{Cu}_2\text{HgGe-VI}_4$ , by replacing the element VI by one from the same group and with higher atomic number, there is an increase in  $\epsilon_\infty$ . Such an increase in  $\epsilon_\infty$  indicates that the polarizability of the system tends to increase. One can see that  $\omega_p$  decreases with the same substitution. Given that the number of valence electrons is the same for all of the studied chalcogenides, the decrease of  $\omega_p$  can be understood as a consequence of the enlargement of the lattice constant with this change in the atomic composition.

Figures 8.7, and 8.8 show the imaginary ( $\epsilon_i$ ) and real ( $\epsilon_r$ ) parts of the dielectric function for Cu-based chalcogenides. Fig. 8.7, and Fig. 8.8 present the component of the dielectric function along x and z direction, respectively. Each sub-plot in these figures consists of three families of plots, namely (a), (b), and (c) which corresponds to the plots for  $\text{Cu}_2\text{Zn-}$ ,  $\text{Cu}_2\text{Cd-}$ ,  $\text{Cu}_2\text{Hg-}$  based compounds, respectively.



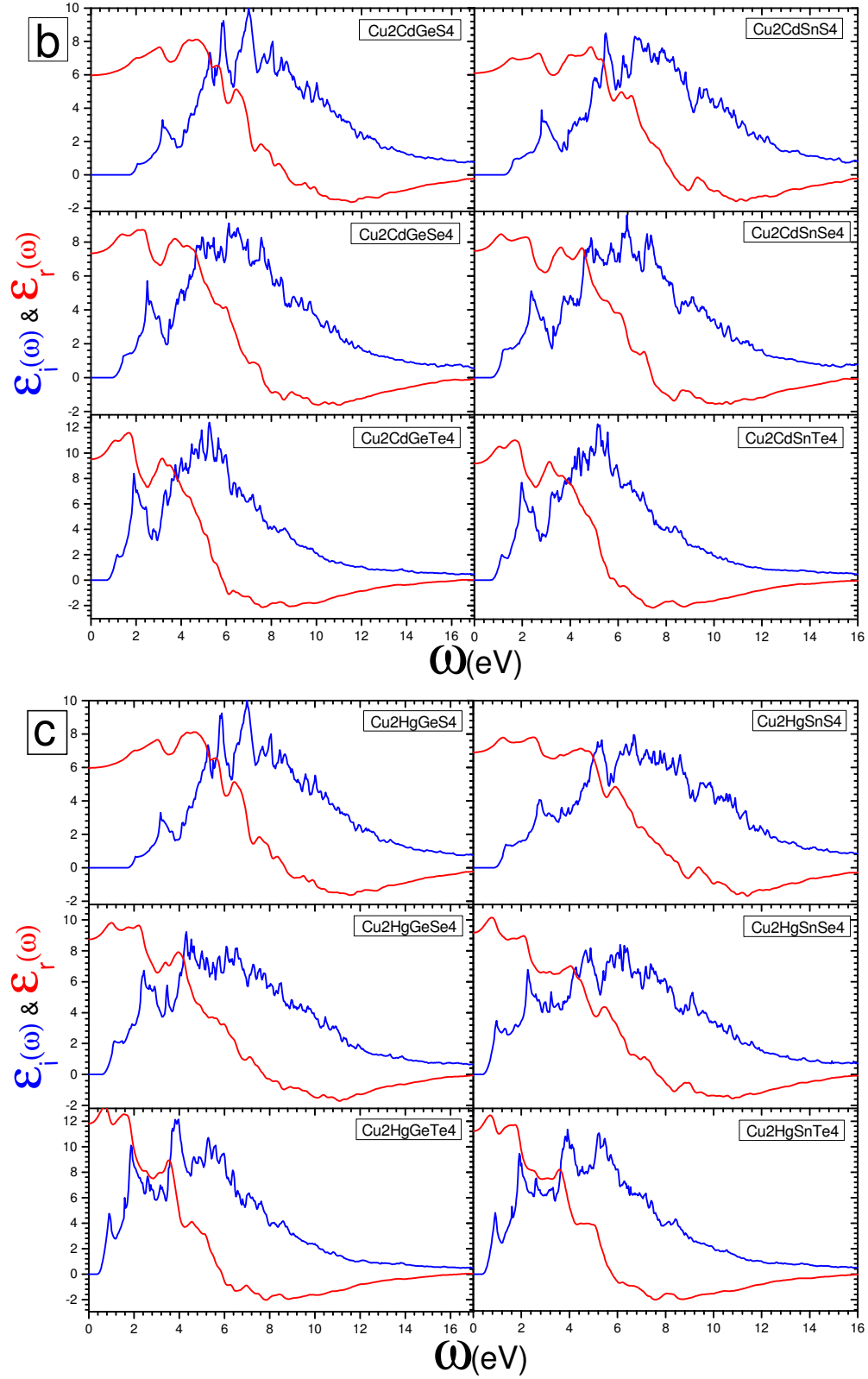
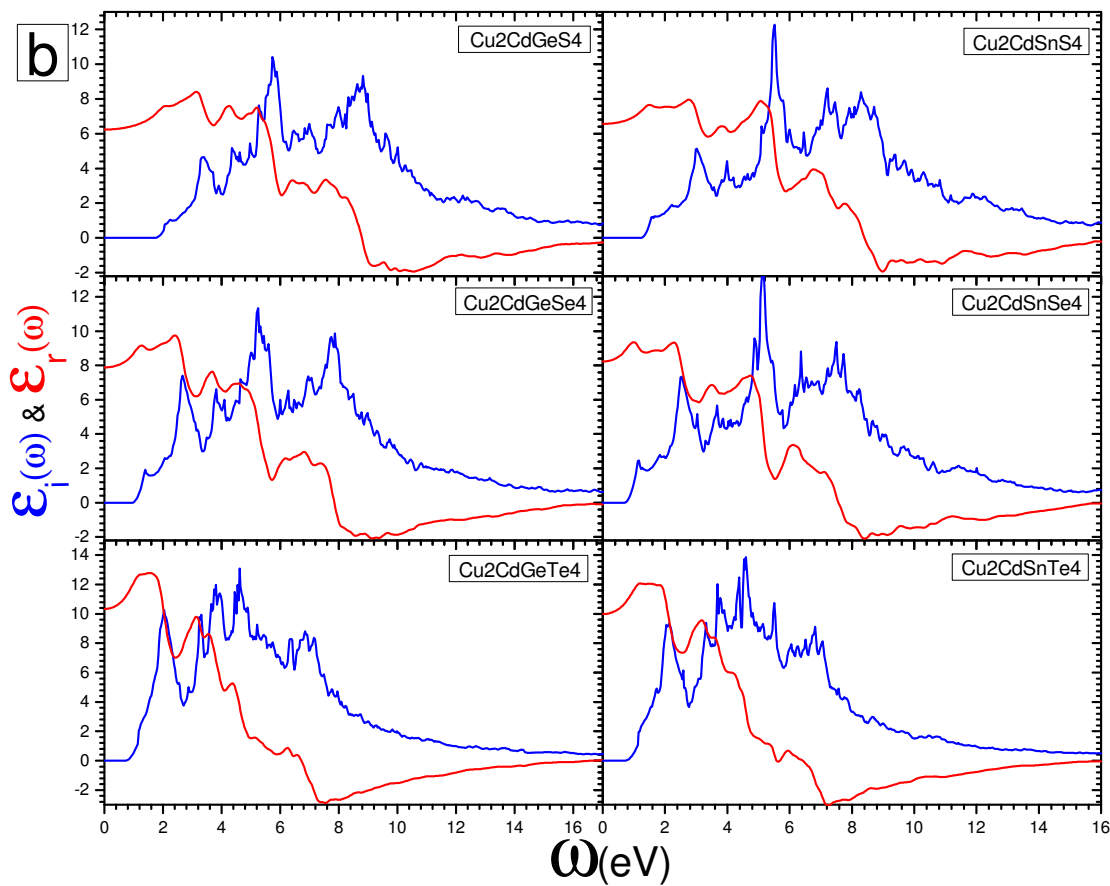
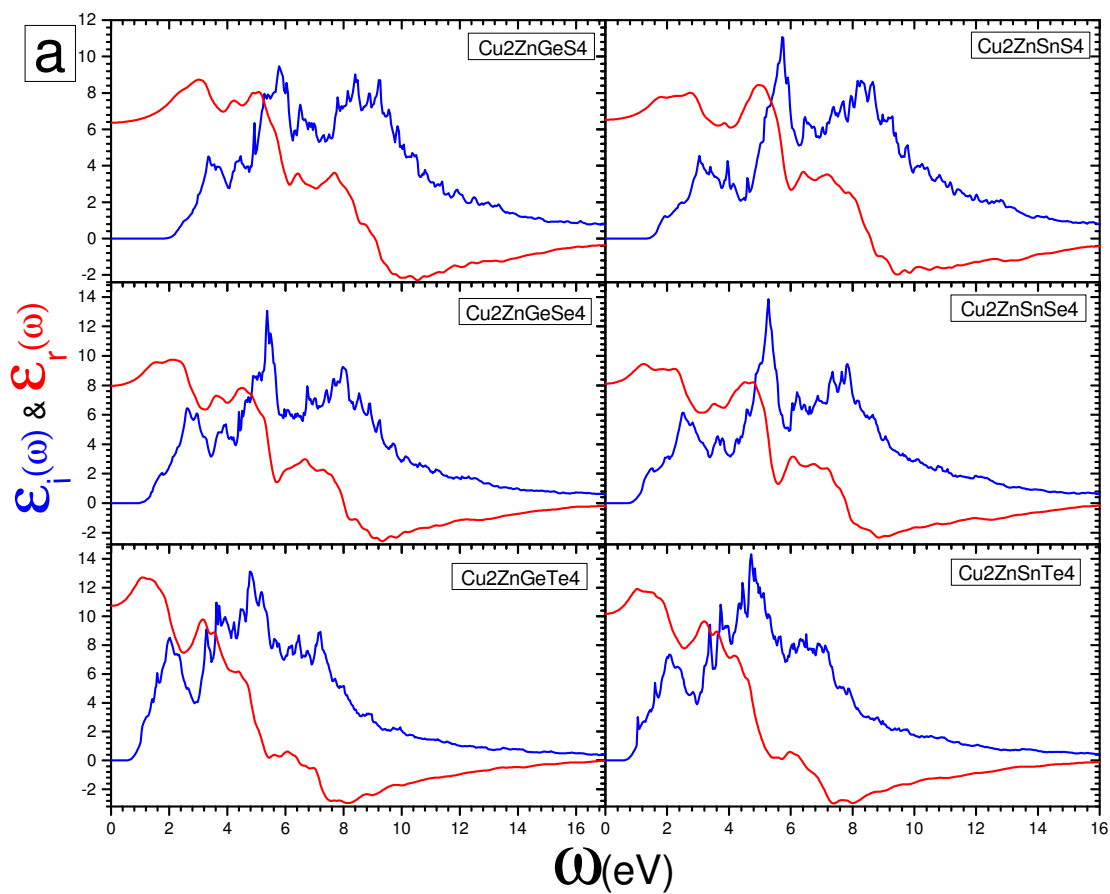


Figure 8.7: Imaginary and real part of the dielectric function ( $\epsilon_i$ , and  $\epsilon_r$ ) along x direction of the studied (a) Cu<sub>2</sub>Zn-based, (b) Cu<sub>2</sub>Cd-based, and (a) Cu<sub>2</sub>Hg-based chalcogenides. For each compound, the blue, and red figure corresponds to  $\epsilon_i$ , and  $\epsilon_r$ , respectively.



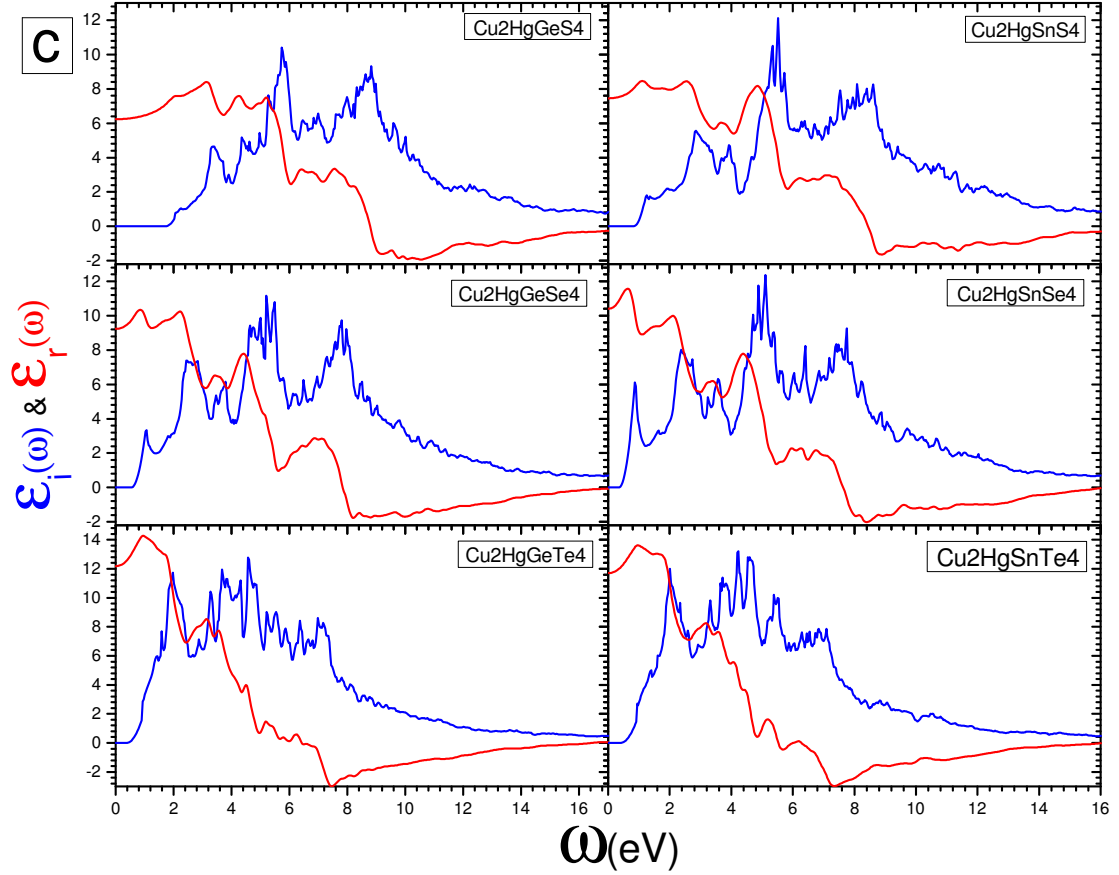
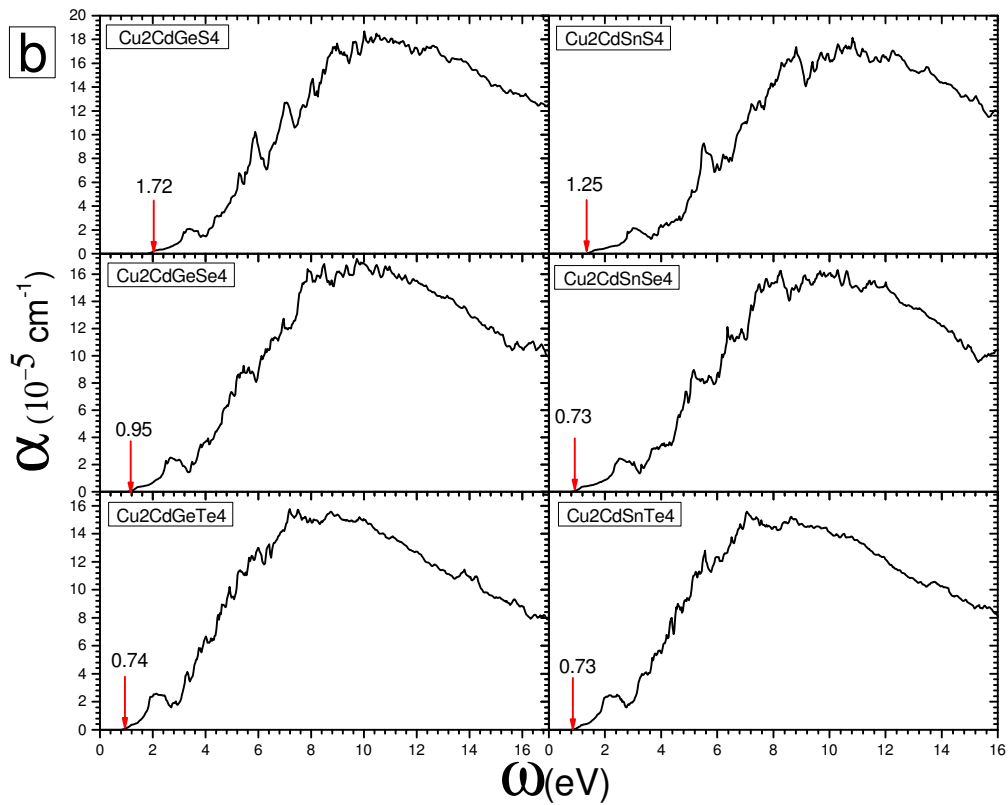
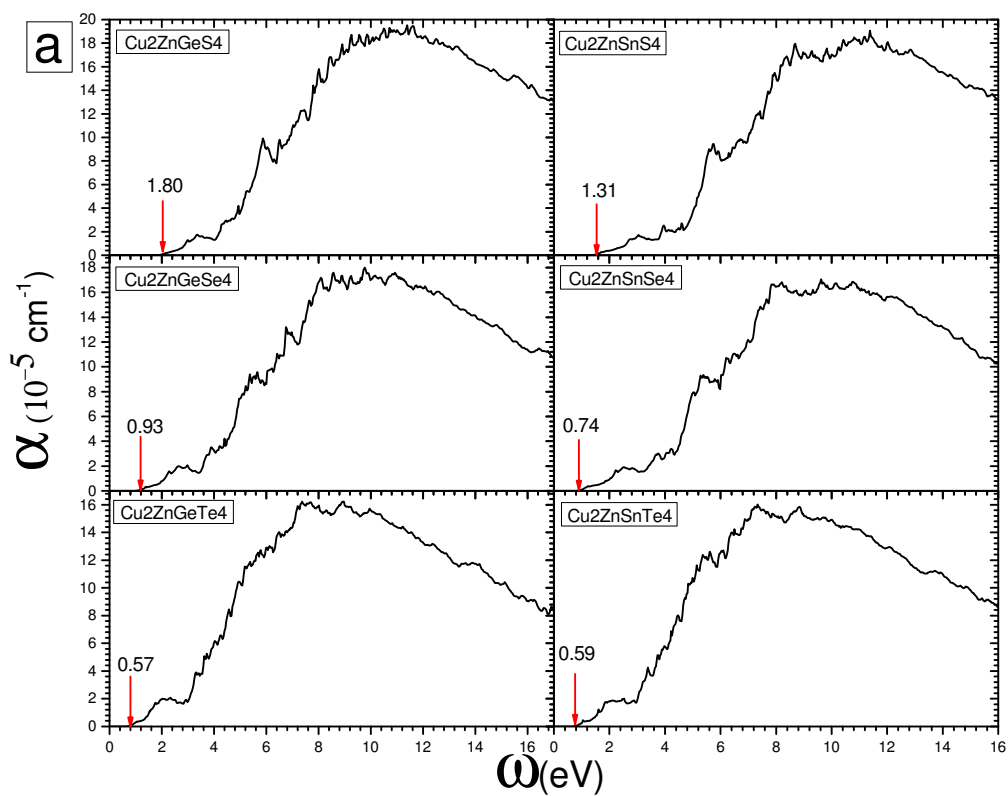


Figure 8.8: Imaginary and real part of the dielectric function ( $\epsilon_i$ , and  $\epsilon_r$ ) along z direction of the studied (a)  $\text{Cu}_2\text{Zn}$ -based, (b)  $\text{Cu}_2\text{Cd}$ -based, and (a)  $\text{Cu}_2\text{Hg}$ -based chalcogenides. For each compound, the blue, and red figure corresponds to  $\epsilon_i$ , and  $\epsilon_r$ , respectively.

There are two aspects about the low frequency behavior of the dielectric function that are relevant to experiment. One is the zero frequency limit of the real part of the dielectric function, i.e. the optical dielectric constant ( $\epsilon_\infty$ ).  $\epsilon_\infty$  is given in table 8.1 and its trend with respect to the composition is already discussed. The other aspect is the absorption edge, determined by onset of the imaginary part of the dielectric function.

Fig. 8.9(a)-(c) present the average absorption spectra. We use Eq. (3.15) to calculate the frequency dependent absorption coefficient for each compound. The absorption matrix is averaged over all components.



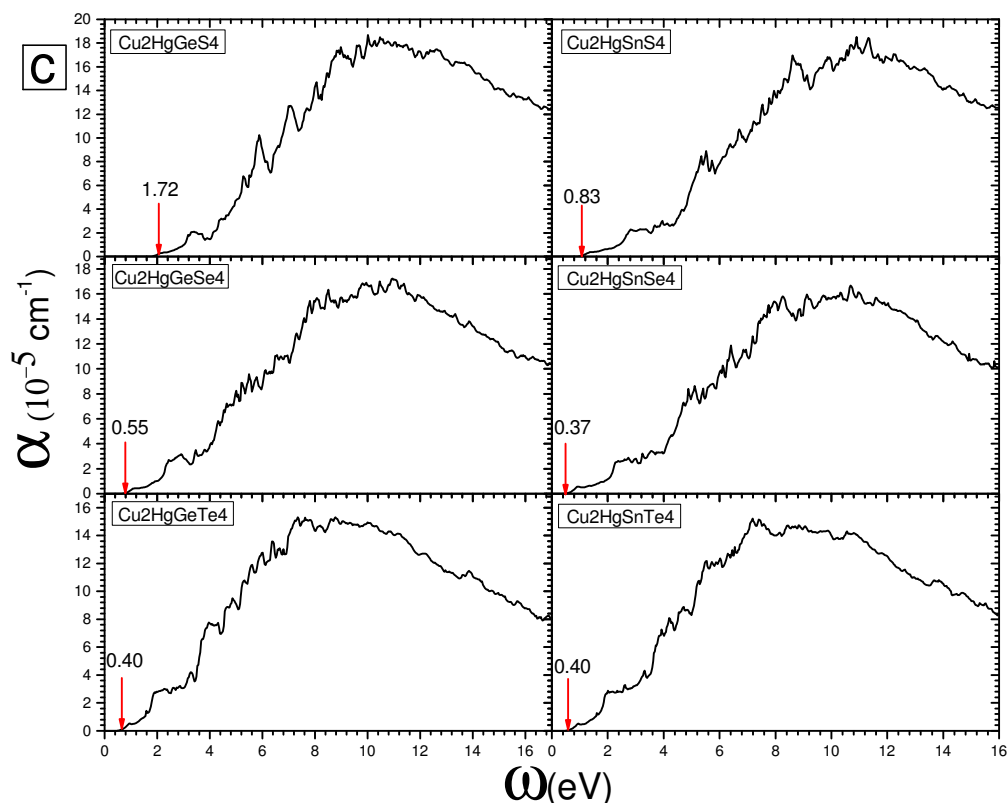
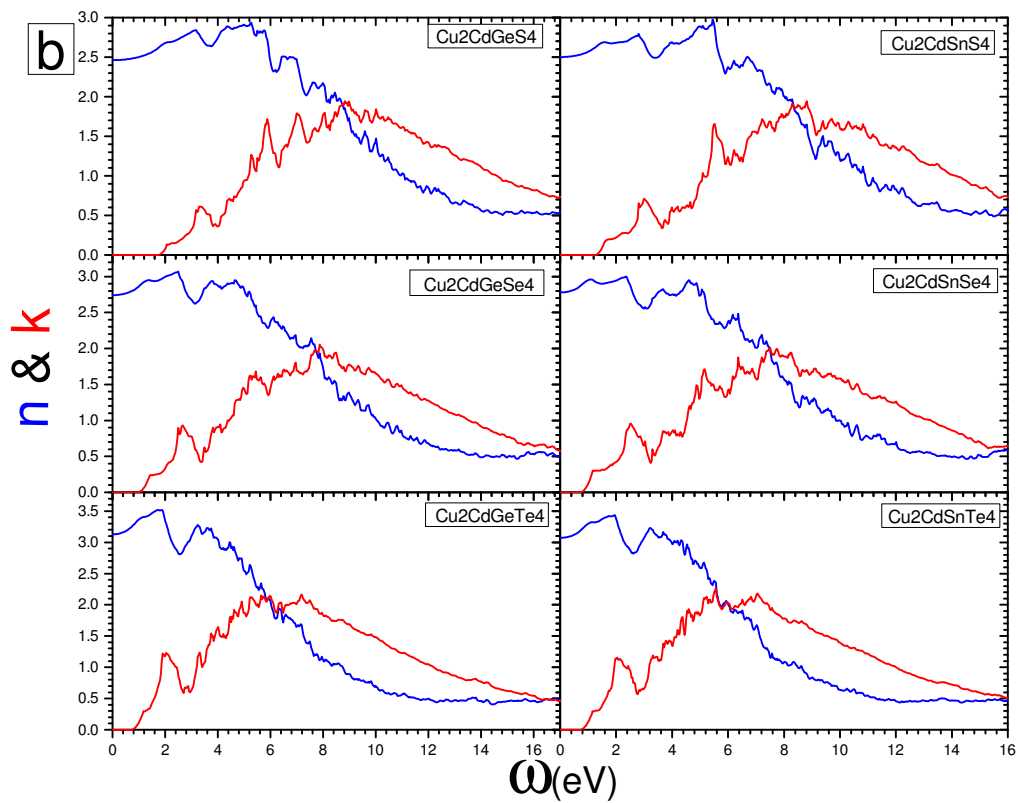
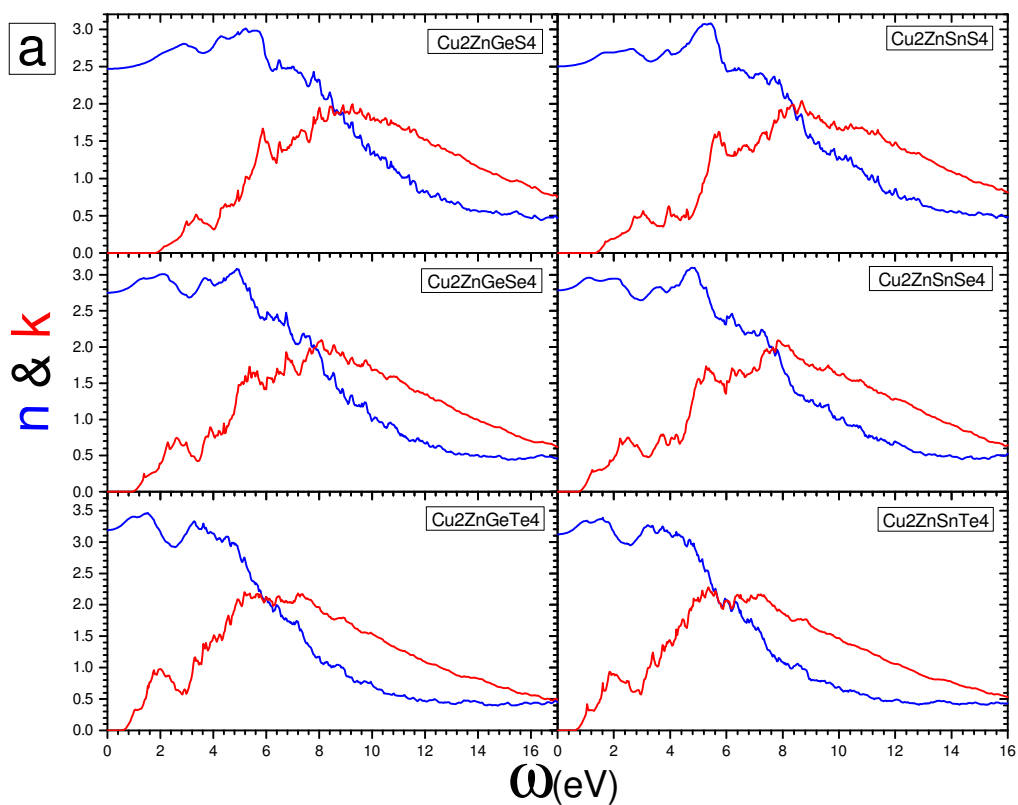


Figure 8.9: Averaged absorption coefficient versus photon energy (eV) for the studied (a) Cu<sub>2</sub>Zn-based, (b) Cu<sub>2</sub>Cd-based, and (a) Cu<sub>2</sub>Hg-based chalcogenides. The value of the first direct allowed transition is given for each compound in the corresponding plot.

The energy of the first direct allowed transition (optical band gap) can be found from the absorption spectra. By replacing element VI by an element with a higher atomic number there is a red shift in the absorption edge and the band gap also shows the same trend. Moreover, the comparison between the optical band gap and the fundamental band gap calculated from the band structure shows that the first transition is allowed for most of the compounds. It is important for an absorber layer to highly absorb most part of the solar spectrum and specifically visible light. By substituting S by Se and then Te (the VI element) there is an increase in the maximum absorption of the Cu<sub>2</sub>-II-IV-VI<sub>4</sub> compounds in the visible range (1.65 to 3.23 eV). For example, the maximum absorption of Cu<sub>2</sub>HgGeS<sub>4</sub>, Cu<sub>2</sub>HgGeSe<sub>4</sub>, and Cu<sub>2</sub>HgGeTe<sub>4</sub> is  $2.06$ ,  $2.40$ , and  $4.17 \times 10^5 \text{ cm}^{-1}$ , respectively. The opposite trend is found for the optical band gap. It means that the optical band gap of Cu<sub>2</sub>HgGeS<sub>4</sub>, 1.72 eV is larger than that of Cu<sub>2</sub>HgGeSe<sub>4</sub>, 0.55 eV, and Cu<sub>2</sub>HgGeTe<sub>4</sub>, 0.40 eV.





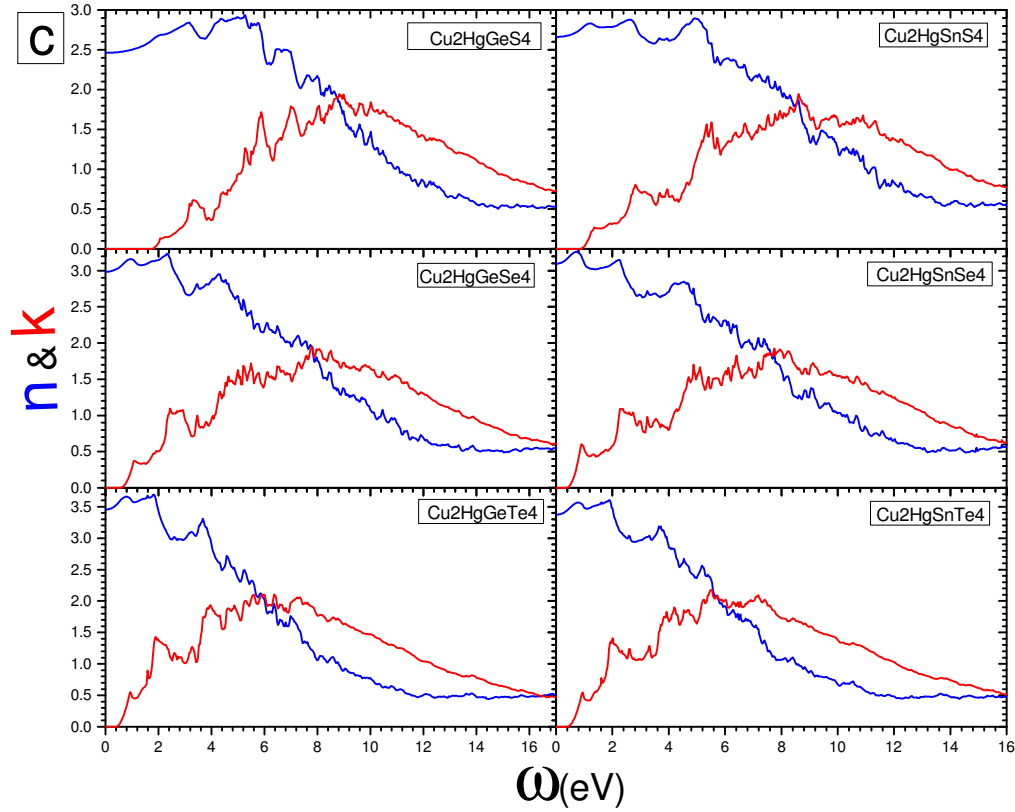


Figure 8.10: Averaged refractive index ( $n$ ), and averaged extinction coefficient ( $k$ ) is presented as a function of photon energy (eV) for the studied (a)  $\text{Cu}_2\text{Zn}$ -based, (b)  $\text{Cu}_2\text{Cd}$ -based, and (a)  $\text{Cu}_2\text{Hg}$ -based chalcogenides.

Figure 8.10 presents the averaged refractive index and averaged extinction coefficient of the studied chalcogenides as a function of the photon energy which are obtained from Eqs. (3.13) and (3.14). Eq. (3.13) gives the zero frequency refractive index ( $n_0 = \sqrt{\epsilon_\infty}$ ). Based on this formula, the same trend in  $\epsilon_\infty$  can be found in  $n_0$ .

We are interested in high efficiency absorber layers that have an efficiency higher than the existing thin film solar cells. Therefore, we limit our further study to the compounds that might yield a theoretical efficiency larger than 25%. It means that our investigations continue with the compounds that have a band gap between 0.8 and 1.9 eV. Such materials can have a maximum theoretical efficiency in the range of 25% and 33% according to the SQ limit.

As it is clear from Eq. (8.2) the efficiency depends on the thickness of the material via the absorptivity of the compound. An increase in  $L$  makes the absorptivity function close to the step function (see Eq. (8.12)) and as a result the efficiency moves toward the SQ limit. In order to include the

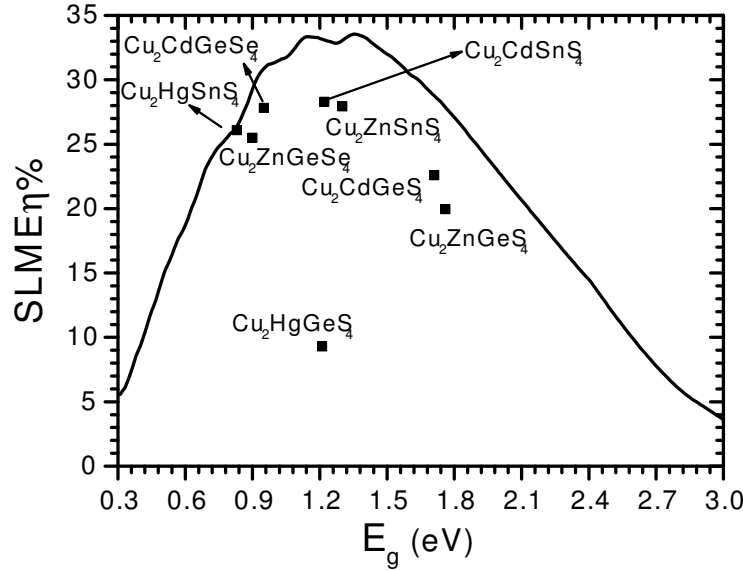


Figure 8.11: SLME ( $\eta$ ) versus the band gap ( $E_g$ ) for the studied chalcogenides at  $L = 0.5 \mu\text{m}$ . The full line presents the SQ limit.

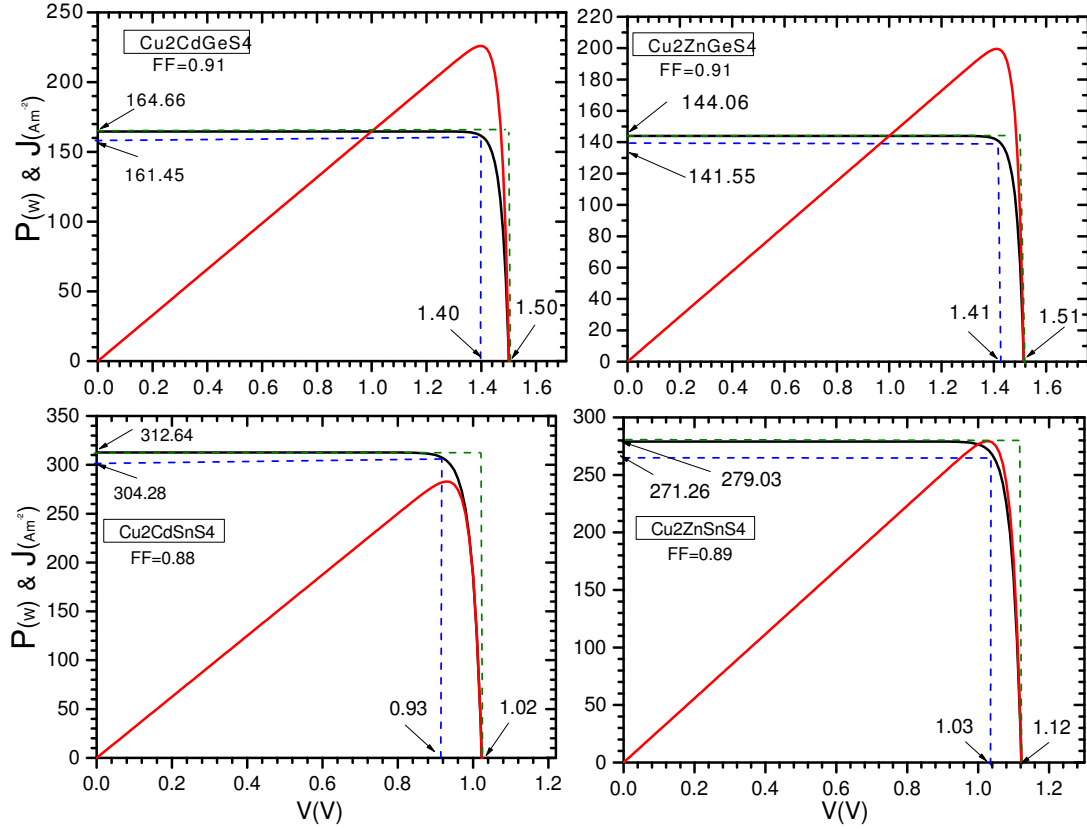
effect of the material optical properties, a reasonable thickness should be used. We use  $L = 0.5 \mu\text{m}$  as the thickness of the studied absorber layers.

Figure 8.11 presents the SLME parameter for the studied compounds as a function of the band gap energy. The SQ limit as the upper limit on the efficiency is also given as a curve. It is clear from Fig. 8.11 that  $\text{Cu}_2\text{HgGeS}_4$  has a band gap of 1.21 eV. Although, its band gap is very close to the band gap that corresponds to the maximum efficiency, this material results in a very low efficiency due to its indirect band gap.

The effect of the direct/indirect band gap is very clear from the comparison between  $\text{Cu}_2\text{HgGeS}_4$  and  $\text{Cu}_2\text{CdSnS}_4$ . The band gap of both compounds is almost 1.2 eV and the two compounds have almost the same absorption coefficient.  $\text{Cu}_2\text{HgGeS}_4$  has an indirect band gap compared with  $\text{Cu}_2\text{CdSnS}_4$  that has a direct one.  $\text{Cu}_2\text{HgGeS}_4$  has a much lower efficiency than  $\text{Cu}_2\text{CdSnS}_4$ . A comparison between  $\text{Cu}_2\text{CdGeSe}_4$  and  $\text{Cu}_2\text{ZnSnS}_4$  shows that it is possible to have a high efficiency absorber layer with the non-optimum band gap material.  $\text{Cu}_2\text{CdGeSe}_4$  has a band gap of 0.95 eV and the band gap of  $\text{Cu}_2\text{ZnSnS}_4$  is 1.30 eV. According to the SQ limit, the latter is expected to have higher efficiency. However, the former one has a high absorption that yields a high efficiency for this material.

For completeness, we plot the current-voltage and power-voltage curve for the studied chalcogenides. The voltage is the difference between the quasi Fermi level for electrons and holes. This value can be changed by applying an electric field (i.e. via incident of photons on the solar cell).

The voltage changes between zero and its maximum value which is the band gap voltage of the material.



$P_m$  and  $P_{nominal}$  are presented by blue and green dashed lines, respectively. Figure 8.12 also gives  $V_m$ , and  $V_{oc}$  as two voltages. For each compound, the lower voltage is  $V_m$ , and the higher one corresponds to  $V_{oc}$ . Each plot gives two more values, namely  $J_m$  (lower one) and  $J_{sc}$  (higher one). According to the definition of  $J_{sc}$  and  $J_m$  (see Eqs. (8.1) and (8.9)),  $J_{sc}$  is always larger than  $J_m$  and this difference depends on the recombination rate. Likewise, Eq. (8.11) implies that  $V_{oc}$  is always larger than  $V_m$ . Altogether,  $P_{nominal}$  is always larger by a factor than  $P_m$ . As already introduced in section 8.2.3, the FF determines the ratio between these two power values. The FF values are given for each compound in the corresponding plot in Fig 8.12.

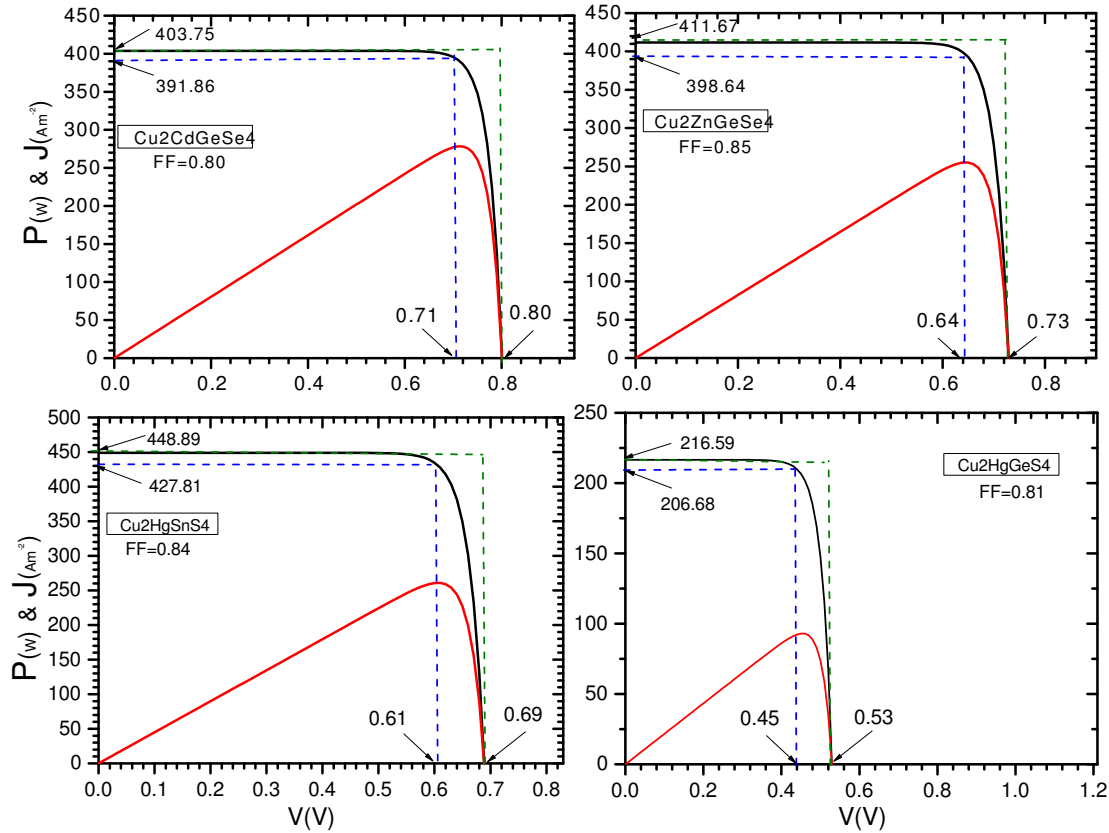


Figure 8.12: current density (black curve) and power (red curve) of the solar cells with respect to the voltage. Blue, and green dashed lines represent the  $P_m$  and  $P_{nominal}$ , respectively. Lower and higher value for voltages indicate  $V_m$ , and  $V_{oc}$ , respectively. Lower and higher value for current density values show  $J_m$ , and  $J_{sc}$ , respectively.

## 8.5 Conclusions

The results of this chapter show that the optoelectronic properties of the studied Cu-based chalcogenides  $Cu_2-II-IV-VI_4$  strongly depend on the element VI in the material composition. The change of element VI has a higher effect than changing element II, or IV in altering the characteristics of the studied chalcogenides. Replacement of the element VI by one from the same group with a higher atomic number decreases the plasma frequency and band gap and at the same time results in an increase in lattice parameters, and optical dielectric constant. A clear red shift in the absorption edge is observed which is correlated with the decrease in the band gap. Further investigations of the compounds of interest show that besides the fundamental band gap that plays a main role in

the efficiency of an absorber layer, its direct/indirect nature is an essential characteristic. The absorption coefficient is important to compare the efficiency of two compounds with the same band gap. In such a case two compounds have the same band gap and the same SQ efficiency, but the one with higher absorptivity has a higher efficiency than the other one. Finally, the results of the calculations identify  $\text{Cu}_2\text{CdGeSe}_4$  and  $\text{Cu}_2\text{-II-SnS}_4$  with  $\text{II}=\text{Cd}$ , and  $\text{Zn}$  as high efficiency absorber layers.

# Appendix A

## Supplementary information for Chapter 5

Table A.1: For each compound the results are given in five lines. They present lattice constant (Å), band gap (eV), position of the CBM (eV), position of the VBM (eV) with respect to the BPE, and the relative size of the stable region with respect to the total area of the stability triangle (in %), respectively.

PBE refers to the calculated results using the PBE functional.

Interp. HSE means that the HSE results of the corresponding binary oxides are used to calculate the values.  $\text{PBE}^{aver.}$  results are the average over the four considered configurations of  $(\text{X}_{0.5}\text{Y}_{0.5})_2\text{O}_3$ . The stability triangle is only plotted based on the PBE calculated results, therefore there is no data in Table A.1 for the HSE interpolated relative size of the stable region with respect to the total area of the stability triangle.

The few cases in which the calculations failed to converge, are denoted by a "×".

| XY   | $(\text{X}_{0.25}\text{Y}_{0.75})_2\text{O}_3$ |                | $(\text{X}_{0.5}\text{Y}_{0.5})_2\text{O}_3$ |                    |                    |                    |                      |                | $(\text{X}_{0.75}\text{Y}_{0.25})_2\text{O}_3$ |                |
|------|--|----------------|--|--------------------|--------------------|--------------------|----------------------|----------------|--|----------------|
|      | PBE  | interp.<br>HSE | PBE <sup>1st</sup>                           | PBE <sup>2nd</sup> | PBE <sup>3rd</sup> | PBE <sup>4th</sup> | PBE <sup>aver.</sup> | interp.<br>HSE | PBE  | interp.<br>HSE |
| BiCe | 11.341   | 11.358         | 11.307                                       | 11.23              | 11.311             | 11.338             | 11.297               | 11.311         | 11.252   | 11.264         |
|      | 2.574  | 4.882          | 2.284  | 2.630              | 2.680              | 2.480              | 2.519                | 4.311          | 2.746  | 3.740          |
|      | 1.170  | 2.221          | -3.696                                       | 1.415              | 1.369              | 1.300              | 0.097                | 2.057          | 1.645  | 1.893          |
|      | -1.404   | -2.662         | -5.980                                       | -1.215             | -1.312             | -1.181             | -2.422               | -2.255         | -1.102   | -1.848         |
|      | 8.771  |                | 19.431                                       | 19.463             | 19.509             | 19.640             | 19.511               |                | 30.309   |                |
| BiDy | 10.811   | 10.812         | 10.946                                       | 10.947             | 10.959             | 10.942             | 10.949               | 10.947         | 11.073   | 11.082         |
|      | 2.582  | 5.214          | 2.418  | 2.537              | 2.499              | 2.532              | 2.497                | 4.533          | 2.738  | 3.851          |
|      | 1.262  | 2.294          | 1.157  | 1.144              | 1.141              | 1.193              | 1.159                | 2.106          | 1.622  | 1.917          |
|      | -1.320   | -2.921         | -1.261                                       | -1.393             | -1.359             | -1.339             | -1.338               | -2.427         | -1.117   | -1.934         |
|      | 8.680  |                | 19.064                                       | 19.318             | 19.148             | 19.228             | 19.189               |                | 28.677   |                |
| BiEr | 10.715   | 10.704         | 10.885                                       | 10.778             | 10.895             | 10.878             | 10.859               | 10.875         | 11.047   | 11.046         |

Table A.1 Continued

| XY   | $(X_{0.25}Y_{0.75})_2O_3$ |                | $(X_{0.5}Y_{0.5})_2O_3$ |                    |                    |                    |                      |                | $(X_{0.75}Y_{0.25})_2O_3$ |                |
|------|---------------------------|----------------|-------------------------|--------------------|--------------------|--------------------|----------------------|----------------|---------------------------|----------------|
|      | PBE                       | interp.<br>HSE | PBE <sup>1st</sup>      | PBE <sup>2nd</sup> | PBE <sup>3rd</sup> | PBE <sup>4th</sup> | PBE <sup>aver.</sup> | interp.<br>HSE | PBE                       | interp.<br>HSE |
|      | 2.546                     | 5.282          | 2.406                   | 2.514              | 2.462              | 2.510              | 2.473                | 4.578          | 2.719                     | 3.873          |
|      | 1.236                     | 2.276          | 1.160                   | 1.143              | 1.114              | 1.173              | 1.148                | 2.094          | 1.592                     | 1.911          |
|      | -1.310                    | -3.006         | -1.246                  | -1.372             | -1.348             | -1.338             | -1.326               | -2.484         | -1.127                    | -1.962         |
|      | 4.808                     |                | 12.589                  | 12.983             | 12.682             | 12.727             | 12.745               |                | 26.018                    |                |
| BiEu | 10.902                    | 10.908         | 10.960                  | 10.961             | 10.965             | 10.965             | 10.963               | 11.011         | 11.023                    | 11.114         |
|      | 2.591                     | 5.180          | 2.412                   | 2.562              | 2.535              | 2.510              | 2.505                | 4.510          | 2.775                     | 3.840          |
|      | 1.268                     | 2.330          | 1.204                   | 1.243              | 1.241              | 1.173              | 1.216                | 2.130          | 1.704                     | 1.929          |
|      | -1.324                    | -2.851         | -1.209                  | -1.319             | -1.294             | -1.338             | -1.290               | -2.381         | -1.072                    | -1.911         |
|      | 5.337                     |                | 13.139                  | 13.257             | 13.194             | 13.204             | 13.397               |                | 26.707                    |                |
| BiFe | 9.528                     | 9.537          | 10.013                  | 9.979              | 10.090             | 10.557             | 10.160               | 10.097         | 10.663                    | 10.657         |
|      | 0                         | 0.812          | 0.001                   | 0                  | 0                  | 0                  | 0.001                | 1.598          | 0                         | 2.383          |
|      | 0.247                     | 1.527          | 0.426                   | 0.434              | 0.357              | 0.419              | 0.409                | 1.594          | -5.894                    | 1.662          |
|      | 0.290                     | 0.715          | 0.426                   | 0.437              | 0.372              | 0.457              | 0.423                | -0.004         | -5.851                    | -0.722         |
|      | 2.401                     |                | 7.118                   | 12.390             | 11.982             | 11.922             | 10.853               |                | 21.443                    |                |
| BiGa | 10.042                    | 9.861          | 10.371                  | 10.310             | 10.844             | 10.557             | 10.521               | 10.313         | 10.824                    | 10.765         |
|      | 1.624                     | 4.133          | 2.354                   | 2.247              | 2.406              | 2.377              | 2.346                | 3.812          | 1.790                     | 3.491          |
|      | 0.908                     | 0.826          | 1.039                   | 0.988              | 1.059              | 1.158              | 1.061                | 1.127          | 0.806                     | 1.428          |
|      | -0.716                    | -3.308         | -1.316                  | -1.260             | -1.347             | -1.220             | -1.286               | -2.686         | -0.985                    | -2.063         |
|      | 1.062                     |                | 13.518                  | 15.429             | 15.911             | 15.446             | 15.076               |                | 24.398                    |                |
| BiGd | 10.916                    | 10.915         | 11.021                  | 11.012             | 11.019             | 11.013             | 11.017               | 11.016         | 11.106                    | 11.117         |
|      | 2.575                     | 5.427          | 2.427                   | 2.544              | 2.518              | 2.540              | 2.508                | 4.674          | 2.729                     | 3.922          |
|      | 1.232                     | 2.467          | 1.156                   | 1.181              | 1.177              | 1.226              | 1.185                | 2.221          | 1.618                     | 1.975          |
|      | -1.344                    | -2.960         | -1.271                  | -1.364             | -1.342             | -1.315             | -1.323               | -2.454         | -1.112                    | -1.947         |
|      | 5.188                     |                | 13.005                  | 13.100             | 13.028             | 13.074             | 13.052               |                | 26.469                    |                |
| BiHo | 10.754                    | 10.758         | 10.914                  | 10.917             | 10.927             | 10.905             | 10.916               | 10.911         | 11.055                    | 11.064         |
|      | 2.567                     | 5.257          | 2.407                   | 2.530              | 2.483              | 2.524              | 2.486                | 4.561          | 2.723                     | 3.865          |
|      | 1.257                     | 2.258          | 1.155                   | 1.136              | 1.129              | 1.187              | 1.152                | 2.082          | 1.604                     | 1.906          |
|      | -1.311                    | -2.999         | -1.253                  | -1.395             | -1.355             | -1.337             | -1.335               | -2.480         | -1.120                    | -1.960         |
|      | 4.886                     |                | 12.654                  | 12.831             | 12.727             | 12.765             | 12.744               |                | 26.066                    |                |
| BiIn | 10.537                    | 10.533         | 10.634                  | 10.784             | 10.826             | 10.752             | 10.749               | 10.761         | 11.041                    | 10.989         |
|      | 1.458                     | 2.929          | 1.921                   | 2.367              | 2.252              | 2.200              | 2.185                | 3.009          | 2.426                     | 3.089          |
|      | 0.436                     | -0.011         | 0.892                   | 1.190              | 1.139              | 1.060              | 1.071                | 0.570          | 1.386                     | 1.149          |
|      | -1.022                    | -2.939         | -1.029                  | -1.177             | -1.114             | -1.140             | -1.115               | -2.440         | -1.041                    | -1.940         |
|      | 6.918                     |                | 17.625                  | 18.371             | 18.117             | 18.013             | 18.032               |                | 27.911                    |                |
| BiLa | 11.356                    | 11.336         | 11.323                  | 11.189             | 11.324             | 11.333             | 11.293               | 11.296         | 11.254                    | 11.257         |
|      | 2.652                     | 4.881          | 2.360                   | 2.696              | 2.744              | 2.562              | 2.591                | 4.311          | 2.773                     | 3.740          |



Table A.1 Continued

| XY   | $(X_{0.25}Y_{0.75})_2O_3$ |                | $(X_{0.5}Y_{0.5})_2O_3$ |                    |                    |                    |                      |                | $(X_{0.75}Y_{0.25})_2O_3$ |                |
|------|---------------------------|----------------|-------------------------|--------------------|--------------------|--------------------|----------------------|----------------|---------------------------|----------------|
|      | PBE                       | interp.<br>HSE | PBE <sup>1st</sup>      | PBE <sup>2nd</sup> | PBE <sup>3rd</sup> | PBE <sup>4th</sup> | PBE <sup>aver.</sup> | interp.<br>HSE | PBE                       | interp.<br>HSE |
|      | 1.341                     | 2.165          | 1.376                   | 1.528              | 1.458              | 1.330              | 1.423                | 2.020          | 1.715                     | 1.874          |
|      | -1.311                    | -2.717         | -0.984                  | -1.168             | -1.286             | -1.232             | -1.168               | -2.291         | -1.059                    | -1.866         |
|      | 7.659                     |                | 18.208                  | 18.692             | 18.466             | 18.372             | 18.435               |                | 30.562                    |                |
| BiLu | 10.577                    | 10.575         | 10.784                  | 10.685             | 10.805             | 10.778             | 10.763               | 10.789         | 11.007                    | 11.003         |
|      | 2.545                     | 5.342          | 2.391                   | 2.479              | 2.414              | 2.469              | 2.439                | 4.618          | 2.696                     | 3.894          |
|      | 1.267                     | 2.259          | 1.170                   | 1.107              | 1.069              | 1.145              | 1.123                | 2.083          | 1.564                     | 1.906          |
|      | -1.279                    | -3.084         | -1.221                  | -1.372             | -1.346             | -1.324             | -1.316               | -2.536         | -1.133                    | -1.988         |
|      | 5.852                     |                | 15.189                  | 15.812             | 15.403             | 15.458             | 15.466               |                | 28.185                    |                |
| BiMn | 9.983                     | 9.580          | 10.339                  | 10.059             | 10.352             | 10.256             | 10.252               | 10.126         | 10.636                    | 10.672         |
|      | 0                         | 2.462          | 0                       | 0                  | 0                  | 0                  | 0                    | 2.698          | 0                         | 2.934          |
|      | 0.711                     | 1.393          | 0.770                   | 0.718              | 0.680              | 0.715              | 0.721                | 1.505          | 0.415                     | 1.617          |
|      | 0.883                     | -1.070         | 0.781                   | 0.726              | 0.692              | 0.742              | 0.736                | -1.193         | 0.604                     | -1.317         |
|      | 5.523                     |                | 8.229                   | 15.196             | 18.252             | 13.188             | 13.716               |                | 0                         |                |
| BiPm | 11.108                    | 11.108         | 11.145                  | 11.139             | 11.131             | 11.146             | 11.141               | 11.144         | 11.171                    | 11.181         |
|      | 2.595                     | 5.047          | 2.361                   | 2.548              | 2.602              | 2.524              | 2.509                | 4.421          | 2.747                     | 3.795          |
|      | 1.213                     | 2.282          | 1.193                   | 1.280              | -3.677             | 1.285              | 0.021                | 2.098          | 1.645                     | 1.914          |
|      | -1.383                    | -2.765         | -1.169                  | -1.269             | -6.278             | -1.24              | -2.489               | -2.323         | -1.102                    | -1.882         |
|      | 8.705                     |                | 18.987                  | 19.139             | 19.01              | 19.098             | 19.059               |                | 29.928                    |                |
| BiPr | 11.273                    | 11.190         | 11.261                  | 11.252             | 11.262             | 11.262             | 11.26                | 11.199         | 11.229                    | 11.208         |
|      | 2.607                     | 5.016          | 2.334                   | 2.602              | 2.653              | 2.523              | 2.528                | 4.401          | 2.754                     | 3.785          |
|      | 1.195                     | 2.285          | 1.263                   | 1.359              | 1.342              | 1.329              | 1.324                | 2.100          | 1.652                     | 1.915          |
|      | -1.412                    | -2.732         | -1.072                  | -1.244             | -1.311             | -1.195             | -1.206               | -2.301         | -1.103                    | -1.871         |
|      | 7.192                     |                | 18.114                  | 18.278             | 18.163             | 18.208             | 18.191               |                | 29.183                    |                |
| BiSc | 10.247                    | 10.241         | 10.546                  | 10.571             | 10.619             | 10.538             | 10.569               | 10.566         | 10.901                    | 10.892         |
|      | 2.048                     | 5.446          | 2.230                   | 2.402              | 2.301              | 2.293              | 2.307                | 4.687          | 2.472                     | 3.928          |
|      | 1.508                     | 2.781          | 1.449                   | 1.379              | 1.315              | 1.392              | 1.384                | 2.430          | 1.520                     | 2.080          |
|      | -0.540                    | -2.666         | -0.781                  | -1.024             | -0.986             | -0.902             | -0.924               | -2.257         | -0.953                    | -1.849         |
|      | 3.271                     |                | 11.164                  | 11.736             | 11.465             | 11.508             | 11.468               |                | 24.839                    |                |
| BiSm | 11.053                    | 11.055         | 11.112                  | 11.099             | 11.102             | 11.106             | 11.105               | 11.109         | 11.153                    | 11.163         |
|      | 2.577                     | 5.065          | 2.383                   | 2.532              | 2.547              | 2.528              | 2.498                | 4.433          | 2.740                     | 3.801          |
|      | 1.207                     | 2.275          | 1.146                   | 1.238              | 1.235              | 1.265              | 1.221                | 2.093          | 1.635                     | 1.911          |
|      | -1.371                    | -2.791         | -1.237                  | -1.295             | -1.312             | -1.263             | -1.277               | -2.341         | -1.105                    | -1.891         |
|      | 7.861                     |                | 17.757                  | 17.878             | 17.761             | 17.853             | 17.812               |                | 29.837                    |                |
| BiTb | 10.859                    | 10.86          | 10.984                  | 10.981             | 10.989             | 10.975             | 10.983               | 10.979         | 11.091                    | 11.098         |
|      | 2.565                     | 5.188          | 2.429                   | 2.539              | 2.517              | 2.539              | 2.506                | 4.515          | 2.742                     | 3.842          |
|      | 1.231                     | 2.296          | 1.159                   | 1.161              | 1.160              | 1.208              | 1.172                | 2.107          | 1.625                     | 1.918          |

Table A.1 Continued

| XY   | $(X_{0.25}Y_{0.75})_2O_3$ |                | $(X_{0.5}Y_{0.5})_2O_3$ |                    |                    |                    |                      |                | $(X_{0.75}Y_{0.25})_2O_3$ |                |
|------|---------------------------|----------------|-------------------------|--------------------|--------------------|--------------------|----------------------|----------------|---------------------------|----------------|
|      | PBE                       | interp.<br>HSE | PBE <sup>1st</sup>      | PBE <sup>2nd</sup> | PBE <sup>3rd</sup> | PBE <sup>4th</sup> | PBE <sup>aver.</sup> | interp.<br>HSE | PBE                       | interp.<br>HSE |
|      | -1.335<br>10.240          | -2.893         | -1.271<br>20.120        | -1.379<br>20.400   | -1.357<br>20.217   | -1.332<br>20.314   | -1.335<br>20.263     | -2.409         | -1.118<br>25.703          | -1.925         |
| BiTl | 10.882                    | 10.879         | 11.014                  | 11.055             | 11.068             | 11.016             | 11.039               | 10.992         | 11.140                    | 11.105         |
|      | 0.880                     | 1.116          | 1.138                   | 1.300              | 1.282              | 1.286              | 1.252                | 1.800          | 1.928                     | 2.485          |
|      | 0.202                     | -1.070         | 0.281                   | 0.359              | 0.364              | 0.403              | 0.352                | -0.137         | 0.962                     | 0.796          |
|      | -0.679                    | -2.185         | -0.858                  | -0.941             | -0.919             | -0.883             | -0.901               | -1.937         | -0.967                    | -1.689         |
|      | 10.945                    |                | 22.365                  | 20.509             | 20.380             | 20.116             | 20.842               |                | 26.153                    |                |
| BiTm | 10.660                    | 10.659         | 10.742                  | 10.851             | 10.863             | 10.835             | 10.823               | 10.845         | 11.033                    | 11.031         |
|      | 2.560                     | 5.301          | 2.399                   | 2.512              | 2.451              | 2.485              | 2.462                | 4.590          | 2.706                     | 3.880          |
|      | 1.266                     | 2.260          | 1.194                   | 1.113              | 1.102              | 1.156              | 1.142                | 2.083          | 1.576                     | 1.906          |
|      | -1.295                    | -3.042         | -1.206                  | -1.399             | -1.349             | -1.329             | -1.321               | -2.508         | -1.131                    | -1.974         |
|      | 4.677                     |                | 12.651                  | 12.714             | 12.584             | 12.625             | 12.643               |                | 25.909                    |                |
| BiV  | 10.204                    | 9.752          | 11.142                  | 10.424             | ×                  | ×                  | 10.793               | 10.240         | 10.683                    | 10.729         |
|      | 0.005                     | 2.583          | 0                       | 0                  | ×                  | ×                  | 2.779                | 0.044          | 0                         | 2.974          |
|      | 1.471                     | 2.219          | 1.214                   | 1.206              | ×                  | ×                  | 1.210                | 2.055          | 1.030                     | 1.892          |
|      | 1.467                     | -0.356         | 1.283                   | 1.228              | ×                  | ×                  | 1.255                | -0.718         | 1.072                     | -1.079         |
|      | 4.266                     |                | 13.969                  | 14.757             | ×                  | ×                  | 14.363               |                | 24.601                    |                |
| BiY  | 10.833                    | 10.833         | 10.959                  | 10.964             | 10.967             | 10.955             | 10.962               | 10.961         | 11.082                    | 11.089         |
|      | 2.555                     | 5.292          | 2.430                   | 2.528              | 2.496              | 2.527              | 2.496                | 4.584          | 2.722                     | 3.877          |
|      | 1.294                     | 2.386          | 1.200                   | 1.180              | 1.178              | 1.229              | 1.197                | 2.167          | 1.620                     | 1.948          |
|      | -1.262                    | -2.906         | -1.230                  | -1.349             | -1.318             | -1.298             | -1.299               | -2.418         | -1.103                    | -1.929         |
|      | 9.767                     |                | 19.931                  | 20.299             | 20.131             | 20.160             | 20.130               |                | 26.480                    |                |
| BiYb | 10.603                    | 10.820         | 10.763                  | 10.815             | 10.810             | 10.791             | 10.795               | 10.952         | 10.987                    | 11.085         |
|      | 2.790                     | 5.321          | 1.510                   | 1.866              | 2.034              | 1.548              | 1.740                | 4.604          | 2.750                     | 3.887          |
|      | 1.837                     | 2.150          | 0.859                   | 1.239              | 1.340              | 0.960              | 1.100                | 2.010          | 1.607                     | 1.869          |
|      | -0.953                    | -3.172         | -0.652                  | -0.628             | -0.694             | -0.588             | -0.641               | -2.595         | -1.143                    | -2.018         |
|      | 20.391                    |                | 33.013                  | 32.563             | 32.469             | 32.864             | 32.727               |                | 39.347                    |                |
| CeDy | 10.850                    | 10.859         | 11.022                  | 10.876             | 11.025             | 11.016             | 10.985               | 11.041         | 11.198                    | 11.223         |
|      | 3.798                     | 5.785          | 3.701                   | 3.740              | 3.540              | 3.681              | 3.666                | 5.675          | 3.312                     | 5.564          |
|      | 1.571                     | 2.458          | 1.515                   | 1.480              | 1.337              | 1.475              | 1.452                | 2.434          | 1.112                     | 2.409          |
|      | -2.228                    | -3.328         | -2.186                  | -2.260             | -2.202             | -2.205             | -2.214               | -3.242         | -2.200                    | -3.155         |
|      | 0                         |                | 0                       | 0                  | 0                  | 0                  | 0                    |                | 0                         |                |
| CeEr | 10.762                    | 10.751         | 10.956                  | 10.816             | 10.981             | 10.964             | 10.93                | 10.969         | 11.167                    | 11.187         |
|      | 3.781                     | 5.853          | 3.683                   | 3.719              | 3.482              | 3.655              | 3.635                | 5.720          | 3.193                     | 5.587          |
|      | 1.555                     | 2.440          | 1.508                   | 1.465              | 1.291              | 1.460              | 1.431                | 2.422          | 1.002                     | 2.403          |
|      | -2.227                    | -3.413         | -2.175                  | -2.255             | -2.191             | -2.195             | -2.204               | -3.299         | -2.191                    | -3.184         |

Table A.1 Continued

| XY   | $(X_{0.25}Y_{0.75})_2O_3$ |                | $(X_{0.5}Y_{0.5})_2O_3$ |                    |                    |                    |                      |                | $(X_{0.75}Y_{0.25})_2O_3$ |                |
|------|---------------------------|----------------|-------------------------|--------------------|--------------------|--------------------|----------------------|----------------|---------------------------|----------------|
|      | PBE                       | interp.<br>HSE | PBE <sup>1st</sup>      | PBE <sup>2nd</sup> | PBE <sup>3rd</sup> | PBE <sup>4th</sup> | PBE <sup>aver.</sup> | interp.<br>HSE | PBE                       | interp.<br>HSE |
|      | 12.759                    |                | 24.497                  | 24.325             | 24.679             | 24.679             | 24.545               |                | 27.155                    |                |
| CeEu | 10.841                    | 10.955         | 10.937                  | 10.937             | 10.937             | 10.934             | 10.937               | 11.105         | 11.036                    | 11.255         |
|      | 3.952                     | 5.752          | 3.882                   | 3.792              | 3.726              | 3.852              | 3.813                | 5.652          | 3.556                     | 5.553          |
|      | 1.664                     | 2.494          | 1.613                   | 1.517              | 1.458              | 1.572              | 1.540                | 2.458          | 1.302                     | 2.421          |
|      | -2.289                    | -3.258         | -2.269                  | -2.275             | -2.268             | -2.28              | -2.273               | -3.195         | -2.255                    | -3.132         |
|      | 13.189                    |                | 24.766                  | 24.885             | 24.860             | 24.844             | 24.838               |                | 27.007                    |                |
| CeFe | 10.011                    | 9.584          | 10.127                  | ×                  | 10.326             | 10.368             | 10.274               | 10.191         | 10.827                    | 10.798         |
|      | 0                         | 1.383          | 0                       | ×                  | 0.011              | 0.026              | 0.013                | 2.740          | 0                         | 4.097          |
|      | 0.433                     | 1.691          | 0.383                   | ×                  | 0.298              | 0.377              | 0.353                | 1.922          | -0.063                    | 2.154          |
|      | 0.475                     | 0.308          | 0.414                   | ×                  | 0.288              | 0.351              | 0.351                | -0.818         | -0.053                    | -1.944         |
|      | 10.350                    |                | 15.876                  | ×                  | 21.494             | 19.990             | 19.120               |                | 0                         |                |
| CeGa | 10.299                    | 9.908          | 10.364                  | 10.247             | 10.554             | 10.553             | 10.430               | 10.407         | 10.945                    | 10.906         |
|      | 2.292                     | 4.705          | 2.098                   | 2.654              | 2.400              | 2.561              | 2.429                | 4.954          | 1.146                     | 5.204          |
|      | 0.149                     | 0.990          | 0.287                   | 0.666              | 0.595              | 0.672              | 0.555                | 1.455          | -0.811                    | 1.920          |
|      | -2.144                    | -3.715         | -1.812                  | -1.989             | -1.805             | -1.889             | -1.874               | -3.500         | -1.957                    | -3.284         |
|      | 7.903                     |                | 20.381                  | 0                  | 24.413             | 23.001             | 16.949               |                | 0                         |                |
| CeGd | 10.950                    | 10.962         | 11.094                  | 10.952             | 11.099             | 11.087             | 11.058               | 11.110         | 11.237                    | 11.258         |
|      | 3.802                     | 5.998          | 3.710                   | 3.747              | 3.579              | 3.687              | 3.681                | 5.816          | 3.412                     | 5.635          |
|      | 1.575                     | 2.631          | 1.516                   | 1.489              | 1.373              | 1.479              | 1.465                | 2.549          | 1.210                     | 2.467          |
|      | -2.228                    | -3.367         | -2.195                  | -2.259             | -2.206             | -2.209             | -2.218               | -3.268         | -2.202                    | -3.168         |
|      | 13.541                    |                | 25.220                  | 24.895             | 25.331             | 25.307             | 25.188               |                | 27.605                    |                |
| CeHo | 10.802                    | 10.805         | 10.987                  | 10.844             | 10.995             | 10.981             | 10.952               | 11.005         | 11.180                    | 11.205         |
|      | 3.792                     | 5.828          | 3.696                   | 3.730              | 3.515              | 3.676              | 3.655                | 5.703          | 3.247                     | 5.578          |
|      | 1.565                     | 2.422          | 1.515                   | 1.472              | 1.316              | 1.473              | 1.444                | 2.410          | 1.052                     | 2.397          |
|      | -2.228                    | -3.406         | -2.181                  | -2.258             | -2.200             | -2.203             | -2.211               | -3.294         | -2.195                    | -3.181         |
|      | 12.880                    |                | 24.571                  | 24.347             | 24.731             | 24.724             | 24.593               |                | 27.218                    |                |
| CeIn | 10.569                    | 10.58          | 10.854                  | 10.561             | 10.821             | 10.845             | 10.771               | 10.855         | 11.050                    | 11.13          |
|      | 1.154                     | 3.500          | 1.791                   | 2.479              | 2.032              | 1.979              | 2.071                | 4.151          | 1.745                     | 4.802          |
|      | -0.852                    | 0.154          | -0.184                  | 0.296              | -0.040             | -0.073             | -0.001               | 0.898          | -0.376                    | 1.641          |
|      | -2.006                    | -3.346         | -1.975                  | -2.183             | -2.071             | -2.051             | -2.070               | -3.254         | -2.120                    | -3.161         |
|      | 0                         |                | 0                       | 0                  | 0                  | 0                  | 0                    |                | 0                         |                |
| CeLa | 11.405                    | 11.383         | 11.401                  | 11.344             | 11.397             | 11.399             | 11.386               | 11.390         | 11.404                    | 11.398         |
|      | 3.444                     | 5.452          | 3.506                   | 3.627              | 3.667              | 3.558              | 3.590                | 5.453          | 3.737                     | 5.453          |
|      | 1.468                     | 2.329          | 1.471                   | 1.545              | 1.569              | -3.545             | 0.260                | 2.348          | 1.595                     | 2.366          |
|      | -1.976                    | -3.124         | -2.036                  | -2.082             | -2.099             | -7.102             | -3.330               | -3.106         | -2.142                    | -3.087         |
|      | 28.200                    |                | 42.394                  | 42.714             | 43.682             | 42.819             | 42.902               |                | 4.406                     |                |

Table A.1 Continued

| XY   | $(X_{0.25}Y_{0.75})_2O_3$ |                | $(X_{0.5}Y_{0.5})_2O_3$ |                    |                    |                    |                      |                | $(X_{0.75}Y_{0.25})_2O_3$ |                |
|------|---------------------------|----------------|-------------------------|--------------------|--------------------|--------------------|----------------------|----------------|---------------------------|----------------|
|      | PBE                       | interp.<br>HSE | PBE <sup>1st</sup>      | PBE <sup>2nd</sup> | PBE <sup>3rd</sup> | PBE <sup>4th</sup> | PBE <sup>aver.</sup> | interp.<br>HSE | PBE                       | interp.<br>HSE |
| CeLu | 10.628                    | 10.622         | 10.878                  | 10.77              | 10.886             | 10.866             | 10.85                | 10.883         | 11.14                     | 11.144         |
|      | 3.737                     | 5.913          | 3.618                   | 3.659              | 3.412              | 3.642              | 3.583                | 5.760          | 3.008                     | 5.607          |
|      | 1.514                     | 2.423          | 1.477                   | 1.425              | 1.235              | 1.457              | 1.399                | 2.410          | 0.836                     | 2.398          |
|      | -2.223                    | -3.491         | -2.140                  | -2.234             | -2.178             | -2.185             | -2.185               | -3.350         | -2.173                    | -3.210         |
|      | 18.309                    |                | 31.820                  | 32.195             | 32.266             | 32.386             | 32.167               |                | 29.320                    |                |
| CeMn | 10.026                    | 9.627          | 10.157                  | 10.049             | 10.116             | 10.477             | 10.200               | 10.220         | 0                         | 10.813         |
|      | 0                         | 3.033          | 0                       | 0.001              | 0.005              | 0                  | 0.002                | 3.840          | 0                         | 4.647          |
|      | 0.835                     | 1.557          | 0.682                   | 0.686              | 0.717              | 0.703              | 0.697                | 1.833          | 0                         | 2.109          |
|      | 0.861                     | -1.477         | 0.770                   | 0.686              | 0.713              | 0.706              | 0.719                | -2.008         | 0                         | -2.538         |
|      | 0                         |                | 0                       | 0                  | 0                  | 0                  | 0                    |                | 0                         |                |
| CePm | 11.139                    | 11.155         | 11.222                  | 11.075             | 11.224             | 11.22              | 11.186               | 11.238         | 11.306                    | 11.322         |
|      | 3.763                     | 5.618          | 3.698                   | 3.763              | 3.630              | 3.682              | 3.694                | 5.563          | 3.545                     | 5.508          |
|      | 1.548                     | 2.446          | 1.501                   | 1.510              | 1.425              | -2.080             | 0.589                | 2.426          | 1.345                     | 2.405          |
|      | -2.216                    | -3.172         | -2.198                  | -2.254             | -2.205             | -5.762             | -3.105               | -3.138         | -2.200                    | -3.103         |
|      | 30.489                    |                | 42.456                  | 32.270             | 43.820             | 43.331             | 40.469               |                | 32.864                    |                |
| CePr | 11.3                      | 11.237         | 11.329                  | 11.18              | 11.332             | 11.330             | 11.293               | 11.293         | 11.363                    | 11.349         |
|      | 3.675                     | 5.588          | 3.651                   | 3.744              | 3.630              | 3.641              | 3.667                | 5.543          | 3.594                     | 5.498          |
|      | 1.477                     | 2.449          | 1.459                   | 1.499              | 1.435              | 1.448              | 1.461                | 2.428          | 1.404                     | 2.406          |
|      | -2.199                    | -3.139         | -2.192                  | -2.246             | -2.196             | -2.193             | -2.207               | -3.115         | -2.19                     | -3.092         |
|      | 0                         |                | 0                       | 0                  | 0                  | 0                  | 0                    |                | 0                         |                |
| CeSc | 10.316                    | 10.288         | 10.617                  | 10.463             | 10.675             | 10.598             | 10.589               | 10.660         | 11.048                    | 11.033         |
|      | 3.303                     | 6.017          | 3.601                   | 3.678              | 3.397              | 3.748              | 3.606                | 5.829          | 2.806                     | 5.641          |
|      | 1.691                     | 2.945          | 1.909                   | 1.781              | 1.629              | 1.898              | 1.805                | 2.758          | 0.918                     | 2.572          |
|      | -1.612                    | -3.073         | -1.692                  | -1.897             | -1.768             | -1.851             | -1.802               | -3.072         | -1.889                    | -3.070         |
|      | 10.880                    |                | 23.162                  | 23.026             | 23.071             | 23.426             | 23.171               |                | 25.767                    |                |
| CeSm | 11.093                    | 11.102         | 11.186                  | 11.038             | 11.189             | 11.184             | 11.150               | 11.203         | 11.287                    | 11.304         |
|      | 3.763                     | 5.636          | 3.700                   | 3.755              | 3.615              | 3.680              | 3.688                | 5.575          | 3.507                     | 5.514          |
|      | 1.547                     | 2.439          | 1.503                   | 1.501              | 1.410              | 1.475              | 1.473                | 2.421          | 1.306                     | 2.403          |
|      | -2.216                    | -3.198         | -2.198                  | -2.255             | -2.206             | -2.205             | -2.216               | -3.155         | -2.201                    | -3.112         |
|      | 27.374                    |                | 40.563                  | 38.418             | 40.889             | 40.791             | 40.165               |                | 33.625                    |                |
| CeTb | 10.897                    | 10.907         | 11.051                  | 10.899             | 11.057             | 11.047             | 11.014               | 11.073         | 11.209                    | 11.239         |
|      | 3.808                     | 5.759          | 3.714                   | 3.756              | 3.562              | 3.690              | 3.681                | 5.657          | 3.361                     | 5.555          |
|      | 1.579                     | 2.460          | 1.520                   | 1.492              | 1.356              | 1.481              | 1.463                | 2.435          | 1.159                     | 2.410          |
|      | -2.229                    | -3.300         | -2.194                  | -2.264             | -2.207             | -2.21              | -2.219               | -3.223         | -2.202                    | -3.146         |
|      | 0                         |                | 0                       | 0                  | 0                  | 0                  | 0                    |                | 0                         |                |
| CeTl | 10.956                    | 10.926         | 11.076                  | 10.907             | 11.101             | 11.075             | 11.040               | 11.086         | 11.24                     | 11.246         |

Table A.1 Continued

| XY   | $(X_{0.25}Y_{0.75})_2O_3$ |                | $(X_{0.5}Y_{0.5})_2O_3$ |                    |                    |                    |                      |                | $(X_{0.75}Y_{0.25})_2O_3$ |                |
|------|---------------------------|----------------|-------------------------|--------------------|--------------------|--------------------|----------------------|----------------|---------------------------|----------------|
|      | PBE                       | interp.<br>HSE | PBE <sup>1st</sup>      | PBE <sup>2nd</sup> | PBE <sup>3rd</sup> | PBE <sup>4th</sup> | PBE <sup>aver.</sup> | interp.<br>HSE | PBE                       | interp.<br>HSE |
|      | 0.273                     | 1.687          | 0.785                   | 1.054              | 0.900              | 0.845              | 0.896                | 2.943          | 1.047                     | 4.198          |
|      | -1.399                    | -0.906         | -1.031                  | -0.787             | -0.921             | -5.358             | -2.025               | 0.192          | -0.995                    | 1.288          |
|      | -1.672                    | -2.592         | -1.815                  | -1.840             | -1.82              | -6.203             | -2.920               | -2.751         | -2.042                    | -2.910         |
|      | 0                         |                | 0                       | 0                  | 0                  | 0                  | 0                    |                | 0                         |                |
| CeTm | 10.708                    | 10.706         | 10.916                  | 10.778             | 10.928             | 10.925             | 10.887               | 10.939         | 11.146                    | 11.172         |
|      | 3.759                     | 5.872          | 3.670                   | 3.706              | 3.464              | 3.652              | 3.623                | 5.732          | 3.123                     | 5.593          |
|      | 1.533                     | 2.424          | 1.504                   | 1.454              | 1.273              | 1.461              | 1.423                | 2.411          | 0.937                     | 2.398          |
|      | -2.226                    | -3.449         | -2.166                  | -2.252             | -2.191             | -2.191             | -2.200               | -3.322         | -2.186                    | -3.196         |
|      | 12.525                    |                | 24.302                  | 24.178             | 24.49              | 24.515             | 24.371               |                | 27.015                    |                |
| CeV  | 10.089                    | 9.799          | 10.222                  | 10.193             | 10.320             | 10.381             | 10.279               | 10.334         | 10.740                    | 10.870         |
|      | 0                         | 3.154          | 0.016                   | 0                  | 0.005              | 0                  | 0.006                | 3.921          | 0                         | 4.687          |
|      | 1.488                     | 2.383          | 1.457                   | 1.375              | 1.371              | 1.338              | 1.386                | 2.383          | 1.095                     | 2.384          |
|      | 1.511                     | -0.763         | 1.441                   | 1.391              | 1.367              | 1.342              | 1.386                | -1.532         | 1.104                     | -2.300         |
|      | 10.312                    |                | 21.704                  | 21.359             | 20.731             | 23.627             | 21.855               |                | 22.845                    |                |
| CeY  | 10.876                    | 10.880         | 11.034                  | 10.883             | 11.039             | 11.027             | 10.996               | 11.055         | 11.204                    | 11.230         |
|      | 3.878                     | 5.863          | 3.753                   | 3.778              | 3.591              | 3.720              | 3.711                | 5.726          | 3.374                     | 5.590          |
|      | 1.704                     | 2.550          | 1.592                   | 1.548              | 1.416              | 1.543              | 1.525                | 2.495          | 1.189                     | 2.440          |
|      | -2.175                    | -3.314         | -2.161                  | -2.231             | -2.175             | -2.178             | -2.187               | -3.232         | -2.186                    | -3.151         |
|      | 0                         |                | 0                       | 0                  | 0                  | 0                  | 0                    |                | 0                         | 0              |
| CeYb | 10.865                    | 10.867         | 11.041                  | 10.825             | 11.076             | 11.034             | 10.994               | 11.046         | 11.211                    | 11.226         |
|      | 4.160                     | 5.892          | 4.165                   | 4.134              | 4.002              | 4.099              | 4.100                | 5.746          | 3.717                     | 5.600          |
|      | 1.562                     | 2.314          | 1.595                   | 1.525              | 1.425              | -1.508             | 0.760                | 2.338          | 1.325                     | 2.361          |
|      | -2.599                    | -3.579         | -2.570                  | -2.609             | -2.577             | -5.606             | -3.341               | -3.409         | -2.392                    | -3.239         |
|      | 30.318                    |                | 42.403                  | 34.375             | 46.581             | 43.142             | 41.625               |                | 2.689                     |                |
| DyEr | 10.580                    | 10.569         | 10.613                  | ×                  | 10.614             | 10.612             | 10.613               | 10.605         | 10.650                    | 10.641         |
|      | 3.991                     | 5.963          | 3.968                   | ×                  | 3.939              | 3.968              | 3.959                | 5.941          | 3.898                     | 5.918          |
|      | 0.777                     | 2.464          | 1.533                   | ×                  | 1.492              | 1.527              | 1.518                | 2.470          | 1.466                     | 2.476          |
|      | 1.541                     | -3.500         | -2.435                  | ×                  | -2.447             | -2.442             | -2.442               | -3.471         | -2.433                    | -3.443         |
|      | 12.472                    |                | 23.537                  | ×                  | 23.567             | 23.549             | 23.551               |                | 22.012                    |                |
| DyEu | 10.749                    | 10.773         | 10.814                  | 10.704             | 10.702             | 10.703             | 10.731               | 10.741         | 10.655                    | 10.709         |
|      | 3.875                     | 5.862          | 3.906                   | 3.956              | 3.971              | 3.934              | 3.942                | 5.873          | 4.029                     | 5.885          |
|      | 0.657                     | 2.518          | 1.509                   | 1.560              | 1.581              | 1.535              | 1.547                | 2.506          | 1.627                     | 2.494          |
|      | 1.485                     | -3.344         | -2.398                  | -2.396             | -2.39              | -2.399             | -2.396               | -3.368         | -2.402                    | -3.391         |
|      | 10.281                    |                | 19.344                  | 19.346             | 19.324             | 19.344             | 19.339               |                | 22.018                    | 0              |
| DyFe | 9.415                     | 9.402          | 9.789                   | 9.713              | 9.888              | 9.845              | 9.809                | 9.827          | 10.282                    | 10.252         |
|      | 0.015                     | 1.493          | 0                       | 0                  | 0                  | 0                  | 0                    | 2.961          | 0                         | 4.428          |

Table A.1 Continued

| XY   | $(X_{0.25}Y_{0.75})_2O_3$ |                | $(X_{0.5}Y_{0.5})_2O_3$ |                    |                    |                    |                      |                | $(X_{0.75}Y_{0.25})_2O_3$ |                |
|------|---------------------------|----------------|-------------------------|--------------------|--------------------|--------------------|----------------------|----------------|---------------------------|----------------|
|      | PBE                       | interp.<br>HSE | PBE <sup>1st</sup>      | PBE <sup>2nd</sup> | PBE <sup>3rd</sup> | PBE <sup>4th</sup> | PBE <sup>aver.</sup> | interp.<br>HSE | PBE                       | interp.<br>HSE |
|      | 0.014                     | 1.715          | 0.266                   | 0.207              | 0.220              | 0.237              | 0.233                | 1.971          | -0.279                    | 2.226          |
|      | 0.148                     | 0.222          | 0.283                   | 0.213              | 0.221              | 0.265              | 0.246                | -0.991         | -0.250                    | -2.203         |
|      | 10.537                    |                | 20.013                  | 23.422             | 21.408             | 22.445             | 21.822               |                | 0                         |                |
| DyGa | 9.840                     | 9.726          | 10.073                  | 10.086             | 10.233             | 10.143             | 10.134               | 10.043         | 10.389                    | 10.36          |
|      | 1.887                     | 4.815          | 2.057                   | 2.658              | 2.539              | 2.460              | 2.429                | 5.175          | 1.808                     | 5.536          |
|      | 2.618                     | 1.014          | 0.139                   | 0.384              | 0.306              | 0.310              | 0.285                | 1.503          | -0.504                    | 1.993          |
|      | -0.083                    | -3.801         | -1.919                  | -2.274             | -2.234             | -2.151             | -2.145               | -3.672         | -2.312                    | -3.543         |
|      | 16.468                    |                | 27.187                  | 27.127             | 26.764             | 27.459             | 27.134               |                | 18.813                    |                |
| DyGd | 10.781                    | 10.780         | 10.746                  | 10.745             | 10.746             | 10.747             | 10.746               | 10.745         | 10.710                    | 10.711         |
|      | 3.858                     | 6.109          | 3.875                   | 3.902              | 3.913              | 3.890              | 3.895                | 6.038          | 3.949                     | 5.967          |
|      | 0.696                     | 2.655          | 1.492                   | 1.521              | 1.537              | 1.507              | 1.515                | 2.598          | 1.565                     | 2.540          |
|      | 1.480                     | -3.454         | -2.384                  | -2.381             | -2.377             | -2.384             | -2.382               | -3.441         | -2.384                    | -3.427         |
|      | 12.613                    |                | 23.689                  | 23.678             | 23.667             | 23.684             | 23.679               |                | 26.861                    |                |
| DyHo | 10.630                    | 10.623         | 10.647                  | 10.646             | 10.644             | 10.641             | 10.645               | 10.641         | 10.659                    | 10.659         |
|      | 3.967                     | 5.939          | 3.954                   | 3.942              | 3.942              | 3.956              | 3.949                | 5.924          | 3.929                     | 5.910          |
|      | 0.746                     | 2.447          | 1.531                   | 1.515              | 1.512              | 1.528              | 1.522                | 2.459          | 1.502                     | 2.470          |
|      | 1.538                     | -3.492         | -2.424                  | -2.428             | -2.431             | -2.429             | -2.428               | -3.466         | -2.427                    | -3.440         |
|      | 12.445                    |                | 23.485                  | 23.495             | 23.498             | 23.489             | 23.492               |                | 22.078                    | 0              |
| DyIn | 10.408                    | 10.398         | 10.497                  | 10.503             | 10.497             | 10.500             | 10.500               | 10.491         | 10.587                    | 10.584         |
|      | 1.565                     | 3.610          | 2.092                   | 2.171              | 2.136              | 2.132              | 2.133                | 4.372          | 2.270                     | 5.134          |
|      | 3.385                     | 0.178          | -0.213                  | -0.139             | -0.189             | -0.169             | -0.178               | 0.946          | -0.133                    | 1.714          |
|      | -0.761                    | -3.432         | -2.305                  | -2.310             | -2.324             | -2.300             | -2.310               | -3.426         | -2.403                    | -3.420         |
|      | 19.807                    |                | 27.982                  | 30.306             | 31.02              | 29.430             | 29.685               |                | 22.022                    |                |
| DyLa | 11.231                    | 11.201         | 11.042                  | 11.019             | 11.026             | 11.037             | 11.031               | 11.026         | 10.854                    | 10.851         |
|      | 3.186                     | 5.563          | 3.332                   | 3.594              | 3.676              | 3.491              | 3.524                | 5.674          | 3.912                     | 5.785          |
|      | 0.835                     | 2.353          | 1.374                   | 1.562              | 1.625              | 1.485              | 1.512                | 2.396          | 1.797                     | 2.439          |
|      | 1.249                     | -3.210         | -1.958                  | -2.033             | -2.051             | -2.007             | -2.013               | -3.278         | -2.116                    | -3.346         |
|      | 22.986                    |                | 36.116                  | 37.123             | 37.053             | 36.66              | 36.738               |                | 30.593                    |                |
| DyLu | 10.442                    | 10.439         | 10.52                   | 10.522             | 10.523             | 10.521             | 10.522               | 10.518         | 10.600                    | 10.597         |
|      | 4.043                     | 6.024          | 3.996                   | 3.961              | 3.925              | 3.981              | 3.966                | 5.981          | 3.816                     | 5.939          |
|      | 0.890                     | 2.447          | 1.544                   | 1.485              | 1.446              | 1.517              | 1.498                | 2.459          | 1.368                     | 2.471          |
|      | 1.560                     | -3.577         | -2.453                  | -2.477             | -2.480             | -2.464             | -2.469               | -3.523         | -2.448                    | -3.469         |
|      | 19.658                    |                | 32.560                  | 32.719             | 32.735             | 32.649             | 32.666               |                | 30.932                    |                |
| DyMn | 9.449                     | 9.445          | 9.807                   | 9.814              | 9.897              | 9.862              | 9.845                | 9.855          | 10.336                    | 10.266         |
|      | 0                         | 3.144          | 0                       | 0                  | 0.002              | 0.001              | 0.001                | 4.061          | 0                         | 4.979          |
|      | 0.010                     | 1.581          | 0.701                   | 0.631              | 0.696              | 0.685              | 0.679                | 1.881          | 0.267                     | 2.182          |

Table A.1 Continued

| XY   | $(X_{0.25}Y_{0.75})_2O_3$ |                | $(X_{0.5}Y_{0.5})_2O_3$ |                    |                    |                    |                      |                | $(X_{0.75}Y_{0.25})_2O_3$ |                |
|------|---------------------------|----------------|-------------------------|--------------------|--------------------|--------------------|----------------------|----------------|---------------------------|----------------|
|      | PBE                       | interp.<br>HSE | PBE <sup>1st</sup>      | PBE <sup>2nd</sup> | PBE <sup>3rd</sup> | PBE <sup>4th</sup> | PBE <sup>aver.</sup> | interp.<br>HSE | PBE                       | interp.<br>HSE |
|      | 0.551<br>0                | -1.563         | 0.774<br>0              | 0.665<br>0         | 0.694<br>0         | 0.684<br>0         | 0.705<br>0           | -2.180         | 0.283<br>0                | -2.797         |
| DyPm | 10.972                    | 10.973         | 10.875                  | 10.869             | 10.869             | 10.875             | 10.872               | 10.874         | 10.772                    | 10.775         |
|      | 3.646                     | 5.728          | 3.710                   | 3.803              | 3.829              | 3.765              | 3.777                | 5.784          | 3.912                     | 5.840          |
|      | 0.714                     | 2.471          | 1.410                   | 1.496              | 1.532              | 1.454              | 1.473                | 2.474          | 1.592                     | 2.478          |
|      | 1.355                     | -3.258         | -2.301                  | -2.308             | -2.298             | -2.311             | -2.305               | -3.310         | -2.321                    | -3.362         |
|      | 30.204                    |                | 42.663                  | 42.759             | 42.396             | 42.764             | 42.645               |                | 32.764                    |                |
| DyPr | 11.139                    | 11.054         | 10.986                  | 10.973             | 10.972             | 10.983             | 10.979               | 10.928         | 10.827                    | 10.802         |
|      | 3.428                     | 5.698          | 3.521                   | 3.684              | 3.727              | 3.616              | 3.637                | 5.764          | 3.840                     | 5.830          |
|      | 0.814                     | 2.474          | 1.310                   | 1.443              | 1.494              | 1.378              | 1.407                | 2.476          | 1.582                     | 2.479          |
|      | 1.207                     | -3.225         | -2.212                  | -2.241             | -2.233             | -2.238             | -2.231               | -3.288         | -2.259                    | -3.351         |
|      | 20.292                    |                | 32.617                  | 33.277             | 32.762             | 33.031             | 32.921               |                | 24.319                    |                |
| DySc | 10.107                    | 10.106         | 10.298                  | 10.301             | 10.304             | 10.294             | 10.300               | 10.296         | 10.487                    | 10.486         |
|      | 3.594                     | 6.128          | 3.842                   | 3.996              | 4.003              | 3.956              | 3.950                | 6.050          | 3.744                     | 5.973          |
|      | 0.746                     | 2.969          | 1.916                   | 2.024              | 2.044              | 1.992              | 1.994                | 2.807          | 1.671                     | 2.644          |
|      | 1.771                     | -3.159         | -1.926                  | -1.973             | -1.960             | -1.964             | -1.956               | -3.244         | -2.074                    | -3.329         |
|      | 11.751                    |                | 23.021                  | 23.201             | 23.155             | 23.131             | 23.127               |                | 26.482                    |                |
| DySm | 10.92                     | 10.919         | 10.840                  | 10.835             | 10.836             | 10.839             | 10.838               | 10.838         | 10.755                    | 10.757         |
|      | 3.709                     | 5.747          | 3.760                   | 3.826              | 3.846              | 3.801              | 3.809                | 5.796          | 3.926                     | 5.846          |
|      | 0.713                     | 2.463          | 1.431                   | 1.497              | 1.526              | 1.467              | 1.481                | 2.470          | 1.585                     | 2.476          |
|      | 1.391                     | -3.284         | -2.329                  | -2.329             | -2.320             | -2.334             | -2.328               | -3.327         | -2.341                    | -3.371         |
|      | 25.139                    |                | 38.168                  | 38.158             | 38.039             | 38.177             | 38.135               |                | 32.527                    |                |
| DyTb | 10.726                    | 10.725         | 10.714                  | 10.713             | 10.714             | 10.713             | 10.714               | 10.709         | 10.697                    | 10.693         |
|      | 3.901                     | 5.869          | 3.909                   | 3.921              | 3.925              | 3.913              | 3.917                | 5.878          | 3.941                     | 5.887          |
|      | 0.707                     | 2.484          | 1.509                   | 1.523              | 1.53               | 1.514              | 1.519                | 2.483          | 1.544                     | 2.483          |
|      | 1.506                     | -3.386         | -2.400                  | -2.399             | -2.396             | -2.400             | -2.399               | -3.395         | -2.398                    | -3.405         |
|      | 0.025                     |                | 0.007                   | 0                  | 0                  | 0                  | 0.002                |                | 0                         |                |
| DyTl | 10.783                    | 10.744         | 10.745                  | 10.740             | 10.738             | 10.730             | 10.739               | 10.721         | 10.706                    | 10.699         |
|      | 0.380                     | 1.798          | 0.865                   | 0.846              | 0.846              | 0.857              | 0.854                | 3.164          | 1.303                     | 4.530          |
|      | 2.661                     | -0.882         | -1.104                  | -1.077             | -1.097             | -1.083             | -1.091               | 0.240          | -0.952                    | 1.361          |
|      | -1.427                    | -2.679         | -1.969                  | -1.922             | -1.942             | -1.939             | -1.943               | -2.924         | -2.254                    | -3.169         |
|      | 0                         |                | 0                       | 0                  | 0                  | 0                  | 0                    |                | 0                         |                |
| DyTm | 10.528                    | 10.523         | 10.576                  | 10.488             | 10.578             | 10.574             | 10.554               | 10.574         | 10.628                    | 10.625         |
|      | 4.007                     | 5.982          | 3.986                   | 4.062              | 3.932              | 3.967              | 3.987                | 5.954          | 3.878                     | 5.925          |
|      | 0.823                     | 2.448          | 1.542                   | 1.568              | 1.475              | 1.521              | 1.527                | 2.459          | 1.435                     | 2.471          |
|      | 1.549                     | -3.535         | -2.444                  | -2.494             | -2.458             | -2.446             | -2.461               | -3.495         | -2.443                    | -3.455         |

Table A.1 Continued

| XY   | $(X_{0.25}Y_{0.75})_2O_3$ |                | $(X_{0.5}Y_{0.5})_2O_3$ |                    |                    |                    |                      |                | $(X_{0.75}Y_{0.25})_2O_3$ |                |
|------|---------------------------|----------------|-------------------------|--------------------|--------------------|--------------------|----------------------|----------------|---------------------------|----------------|
|      | PBE                       | interp.<br>HSE | PBE <sup>1st</sup>      | PBE <sup>2nd</sup> | PBE <sup>3rd</sup> | PBE <sup>4th</sup> | PBE <sup>aver.</sup> | interp.<br>HSE | PBE                       | interp.<br>HSE |
|      | 12.421                    |                | 19.561                  | 19.481             | 23.546             | 23.52              | 21.527               |                | 26.835                    |                |
| DyV  | 9.679                     | 9.617          | 9.947                   | 9.969              | 10.014             | 9.904              | 9.959                | 9.970          | 10.353                    | 10.323         |
|      | 0                         | 3.265          | 0                       | 0.007              | 0                  | 0                  | 0.002                | 4.142          | 0                         | 5.019          |
|      | 0.073                     | 2.407          | 1.515                   | 1.397              | 1.422              | 1.398              | 1.433                | 2.432          | 1.306                     | 2.457          |
|      | 1.552                     | -0.849         | 1.545                   | 1.390              | 1.437              | 1.481              | 1.464                | -1.704         | 1.314                     | -2.559         |
|      | 8.787                     |                | 19.763                  | 20.419             | 20.264             | 20.366             | 20.203               |                | 22.959                    |                |
| DyY  | 10.698                    | 10.698         | 10.692                  | 10.689             | 10.691             | 10.691             | 10.691               | 10.691         | 10.685                    | 10.684         |
|      | 4.021                     | 5.973          | 3.989                   | 4.001              | 4.001              | 3.994              | 3.997                | 5.948          | 3.979                     | 5.922          |
|      | 0.545                     | 2.574          | 1.611                   | 1.627              | 1.633              | 1.618              | 1.623                | 2.543          | 1.600                     | 2.513          |
|      | 1.656                     | -3.400         | -2.378                  | -2.374             | -2.368             | -2.376             | -2.374               | -3.405         | -2.38                     | -3.41          |
|      | 0                         |                | 0                       | 0                  | 0.039              | 0                  | 0.010                |                | 0.109                     |                |
| DyYb | 10.698                    | 10.685         | 10.702                  | 10.704             | 10.700             | 10.701             | 10.702               | 10.682         | 10.689                    | 10.679         |
|      | 4.026                     | 6.003          | 4.407                   | 4.432              | 4.463              | 4.415              | 4.430                | 5.967          | 4.263                     | 5.932          |
|      | 1.532                     | 2.338          | 1.550                   | 1.556              | 1.586              | 1.549              | 1.561                | 2.386          | 1.633                     | 2.434          |
|      | -2.494                    | -3.665         | -2.857                  | -2.877             | -2.878             | -2.866             | -2.870               | -3.582         | -2.630                    | -3.498         |
|      | 4.715                     |                | 7.041                   | 7.136              | 7.252              | 7.072              | 7.125                |                | 6.614                     |                |
| ErEu | 10.721                    | 10.737         | 10.647                  | 10.640             | 10.640             | 10.645             | 10.643               | 10.669         | 10.567                    | 10.601         |
|      | 3.796                     | 5.885          | 3.858                   | 3.949              | 3.979              | 3.913              | 3.925                | 5.918          | 4.043                     | 5.952          |
|      | 1.402                     | 2.512          | 1.450                   | 1.540              | 1.579              | 1.500              | 1.518                | 2.494          | 1.627                     | 2.476          |
|      | -2.394                    | -3.373         | -2.409                  | -2.41              | -2.400             | -2.412             | -2.408               | -3.425         | -2.417                    | -3.476         |
|      | 0                         |                | 0.538                   | 0                  | 0                  | 0                  | 0.135                |                | 0.662                     |                |
| ErFe | 9.386                     | 9.366          | 9.737                   | 9.692              | 9.815              | 9.781              | 9.757                | 9.755          | 10.188                    | 10.144         |
|      | 0.012                     | 1.516          | 0                       | 0                  | 0                  | 0                  | 0                    | 3.006          | 0                         | 4.496          |
|      | 0.149                     | 1.709          | 0.247                   | 0.189              | 0.203              | 0.222              | 0.216                | 1.959          | -0.328                    | 2.208          |
|      | 0.137                     | 0.193          | 0.255                   | 0.198              | 0.205              | 0.257              | 0.229                | -1.048         | -0.294                    | -2.288         |
|      | 0                         |                | 0                       | 0                  | 0                  | 0                  | 0                    |                | 0                         |                |
| ErGa | 9.784                     | 9.690          | 10.007                  | 9.929              | 10.023             | 10.066             | 10.007               | 9.971          | 10.293                    | 10.252         |
|      | 1.859                     | 4.838          | 2.123                   | 2.867              | 2.547              | 2.481              | 2.505                | 5.220          | 1.945                     | 5.603          |
|      | -0.157                    | 1.008          | 0.119                   | 0.469              | 0.208              | 0.254              | 0.263                | 1.492          | -0.450                    | 1.975          |
|      | -2.016                    | -3.830         | -2.005                  | -2.398             | -2.34              | -2.227             | -2.243               | -3.729         | -2.395                    | -3.629         |
|      | 0                         |                | 0                       | 0                  | 0                  | 0                  | 0                    |                | 0                         |                |
| ErGd | 10.750                    | 10.744         | 10.684                  | 10.602             | 10.683             | 10.688             | 10.665               | 10.674         | 10.616                    | 10.604         |
|      | 3.804                     | 6.131          | 3.849                   | 3.996              | 3.925              | 3.877              | 3.912                | 6.083          | 3.981                     | 6.034          |
|      | 1.414                     | 2.649          | 1.444                   | 1.561              | 1.534              | 1.474              | 1.504                | 2.586          | 1.574                     | 2.522          |
|      | -2.391                    | -3.482         | -2.406                  | -2.435             | -2.392             | -2.403             | -2.409               | -3.497         | -2.408                    | -3.513         |
|      | 0                         |                | 0                       | 11.798             | 0                  | 0                  | 2.95                 |                | 0                         |                |



Table A.1 Continued

| XY   | $(X_{0.25}Y_{0.75})_2O_3$ |                | $(X_{0.5}Y_{0.5})_2O_3$ |                    |                    |                    |                      |                | $(X_{0.75}Y_{0.25})_2O_3$ |                |
|------|---------------------------|----------------|-------------------------|--------------------|--------------------|--------------------|----------------------|----------------|---------------------------|----------------|
|      | PBE                       | interp.<br>HSE | PBE <sup>1st</sup>      | PBE <sup>2nd</sup> | PBE <sup>3rd</sup> | PBE <sup>4th</sup> | PBE <sup>aver.</sup> | interp.<br>HSE | PBE                       | interp.<br>HSE |
| ErHo | 10.600                    | 10.587         | 10.582                  | 10.501             | 10.578             | 10.578             | 10.56                | 10.569         | 10.566                    | 10.551         |
|      | 3.941                     | 5.961          | 3.956                   | 4.069              | 3.976              | 3.965              | 3.992                | 5.969          | 3.986                     | 5.978          |
|      | 1.488                     | 2.441          | 1.493                   | 1.571              | 1.516              | 1.502              | 1.521                | 2.447          | 1.523                     | 2.452          |
|      | -2.453                    | -3.521         | -2.463                  | -2.498             | -2.46              | -2.464             | -2.472               | -3.523         | -2.463                    | -3.526         |
|      | 0.132                     |                | 0.176                   | 0.324              | 48.883             | 0.173              | 12.389               |                | 35.376                    |                |
| ErIn | 10.374                    | 10.362         | 10.436                  | 10.281             | 10.434             | 10.427             | 10.395               | 10.419         | 10.489                    | 10.476         |
|      | 1.604                     | 3.633          | 2.127                   | 2.405              | 2.138              | 2.159              | 2.208                | 4.417          | 2.368                     | 5.202          |
|      | -0.765                    | 0.172          | -0.235                  | -0.026             | -0.228             | -0.195             | -0.171               | 0.934          | -0.099                    | 1.696          |
|      | -2.369                    | -3.461         | -2.362                  | -2.431             | -2.366             | -2.354             | -2.379               | -3.483         | -2.467                    | -3.506         |
|      | 0                         |                | 0                       | 0                  | 0                  | 0                  | 0                    |                | 0                         |                |
| ErLa | 11.188                    | 11.165         | 10.979                  | 10.853             | 10.952             | 10.972             | 10.939               | 10.954         | 10.769                    | 10.744         |
|      | 3.107                     | 5.586          | 3.261                   | 3.633              | 3.653              | 3.451              | 3.500                | 5.719          | 3.881                     | 5.852          |
|      | 1.179                     | 2.347          | 1.326                   | 1.583              | 1.624              | 1.464              | 1.500                | 2.384          | 1.781                     | 2.421          |
|      | -1.928                    | -3.239         | -1.935                  | -2.05              | -2.030             | -1.987             | -2.001               | -3.335         | -2.100                    | -3.432         |
|      | 0                         |                | 0                       | 0                  | 0                  | 0                  | 0                    |                | 0                         |                |
| ErLu | 10.412                    | 10.404         | 10.460                  | 10.415             | 10.459             | 10.458             | 10.448               | 10.447         | 10.501                    | 10.490         |
|      | 4.052                     | 6.046          | 4.024                   | 4.061              | 3.973              | 4.004              | 4.016                | 6.026          | 3.915                     | 6.006          |
|      | 1.522                     | 2.442          | 1.521                   | 1.520              | 1.461              | 1.493              | 1.499                | 2.447          | -2.303                    | 2.453          |
|      | -2.531                    | -3.605         | -2.504                  | -2.541             | -2.512             | -2.510             | -2.517               | -3.580         | -6.223                    | -3.554         |
|      | 0                         |                | 0                       | 0.325              | 0                  | 0                  | 0.082                |                | 0                         |                |
| ErMn | 9.416                     | 9.409          | 9.748                   | 9.700              | 9.825              | 9.804              | 9.77                 | 9.784          | 10.221                    | 10.159         |
|      | 0.004                     | 3.166          | 0                       | 0                  | 0                  | 0.003              | 0.001                | 4.106          | 0                         | 5.046          |
|      | 0.555                     | 1.575          | 0.685                   | 0.628              | 0.683              | 0.686              | 0.671                | 1.870          | 0.229                     | 2.164          |
|      | 0.552                     | -1.592         | 0.764                   | 0.672              | 0.686              | 0.684              | 0.702                | -2.237         | 0.257                     | -2.883         |
|      | 0                         |                | 0                       | 0                  | 0                  | 0                  | 0                    |                | 0                         |                |
| ErPm | 10.938                    | 10.937         | 10.813                  | 10.706             | 10.805             | 10.814             | 10.785               | 10.802         | 10.678                    | 10.668         |
|      | 3.565                     | 5.751          | 3.649                   | 3.886              | 3.826              | 3.733              | 3.774                | 5.829          | 3.923                     | 5.908          |
|      | 1.273                     | 2.465          | 1.519                   | 1.533              | 1.525              | 1.418              | 1.499                | 2.463          | 1.591                     | 2.460          |
|      | -2.293                    | -3.287         | -2.429                  | -2.354             | -2.301             | -2.316             | -2.350               | -3.367         | -2.333                    | -3.448         |
|      | 0                         |                | 0                       | 0                  | 0                  | 0                  | 0                    |                | 0                         |                |
| ErPr | 11.108                    | 11.019         | 10.923                  | 10.810             | 10.907             | 10.920             | 10.890               | 10.857         | 10.736                    | 10.695         |
|      | 3.315                     | 5.721          | 3.440                   | 3.754              | 3.719              | 3.577              | 3.623                | 5.809          | 3.832                     | 5.897          |
|      | 1.099                     | 2.468          | 1.241                   | 1.476              | 1.489              | 1.341              | 1.387                | 2.465          | 1.569                     | 2.461          |
|      | -2.216                    | -3.253         | -2.2                    | -2.278             | -2.23              | -2.236             | -2.236               | -3.345         | -2.264                    | -3.437         |
|      | 0                         |                | 0                       | 0                  | 0                  | 0                  | 0                    |                | 0                         |                |
| ErSc | 10.077                    | 10.070         | 10.236                  | 10.156             | 10.239             | 10.231             | 10.216               | 10.224         | 10.598                    | 10.379         |

Table A.1 Continued

| XY   | $(X_{0.25}Y_{0.75})_2O_3$ |                | $(X_{0.5}Y_{0.5})_2O_3$ |                    |                    |                    |                      |                | $(X_{0.75}Y_{0.25})_2O_3$ |                |
|------|---------------------------|----------------|-------------------------|--------------------|--------------------|--------------------|----------------------|----------------|---------------------------|----------------|
|      | PBE                       | interp.<br>HSE | PBE <sup>1st</sup>      | PBE <sup>2nd</sup> | PBE <sup>3rd</sup> | PBE <sup>4th</sup> | PBE <sup>aver.</sup> | interp.<br>HSE | PBE                       | interp.<br>HSE |
|      | 3.656                     | 6.150          | 3.900                   | 4.121              | 4.088              | 4.009              | 4.030                | 6.095          | 4.006                     | 6.041          |
|      | 1.796                     | 2.963          | 1.944                   | 2.087              | 2.116              | 2.024              | 2.043                | 2.795          | 2.187                     | 2.626          |
|      | -1.861                    | -3.188         | -1.956                  | -2.034             | -1.973             | -1.986             | -1.988               | -3.301         | 2.200                     | -3.415         |
|      | 0                         |                | 0                       | 0                  | 0                  | 0                  | 0                    |                | 0                         |                |
| ErSm | 10.891                    | 10.884         | 10.777                  | 10.685             | 10.772             | 10.779             | 10.754               | 10.767         | 10.398                    | 10.650         |
|      | 3.628                     | 5.769          | 3.709                   | 3.908              | 3.846              | 3.774              | 3.810                | 5.841          | 3.869                     | 5.914          |
|      | 1.310                     | 2.457          | 1.377                   | 1.532              | 1.520              | 1.432              | 1.466                | 2.458          | 2.097                     | 2.458          |
|      | -2.318                    | -3.312         | -2.332                  | -2.376             | -2.326             | -2.342             | -2.344               | -3.384         | 2.149                     | -3.456         |
|      | 0                         |                | 0                       | 0                  | 0                  | 0                  | 0                    |                | 0                         |                |
| ErTb | 10.702                    | 10.689         | 10.650                  | 10.556             | 10.652             | 10.649             | 10.627               | 10.637         | 10.665                    | 10.585         |
|      | 3.859                     | 5.892          | 3.890                   | 4.038              | 3.942              | 3.909              | 3.945                | 5.923          | 3.990                     | 5.955          |
|      | 1.446                     | 2.478          | 1.463                   | 1.576              | 1.527              | 1.484              | 1.513                | 2.471          | 1.561                     | 2.465          |
|      | -2.413                    | -3.414         | -2.428                  | -2.462             | -2.415             | -2.426             | -2.433               | -3.452         | -2.43                     | -3.490         |
|      | 0                         |                | 0                       | 0.131              | 0                  | 0                  | 0.033                |                | 0                         |                |
| ErTl | 10.740                    | 10.708         | 10.675                  | 10.565             | 10.672             | 10.666             | 10.645               | 10.650         | 10.617                    | 10.592         |
|      | 0.374                     | 1.820          | 0.876                   | 0.930              | 0.832              | 0.853              | 0.873                | 3.209          | 1.321                     | 4.597          |
|      | -1.448                    | -0.888         | -1.125                  | -1.052             | -1.136             | -1.116             | -1.108               | 0.228          | -0.957                    | 1.343          |
|      | -1.822                    | -2.707         | -2.001                  | -1.981             | -1.967             | -1.968             | -1.980               | -2.981         | -2.278                    | -3.255         |
|      | 0                         |                | 0                       | 0                  | 0                  | 0                  | 0                    |                | 0                         |                |
| ErTm | 10.495                    | 10.488         | 10.466                  | 10.438             | 10.513             | 10.513             | 10.483               | 10.503         | 10.534                    | 10.518         |
|      | 4.007                     | 6.005          | 4.063                   | 4.086              | 3.977              | 3.992              | 4.030                | 5.999          | 3.955                     | 5.992          |
|      | 1.516                     | 2.442          | 1.553                   | 1.558              | 1.481              | 1.501              | 1.524                | 2.447          | 1.466                     | 2.453          |
|      | -2.492                    | -3.563         | -2.510                  | -2.528             | -2.496             | -2.492             | -2.507               | -3.552         | -2.490                    | -3.540         |
|      | 0                         |                | 37.487                  | 41.741             | 0.492              | 0                  | 19.930               |                | 9.697                     |                |
| ErV  | 9.641                     | 9.581          | 9.911                   | 9.805              | 9.957              | 9.865              | 9.885                | 9.898          | 10.261                    | 10.216         |
|      | 0                         | 3.287          | 0                       | 0                  | 0.012              | 0                  | 0.003                | 4.187          | 0                         | 5.086          |
|      | 1.542                     | 2.401          | 1.527                   | 1.425              | 1.458              | 1.413              | 1.456                | 2.420          | 1.301                     | 2.439          |
|      | 1.585                     | -0.878         | 1.561                   | 1.477              | 1.447              | 1.492              | 1.495                | -1.761         | 1.310                     | -2.645         |
|      | 0                         |                | 0                       | 0                  | 0                  | 0                  | 0                    |                | 0                         |                |
| ErY  | 10.672                    | 10.662         | 10.630                  | 10.539             | 10.625             | 10.631             | 10.607               | 10.619         | 10.589                    | 10.576         |
|      | 3.973                     | 5.996          | 3.981                   | 4.119              | 4.029              | 3.996              | 4.032                | 5.993          | 4.031                     | 5.989          |
|      | -2.136                    | 2.568          | 1.576                   | 1.684              | 1.641              | 1.596              | 1.625                | 2.531          | 1.623                     | 2.495          |
|      | -6.109                    | -3.428         | -2.406                  | -2.435             | -2.388             | -2.401             | -2.408               | -3.462         | -2.408                    | -3.495         |
|      | 0                         |                | 0                       | 0.128              | 0                  | 0                  | 0.032                |                | 0                         |                |
| ErYb | 10.664                    | 10.649         | 10.631                  | 10.508             | 10.632             | 10.631             | 10.601               | 10.610         | 10.589                    | 10.572         |
|      | 3.990                     | 6.025          | 4.420                   | 4.634              | 4.520              | 4.445              | 4.505                | 6.012          | 4.315                     | 5.999          |

Table A.1 Continued

| XY   | $(X_{0.25}Y_{0.75})_2O_3$ |                | $(X_{0.5}Y_{0.5})_2O_3$ |                    |                    |                    |                      |                | $(X_{0.75}Y_{0.25})_2O_3$ |                |
|------|---------------------------|----------------|-------------------------|--------------------|--------------------|--------------------|----------------------|----------------|---------------------------|----------------|
|      | PBE                       | interp.<br>HSE | PBE <sup>1st</sup>      | PBE <sup>2nd</sup> | PBE <sup>3rd</sup> | PBE <sup>4th</sup> | PBE <sup>aver.</sup> | interp.<br>HSE | PBE                       | interp.<br>HSE |
|      | -1.378                    | 2.332          | 1.510                   | 1.648              | 1.582              | 1.524              | 1.566                | 2.374          | 1.639                     | 2.416          |
|      | -5.368                    | -3.694         | -2.911                  | -2.986             | -2.939             | -2.922             | -2.940               | -3.638         | -2.676                    | -3.583         |
|      | 0.040                     |                | 0.047                   | 0.058              | 0.057              | 0.049              | 0.053                |                | 0.045                     |                |
| EuFe | 9.442                     | 9.434          | 9.812                   | 9.809              | 9.908              | 9.833              | 9.841                | 9.891          | 10.267                    | 10.348         |
|      | 0                         | 1.482          | 0                       | 0.005              | 0                  | 0                  | 0.002                | 2.938          | 0                         | 4.395          |
|      | 0.127                     | 1.727          | -3.842                  | 0.231              | 0.256              | 0.263              | -0.773               | 1.995          | -0.112                    | 2.263          |
|      | 0.137                     | 0.245          | -3.808                  | 0.227              | 0.261              | 0.277              | -0.761               | -0.944         | -0.088                    | -2.132         |
|      | 0                         |                | 0                       | 0                  | 0                  | 0                  | 0                    |                | 0                         |                |
| EuGa | 9.817                     | 9.758          | 10.113                  | 10.087             | 10.147             | 10.059             | 10.102               | 10.107         | 10.41                     | 10.456         |
|      | 2.074                     | 4.804          | 2.091                   | 2.745              | 2.622              | 2.411              | 2.468                | 5.153          | 1.638                     | 5.502          |
|      | 0.069                     | 1.026          | 0.249                   | 0.547              | 0.497              | 0.434              | 0.432                | 1.528          | -0.591                    | 2.029          |
|      | -2.005                    | -3.778         | -1.843                  | -2.199             | -2.125             | -1.977             | -2.036               | -3.626         | -2.229                    | -3.473         |
|      | 0                         |                | 0                       | 0                  | 0                  | 0                  | 0                    |                | 0                         |                |
| EuGd | 10.753                    | 10.812         | 10.806                  | 10.774             | 10.773             | 10.772             | 10.782               | 10.810         | 10.793                    | 10.808         |
|      | 3.977                     | 6.097          | 3.914                   | 3.941              | 3.935              | 3.945              | 3.934                | 6.015          | 3.911                     | 5.933          |
|      | 1.598                     | 2.668          | 1.560                   | 1.566              | 1.558              | 1.571              | 1.564                | 2.622          | 1.540                     | 2.576          |
|      | -2.379                    | -3.430         | -2.355                  | -2.376             | -2.377             | -2.374             | -2.371               | -3.394         | -2.371                    | -3.357         |
|      | 24.452                    |                | 38.507                  | 47.578             | 47.610             | 47.443             | 45.285               |                | 0.065                     |                |
| EuHo | 10.607                    | 10.655         | 10.700                  | 10.666             | 10.671             | 10.671             | 10.677               | 10.705         | 10.735                    | 10.755         |
|      | 4.051                     | 5.927          | 3.959                   | 3.963              | 3.925              | 3.973              | 3.955                | 5.902          | 3.839                     | 5.876          |
|      | 1.638                     | 2.459          | 1.587                   | 1.556              | 1.518              | 1.577              | 1.560                | 2.483          | 1.445                     | 2.507          |
|      | -2.414                    | -3.469         | -2.373                  | -2.408             | -2.407             | -2.395             | -2.396               | -3.420         | -2.395                    | -3.370         |
|      | 0.341                     |                | 42.689                  | 0.449              | 0.462              | 0.449              | 11.012               |                | 0.340                     |                |
| EuIn | 10.330                    | 10.430         | 10.493                  | 10.451             | 10.449             | 10.439             | 10.458               | 10.555         | 10.570                    | 10.680         |
|      | 1.639                     | 3.599          | 2.193                   | 2.396              | 2.330              | 2.348              | 2.317                | 4.350          | 2.255                     | 5.100          |
|      | -0.657                    | 0.191          | -0.086                  | 0.080              | -0.001             | -5.523             | -1.383               | 0.971          | -0.128                    | 1.751          |
|      | -2.296                    | -3.409         | -2.278                  | -2.316             | -2.331             | -7.871             | -3.699               | -3.380         | -2.382                    | -3.350         |
|      | 0                         |                | 0                       | 0                  | 0                  | 0                  | 0                    |                | 0                         |                |
| EuLa | 11.209                    | 11.233         | 11.120                  | 11.084             | 11.085             | 11.092             | 11.096               | 11.090         | 10.977                    | 10.948         |
|      | 3.315                     | 5.552          | 3.432                   | 3.659              | 3.740              | 3.570              | 3.601                | 5.651          | 3.928                     | 5.751          |
|      | 1.358                     | 2.365          | 1.430                   | 1.583              | 1.640              | 1.517              | 1.543                | 2.420          | 1.781                     | 2.475          |
|      | -1.957                    | -3.187         | -2.003                  | -2.076             | -2.100             | -2.053             | -2.058               | -3.232         | -2.148                    | -3.276         |
|      | 0                         |                | 0                       | 0                  | 0                  | 0                  | 0                    |                | 0                         |                |
| EuLu | 10.461                    | 10.472         | 10.604                  | 10.543             | 10.543             | 10.538             | 10.557               | 10.583         | 10.706                    | 10.694         |
|      | 4.026                     | 6.013          | 3.929                   | 3.944              | 3.878              | 3.986              | 3.935                | 5.959          | 3.643                     | 5.905          |
|      | 1.601                     | 2.460          | 1.567                   | 1.519              | 1.449              | 1.576              | 1.528                | 2.483          | 1.259                     | 2.507          |

Table A.1 Continued

| XY   | $(X_{0.25}Y_{0.75})_2O_3$ |                | $(X_{0.5}Y_{0.5})_2O_3$ |                    |                    |                    |                      |                | $(X_{0.75}Y_{0.25})_2O_3$ |                |
|------|---------------------------|----------------|-------------------------|--------------------|--------------------|--------------------|----------------------|----------------|---------------------------|----------------|
|      | PBE                       | interp.<br>HSE | PBE <sup>1st</sup>      | PBE <sup>2nd</sup> | PBE <sup>3rd</sup> | PBE <sup>4th</sup> | PBE <sup>aver.</sup> | interp.<br>HSE | PBE                       | interp.<br>HSE |
|      | -2.426<br>0               | -3.554         | -2.363<br>0             | -2.426<br>0        | -2.429<br>0        | -2.41<br>0         | -2.407<br>0          | -3.476         | -2.383<br>0               | -3.398         |
| EuMn | 9.536                     | 9.477          | 9.878                   | 9.854              | 9.942              | 9.858              | 9.883                | 9.920          | 0                         | 10.363         |
|      | 0                         | 3.133          | 0                       | 0                  | 0.012              | 0                  | 0.003                | 4.039          | 0                         | 4.945          |
|      | 0.686                     | 1.593          | 0.705                   | 0.629              | 0.705              | 0.693              | 0.683                | 1.906          | 0                         | 2.218          |
|      | 0.693                     | -1.540         | 0.790                   | 0.669              | 0.694              | 0.710              | 0.716                | -2.134         | 0                         | -2.727         |
|      | 0                         |                | 0                       | 0                  | 0                  | 0                  | 0                    |                | 0                         |                |
| EuPm | 10.931                    | 11.005         | 10.927                  | 10.892             | 10.994             | 10.897             | 10.928               | 10.938         | 10.854                    | 10.872         |
|      | 3.818                     | 5.717          | 3.812                   | 3.880              | 3.890              | 3.856              | 3.860                | 5.762          | 3.939                     | 5.806          |
|      | 1.499                     | 2.483          | 1.501                   | 1.554              | 1.569              | 1.531              | 1.539                | 2.499          | 1.607                     | 2.515          |
|      | -2.320                    | -3.235         | -2.312                  | -2.326             | -2.321             | -2.325             | -2.321               | -3.264         | -2.333                    | -3.292         |
|      | 0.007                     |                | 0                       | 0.003              | 0.003              | 0.004              | 0.003                |                | 0                         |                |
| EuPr | 11.081                    | 11.087         | 11.034                  | 10.993             | 10.329             | 10.996             | 10.838               | 10.993         | 10.918                    | 10.899         |
|      | 3.635                     | 5.687          | 3.654                   | 3.773              | 3.810              | 3.736              | 3.744                | 5.742          | 3.878                     | 5.796          |
|      | 1.368                     | 2.486          | 1.412                   | 1.503              | 1.542              | 1.465              | 1.481                | 2.501          | 1.600                     | 2.516          |
|      | -2.267                    | -3.202         | -2.242                  | -2.271             | -2.269             | -2.271             | -2.264               | -3.241         | -2.278                    | -3.281         |
|      | 0                         |                | 0                       | 0                  | 0                  | 0                  | 0                    |                | 0                         |                |
| EuSc | 10.116                    | 10.138         | 10.348                  | 10.320             | 10.861             | 10.307             | 10.459               | 10.360         | 10.528                    | 10.583         |
|      | 3.529                     | 6.116          | 3.784                   | 3.931              | 3.868              | 3.929              | 3.878                | 6.028          | 3.520                     | 5.939          |
|      | 1.748                     | 2.981          | 1.890                   | 1.960              | 1.926              | 1.962              | 1.935                | 2.831          | 1.445                     | 2.681          |
|      | -1.782                    | -3.136         | -1.895                  | -1.972             | -1.942             | -1.967             | -1.944               | -3.198         | -2.075                    | -3.259         |
|      | 0                         |                | 0                       | 0                  | 0                  | 0                  | 0                    |                | 0                         |                |
| EuSm | 10.877                    | 10.952         | 10.894                  | 10.861             | 10.726             | 10.862             | 10.836               | 10.903         | 10.839                    | 10.854         |
|      | 3.868                     | 5.735          | 3.845                   | 3.894              | 3.903              | 3.886              | 3.882                | 5.774          | 3.926                     | 5.812          |
|      | 1.529                     | 2.475          | 1.518                   | 1.554              | 1.564              | 1.543              | 1.545                | 2.494          | 1.584                     | 2.512          |
|      | -2.34                     | -3.261         | -2.327                  | -2.341             | -2.339             | -2.343             | -2.338               | -3.281         | -2.343                    | -3.301         |
|      | 0.067                     |                | 0.013                   | 0.034              | 0.031              | 0.036              | 0.028                |                | 0.011                     |                |
| EuTb | 10.694                    | 10.757         | 10.728                  | 10.728             | 10.737             | 10.725             | 10.73                | 10.773         | 10.760                    | 10.789         |
|      | 4.013                     | 5.858          | 3.964                   | 3.964              | 3.947              | 3.977              | 3.963                | 5.856          | 3.904                     | 5.853          |
|      | 1.619                     | 2.496          | 1.572                   | 1.572              | 1.554              | 1.588              | 1.572                | 2.507          | 1.519                     | 2.519          |
|      | -2.394                    | -3.363         | -2.393                  | -2.392             | -2.394             | -2.389             | -2.392               | -3.349         | -2.385                    | -3.335         |
|      | 0.125                     |                | 0.045                   | 0.045              | 0.047              | 0.031              | 0.042                |                | 0.009                     |                |
| EuTl | 10.709                    | 10.776         | 10.776                  | 10.743             | 10.597             | 10.731             | 10.712               | 10.786         | 10.768                    | 10.796         |
|      | 0.419                     | 1.786          | 0.905                   | 0.965              | 0.968              | 0.962              | 0.950                | 3.141          | 1.361                     | 4.496          |
|      | -1.390                    | -0.870         | -1.038                  | -0.950             | -0.965             | -0.969             | -0.981               | 0.265          | -0.884                    | 1.398          |
|      | -1.809                    | -2.655         | -1.942                  | -1.915             | -1.932             | -1.930             | -1.930               | -2.877         | -2.244                    | -3.099         |

Table A.1 Continued

| XY   | $(X_{0.25}Y_{0.75})_2O_3$ |                | $(X_{0.5}Y_{0.5})_2O_3$ |                    |                    |                    |                      |                | $(X_{0.75}Y_{0.25})_2O_3$ |                |
|------|---------------------------|----------------|-------------------------|--------------------|--------------------|--------------------|----------------------|----------------|---------------------------|----------------|
|      | PBE                       | interp.<br>HSE | PBE <sup>1st</sup>      | PBE <sup>2nd</sup> | PBE <sup>3rd</sup> | PBE <sup>4th</sup> | PBE <sup>aver.</sup> | interp.<br>HSE | PBE                       | interp.<br>HSE |
|      | 0                         |                | 0                       | 0                  | 0                  | 0                  | 0                    |                | 0                         |                |
| EuTm | 10.519                    | 10.556         | 10.636                  | 10.609             | 10.597             | 10.604             | 10.612               | 10.639         | 10.699                    | 10.722         |
|      | 4.043                     | 5.971          | 3.958                   | 3.935              | 3.902              | 3.972              | 3.942                | 5.931          | 3.750                     | 5.891          |
|      | 1.622                     | 2.460          | 1.586                   | 1.523              | 1.480              | 1.571              | 1.540                | 2.484          | 1.353                     | 2.507          |
|      | -2.421                    | -3.512         | -2.373                  | -2.413             | -2.422             | -2.401             | -2.403               | -3.448         | -2.397                    | -3.384         |
|      | 32.125                    |                | 29.800                  | 41.823             | 38.965             | 38.257             | 37.211               |                | 25.572                    |                |
| EuV  | 9.722                     | 9.649          | 9.955                   | 9.722              | 10.021             | 9.904              | 9.901                | 10.034         | 10.334                    | 10.420         |
|      | 0                         | 3.254          | 0                       | 0.278              | 0                  | 0                  | 0.070                | 4.119          | 0                         | 4.985          |
|      | 1.552                     | 2.419          | -0.029                  | 0.936              | 1.428              | 1.411              | 0.937                | 2.456          | 1.331                     | 2.493          |
|      | 1.562                     | -0.826         | 0.072                   | 0.658              | 1.463              | 1.43               | 0.906                | -1.658         | 1.332                     | -2.489         |
|      | 0                         |                | 0                       | 0                  | 0                  | 0                  | 0                    |                | 0                         |                |
| EuY  | 10.666                    | 10.730         | 10.745                  | 10.713             | 10.712             | 10.707             | 10.72                | 10.755         | 10.754                    | 10.78          |
|      | 4.127                     | 5.962          | 4.011                   | 4.014              | 3.999              | 4.032              | 4.014                | 5.925          | 3.924                     | 5.888          |
|      | 1.768                     | 2.586          | 1.671                   | 1.655              | 1.641              | 1.674              | 1.661                | 2.568          | 1.561                     | 2.549          |
|      | -2.359                    | -3.376         | -2.341                  | -2.359             | -2.359             | -2.359             | -2.355               | -3.358         | -2.364                    | -3.339         |
|      | 0.046                     |                | 0.058                   | 0.037              | 0.047              | 0.008              | 0.038                |                | 0.023                     |                |
| EuYb | 10.626                    | 10.717         | 10.733                  | 10.686             | 10.690             | 10.688             | 10.700               | 10.746         | 10.737                    | 10.776         |
|      | 4.355                     | 5.992          | 4.440                   | 4.439              | 4.445              | 4.451              | 4.444                | 5.945          | 4.237                     | 5.898          |
|      | 1.661                     | 2.350          | 1.642                   | 1.617              | 1.628              | 1.637              | 1.631                | 2.410          | 1.638                     | 2.470          |
|      | -2.695                    | -3.642         | -2.799                  | -2.822             | -2.818             | -2.815             | -2.814               | -3.535         | -2.599                    | -3.428         |
|      | 0.011                     |                | 0.037                   | 0.032              | 0.046              | 0.026              | 0.035                |                | 0.045                     |                |
| FeGa | 9.318                     | 9.301          | 9.203                   | 9.204              | 9.219              | 9.203              | 9.208                | 9.193          | 9.108                     | 9.085          |
|      | 0                         | 3.348          | 0.010                   | 0.005              | 0                  | 0                  | 0.004                | 2.240          | 0                         | 1.133          |
|      | -0.487                    | 0.758          | 0.076                   | 0.120              | 0.153              | 0.088              | 0.110                | 0.992          | 0.266                     | 1.226          |
|      | -0.420                    | -2.590         | 0.066                   | 0.116              | 0.177              | 0.088              | 0.112                | -1.249         | 0.273                     | 0.093          |
|      | 0                         |                | 0                       | 0                  | 0                  | 0                  | 0                    |                | 0                         |                |
| FeGd | 10.387                    | 10.355         | 9.915                   | 9.837              | 9.716              | 9.931              | 9.850                | 9.896          | 9.449                     | 9.437          |
|      | 0                         | 4.641          | 0                       | 0                  | 0                  | 0                  | 0                    | 3.103          | 0.008                     | 1.564          |
|      | -0.224                    | 2.400          | 0.213                   | 0.228              | 0.249              | 0.242              | 0.233                | 2.086          | 0.137                     | 1.773          |
|      | -0.200                    | -2.242         | 0.286                   | 0.237              | 0.271              | 0.258              | 0.263                | -1.017         | 0.129                     | 0.209          |
|      | 9.597                     |                | 21.468                  | 23.692             | 23.630             | 23.020             | 22.953               |                | 22.890                    |                |
| FeHo | 10.239                    | 10.198         | 9.813                   | 9.697              | 9.655              | 9.845              | 9.753                | 9.791          | 9.400                     | 9.384          |
|      | 0                         | 4.471          | 0                       | 0                  | 0                  | 0                  | 0                    | 2.989          | 0.017                     | 1.508          |
|      | -0.303                    | 2.191          | 0.205                   | 0.189              | 0.230              | 0.212              | 0.209                | 1.947          | 0.152                     | 1.703          |
|      | -0.200                    | -2.281         | 0.268                   | 0.198              | 0.262              | 0.212              | 0.235                | -1.043         | 0.136                     | 0.196          |
|      | 10.307                    |                | 22.349                  | 24.038             | 23.779             | 23.417             | 23.395               |                | 23.834                    |                |

Table A.1 Continued

| XY   | $(X_{0.25}Y_{0.75})_2O_3$ |                | $(X_{0.5}Y_{0.5})_2O_3$ |                    |                    |                    |                      |                | $(X_{0.75}Y_{0.25})_2O_3$ |                |
|------|---------------------------|----------------|-------------------------|--------------------|--------------------|--------------------|----------------------|----------------|---------------------------|----------------|
|      | PBE                       | interp.<br>HSE | PBE <sup>1st</sup>      | PBE <sup>2nd</sup> | PBE <sup>3rd</sup> | PBE <sup>4th</sup> | PBE <sup>aver.</sup> | interp.<br>HSE | PBE                       | interp.<br>HSE |
| FeIn | 9.982                     | 9.973          | 9.657                   | 9.533              | 9.669              | 9.705              | 9.641                | 9.641          | 0                         | 9.309          |
|      | 0                         | 2.143          | 0                       | 0                  | 0                  | 0                  | 0                    | 1.437          | 0                         | 0.732          |
|      | -0.271                    | -0.078         | 0.123                   | 0.146              | 0.171              | 0.188              | 0.157                | 0.435          | 0                         | 0.947          |
|      | -0.211                    | -2.221         | 0.145                   | 0.167              | 0.196              | 0.197              | 0.177                | -1.003         | 0                         | 0.216          |
|      | 0                         |                | 0                       | 0                  | 0                  | 0                  | 0                    |                | 0                         |                |
| FeLa | 10.804                    | 10.776         | 10.199                  | 10.006             | 10.066             | 10.014             | 10.072               | 10.176         | 9.986                     | 9.577          |
|      | 0                         | 4.096          | 0                       | 0                  | 0.020              | 0.031              | 0.013                | 2.739          | 0                         | 1.383          |
|      | -0.009                    | 2.098          | 0.199                   | 0.274              | 0.379              | 0.285              | 0.285                | 1.885          | 0.419                     | 1.672          |
|      | 0.052                     | -1.998         | 0.279                   | 0.288              | 0.359              | 0.254              | 0.295                | -0.855         | 0.457                     | 0.290          |
|      | 0                         |                | 0                       | 0                  | 0                  | 0                  | 0                    |                | 0                         |                |
| FeLu | 10.054                    | 10.015         | 9.690                   | 9.665              | 9.613              | 9.716              | 9.671                | 9.669          | 9.340                     | 9.323          |
|      | 0                         | 4.556          | 0                       | 0                  | 0                  | 0                  | 0                    | 3.046          | 0.018                     | 1.536          |
|      | -0.398                    | 2.192          | 0.185                   | 0.167              | 0.205              | 0.175              | 0.183                | 1.948          | 0.163                     | 1.703          |
|      | -0.357                    | -2.365         | 0.238                   | 0.202              | 0.237              | 0.179              | 0.214                | -1.099         | 0.145                     | 0.168          |
|      | 13.513                    |                | 23.382                  | 25.940             | 25.108             | 25.139             | 24.892               |                | 17.108                    |                |
| FeMn | 9.020                     | 9.020          | 9.011                   | 9.009              | 9.015              | 9.012              | 9.012                | 9.006          | 8.987                     | 8.992          |
|      | 0                         | 1.676          | 0                       | 0                  | 0                  | 0                  | 0                    | 1.126          | 0                         | 0.576          |
|      | 0.310                     | 1.325          | 0.205                   | 0.198              | 0.201              | 0.198              | 0.201                | 1.370          | 0.101                     | 1.415          |
|      | 0.310                     | -0.352         | 0.247                   | 0.228              | 0.246              | 0.220              | 0.236                | 0.244          | 0.162                     | 0.839          |
|      | 0.744                     |                | 0.302                   | 0.015              | 0                  | 0.178              | 0.124                |                | 0                         |                |
| FePm | 10.567                    | 10.548         | 10.044                  | 9.99               | 9.815              | 10.085             | 9.984                | 10.024         | 9.513                     | 9.501          |
|      | 0                         | 4.261          | 0                       | 0                  | 0                  | 0                  | 0                    | 2.849          | 0                         | 1.438          |
|      | -0.146                    | 2.215          | 0.225                   | 0.263              | 0.272              | 0.333              | 0.274                | 1.963          | 0.118                     | 1.711          |
|      | -0.127                    | -2.046         | 0.304                   | 0.284              | 0.310              | 0.347              | 0.312                | -0.887         | 0.122                     | 0.274          |
|      | 0                         |                | 0                       | 0                  | 0                  | 0                  | 0                    |                | 0                         | 0              |
| FePr | 10.710                    | 10.63          | 10.153                  | 9.960              | 9.969              | 10.202             | 10.071               | 10.079         | 9.928                     | 9.528          |
|      | 0                         | 4.231          | 0                       | 0                  | 0.028              | 0                  | 0.007                | 2.829          | 0                         | 1.428          |
|      | -0.076                    | 2.218          | 0.242                   | 0.285              | 0.367              | 0.326              | 0.305                | 1.965          | 0.429                     | 1.712          |
|      | -0.065                    | -2.013         | 0.313                   | 0.293              | 0.339              | 0.341              | 0.322                | -0.865         | 0.462                     | 0.285          |
|      | 0                         |                | 0                       | 0                  | 0                  | 0                  | 0                    |                | 0                         |                |
| FeSc | 9.698                     | 9.681          | 9.452                   | 9.434              | 9.443              | 9.460              | 9.448                | 9.446          | 9.226                     | 9.212          |
|      | 0                         | 4.66           | 0                       | 0                  | 0                  | 0                  | 0                    | 3.115          | 0.001                     | 1.571          |
|      | -0.041                    | 2.713          | 0.242                   | 0.226              | 0.259              | 0.234              | 0.241                | 2.295          | 0.142                     | 1.877          |
|      | 0.001                     | -1.947         | 0.271                   | 0.255              | 0.286              | 0.234              | 0.262                | -0.821         | 0.142                     | 0.307          |
|      | 13.567                    |                | 26.107                  | 26.681             | 26.15              | 26.558             | 26.374               |                | 26.305                    |                |
| FeSm | 10.513                    | 10.495         | 10.007                  | 9.756              | 9.787              | 10.013             | 9.891                | 9.989          | 9.492                     | 9.483          |

Table A.1 Continued

| XY   | $(X_{0.25}Y_{0.75})_2O_3$ |                | $(X_{0.5}Y_{0.5})_2O_3$ |                    |                    |                    |                      |                | $(X_{0.75}Y_{0.25})_2O_3$ |                |
|------|---------------------------|----------------|-------------------------|--------------------|--------------------|--------------------|----------------------|----------------|---------------------------|----------------|
|      | PBE                       | interp.<br>HSE | PBE <sup>1st</sup>      | PBE <sup>2nd</sup> | PBE <sup>3rd</sup> | PBE <sup>4th</sup> | PBE <sup>aver.</sup> | interp.<br>HSE | PBE                       | interp.<br>HSE |
|      | 0                         | 4.279          | 0                       | 0                  | 0                  | 0                  | 0                    | 2.862          | -0.004                    | 1.444          |
|      | -0.166                    | 2.207          | 0.221                   | 0.228              | 0.267              | 0.339              | 0.264                | 1.958          | 0.120                     | 1.709          |
|      | -0.146                    | -2.072         | 0.297                   | 0.234              | 0.302              | 0.351              | 0.296                | -0.904         | 0.124                     | 0.265          |
|      | 0                         |                | 0                       | 0                  | 0                  | 0                  | 0                    |                | 0                         |                |
| FeTb | 10.328                    | 10.300         | 9.879                   | 9.749              | 9.692              | 9.899              | 9.805                | 9.859          | 9.433                     | 9.418          |
|      | 0                         | 4.402          | 0                       | 0                  | 0                  | 0                  | 0                    | 2.943          | 0.012                     | 1.485          |
|      | -0.256                    | 2.228          | 0.212                   | 0.203              | 0.243              | 0.227              | 0.222                | 1.972          | 0.142                     | 1.715          |
|      | -0.229                    | -2.174         | 0.280                   | 0.205              | 0.270              | 0.232              | 0.247                | -0.972         | 0.131                     | 0.231          |
|      | 0                         |                | 0                       | 0                  | 0                  | 0                  | 0                    |                | 0                         |                |
| FeTl | 10.307                    | 10.319         | 9.919                   | 10.076             | 11.130             | 10.121             | 10.312               | 9.872          | 9.452                     | 9.425          |
|      | 0                         | 0.330          | 0                       | 0                  | 0.004              | 0.010              | 0.004                | 0.229          | -0.034                    | 0.127          |
|      | 0.016                     | -1.137         | 0.193                   | 0.243              | 0.577              | 0.383              | 0.349                | -0.272         | 0.163                     | 0.594          |
|      | -0.052                    | -1.467         | 0.198                   | 0.243              | 0.574              | 0.373              | 0.347                | -0.500         | 0.196                     | 0.467          |
|      | 0                         |                | 0                       | 0                  | 0.033              | 0                  | 0.009                |                | 0                         |                |
| FeTm | 10.13                     | 10.099         | 9.693                   | 9.574              | 9.622              | 9.775              | 9.666                | 9.725          | 9.369                     | 9.351          |
|      | 0                         | 4.515          | 0                       | 0                  | 0                  | 0                  | 0                    | 3.019          | 0.022                     | 1.522          |
|      | -0.352                    | 2.192          | 0.206                   | 0.184              | 0.218              | 0.192              | 0.200                | 1.948          | 0.162                     | 1.703          |
|      | -0.316                    | -2.323         | 0.264                   | 0.195              | 3.000              | 0.196              | 0.914                | -1.071         | 0.140                     | 0.182          |
|      | 10.871                    |                | 23.075                  | 24.691             | 24.082             | 23.936             | 23.946               |                | 24.378                    | 0              |
| FeV  | 9.213                     | 9.192          | 9.132                   | 9.138              | 9.138              | 9.158              | 9.142                | 9.120          | 9.050                     | 9.049          |
|      | 0                         | 1.797          | 0                       | 0                  | 0.018              | 0                  | 0.005                | 1.207          | 0                         | 0.616          |
|      | 1.046                     | 2.151          | 0.662                   | 0.626              | 0.673              | 0.660              | 0.656                | 1.920          | 0.290                     | 1.690          |
|      | 1.118                     | 0.363          | 0.668                   | 0.654              | 0.655              | 0.664              | 0.661                | 0.720          | 0.426                     | 1.077          |
|      | 10.194                    |                | 17.585                  | 17.484             | 17.415             | 17.831             | 17.579               |                | 16.710                    |                |
| FeY  | 10.294                    | 10.273         | 9.858                   | 9.749              | 9.695              | 9.895              | 9.800                | 9.841          | 9.423                     | 9.409          |
|      | 0                         | 4.506          | 0                       | 0                  | 0                  | 0.002              | 0.001                | 3.013          | 0.012                     | 1.519          |
|      | -0.230                    | 2.318          | 0.214                   | 0.205              | 0.241              | 0.234              | 0.224                | 2.032          | 0.147                     | 1.745          |
|      | -0.201                    | -2.188         | 0.276                   | 0.216              | 0.273              | 0.233              | 0.250                | -0.981         | 0.136                     | 0.227          |
|      | 0                         |                | 0                       | 0                  | 0                  | 0                  | 0                    |                | 0                         |                |
| FeYb | 10.03                     | 10.260         | 9.653                   | 9.549              | 9.521              | 9.774              | 9.625                | 9.832          | 9.302                     | 9.405          |
|      | 0                         | 4.535          | 0                       | 0                  | 0                  | 0.001              | 0.001                | 3.032          | 0.003                     | 1.529          |
|      | -1.525                    | 2.083          | -0.135                  | -0.028             | -0.028             | -0.128             | -0.080               | 1.875          | 0.087                     | 1.667          |
|      | -1.469                    | -2.453         | -0.122                  | -0.015             | -0.011             | -0.129             | -0.070               | -1.158         | 0.084                     | 0.138          |
|      | 8.560                     |                | 17.411                  | 16.493             | 16.751             | 16.879             | 16.884               |                | 15.148                    |                |
| GaGd | 10.498                    | 10.463         | 10.198                  | 10.010             | 10.169             | 10.27              | 10.162               | 10.112         | 9.920                     | 9.761          |
|      | 1.662                     | 5.748          | 2.229                   | 2.529              | 2.372              | 2.543              | 2.419                | 5.317          | 1.993                     | 4.886          |

Table A.1 Continued

| XY   | $(X_{0.25}Y_{0.75})_2O_3$ |                | $(X_{0.5}Y_{0.5})_2O_3$ |                    |                    |                    |                      |                | $(X_{0.75}Y_{0.25})_2O_3$ |                |
|------|---------------------------|----------------|-------------------------|--------------------|--------------------|--------------------|----------------------|----------------|---------------------------|----------------|
|      | PBE                       | interp.<br>HSE | PBE <sup>1st</sup>      | PBE <sup>2nd</sup> | PBE <sup>3rd</sup> | PBE <sup>4th</sup> | PBE <sup>aver.</sup> | interp.<br>HSE | PBE                       | interp.<br>HSE |
|      | -0.564                    | 2.166          | 0.141                   | 0.402              | 0.409              | 0.438              | 0.348                | 1.619          | -0.298                    | 1.072          |
|      | -2.226                    | -3.583         | -2.088                  | -2.127             | -1.963             | -2.105             | -2.071               | -3.699         | -2.291                    | -3.815         |
|      | 11.762                    |                | 24.219                  | 24.577             | 24.785             | 24.779             | 24.590               |                | 23.781                    |                |
| GaHo | 10.339                    | 10.306         | 10.088                  | 9.961              | 9.898              | 10.034             | 9.996                | 10.007         | 9.808                     | 9.708          |
|      | 1.879                     | 5.578          | 2.311                   | 2.677              | 2.472              | 2.522              | 2.496                | 5.204          | 1.865                     | 4.829          |
|      | -0.475                    | 1.957          | 0.153                   | 0.365              | 0.282              | 0.226              | 0.257                | 1.480          | -0.827                    | 1.002          |
|      | -2.353                    | -3.621         | -2.159                  | -2.312             | -2.190             | -2.296             | -2.240               | -3.725         | -2.692                    | -3.828         |
|      | 12.421                    |                | 24.606                  | 24.841             | 24.901             | 24.574             | 24.730               |                | 26.267                    |                |
| GaIn | 10.066                    | 10.081         | 9.855                   | 9.854              | 9.838              | 9.860              | 9.852                | 9.857          | 9.632                     | 9.633          |
|      | 1.068                     | 3.250          | 1.262                   | 1.284              | 1.287              | 1.278              | 1.278                | 3.652          | 1.614                     | 4.053          |
|      | -1.300                    | -0.312         | -1.114                  | -1.108             | -1.097             | -1.101             | -1.105               | -0.033         | -0.896                    | 0.246          |
|      | -2.368                    | -3.562         | -2.376                  | -2.391             | -2.384             | -2.378             | -2.383               | -3.685         | -2.509                    | -3.808         |
|      | 0                         |                | 0                       | 0                  | 0                  | 0                  | 0                    |                | 0                         |                |
| GaLa | 10.935                    | 10.884         | 10.537                  | 10.246             | 10.598             | 10.514             | 10.474               | 10.392         | 10.288                    | 9.901          |
|      | 1.299                     | 5.203          | 1.854                   | 2.727              | 2.919              | 2.452              | 2.488                | 4.953          | 2.462                     | 4.704          |
|      | -0.428                    | 1.864          | 0.265                   | 1.065              | 1.196              | 0.983              | 0.878                | 1.418          | 0.480                     | 0.971          |
|      | -1.726                    | -3.339         | -1.589                  | -1.663             | -1.723             | -1.470             | -1.612               | -3.536         | -1.983                    | -3.733         |
|      | 0                         |                | 0                       | 0                  | 0                  | 0                  | 0                    |                | 0                         |                |
| GaLu | 10.146                    | 10.123         | 9.915                   | 9.791              | 9.839              | 9.908              | 9.864                | 9.885          | 9.685                     | 9.647          |
|      | 2.153                     | 5.664          | 2.287                   | 2.930              | 2.583              | 2.648              | 2.612                | 5.261          | 1.910                     | 4.858          |
|      | -0.360                    | 1.958          | -0.152                  | 0.416              | 0.207              | 0.174              | 0.162                | 1.480          | -0.28                     | 1.003          |
|      | -2.513                    | -3.706         | -2.438                  | -2.514             | -2.377             | -2.474             | -2.451               | -3.781         | -2.19                     | -3.856         |
|      | 19.010                    |                | 30.760                  | 32.408             | 31.458             | 31.443             | 31.517               |                | 25.427                    |                |
| GaMn | 9.115                     | 9.128          | 9.248                   | 9.215              | 9.236              | 7.997              | 8.924                | 9.222          | 9.338                     | 9.316          |
|      | 3.854                     | 2.784          | 0                       | 0.01               | 0                  | 0                  | 0.003                | 3.341          | 0                         | 3.898          |
|      | 0.607                     | 1.092          | 0.674                   | 0.643              | 0.609              | 0.648              | 0.644                | 0.903          | -                         | 0.714          |
|      |                           |                |                         |                    |                    |                    |                      |                | 13.920                    |                |
|      | 0.644                     | -1.692         | 0.700                   | 0.632              | 0.610              | 0.658              | 0.650                | -2.438         | -                         | -3.184         |
|      | 0                         |                | 0                       | 0                  | 0                  | 0                  | 0                    |                | 13.871                    |                |
| GaPm | 10.687                    | 10.656         | 10.333                  | 10.100             | 10.238             | 10.579             | 10.313               | 10.24          | 10.120                    | 9.825          |
|      | 1.421                     | 5.368          | 2.108                   | 2.422              | 2.439              | 2.620              | 2.398                | 5.064          | 2.178                     | 4.759          |
|      | -0.670                    | 1.981          | 0.105                   | 0.435              | 0.483              | 0.530              | 0.389                | 1.496          | -0.045                    | 1.010          |
|      | -2.090                    | -3.387         | -2.004                  | -1.987             | -1.957             | -2.090             | -2.010               | -3.568         | -2.223                    | -3.749         |
|      | 0                         |                | 0                       | 0                  | 0                  | 0                  | 0                    |                | 0                         |                |
| GaPr | 10.850                    | 10.738         | 10.453                  | 10.293             | 10.315             | 10.459             | 10.380               | 10.295         | 10.238                    | 9.852          |



Table A.1 Continued

| XY   | $(X_{0.25}Y_{0.75})_2O_3$ |                | $(X_{0.5}Y_{0.5})_2O_3$ |                    |                    |                    |                      |                | $(X_{0.75}Y_{0.25})_2O_3$ |                |
|------|---------------------------|----------------|-------------------------|--------------------|--------------------|--------------------|----------------------|----------------|---------------------------|----------------|
|      | PBE                       | interp.<br>HSE | PBE <sup>1st</sup>      | PBE <sup>2nd</sup> | PBE <sup>3rd</sup> | PBE <sup>4th</sup> | PBE <sup>aver.</sup> | interp.<br>HSE | PBE                       | interp.<br>HSE |
|      | 1.237                     | 5.338          | 1.900                   | 2.531              | 2.419              | 2.474              | 2.331                | 5.044          | 2.277                     | 4.749          |
|      | -0.762                    | 1.984          | 0.038                   | 0.566              | 0.510              | 0.684              | 0.450                | 1.498          | 0.106                     | 1.011          |
|      | -1.999                    | -3.354         | -1.863                  | -1.966             | -1.909             | -1.791             | -1.883               | -3.546         | -2.171                    | -3.738         |
|      | 0                         |                | 0                       | 0                  | 0                  | 0                  | 0                    |                | 0                         |                |
| GaSc | 9.798                     | 9.789          | 9.670                   | 9.663              | 9.660              | 9.672              | 9.667                | 9.662          | 9.554                     | 9.536          |
|      | 2.639                     | 5.767          | 2.812                   | 3.254              | 3.146              | 3.136              | 3.087                | 5.330          | 2.627                     | 4.892          |
|      | 0.739                     | 2.480          | 0.886                   | 1.36               | 1.274              | 1.224              | 1.186                | 1.828          | 0.492                     | 1.176          |
|      | -1.901                    | -3.288         | -1.926                  | -1.894             | -1.873             | -1.913             | -1.902               | -3.502         | -2.136                    | -3.716         |
|      | 15.172                    |                | 27.186                  | 27.193             | 27.044             | 27.254             | 27.169               |                | 27.529                    |                |
| GaSm | 10.640                    | 10.603         | 10.292                  | 9.980              | 10.227             | 10.501             | 10.250               | 10.205         | 10.067                    | 9.807          |
|      | 1.481                     | 5.386          | 2.153                   | 2.682              | 2.378              | 2.688              | 2.476                | 5.076          | 2.139                     | 4.765          |
|      | -0.641                    | 1.974          | 0.113                   | 0.563              | 0.457              | 0.567              | 0.425                | 1.491          | -0.107                    | 1.008          |
|      | -2.122                    | -3.413         | -2.040                  | -2.120             | -1.921             | -2.120             | -2.051               | -3.586         | -2.245                    | -3.758         |
|      | 11.923                    |                | 0                       | 0                  | 20.505             | 24.033             | 11.135               |                | 0                         |                |
| GaTb | 10.438                    | 10.408         | 10.161                  | 9.988              | 9.941              | 10.216             | 10.077               | 10.075         | 9.876                     | 9.742          |
|      | 1.741                     | 5.509          | 2.256                   | 2.615              | 2.441              | 2.561              | 2.469                | 5.158          | 1.902                     | 4.806          |
|      | -0.531                    | 1.994          | 0.147                   | 0.394              | 0.339              | 0.406              | 0.322                | 1.505          | -0.049                    | 1.015          |
|      | -2.271                    | -3.515         | -2.109                  | -2.221             | -2.102             | -2.156             | -2.147               | -3.654         | -1.950                    | -3.792         |
|      | 0                         |                | 0                       | 0                  | 0                  | 0                  | 0                    |                | 0                         |                |
| GaTl | 10.41                     | 10.427         | 10.083                  | 10.074             | 10.037             | 10.121             | 10.079               | 10.088         | 9.798                     | 9.749          |
|      | 0                         | 1.437          | 0.034                   | 0.007              | 0.010              | 0.018              | 0.018                | 2.443          | 0.711                     | 3.449          |
|      | -1.737                    | -1.371         | -1.758                  | -1.838             | -1.789             | -1.802             | -1.797               | -0.739         | -1.533                    | -0.108         |
|      | -1.707                    | -2.808         | -1.791                  | -1.844             | -1.798             | -1.819             | -1.813               | -3.182         | -2.243                    | -3.556         |
|      | 0                         |                | 0                       | 0                  | 0                  | 0                  | 0                    |                | 0                         |                |
| GaTm | 10.235                    | 10.207         | 10.015                  | 9.807              | 9.859              | 9.960              | 9.911                | 9.941          | 9.752                     | 9.675          |
|      | 2.018                     | 5.622          | 2.379                   | 2.927              | 2.506              | 2.579              | 2.598                | 5.233          | 1.867                     | 4.844          |
|      | -0.423                    | 1.959          | 0.139                   | 0.479              | 0.231              | 0.195              | 0.261                | 1.481          | -0.189                    | 1.003          |
|      | -2.440                    | -3.664         | -2.241                  | -2.449             | -2.276             | -2.384             | -2.338               | -3.753         | -2.056                    | -3.842         |
|      | 12.973                    |                | 25.454                  | 25.504             | 25.260             | 25.140             | 25.339               |                | 26.424                    |                |
| GaV  | 9.353                     | 9.300          | 9.373                   | 9.345              | 9.485              | 9.389              | 9.398                | 9.336          | 9.431                     | 9.373          |
|      | 0                         | 2.905          | 0                       | 0.015              | 0                  | 0                  | 0.004                | 3.421          | 0                         | 3.938          |
|      | 1.551                     | 1.918          | 1.479                   | 1.436              | 1.309              | 1.343              | 1.392                | 1.453          | 1.111                     | 0.989          |
|      | 1.603                     | -0.979         | 1.564                   | 1.421              | 1.322              | 1.393              | 1.425                | -1.963         | 1.175                     | -2.947         |
|      | 13.516                    |                | 26.127                  | 26.882             | 26.899             | 26.835             | 26.686               |                | 26.850                    |                |
| GaY  | 10.399                    | 10.381         | 10.138                  | 9.890              | 9.938              | 10.168             | 10.034               | 10.057         | 9.850                     | 9.733          |
|      | 1.878                     | 5.613          | 2.328                   | 2.952              | 2.500              | 2.597              | 2.595                | 5.227          | 1.925                     | 4.841          |

Table A.1 Continued

| XY   | $(X_{0.25}Y_{0.75})_2O_3$ |                | $(X_{0.5}Y_{0.5})_2O_3$ |                    |                    |                    |                      |                | $(X_{0.75}Y_{0.25})_2O_3$ |                |
|------|---------------------------|----------------|-------------------------|--------------------|--------------------|--------------------|----------------------|----------------|---------------------------|----------------|
|      | PBE                       | interp.<br>HSE | PBE <sup>1st</sup>      | PBE <sup>2nd</sup> | PBE <sup>3rd</sup> | PBE <sup>4th</sup> | PBE <sup>aver.</sup> | interp.<br>HSE | PBE                       | interp.<br>HSE |
|      | -0.379                    | 2.085          | 0.270                   | 0.678              | 0.419              | 0.444              | 0.453                | 1.565          | 0.022                     | 1.045          |
|      | -2.256                    | -3.529         | -2.058                  | -2.274             | -2.081             | -2.154             | -2.142               | -3.663         | -1.903                    | -3.797         |
|      | 0                         |                | 0                       | 0                  | 0                  | 0                  | 0                    |                | 0                         |                |
| GaYb | 10.302                    | 10.368         | 10.056                  | 10.035             | 10.023             | 10.257             | 10.093               | 10.048         | 9.836                     | 9.729          |
|      | 3.134                     | 5.643          | 0.065                   | 0.022              | 0                  | 0                  | 0.022                | 5.247          | 2.302                     | 4.851          |
|      | -0.163                    | 1.849          | 0.884                   | 0.982              | 1.120              | 1.549              | 1.134                | 1.408          | -0.333                    | 0.966          |
|      | -3.296                    | -3.794         | 0.819                   | 0.960              | 1.043              | 2.061              | 1.221                | -3.840         | -2.634                    | -3.885         |
|      | 3.505                     |                | 18.450                  | 24.365             | 25.149             | 25.723             | 23.422               |                | 2.434                     |                |
| GdHo | 10.658                    | 10.658         | 10.715                  | 10.715             | 10.712             | 10.711             | 10.714               | 10.710         | 10.768                    | 10.762         |
|      | 3.968                     | 6.010          | 3.931                   | 3.909              | 3.883              | 3.924              | 3.912                | 6.066          | 3.828                     | 6.123          |
|      | 1.572                     | 2.504          | 1.556                   | 1.517              | 1.489              | 1.539              | 1.526                | 2.574          | 1.445                     | 2.644          |
|      | -2.397                    | -3.506         | -2.376                  | -2.392             | -2.394             | -2.386             | -2.387               | -3.493         | -2.383                    | -3.480         |
|      | 31.820                    |                | 44.113                  | 46.263             | 46.706             | 45.255             | 45.584               |                | 36.181                    |                |
| GdIn | 10.446                    | 10.433         | 10.575                  | 10.583             | 10.571             | 10.569             | 10.575               | 10.560         | 10.690                    | 10.687         |
|      | 1.486                     | 3.681          | 2.047                   | 2.157              | 2.121              | 2.111              | 2.109                | 4.514          | 2.159                     | 5.347          |
|      | -0.769                    | 0.236          | -0.206                  | -0.106             | -0.158             | -0.138             | -0.152               | 1.062          | -0.180                    | 1.888          |
|      | -2.254                    | -3.446         | -2.252                  | -2.263             | -2.279             | -2.249             | -2.261               | -3.453         | -2.338                    | -3.460         |
|      | 0                         |                | 0                       | 0                  | 0                  | 0                  | 0                    |                | 0                         |                |
| GdLa | 11.256                    | 11.235         | 11.116                  | 10.996             | 11.097             | 11.109             | 11.080               | 11.095         | 10.957                    | 10.955         |
|      | 3.281                     | 5.634          | 3.410                   | 3.684              | 3.699              | 3.533              | 3.582                | 5.816          | 3.910                     | 5.998          |
|      | 1.330                     | 2.411          | 1.421                   | 1.6                | 1.629              | 1.505              | 1.539                | 2.512          | 1.784                     | 2.613          |
|      | -1.951                    | -3.223         | -1.990                  | -2.084             | -2.070             | -2.029             | -2.044               | -3.304         | -2.127                    | -3.386         |
|      | 0                         |                | 0                       | 0                  | 0                  | 0                  | 0                    |                | 0                         |                |
| GdLu | 10.475                    | 10.474         | 10.591                  | 10.596             | 10.593             | 10.589             | 10.593               | 10.587         | 10.706                    | 10.701         |
|      | 3.998                     | 6.095          | 3.954                   | 3.897              | 3.844              | 3.927              | 3.906                | 6.123          | 3.688                     | 6.151          |
|      | 1.566                     | 2.505          | 1.563                   | 1.479              | 1.422              | 1.525              | 1.498                | 2.575          | 1.293                     | 2.644          |
|      | -2.433                    | -3.590         | -2.391                  | -2.418             | -2.423             | -2.403             | -2.409               | -3.549         | -2.395                    | -3.508         |
|      | 0                         |                | 0                       | 0                  | 0                  | 0                  | 0                    |                | 0                         |                |
| GdMn | 9.500                     | 9.479          | 9.875                   | 9.946              | 9.987              | 9.951              | 9.940                | 9.924          | 10.401                    | 10.369         |
|      | 0.004                     | 3.215          | 0                       | 0                  | 0                  | 0                  | 0                    | 4.203          | 0                         | 5.191          |
|      | 0.592                     | 1.639          | 0.710                   | 0.664              | 0.627              | 0.707              | 0.677                | 1.997          | -6.794                    | 2.355          |
|      | 0.589                     | -1.576         | 0.787                   | 0.683              | 0.631              | 0.726              | 0.707                | -2.207         | -6.791                    | -2.837         |
|      | 0                         |                | 0                       | 0                  | 0                  | 0                  | 0                    |                | 0                         |                |
| GdPm | 11.01                     | 11.007         | 10.945                  | 10.941             | 10.944             | 10.944             | 10.944               | 10.943         | 10.883                    | 10.879         |
|      | 3.719                     | 5.799          | 3.763                   | 3.812              | 3.823              | 3.789              | 3.797                | 5.926          | 3.880                     | 6.053          |
|      | 1.432                     | 2.528          | 1.464                   | 1.514              | 1.533              | 1.489              | 1.500                | 2.590          | 1.577                     | 2.652          |

Table A.1 Continued

| XY   | $(X_{0.25}Y_{0.75})_2O_3$ |                | $(X_{0.5}Y_{0.5})_2O_3$ |                    |                    |                    |                      |                | $(X_{0.75}Y_{0.25})_2O_3$ |                |
|------|---------------------------|----------------|-------------------------|--------------------|--------------------|--------------------|----------------------|----------------|---------------------------|----------------|
|      | PBE                       | interp.<br>HSE | PBE <sup>1st</sup>      | PBE <sup>2nd</sup> | PBE <sup>3rd</sup> | PBE <sup>4th</sup> | PBE <sup>aver.</sup> | interp.<br>HSE | PBE                       | interp.<br>HSE |
|      | -2.288<br>0               | -3.271         | -2.300<br>0             | -2.298<br>0        | -2.29<br>0         | -2.301<br>0        | -2.298<br>0          | -3.336         | -2.304<br>0               | -3.402         |
| GdPr | 11.169                    | 11.089         | 11.056                  | 11.047             | 11.047             | 11.053             | 11.051               | 10.997         | 10.936                    | 10.906         |
|      | 3.519                     | 5.769          | 3.592                   | 3.700              | 3.731              | 3.657              | 3.670                | 5.906          | 3.825                     | 6.043          |
|      | 1.294                     | 2.531          | 1.372                   | 1.461              | 1.499              | 1.418              | 1.438                | 2.592          | 1.574                     | 2.653          |
|      | -2.226                    | -3.238         | -2.220                  | -2.239             | -2.232             | -2.240             | -2.233               | -3.314         | -2.252                    | -3.391         |
|      | 0                         |                | 0                       | 0                  | 0                  | 0                  | 0                    |                | 0                         |                |
| GdSc | 10.149                    | 10.140         | 10.367                  | 10.371             | 10.377             | 10.361             | 10.369               | 10.365         | 10.598                    | 10.590         |
|      | 3.530                     | 6.199          | 3.777                   | 3.917              | 3.884              | 3.895              | 3.869                | 6.192          | 3.564                     | 6.186          |
|      | 1.752                     | 3.027          | 1.889                   | 1.971              | 1.960              | 1.958              | 1.945                | 2.922          | 1.527                     | 2.818          |
|      | -1.778                    | -3.172         | -1.889                  | -1.946             | -1.925             | -1.937             | -1.925               | -3.270         | -2.037                    | -3.369         |
|      | 0                         |                | 0                       | 0                  | 0                  | 0                  | 0                    |                | 0                         |                |
| GdSm | 10.956                    | 10.954         | 10.911                  | 10.908             | 10.909             | 10.912             | 10.91                | 10.907         | 10.865                    | 10.861         |
|      | 3.765                     | 5.818          | 3.792                   | 3.824              | 3.834              | 3.810              | 3.815                | 5.938          | 3.882                     | 6.059          |
|      | 1.458                     | 2.521          | 1.478                   | 1.511              | 1.526              | 1.495              | 1.503                | 2.585          | 1.563                     | 2.649          |
|      | -2.307                    | -3.297         | -2.315                  | -2.313             | -2.309             | -2.316             | -2.314               | -3.354         | -2.32                     | -3.410         |
|      | 0                         |                | 0                       | 0                  | 0                  | 0                  | 0                    |                | 0                         |                |
| GdTb | 10.764                    | 10.760         | 10.783                  | 10.784             | 10.781             | 10.778             | 10.782               | 10.778         | 10.801                    | 10.796         |
|      | 3.920                     | 5.940          | 3.903                   | 3.894              | 3.891              | 3.904              | 3.898                | 6.020          | 3.871                     | 6.100          |
|      | 1.550                     | 2.542          | 1.540                   | 1.526              | 1.521              | 1.537              | 1.531                | 2.599          | 1.507                     | 2.656          |
|      | -2.371                    | -3.399         | -2.363                  | -2.369             | -2.371             | -2.367             | -2.368               | -3.422         | -2.365                    | -3.444         |
|      | 0                         |                | 0                       | 0                  | 0                  | 0                  | 0                    |                | 0.004                     |                |
| GdTl | 10.815                    | 10.778         | 10.815                  | 10.817             | 10.811             | 10.804             | 10.812               | 10.790         | 10.824                    | 10.802         |
|      | 0.372                     | 1.869          | 0.848                   | 0.861              | 0.861              | 0.860              | 0.858                | 3.306          | 1.250                     | 4.742          |
|      | -1.416                    | -0.824         | -1.090                  | -1.035             | -1.053             | -1.051             | -1.058               | 0.356          | -0.968                    | 1.535          |
|      | -1.788                    | -2.692         | -1.937                  | -1.896             | -1.913             | -1.910             | -1.914               | -2.950         | -2.217                    | -3.208         |
|      | 0                         |                | 0                       | 0                  | 0                  | 0                  | 0                    |                | 0                         |                |
| GdTm | 10.559                    | 10.558         | 10.647                  | 10.569             | 10.647             | 10.645             | 10.627               | 10.643         | 10.734                    | 10.729         |
|      | 3.992                     | 6.053          | 3.947                   | 3.990              | 3.863              | 3.922              | 3.931                | 6.095          | 3.759                     | 6.137          |
|      | 1.572                     | 2.506          | 1.558                   | 1.548              | 1.452              | 1.526              | 1.521                | 2.575          | 1.366                     | 2.644          |
|      | -2.421                    | -3.548         | -2.389                  | -2.442             | -2.412             | -2.396             | -2.410               | -3.521         | -2.394                    | -3.494         |
|      | 23.834                    |                | 0.324                   | 0.315              | 36.771             | 34.343             | 17.938               |                | 27.581                    |                |
| GdV  | 9.750                     | 9.651          | 9.998                   | 9.937              | 10.086             | 9.950              | 9.993                | 10.039         | 10.447                    | 10.427         |
|      | 0.005                     | 3.336          | 0                       | 0.011              | 0                  | 0                  | 0.003                | 4.284          | 0                         | 5.232          |
|      | 1.555                     | 2.465          | 1.500                   | 1.407              | 1.411              | 1.383              | 1.426                | 2.548          | 1.314                     | 2.630          |
|      | 1.551                     | -0.863         | 1.554                   | 1.396              | 1.440              | 1.439              | 1.458                | -1.731         | 1.318                     | -2.599         |

Table A.1 Continued

| XY   | $(X_{0.25}Y_{0.75})_2O_3$ |                | $(X_{0.5}Y_{0.5})_2O_3$ |                    |                    |                    |                      |                | $(X_{0.75}Y_{0.25})_2O_3$ |                |
|------|---------------------------|----------------|-------------------------|--------------------|--------------------|--------------------|----------------------|----------------|---------------------------|----------------|
|      | PBE                       | interp.<br>HSE | PBE <sup>1st</sup>      | PBE <sup>2nd</sup> | PBE <sup>3rd</sup> | PBE <sup>4th</sup> | PBE <sup>aver.</sup> | interp.<br>HSE | PBE                       | interp.<br>HSE |
|      | 0                         |                | 0                       | 0                  | 0                  | 0                  | 0                    |                | 0                         |                |
| GdY  | 10.735                    | 10.733         | 10.762                  | 10.763             | 10.760             | 10.761             | 10.762               | 10.760         | 10.792                    | 10.787         |
|      | 4.033                     | 6.044          | 3.974                   | 3.961              | 3.951              | 3.966              | 3.963                | 6.089          | 3.899                     | 6.134          |
|      | 1.696                     | 2.632          | 1.637                   | 1.620              | 1.612              | 1.627              | 1.624                | 2.659          | 1.554                     | 2.686          |
|      | -2.337                    | -3.413         | -2.337                  | -2.342             | -2.339             | -2.340             | -2.340               | -3.431         | -2.345                    | -3.449         |
|      | 0                         |                | 0                       | 0                  | 0.002              | 0                  | 0.001                |                | 0.017                     |                |
| GdYb | 10.739                    | 10.719         | 10.781                  | 10.775             | 10.774             | 10.778             | 10.777               | 10.751         | 10.798                    | 10.783         |
|      | 4.039                     | 6.074          | 4.376                   | 4.375              | 4.390              | 4.369              | 4.378                | 6.109          | 4.193                     | 6.144          |
|      | 1.559                     | 2.396          | 1.580                   | 1.558              | 1.579              | 1.562              | 1.57                 | 2.502          | 1.613                     | 2.608          |
|      | -2.481                    | -3.678         | -2.796                  | -2.817             | -2.811             | -2.807             | -2.808               | -3.608         | -2.581                    | -3.537         |
|      | 0.019                     |                | 0.034                   | 0.043              | 0.053              | 0.037              | 0.042                |                | 0.050                     |                |
| HoIn | 10.392                    | 10.380         | 10.466                  | 10.476             | 10.465             | 10.468             | 10.469               | 10.455         | 10.533                    | 10.530         |
|      | 1.587                     | 3.625          | 2.111                   | 2.161              | 2.139              | 2.139              | 2.138                | 4.401          | 2.322                     | 5.177          |
|      | -0.763                    | 0.167          | -0.223                  | -0.166             | -0.206             | -0.186             | -0.196               | 0.923          | -0.114                    | 1.679          |
|      | -2.349                    | -3.459         | -2.334                  | -2.327             | -2.345             | -2.324             | -2.333               | -3.478         | -2.436                    | -3.498         |
|      | 0                         |                | 0                       | 0                  | 0                  | 0                  | 0                    |                | 0                         |                |
| HoLa | 11.209                    | 11.183         | 11.009                  | 10.884             | 10.987             | 11.004             | 10.971               | 10.990         | 10.806                    | 10.798         |
|      | 3.155                     | 5.577          | 3.294                   | 3.646              | 3.670              | 3.470              | 3.520                | 5.702          | 3.907                     | 5.828          |
|      | 1.221                     | 2.342          | 1.351                   | 1.589              | 1.627              | 1.475              | 1.511                | 2.373          | 1.798                     | 2.404          |
|      | -1.935                    | -3.236         | -1.944                  | -2.057             | -2.043             | -1.996             | -2.010               | -3.330         | -2.11                     | -3.424         |
|      | 0                         |                | 0                       | 0                  | 0                  | 0                  | 0                    |                | 0                         |                |
| HoLu | 10.423                    | 10.422         | 10.489                  | 10.488             | 10.490             | 10.488             | 10.489               | 10.483         | 10.550                    | 10.544         |
|      | 4.053                     | 6.038          | 4.011                   | 3.981              | 3.953              | 3.999              | 3.986                | 6.010          | 3.872                     | 5.981          |
|      | 1.543                     | 2.436          | 1.531                   | 1.480              | 1.448              | 1.505              | 1.491                | 2.435          | 1.398                     | 2.435          |
|      | -2.510                    | -3.603         | -2.481                  | -2.502             | -2.506             | -2.495             | -2.496               | -3.575         | -2.475                    | -3.547         |
|      | 0                         |                | 0                       | 0                  | 0                  | 0                  | 0                    |                | 0                         |                |
| HoMn | 9.434                     | 9.427          | 9.779                   | 9.712              | 9.859              | 9.829              | 9.795                | 9.820          | 10.245                    | 10.213         |
|      | 0.003                     | 3.158          | 0                       | 0                  | 0.005              | 0.002              | 0.002                | 4.090          | 0                         | 5.021          |
|      | 0.552                     | 1.569          | 0.692                   | 0.624              | 0.695              | 0.685              | 0.674                | 1.858          | -6.675                    | 2.146          |
|      | 0.550                     | -1.589         | 0.768                   | 0.674              | 0.690              | 0.683              | 0.704                | -2.232         | -6.675                    | -2.875         |
|      | 0                         |                | 0                       | 0                  | 0                  | 0                  | 0                    |                | 0                         |                |
| HoPm | 10.959                    | 10.955         | 10.845                  | 10.752             | 10.835             | 10.841             | 10.819               | 10.838         | 10.726                    | 10.722         |
|      | 3.608                     | 5.743          | 3.681                   | 3.884              | 3.830              | 3.751              | 3.787                | 5.813          | 3.921                     | 5.883          |
|      | 1.317                     | 2.459          | 1.382                   | 1.538              | 1.529              | 1.437              | 1.472                | 2.451          | 1.595                     | 2.443          |
|      | -2.292                    | -3.284         | -2.300                  | -2.347             | -2.301             | -2.314             | -2.316               | -3.362         | -2.327                    | -3.440         |
|      | 0                         |                | 0                       | 0                  | 0                  | 0                  | 0                    |                | 0                         |                |

Table A.1 Continued

| XY   | $(X_{0.25}Y_{0.75})_2O_3$ |                | $(X_{0.5}Y_{0.5})_2O_3$ |                    |                    |                    |                      |                | $(X_{0.75}Y_{0.25})_2O_3$ |                |
|------|---------------------------|----------------|-------------------------|--------------------|--------------------|--------------------|----------------------|----------------|---------------------------|----------------|
|      | PBE                       | interp.<br>HSE | PBE <sup>1st</sup>      | PBE <sup>2nd</sup> | PBE <sup>3rd</sup> | PBE <sup>4th</sup> | PBE <sup>aver.</sup> | interp.<br>HSE | PBE                       | interp.<br>HSE |
| HoPr | 11.12                     | 11.037         | 10.953                  | 10.841             | 10.939             | 10.949             | 10.921               | 10.893         | 10.777                    | 10.749         |
|      | 3.378                     | 5.712          | 3.482                   | 3.762              | 3.723              | 3.599              | 3.642                | 5.793          | 3.846                     | 5.873          |
|      | 1.157                     | 2.462          | 1.276                   | 1.484              | 1.492              | 1.361              | 1.404                | 2.453          | 1.584                     | 2.444          |
|      | -2.221                    | -3.251         | -2.206                  | -2.279             | -2.232             | -2.239             | -2.239               | -3.340         | -2.262                    | -3.429         |
|      | 0                         |                | 0                       | 0                  | 0                  | 0                  | 0                    |                | 0                         | 0              |
| HoSc | 10.097                    | 10.088         | 10.265                  | 10.268             | 10.276             | 10.265             | 10.269               | 10.260         | 10.443                    | 10.433         |
|      | 3.620                     | 6.142          | 3.874                   | 4.033              | 4.044              | 3.980              | 3.983                | 6.079          | 3.804                     | 6.016          |
|      | 1.783                     | 2.957          | 1.931                   | 2.050              | 2.079              | 2.008              | 2.017                | 2.783          | 1.718                     | 2.609          |
|      | -1.838                    | -3.185         | -1.944                  | -1.983             | -1.965             | -1.973             | -1.967               | -3.296         | -2.087                    | -3.407         |
|      | 0                         |                | 0                       | 0                  | 0                  | 0                  | 0                    |                | 0                         |                |
| HoSm | 10.906                    | 10.902         | 10.807                  | 10.801             | 10.802             | 10.810             | 10.805               | 10.803         | 10.712                    | 10.704         |
|      | 3.670                     | 5.761          | 3.733                   | 3.824              | 3.850              | 3.785              | 3.798                | 5.825          | 3.930                     | 5.889          |
|      | 1.353                     | 2.451          | 1.405                   | 1.490              | 1.526              | 1.448              | 1.468                | 2.446          | 1.583                     | 2.440          |
|      | -2.318                    | -3.310         | -2.328                  | -2.334             | -2.325             | -2.337             | -2.331               | -3.380         | -2.348                    | -3.449         |
|      | 0                         |                | 0                       | 0                  | 0                  | 0                  | 0                    |                | 0                         |                |
| HoTb | 10.713                    | 10.707         | 10.681                  | 10.801             | 10.677             | 10.676             | 10.709               | 10.673         | 10.643                    | 10.639         |
|      | 3.882                     | 5.884          | 3.907                   | 3.894              | 3.938              | 3.916              | 3.914                | 5.907          | 3.973                     | 5.930          |
|      | 1.476                     | 2.472          | 1.509                   | 1.496              | 1.532              | 1.503              | 1.510                | 2.460          | 1.559                     | 2.447          |
|      | -2.407                    | -3.412         | -2.398                  | -2.398             | -2.407             | -2.414             | -2.404               | -3.448         | -2.415                    | -3.483         |
|      | 0.004                     |                | 0                       | 0                  | 0                  | 0                  | 0                    |                | 0                         |                |
| HoTl | 10.757                    | 10.726         | 10.707                  | 10.705             | 10.706             | 10.693             | 10.703               | 10.686         | 10.662                    | 10.646         |
|      | 0.382                     | 1.812          | 0.871                   | 0.840              | 0.836              | 0.856              | 0.851                | 3.192          | 1.307                     | 4.573          |
|      | -1.435                    | -0.893         | -1.115                  | -1.096             | -1.119             | -1.098             | -1.107               | 0.217          | -0.959                    | 1.326          |
|      | -1.816                    | -2.705         | -1.986                  | -1.936             | -1.954             | -1.954             | -1.958               | -2.976         | -2.265                    | -3.247         |
|      | 0                         |                | 0                       | 0                  | 0                  | 0                  | 0                    |                | 0                         |                |
| HoTm | 10.51                     | 10.506         | 10.546                  | 10.502             | 10.545             | 10.543             | 10.534               | 10.539         | 10.577                    | 10.572         |
|      | 4.008                     | 5.997          | 3.994                   | 4.026              | 3.958              | 3.982              | 3.990                | 5.982          | 3.920                     | 5.967          |
|      | 1.534                     | 2.436          | 1.527                   | 1.532              | 1.482              | 1.513              | 1.514                | 2.436          | 1.456                     | 2.435          |
|      | -2.475                    | -3.561         | -2.468                  | -2.494             | -2.477             | -2.469             | -2.477               | -3.547         | -2.465                    | -3.533         |
|      | 0                         |                | 24.231                  | 24.050             | 0                  | 0                  | 12.070               |                | 0.076                     | 0              |
| HoV  | 9.652                     | 9.599          | 9.932                   | 9.939              | 9.986              | 9.882              | 9.935                | 9.934          | 10.308                    | 10.27          |
|      | 0                         | 3.279          | 0                       | 0                  | 0.002              | 0                  | 0.001                | 4.170          | 0                         | 5.062          |
|      | 1.545                     | 2.395          | 1.522                   | 1.414              | 1.437              | 1.406              | 1.445                | 2.408          | -2.113                    | 2.422          |
|      | 1.576                     | -0.875         | 1.544                   | 1.455              | 1.435              | 1.493              | 1.482                | -1.756         | -2.105                    | -2.637         |
|      | 0                         |                | 0                       | 0                  | 0                  | 0                  | 0                    |                | 0                         |                |
| HoY  | 10.687                    | 10.68          | 10.658                  | 10.657             | 10.655             | 10.657             | 10.657               | 10.655         | 10.634                    | 10.630         |

Table A.1 Continued

| XY   | $(X_{0.25}Y_{0.75})_2O_3$ |                | $(X_{0.5}Y_{0.5})_2O_3$ |                    |                    |                    |                      |                | $(X_{0.75}Y_{0.25})_2O_3$ |                |
|------|---------------------------|----------------|-------------------------|--------------------|--------------------|--------------------|----------------------|----------------|---------------------------|----------------|
|      | PBE                       | interp.<br>HSE | PBE <sup>1st</sup>      | PBE <sup>2nd</sup> | PBE <sup>3rd</sup> | PBE <sup>4th</sup> | PBE <sup>aver.</sup> | interp.<br>HSE | PBE                       | interp.<br>HSE |
|      | 3.997                     | 5.988          | 3.988                   | 4.009              | 4.021              | 3.997              | 4.004                | 5.976          | 4.001                     | 5.964          |
|      | 1.627                     | 2.562          | 1.595                   | 1.624              | 1.642              | 1.607              | 1.617                | 2.520          | 1.610                     | 2.477          |
|      | -2.370                    | -3.426         | -2.394                  | -2.385             | -2.380             | -2.390             | -2.388               | -3.457         | -2.392                    | -3.488         |
|      | 0                         |                | 0                       | 0                  | 0                  | 0                  | 0                    |                | 0.006                     |                |
| HoYb | 10.682                    | 10.667         | 10.668                  | 10.538             | 10.662             | 10.666             | 10.634               | 10.646         | 10.638                    | 10.626         |
|      | 3.972                     | 6.017          | 4.426                   | 4.610              | 4.494              | 4.431              | 4.491                | 5.996          | 4.296                     | 5.974          |
|      | 1.504                     | 2.327          | 1.534                   | 1.651              | 1.585              | 1.537              | 1.577                | 2.363          | 1.644                     | 2.399          |
|      | -2.469                    | -3.691         | -2.892                  | -2.959             | -2.909             | -2.894             | -2.914               | -3.634         | -2.653                    | -3.576         |
|      | 0.033                     |                | 0.057                   | 0.050              | 0.050              | 0.042              | 0.050                |                | 0.040                     | 0              |
| InLa | 11.149                    | 11.108         | 10.872                  | 10.799             | 10.79              | 10.856             | 10.830               | 10.84          | 10.587                    | 10.573         |
|      | 1.778                     | 4.801          | 1.693                   | 2.134              | 2.048              | 1.981              | 1.964                | 4.150          | 1.201                     | 3.499          |
|      | -0.070                    | 1.585          | -0.105                  | 0.235              | 0.142              | 0.158              | 0.108                | 0.860          | -0.732                    | 0.135          |
|      | -1.847                    | -3.216         | -1.797                  | -1.899             | -1.907             | -1.824             | -1.857               | -3.290         | -1.933                    | -3.364         |
|      | 16.777                    |                | 26.720                  | 28.699             | 28.343             | 27.800             | 27.891               |                | 17.725                    |                |
| InLu | 10.354                    | 10.347         | 10.342                  | 10.340             | 10.346             | 10.348             | 10.344               | 10.333         | 10.335                    | 10.319         |
|      | 2.507                     | 5.262          | 2.084                   | 2.159              | 2.169              | 2.130              | 2.136                | 4.458          | 1.640                     | 3.653          |
|      | -0.051                    | 1.680          | -0.362                  | -0.255             | -0.256             | -0.293             | -0.292               | 0.923          | -0.784                    | 0.167          |
|      | -2.557                    | -3.583         | -2.446                  | -2.413             | -2.424             | -2.423             | -2.427               | -3.535         | -2.423                    | -3.487         |
|      | 20.369                    |                | 33.011                  | 32.714             | 32.600             | 32.912             | 32.809               |                | 29.740                    |                |
| InMn | 9.387                     | 9.352          | 9.701                   | 9.741              | 10.673             | 9.793              | 9.977                | 9.670          | 10.010                    | 9.988          |
|      | 0                         | 2.382          | 0                       | 0                  | 0.005              | 0                  | 0.002                | 2.538          | 0                         | 2.693          |
|      | 0.493                     | 0.813          | 0.648                   | 0.623              | 0.678              | 0.594              | 0.636                | 0.346          | -19.13                    | -0.123         |
|      | 0.629                     | -1.569         | 0.677                   | 0.667              | 0.673              | 0.659              | 0.669                | -2.192         | -                         | -2.815         |
|      | 0                         |                | 0                       | 0                  | 0                  | 0                  | 0                    |                | 19.078                    |                |
| InPm | 10.878                    | 10.88          | 10.709                  | 10.665             | 10.673             | 10.701             | 10.687               | 10.688         | 10.516                    | 10.497         |
|      | 1.966                     | 4.967          | 1.838                   | 2.153              | 2.069              | 2.074              | 2.034                | 4.261          | 1.324                     | 3.555          |
|      | -0.263                    | 1.703          | -0.332                  | -0.036             | -0.094             | -0.120             | -0.146               | 0.939          | -0.802                    | 0.175          |
|      | -2.228                    | -3.264         | -2.170                  | -2.188             | -2.162             | -2.194             | -2.179               | -3.322         | -2.125                    | -3.380         |
|      | 18.444                    |                | 23.849                  | 24.754             | 23.671             | 24.673             | 24.237               |                | 0                         |                |
| InPr | 11.038                    | 10.962         | 10.807                  | 10.749             | 10.751             | 10.804             | 10.778               | 10.743         | 10.565                    | 10.524         |
|      | 1.795                     | 4.936          | 1.731                   | 2.118              | 2.016              | 1.993              | 1.965                | 4.240          | 1.192                     | 3.544          |
|      | -0.348                    | 1.706          | -0.348                  | -0.002             | -0.075             | -0.102             | -0.132               | 0.941          | -0.843                    | 0.176          |
|      | -2.143                    | -3.231         | -2.079                  | -2.120             | -2.090             | -2.095             | -2.096               | -3.300         | -2.035                    | -3.369         |
|      | 0                         |                | 0                       | 0                  | 0                  | 0                  | 0                    |                | 0                         |                |
| InSc | 10.012                    | 10.013         | 10.116                  | 10.114             | 10.129             | 10.118             | 10.120               | 10.110         | 10.215                    | 10.208         |

Table A.1 Continued

| XY   | $(X_{0.25}Y_{0.75})_2O_3$ |                | $(X_{0.5}Y_{0.5})_2O_3$ |                    |                    |                    |                      |                | $(X_{0.75}Y_{0.25})_2O_3$ |                |
|------|---------------------------|----------------|-------------------------|--------------------|--------------------|--------------------|----------------------|----------------|---------------------------|----------------|
|      | PBE                       | interp.<br>HSE | PBE <sup>1st</sup>      | PBE <sup>2nd</sup> | PBE <sup>3rd</sup> | PBE <sup>4th</sup> | PBE <sup>aver.</sup> | interp.<br>HSE | PBE                       | interp.<br>HSE |
|      | 2.921                     | 5.366          | 2.398                   | 2.450              | 2.464              | 2.412              | 2.431                | 4.527          | 1.880                     | 3.688          |
|      | 1.024                     | 2.201          | 0.551                   | 0.655              | 0.660              | 0.593              | 0.615                | 1.271          | -0.061                    | 0.341          |
|      | -1.897                    | -3.165         | -1.848                  | -1.795             | -1.804             | -1.819             | -1.817               | -3.256         | -1.941                    | -3.347         |
|      | 13.051                    |                | 24.423                  | 24.249             | 24.236             | 24.351             | 24.315               |                | 26.877                    |                |
| InSm | 10.823                    | 10.827         | 10.662                  | 10.634             | 10.645             | 10.664             | 10.652               | 10.653         | 10.497                    | 10.479         |
|      | 2.023                     | 4.985          | 1.880                   | 2.151              | 2.074              | 2.081              | 2.047                | 4.273          | 1.383                     | 3.561          |
|      | -0.236                    | 1.695          | -0.327                  | -0.059             | -0.112             | -0.137             | -0.159               | 0.934          | -0.789                    | 0.172          |
|      | -2.259                    | -3.290         | -2.206                  | -2.209             | -2.185             | -2.218             | -2.205               | -3.340         | -2.171                    | -3.389         |
|      | 21.285                    |                | 33.206                  | 33.482             | 32.937             | 33.547             | 33.293               |                | 25.197                    | 0              |
| InTb | 10.635                    | 10.632         | 10.527                  | 10.514             | 10.520             | 10.527             | 10.522               | 10.523         | 10.431                    | 10.414         |
|      | 2.222                     | 5.107          | 2.001                   | 2.176              | 2.138              | 2.134              | 2.113                | 4.354          | 1.528                     | 3.602          |
|      | -0.151                    | 1.716          | -0.319                  | -0.115             | -0.143             | -0.170             | -0.187               | 0.947          | -0.764                    | 0.179          |
|      | -2.373                    | -3.392         | -2.320                  | -2.291             | -2.28              | -2.304             | -2.299               | -3.408         | -2.291                    | -3.423         |
|      | 0                         |                | 0                       | 0                  | 0                  | 0                  | 0                    |                | 0                         |                |
| InTl | 10.631                    | 10.651         | 10.518                  | 10.514             | 10.519             | 10.516             | 10.517               | 10.536         | 10.416                    | 10.421         |
|      | 0.001                     | 1.036          | 0.042                   | 0.001              | 0.009              | 0.021              | 0.019                | 1.640          | 0.241                     | 2.244          |
|      | -1.759                    | -1.650         | -1.874                  | -1.891             | -1.868             | -1.886             | -1.88                | -1.297         | -1.811                    | -0.944         |
|      | -1.759                    | -2.685         | -1.915                  | -1.891             | -1.876             | -1.906             | -1.897               | -2.936         | -2.052                    | -3.187         |
|      | 0                         |                | 0                       | 0                  | 0                  | 0                  | 0                    |                | 0                         |                |
| InTm | 10.435                    | 10.431         | 10.296                  | 10.318             | 10.393             | 10.393             | 10.350               | 10.389         | 10.353                    | 10.347         |
|      | 2.412                     | 5.221          | 2.208                   | 2.179              | 2.164              | 2.141              | 2.173                | 4.430          | 1.618                     | 3.639          |
|      | -0.087                    | 1.680          | -0.250                  | -0.271             | -0.216             | -0.248             | -0.247               | 0.924          | -0.772                    | 0.167          |
|      | -2.499                    | -3.541         | -2.458                  | -2.449             | -2.379             | -2.388             | -2.419               | -3.507         | -2.39                     | -3.473         |
|      | 12.831                    |                | 24.311                  | 24.384             | 23.935             | 24.088             | 24.179               |                | 26.646                    |                |
| InV  | 10.614                    | 9.524          | 10.819                  | 9.893              | 10.166             | 9.976              | 10.214               | 9.784          | 10.103                    | 10.045         |
|      | 0                         | 2.503          | 0                       | 0                  | 0                  | 0                  | 0                    | 2.618          | 0                         | 2.733          |
|      | 1.619                     | 1.639          | 1.235                   | 1.378              | 1.221              | 1.320              | 1.289                | 0.896          | 0.973                     | 0.153          |
|      | 1.650                     | -0.856         | 1.249                   | 1.420              | 1.239              | 1.356              | 1.316                | -1.717         | 1.041                     | -2.578         |
|      | 9.287                     |                | 18.847                  | 22.128             | 23.215             | 22.522             | 21.678               |                | 25.275                    |                |
| InY  | 9.604                     | 10.605         | 10.514                  | 10.506             | 10.501             | 10.509             | 10.508               | 10.505         | 10.414                    | 10.405         |
|      | 2.340                     | 5.212          | 2.059                   | 2.218              | 2.200              | 2.184              | 2.166                | 4.424          | 1.600                     | 3.636          |
|      | -0.010                    | 1.806          | -0.219                  | -0.025             | -0.042             | -0.074             | -0.090               | 1.008          | -0.682                    | 0.209          |
|      | -2.350                    | -3.406         | -2.278                  | -2.242             | -2.242             | -2.258             | -2.255               | -3.417         | -2.281                    | -3.428         |
|      | 0                         |                | 0                       | 0                  | 0                  | 0                  | 0                    |                | 0                         |                |
| InYb | 10.545                    | 10.592         | 10.477                  | 10.449             | 10.457             | 10.479             | 10.466               | 10.496         | 10.382                    | 10.401         |
|      | 3.355                     | 5.241          | 2.558                   | 2.724              | 2.671              | 2.651              | 2.651                | 4.444          | 1.707                     | 3.646          |

Table A.1 Continued

| XY   | $(X_{0.25}Y_{0.75})_2O_3$ |                | $(X_{0.5}Y_{0.5})_2O_3$ |                    |                    |                    |                      |                | $(X_{0.75}Y_{0.25})_2O_3$ |                |
|------|---------------------------|----------------|-------------------------|--------------------|--------------------|--------------------|----------------------|----------------|---------------------------|----------------|
|      | PBE                       | interp.<br>HSE | PBE <sup>1st</sup>      | PBE <sup>2nd</sup> | PBE <sup>3rd</sup> | PBE <sup>4th</sup> | PBE <sup>aver.</sup> | interp.<br>HSE | PBE                       | interp.<br>HSE |
|      | 0.033                     | 1.570          | -0.432                  | -0.300             | -0.334             | -0.369             | -0.359               | 0.850          | -0.968                    | 0.130          |
|      | -3.323                    | -3.671         | -2.990                  | -3.023             | -3.005             | -3.019             | -3.010               | -3.594         | -2.675                    | -3.516         |
|      | 3.237                     |                | 4.562                   | 4.598              | 4.519              | 4.540              | 4.555                |                | 3.430                     |                |
| LaLu | 10.619                    | 10.614         | 10.777                  | 10.773             | ×                  | ×                  | 10.775               | 10.868         | 11.148                    | 11.122         |
|      | 3.859                     | 5.913          | 3.761                   | 3.599              | ×                  | ×                  | 3.680                | 5.759          | 2.955                     | 5.606          |
|      | 1.776                     | 2.405          | 1.752                   | 1.584              | ×                  | ×                  | 1.668                | 2.373          | 1.044                     | 2.342          |
|      | -2.083                    | -3.509         | -2.010                  | -2.015             | ×                  | ×                  | -2.013               | -3.387         | -1.911                    | -3.264         |
|      | 21.198                    |                | 35.043                  | 35.746             | ×                  | ×                  | 35.396               |                | 28.273                    |                |
| LaMn | 10.006                    | 9.620          | 10.675                  | 10.541             | 10.325             | 10.615             | 10.539               | 10.205         | 0                         | 10.790         |
|      | 0                         | 3.033          | 0                       | 0                  | 0                  | 0                  | 0                    | 3.839          | 0                         | 4.646          |
|      | 0.816                     | 1.538          | 0.457                   | 0.397              | 0.660              | 0.676              | 0.548                | 1.796          | 0                         | 2.053          |
|      | 0.858                     | -1.495         | 0.473                   | 0.427              | 0.677              | 0.696              | 0.569                | -2.044         | 0                         | -2.593         |
|      | 0                         |                | 0                       | 0                  | 0                  | 0                  | 0                    |                | 0                         |                |
| LaPm | 11.149                    | 11.147         | 11.236                  | 11.242             | 11.242             | 11.233             | 11.239               | 11.223         | 11.322                    | 11.299         |
|      | 3.873                     | 5.617          | 3.775                   | 3.646              | 3.576              | 3.714              | 3.678                | 5.562          | 3.380                     | 5.507          |
|      | 1.735                     | 2.428          | 1.679                   | 1.574              | 1.521              | 1.624              | 1.600                | 2.389          | 1.415                     | 2.350          |
|      | -2.138                    | -3.190         | -2.096                  | -2.072             | -2.055             | -2.091             | -2.079               | -3.174         | -1.965                    | -3.158         |
|      | 0                         |                | 0                       | 0                  | 0                  | 0                  | 0                    |                | 0                         |                |
| LaPr | 11.313                    | 11.229         | 11.344                  | 11.242             | 11.349             | 11.345             | 11.32                | 11.278         | 11.377                    | 11.327         |
|      | 3.788                     | 5.587          | 3.752                   | 3.633              | 3.579              | 3.695              | 3.665                | 5.542          | 3.437                     | 5.497          |
|      | 1.649                     | 2.431          | 1.642                   | 1.553              | 1.518              | 1.596              | 1.578                | 2.391          | 1.463                     | 2.350          |
|      | -2.139                    | -3.157         | -2.111                  | -2.08              | -2.062             | -2.099             | -2.088               | -3.152         | -1.974                    | -3.147         |
|      | 0                         |                | 0                       | 0                  | 0                  | 0                  | 0                    |                | 0                         |                |
| LaSc | 10.308                    | 10.280         | 10.634                  | 10.645             | 10.678             | 10.615             | 10.643               | 10.645         | 11.040                    | 11.010         |
|      | 3.229                     | 6.017          | 3.576                   | 3.526              | 3.337              | 3.631              | 3.518                | 5.828          | 2.778                     | 5.640          |
|      | 1.626                     | 2.926          | 1.906                   | 1.766              | 1.660              | 1.846              | 1.795                | 2.721          | 1.021                     | 2.516          |
|      | -1.603                    | -3.091         | -1.671                  | -1.760             | -1.677             | -1.786             | -1.724               | -3.108         | -1.758                    | -3.125         |
|      | 13.056                    |                | 25.869                  | 26.163             | 25.618             | 26.089             | 25.935               |                | 26.414                    |                |
| LaSm | 11.094                    | 11.094         | 11.196                  | 11.204             | 11.206             | 11.195             | 11.201               | 11.188         | 11.309                    | 11.282         |
|      | 3.877                     | 5.636          | 3.777                   | 3.634              | 3.564              | 3.709              | 3.671                | 5.575          | 3.351                     | 5.513          |
|      | 1.742                     | 2.420          | 1.688                   | 1.568              | 1.515              | 1.623              | 1.599                | 2.384          | 1.391                     | 2.347          |
|      | -2.135                    | -3.216         | -2.090                  | -2.067             | -2.050             | -2.086             | -2.074               | -3.191         | -1.96                     | -3.167         |
|      | 31.851                    |                | 42.713                  | 42.208             | 41.458             | 42.574             | 42.238               |                | 28.524                    |                |
| LaTb | 10.903                    | 10.900         | 11.067                  | 11.077             | 11.077             | 11.064             | 11.072               | 11.058         | 11.243                    | 11.217         |
|      | 3.922                     | 5.758          | 3.758                   | 3.607              | 3.512              | 3.690              | 3.642                | 5.656          | 3.237                     | 5.554          |
|      | 1.799                     | 2.441          | 1.702                   | 1.566              | 1.494              | 1.628              | 1.598                | 2.397          | 1.292                     | 2.354          |



Table A.1 Continued

| XY   | $(X_{0.25}Y_{0.75})_2O_3$ |                | $(X_{0.5}Y_{0.5})_2O_3$ |                    |                    |                    |                      |                | $(X_{0.75}Y_{0.25})_2O_3$ |                |
|------|---------------------------|----------------|-------------------------|--------------------|--------------------|--------------------|----------------------|----------------|---------------------------|----------------|
|      | PBE                       | interp.<br>HSE | PBE <sup>1st</sup>      | PBE <sup>2nd</sup> | PBE <sup>3rd</sup> | PBE <sup>4th</sup> | PBE <sup>aver.</sup> | interp.<br>HSE | PBE                       | interp.<br>HSE |
|      | -2.124<br>0               | -3.318         | -2.056<br>0             | -2.042<br>0        | -2.019<br>0        | -2.063<br>0        | -2.045<br>0          | -3.259         | -1.945<br>0               | -3.201         |
| LaTl | 10.963                    | 10.919         | 11.098                  | 11.137             | 11.135             | 11.104             | 11.119               | 11.071         | 11.279                    | 11.223         |
|      | 0.366                     | 1.687          | 0.834                   | 0.924              | 0.946              | 0.892              | 0.899                | 2.942          | 1.052                     | 4.197          |
|      | -1.243                    | -0.925         | -0.873                  | -0.756             | -0.736             | -0.818             | -0.796               | 0.154          | -0.731                    | 1.232          |
|      | -1.609                    | -2.611         | -1.706                  | -1.68              | -1.682             | -1.709             | -1.695               | -2.788         | -1.783                    | -2.965         |
|      | 0                         |                | 0                       | 0                  | 0                  | 0                  | 0                    |                | 0                         |                |
| LaTm | 10.698                    | 10.698         | 10.878                  | 10.879             | 10.945             | 10.919             | 10.906               | 10.924         | 11.175                    | 11.150         |
|      | 3.886                     | 5.871          | 3.747                   | 3.587              | 3.415              | 3.642              | 3.598                | 5.732          | 3.048                     | 5.592          |
|      | 1.791                     | 2.405          | 1.721                   | 1.566              | 1.449              | 1.618              | 1.589                | 2.373          | 1.126                     | 2.342          |
|      | -2.096                    | -3.467         | -2.027                  | -2.021             | -1.967             | -2.025             | -2.010               | -3.359         | -1.922                    | -3.250         |
|      | 14.857                    |                | 27.537                  | 27.747             | 27.189             | 27.320             | 27.448               |                | 27.894                    |                |
| LaV  | 10.049                    | 9.791          | 10.225                  | 10.338             | 10.337             | 10.302             | 10.301               | 10.319         | 10.795                    | 10.847         |
|      | 0                         | 3.154          | 0.016                   | 0.006              | 0                  | 0.013              | 0.009                | 3.920          | 0                         | 4.686          |
|      | 1.470                     | 2.364          | 1.470                   | 1.377              | 1.337              | 1.322              | 1.377                | 2.346          | 1.077                     | 2.328          |
|      | 1.516                     | -0.781         | 1.454                   | 1.372              | 1.352              | 1.310              | 1.372                | -1.568         | 1.136                     | -2.355         |
|      | 11.974                    |                | 24.301                  | 24.092             | 23.14              | 24.722             | 24.064               |                | 22.988                    |                |
| LaY  | 10.878                    | 10.873         | 11.051                  | 10.977             | 11.062             | 11.046             | 11.034               | 11.040         | 11.238                    | 11.208         |
|      | 3.999                     | 5.862          | 3.791                   | 3.680              | 3.532              | 3.712              | 3.679                | 5.726          | 3.242                     | 5.589          |
|      | 1.914                     | 2.531          | 1.758                   | 1.635              | 1.538              | 1.674              | 1.652                | 2.458          | 1.312                     | 2.384          |
|      | -2.085                    | -3.332         | -2.034                  | -2.046             | -1.994             | -2.039             | -2.029               | -3.269         | -1.930                    | -3.205         |
|      | 0                         |                | 0                       | 0                  | 0                  | 0                  | 0                    |                | 0                         |                |
| LaYb | 10.860                    | 10.859         | 11.049                  | 10.912             | 11.051             | 11.048             | 11.015               | 11.031         | 11.233                    | 11.203         |
|      | 4.603                     | 5.892          | 4.186                   | 4.067              | 3.958              | 4.095              | 4.077                | 5.745          | 3.542                     | 5.599          |
|      | 2.113                     | 2.295          | 1.872                   | 1.780              | 1.703              | 1.777              | 1.783                | 2.300          | 1.484                     | 2.305          |
|      | -2.491                    | -3.597         | -2.314                  | -2.287             | -2.256             | -2.318             | -2.294               | -3.445         | -2.059                    | -3.294         |
|      | 1.889                     |                | 0                       | 0.916              | 0.878              | 0                  | 0.449                |                | 1.615                     |                |
| LuMn | 9.380                     | 9.366          | 9.670                   | 9.681              | 9.712              | 9.672              | 9.684                | 9.697          | 0                         | 10.029         |
|      | 0                         | 3.187          | 0                       | 0                  | 0                  | 0                  | 0                    | 4.147          | 0                         | 5.107          |
|      | 0.540                     | 1.570          | 0.675                   | 0.640              | 0.663              | 0.655              | 0.659                | 1.858          | 0                         | 2.147          |
|      | 0.556                     | -1.618         | 0.738                   | 0.664              | 0.688              | 0.673              | 0.691                | -2.289         | 0                         | -2.960         |
|      | 0                         |                | 0                       | 0                  | 0                  | 0                  | 0                    |                | 0                         |                |
| LuPm | 10.896                    | 10.894         | 10.723                  | 10.610             | 10.709             | 10.721             | 10.691               | 10.716         | 10.542                    | 10.538         |
|      | 3.409                     | 5.771          | 3.539                   | 3.862              | 3.813              | 3.675              | 3.723                | 5.870          | 3.913                     | 5.968          |
|      | 1.128                     | 2.459          | 1.251                   | 1.508              | 1.514              | 1.359              | 1.408                | 2.451          | 1.570                     | 2.444          |
|      | -2.281                    | -3.312         | -2.289                  | -2.355             | -2.300             | -2.317             | -2.316               | -3.419         | -2.344                    | -3.525         |

Table A.1 Continued

| XY   | $(X_{0.25}Y_{0.75})_2O_3$ |                | $(X_{0.5}Y_{0.5})_2O_3$ |                    |                    |                    |                      |                | $(X_{0.75}Y_{0.25})_2O_3$ |                |
|------|---------------------------|----------------|-------------------------|--------------------|--------------------|--------------------|----------------------|----------------|---------------------------|----------------|
|      | PBE                       | interp.<br>HSE | PBE <sup>1st</sup>      | PBE <sup>2nd</sup> | PBE <sup>3rd</sup> | PBE <sup>4th</sup> | PBE <sup>aver.</sup> | interp.<br>HSE | PBE                       | interp.<br>HSE |
|      | 0                         |                | 0                       | 0                  | 0                  | 0                  | 0                    |                | 0                         |                |
| LuPr | 11.067                    | 10.975         | 10.833                  | 10.717             | 10.803             | 10.827             | 10.795               | 10.770         | 10.595                    | 10.565         |
|      | 3.152                     | 5.741          | 3.306                   | 3.720              | 3.704              | 3.505              | 3.559                | 5.849          | 3.807                     | 5.958          |
|      | 0.947                     | 2.462          | 1.129                   | 1.451              | 1.482              | 1.281              | 1.336                | 2.453          | 1.543                     | 2.445          |
|      | -2.205                    | -3.279         | -2.177                  | -2.269             | -2.222             | -2.224             | -2.223               | -3.397         | -2.265                    | -3.514         |
|      | 0                         |                | 0                       | 0                  | 0                  | 0                  | 0                    |                | 0                         |                |
| LuSc | 10.029                    | 10.027         | 10.140                  | 10.058             | 10.146             | 10.141             | 10.122               | 10.138         | 10.258                    | 10.249         |
|      | 3.721                     | 6.170          | 3.988                   | 4.211              | 4.197              | 4.078              | 4.119                | 6.136          | 4.050                     | 6.101          |
|      | 1.820                     | 2.957          | 1.992                   | 2.162              | 2.216              | 2.076              | 2.112                | 2.784          | 1.902                     | 2.610          |
|      | -1.901                    | -3.213         | -1.997                  | -2.050             | -1.982             | -2.003             | -2.008               | -3.353         | -2.149                    | -3.492         |
|      | 22.382                    |                | 35.520                  | 36.168             | 35.650             | 35.602             | 35.735               |                | 31.916                    |                |
| LuSm | 10.847                    | 10.840         | 10.685                  | 10.622             | 10.675             | 10.683             | 10.667               | 10.680         | 10.527                    | 10.520         |
|      | 2.432                     | 5.789          | 3.607                   | 3.852              | 3.837              | 3.722              | 3.755                | 5.882          | 3.938                     | 5.974          |
|      | 0.141                     | 2.452          | 1.281                   | 1.483              | 1.509              | 1.374              | 1.412                | 2.446          | 1.568                     | 2.441          |
|      | -2.292                    | -3.338         | -2.327                  | -2.369             | -2.328             | -2.349             | -2.344               | -3.436         | -2.371                    | -3.534         |
|      | 0                         |                | 0                       | 0                  | 0                  | 0                  | 0                    |                | 0                         |                |
| LuTb | 10.654                    | 10.646         | 10.557                  | 10.553             | 10.553             | 10.559             | 10.556               | 10.551         | 10.457                    | 10.456         |
|      | 0.711                     | 5.912          | 3.832                   | 3.927              | 3.956              | 3.889              | 3.901                | 5.964          | 4.033                     | 6.015          |
|      | -1.679                    | 2.472          | 1.383                   | 1.482              | 1.523              | 1.437              | 1.457                | 2.460          | 1.573                     | 2.448          |
|      | -2.389                    | -3.440         | -2.450                  | -2.445             | -2.433             | -2.453             | -2.446               | -3.504         | -2.461                    | -3.568         |
|      | 0                         |                | 0                       | 0                  | 0                  | 0                  | 0                    |                | 0                         |                |
| LuTl | 10.694                    | 10.665         | 10.581                  | 10.571             | 10.574             | 10.565             | 10.573               | 10.563         | 10.478                    | 10.462         |
|      | 0                         | 1.840          | 0.885                   | 0.805              | 0.796              | 0.844              | 0.833                | 3.249          | 1.376                     | 4.658          |
|      | -                         | -0.893         | -1.158                  | -1.181             | -1.208             | -1.167             | -1.179               | 0.217          | -0.942                    | 1.327          |
|      | 16.554                    |                |                         |                    |                    |                    |                      |                |                           |                |
|      | -                         | -2.733         | -2.042                  | -1.986             | -2.004             | -2.010             | -2.011               | -3.032         | -2.318                    | -3.332         |
| LuTm | 16.912                    |                |                         |                    |                    |                    |                      |                |                           |                |
|      | 0                         |                | 0                       | 0                  | 0                  | 0                  | 0                    |                | 0                         |                |
|      | 10.449                    | 10.444         | 10.419                  | 10.377             | 10.421             | 10.421             | 10.410               | 10.416         | 10.392                    | 10.388         |
|      | 3.960                     | 6.025          | 3.987                   | 4.076              | 4.020              | 3.994              | 4.020                | 6.039          | 4.052                     | 6.053          |
|      | 1.440                     | 2.436          | 1.440                   | 1.510              | 1.482              | 1.453              | 1.472                | 2.436          | 1.509                     | 2.436          |
| LuV  | -2.521                    | -3.589         | -2.547                  | -2.566             | -2.538             | -2.541             | -2.548               | -3.603         | -2.543                    | -3.617         |
|      | 8.125                     |                | 13.093                  | 13.066             | 35.598             | 35.627             | 24.346               |                | 32.056                    |                |
|      | 9.581                     | 9.538          | 9.827                   | 9.729              | 9.884              | 9.802              | 9.811                | 9.812          | 10.133                    | 10.086         |
|      | 0                         | 3.308          | 0                       | 0                  | 0                  | 0                  | 0                    | 4.227          | 0                         | 5.147          |
|      | 1.592                     | 2.395          | 1.542                   | 1.449              | 1.425              | 1.440              | 1.464                | 2.409          | 1.283                     | 2.422          |

Table A.1 Continued

| XY   | $(X_{0.25}Y_{0.75})_2O_3$ |                | $(X_{0.5}Y_{0.5})_2O_3$ |                    |                    |                    |                      |                | $(X_{0.75}Y_{0.25})_2O_3$ |                |
|------|---------------------------|----------------|-------------------------|--------------------|--------------------|--------------------|----------------------|----------------|---------------------------|----------------|
|      | PBE                       | interp.<br>HSE | PBE <sup>1st</sup>      | PBE <sup>2nd</sup> | PBE <sup>3rd</sup> | PBE <sup>4th</sup> | PBE <sup>aver.</sup> | interp.<br>HSE | PBE                       | interp.<br>HSE |
|      | 1.606<br>16.323           | -0.904         | 1.584<br>29.281         | 1.476<br>30.651    | 1.435<br>30.737    | 1.503<br>30.275    | 1.500<br>30.236      | -1.813         | 1.289<br>25.683           | -2.722         |
| LuY  | 10.625                    | 10.619         | 10.535                  | 10.531             | 10.532             | 10.537             | 10.534               | 10.533         | 10.447                    | 10.447         |
|      | 0                         | 6.016          | 3.929                   | 4.029              | 4.052              | 3.980              | 3.998                | 6.033          | 4.081                     | 6.050          |
|      | -9.843                    | 2.562          | 1.503                   | 1.608              | 1.647              | 1.559              | 1.580                | 2.520          | 1.637                     | 2.478          |
|      | -                         | -3.454         | -2.426                  | -2.421             | -2.405             | -2.422             | -2.419               | -3.513         | -2.444                    | -3.572         |
|      | 13.697                    |                |                         |                    |                    |                    |                      |                |                           |                |
|      | 0                         |                | 0                       | 0                  | 0                  | 0                  | 0                    |                | 0                         |                |
| LuYb | 10.612                    | 10.606         | 10.528                  | 10.528             | 10.529             | 10.528             | 10.529               | 10.524         | 10.442                    | 10.442         |
|      | 0                         | 6.046          | 4.424                   | 4.540              | 4.583              | 4.483              | 4.508                | 6.053          | 4.361                     | 6.060          |
|      | -4.441                    | 2.327          | 1.434                   | 1.520              | 1.560              | 1.477              | 1.498                | 2.363          | 1.622                     | 2.400          |
|      | -8.383                    | -3.719         | -2.99                   | -3.020             | -3.023             | -3.007             | -3.010               | -3.690         | -2.740                    | -3.661         |
|      | 0                         |                | 1.272                   | 1.416              | 1.543              | 1.317              | 1.387                |                | 1.286                     |                |
| MnPm | 10.596                    | 10.562         | 10.120                  | 9.777              | 9.822              | 10.147             | 9.967                | 10.053         | 9.868                     | 9.544          |
|      | 0                         | 4.811          | 0                       | 0                  | 0.004              | 0.025              | 0.008                | 3.950          | 0                         | 3.088          |
|      | 0.358                     | 2.170          | 0.708                   | 0.646              | 0.730              | 0.630              | 0.679                | 1.874          | 0.845                     | 1.577          |
|      | 0.380                     | -2.641         | 0.766                   | 0.691              | 0.726              | 0.606              | 0.698                | -2.076         | 0.853                     | -1.511         |
|      | 1.124                     |                | 10.329                  | 13.404             | 13.907             | 13.539             | 12.795               |                | 17.292                    |                |
| MnPr | 10.747                    | 10.644         | 10.237                  | 9.933              | 9.952              | 10.280             | 10.101               | 10.107         | 9.964                     | 9.571          |
|      | 0                         | 4.781          | 0                       | 0                  | 0                  | 0                  | 0                    | 3.929          | 0                         | 3.078          |
|      | 0.396                     | 2.173          | 0.712                   | 0.670              | 0.691              | 0.676              | 0.688                | 1.876          | 0.838                     | 1.578          |
|      | 0.418                     | -2.608         | 0.745                   | 0.690              | 0.695              | 0.710              | 0.710                | -2.054         | 0.856                     | -1.500         |
|      | 1.662                     |                | 8.417                   | 11.806             | 12.208             | 14.206             | 11.660               |                | 17.605                    | 0              |
| MnSc | 9.739                     | 9.695          | 9.477                   | 9.461              | 9.460              | 9.477              | 9.469                | 9.475          | 9.274                     | 9.255          |
|      | 0                         | 5.210          | 0                       | 0.006              | 0                  | 0                  | 0.002                | 4.216          | 0                         | 3.221          |
|      | 0.483                     | 2.669          | 0.600                   | 0.649              | 0.661              | 0.620              | 0.633                | 2.206          | 0.514                     | 1.743          |
|      | 0.513                     | -2.542         | 0.603                   | 0.644              | 0.684              | 0.638              | 0.643                | -2.010         | 0.531                     | -1.478         |
|      | 4.239                     |                | 13.459                  | 13.899             | 13.633             | 13.735             | 13.682               |                | 25.538                    |                |
| MnSm | 10.531                    | 10.509         | 10.027                  | 9.746              | 9.799              | 10.106             | 9.920                | 10.017         | 9.856                     | 9.526          |
|      | 0                         | 4.829          | 0                       | 0                  | 0                  | 0.028              | 0.007                | 3.962          | 0                         | 3.094          |
|      | -                         | 2.163          | 0.583                   | 0.644              | 0.724              | 0.632              | 0.646                | 1.869          | 0.852                     | 1.575          |
|      | 13.088                    |                |                         |                    |                    |                    |                      |                |                           |                |
|      | -                         | -2.667         | 0.597                   | 0.688              | 0.732              | 0.605              | 0.656                | -2.093         | 0.863                     | -1.520         |
|      | 13.088                    |                |                         |                    |                    |                    |                      |                |                           |                |
|      | 0                         |                | 10.437                  | 13.798             | 14.116             | 13.821             | 13.043               |                | 20.059                    |                |
| MnTb | 10.357                    | 10.315         | 9.897                   | 9.683              | 9.705              | 10.091             | 9.844                | 9.888          | 9.469                     | 9.461          |

Table A.1 Continued

| XY   | $(X_{0.25}Y_{0.75})_2O_3$ |                | $(X_{0.5}Y_{0.5})_2O_3$ |                    |                    |                    |                      |                | $(X_{0.75}Y_{0.25})_2O_3$ |                |
|------|---------------------------|----------------|-------------------------|--------------------|--------------------|--------------------|----------------------|----------------|---------------------------|----------------|
|      | PBE                       | interp.<br>HSE | PBE <sup>1st</sup>      | PBE <sup>2nd</sup> | PBE <sup>3rd</sup> | PBE <sup>4th</sup> | PBE <sup>aver.</sup> | interp.<br>HSE | PBE                       | interp.<br>HSE |
|      | 0                         | 4.952          | 0                       | 0                  | 0                  | 0                  | 0                    | 4.044          | 0                         | 3.135          |
|      | 0.285                     | 2.183          | 0.576                   | 0.627              | 0.688              | 0.703              | 0.649                | 1.883          | 0.543                     | 1.582          |
|      | 0.312                     | -2.769         | 0.598                   | 0.675              | 0.695              | 0.710              | 0.670                | -2.161         | 0.560                     | -1.554         |
|      | 2.332                     |                | 9.905                   | 14.892             | 14.445             | 15.757             | 13.750               |                | 11.544                    |                |
| MnTl | 10.368                    | 10.333         | 11.276                  | 10.338             | 11.49              | 12.031             | 11.284               | 9.900          | 10.494                    | 9.467          |
|      | 0                         | 0.880          | 0                       | 0                  | 0.027              | 0                  | 0.007                | 1.329          | 0                         | 1.778          |
|      | 0.178                     | -1.182         | 0.833                   | 0.702              | 0.914              | 0.858              | 0.827                | -0.361         | 0.784                     | 0.460          |
|      | 0.290                     | -2.062         | 0.851                   | 0.723              | 0.888              | 0.884              | 0.837                | -1.690         | 0.850                     | -1.318         |
|      | 15.852                    |                | 27.659                  | 24.243             | 28.419             | 27.787             | 27.027               |                | 25.971                    |                |
| MnTm | 10.164                    | 10.113         | 9.762                   | 9.615              | 9.635              | 9.810              | 9.706                | 9.753          | 9.398                     | 9.394          |
|      | 0                         | 5.065          | 0                       | 0                  | 0                  | 0                  | 0                    | 4.119          | 0                         | 3.173          |
|      | 0.205                     | 2.148          | 0.585                   | 0.627              | 0.673              | 0.662              | 0.637                | 1.859          | 0.551                     | 1.570          |
|      | 0.232                     | -2.918         | 0.605                   | 0.669              | 0.681              | 0.699              | 0.664                | -2.261         | 0.551                     | -1.604         |
|      | 2.800                     |                | 11.537                  | 12.655             | 12.252             | 11.993             | 12.109               |                | 23.858                    |                |
| MnV  | 9.204                     | 9.206          | 9.145                   | 9.166              | 9.151              | 9.133              | 9.149                | 9.149          | 9.105                     | 9.092          |
|      | 0                         | 2.348          | 0                       | 0                  | 0                  | 0                  | 0                    | 2.307          | 0                         | 2.267          |
|      | 1.202                     | 2.107          | 0.889                   | 0.849              | 0.770              | 0.850              | 0.840                | 1.831          | 0.609                     | 1.556          |
|      | 1.261                     | -0.232         | 0.937                   | 0.851              | 0.791              | 0.863              | 0.861                | -0.470         | 0.662                     | -0.708         |
|      | 7.253                     |                | 17.153                  | 18.084             | 18.087             | 18.344             | 17.917               |                | 28.725                    |                |
| MnY  | 10.359                    | 10.288         | 9.878                   | 9.813              | 9.702              | 9.942              | 9.834                | 9.870          | 9.453                     | 9.452          |
|      | 0                         | 5.056          | 0                       | 0                  | 0                  | 0.001              | 0.001                | 4.113          | 0                         | 3.170          |
|      | 0.274                     | 2.274          | 0.578                   | 0.667              | 0.687              | 0.705              | 0.66                 | 1.943          | 0.551                     | 1.612          |
|      | 0.310                     | -2.783         | 0.597                   | 0.683              | 0.688              | 0.704              | 0.668                | -2.171         | 0.590                     | -1.559         |
|      | 2.816                     |                | 10.269                  | 13.755             | 13.951             | 12.784             | 12.690               |                | 13.073                    |                |
| MnYb | 10.038                    | 10.274         | 9.750                   | 9.564              | 9.545              | 9.796              | 9.664                | 9.861          | 9.719                     | 9.448          |
|      | 0                         | 5.086          | 0                       | 0                  | 0.009              | 0                  | 0.003                | 4.133          | 0                         | 3.180          |
|      | -0.622                    | 2.038          | 0.469                   | 0.401              | 0.496              | 0.421              | 0.447                | 1.786          | 0.799                     | 1.533          |
|      | -0.473                    | -3.048         | 0.504                   | 0.450              | 0.488              | 0.430              | 0.468                | -2.347         | 0.837                     | -1.647         |
|      | 21.706                    |                | 35.511                  | 36.583             | 36.399             | 36.139             | 36.158               |                | 38.624                    |                |
| PmPr | 11.233                    | 11.153         | 11.181                  | 11.179             | 11.177             | 11.181             | 11.180               | 11.126         | 11.123                    | 11.099         |
|      | 3.637                     | 5.642          | 3.667                   | 3.702              | 3.718              | 3.682              | 3.693                | 5.652          | 3.776                     | 5.662          |
|      | 1.417                     | 2.470          | 1.444                   | 1.479              | 1.497              | 1.458              | 1.470                | 2.469          | 1.544                     | 2.468          |
|      | -2.221                    | -3.173         | -2.223                  | -2.223             | -2.221             | -2.224             | -2.223               | -3.184         | -2.233                    | -3.195         |
|      | 0                         |                | 0                       | 0                  | 0                  | 0                  | 0                    |                | 0                         | 0              |
| PmSc | 10.217                    | 10.204         | 10.489                  | 10.492             | 10.510             | 10.477             | 10.492               | 10.493         | 10.786                    | 10.782         |
|      | 3.418                     | 6.072          | 3.675                   | 3.785              | 3.665              | 3.812              | 3.735                | 5.939          | 3.247                     | 5.806          |

Table A.1 Continued

| XY   | $(X_{0.25}Y_{0.75})_2O_3$ |                | $(X_{0.5}Y_{0.5})_2O_3$ |                    |                    |                    |                      |                | $(X_{0.75}Y_{0.25})_2O_3$ |                |
|------|---------------------------|----------------|-------------------------|--------------------|--------------------|--------------------|----------------------|----------------|---------------------------|----------------|
|      | PBE                       | interp.<br>HSE | PBE <sup>1st</sup>      | PBE <sup>2nd</sup> | PBE <sup>3rd</sup> | PBE <sup>4th</sup> | PBE <sup>aver.</sup> | interp.<br>HSE | PBE                       | interp.<br>HSE |
|      | 1.719                     | 2.965          | 1.869                   | 1.889              | 1.813              | 1.922              | 1.874                | 2.799          | 1.274                     | 2.633          |
|      | -1.699                    | -3.107         | -1.806                  | -1.896             | -1.852             | -1.891             | -1.862               | -3.140         | -1.974                    | -3.173         |
|      | 12.497                    |                | 24.678                  | 25.026             | 24.795             | 24.901             | 24.85                |                | 26.933                    |                |
| PmSm | 11.017                    | 11.018         | 11.039                  | 11.034             | 11.036             | 11.036             | 11.037               | 11.036         | 11.057                    | 11.054         |
|      | 3.803                     | 5.691          | 3.792                   | 3.787              | 3.778              | 3.789              | 3.787                | 5.685          | 3.760                     | 5.679          |
|      | 1.530                     | 2.459          | 1.523                   | 1.513              | 1.504              | 1.518              | 1.515                | 2.462          | 1.492                     | 2.464          |
|      | -2.274                    | -3.232         | -2.269                  | -2.275             | -2.275             | -2.272             | -2.273               | -3.223         | -2.269                    | -3.215         |
|      | 29.924                    |                | 43.061                  | 43.117             | 43.141             | 43.092             | 43.103               |                | 5.316                     |                |
| PmTb | 10.829                    | 10.824         | 10.908                  | 10.911             | 10.91              | 10.907             | 10.909               | 10.906         | 10.992                    | 10.989         |
|      | 3.894                     | 5.813          | 3.843                   | 3.805              | 3.779              | 3.827              | 3.814                | 5.766          | 3.683                     | 5.719          |
|      | 1.583                     | 2.480          | 1.558                   | 1.503              | 1.473              | 1.533              | 1.517                | 2.476          | 1.393                     | 2.471          |
|      | -2.312                    | -3.334         | -2.285                  | -2.302             | -2.306             | -2.295             | -2.297               | -3.291         | -2.290                    | -3.249         |
|      | 0                         |                | 0                       | 0                  | 0                  | 0                  | 0                    |                | 0                         |                |
| PmTl | 10.890                    | 10.843         | 10.942                  | 10.956             | 10.948             | 10.934             | 10.945               | 10.919         | 11.020                    | 10.995         |
|      | 0.356                     | 1.742          | 0.813                   | 0.878              | 0.878              | 0.854              | 0.856                | 3.052          | 1.161                     | 4.362          |
|      | -1.383                    | -0.885         | -1.066                  | -0.972             | -0.987             | -1.004             | -1.008               | 0.233          | -0.990                    | 1.350          |
|      | -1.739                    | -2.627         | -1.878                  | -1.850             | -1.865             | -1.858             | -1.863               | -2.820         | -2.150                    | -3.013         |
|      | 0                         |                | 0                       | 0                  | 0                  | 0                  | 0                    |                | 0                         |                |
| PmTm | 10.626                    | 10.622         | 10.773                  | 10.688             | 10.775             | 10.770             | 10.752               | 10.772         | 10.920                    | 10.922         |
|      | 3.915                     | 5.927          | 3.835                   | 3.862              | 3.709              | 3.816              | 3.806                | 5.842          | 3.500                     | 5.757          |
|      | 1.579                     | 2.444          | 1.555                   | 1.512              | 1.392              | 1.516              | 1.494                | 2.452          | 1.211                     | 2.459          |
|      | -2.336                    | -3.483         | -2.281                  | -2.351             | -2.318             | -2.300             | -2.313               | -3.391         | -2.290                    | -3.298         |
|      | 13.862                    |                | 25.700                  | 26.151             | 25.866             | 25.816             | 25.883               |                | 27.872                    |                |
| PmV  | 9.896                     | 9.715          | 10.093                  | 10.332             | 10.200             | 10.046             | 10.168               | 10.167         | 10.574                    | 10.619         |
|      | 0                         | 3.209          | 0                       | 0                  | 0                  | 0                  | 0                    | 4.03           | 0.011                     | 4.851          |
|      | 1.505                     | 2.403          | 1.509                   | 1.155              | 1.396              | 1.369              | 1.358                | 2.424          | 1.231                     | 2.446          |
|      | 1.550                     | -0.797         | 1.525                   | 1.175              | 1.415              | 1.400              | 1.379                | -1.600         | 1.220                     | -2.403         |
|      | 10.503                    |                | 22.159                  | 23.337             | 21.990             | 22.493             | 22.495               |                | 23.131                    |                |
| PmY  | 10.799                    | 10.797         | 10.888                  | 10.891             | 10.890             | 10.886             | 10.889               | 10.888         | 10.979                    | 10.980         |
|      | 3.997                     | 5.918          | 3.899                   | 3.849              | 3.819              | 3.877              | 3.861                | 5.836          | 3.699                     | 5.754          |
|      | 1.726                     | 2.570          | 1.644                   | 1.579              | 1.548              | 1.613              | 1.596                | 2.536          | 1.428                     | 2.501          |
|      | -2.271                    | -3.348         | -2.256                  | -2.270             | -2.272             | -2.265             | -2.266               | -3.301         | -2.272                    | -3.253         |
|      | 0                         |                | 0                       | 0                  | 0                  | 0                  | 0                    |                | 0                         | 0              |
| PmYb | 10.806                    | 10.783         | 10.910                  | 10.907             | 10.904             | 10.910             | 10.908               | 10.879         | 10.994                    | 10.975         |
|      | 3.990                     | 5.947          | 4.296                   | 4.236              | 4.239              | 4.252              | 4.256                | 5.856          | 4.013                     | 5.764          |
|      | 1.580                     | 2.335          | 1.608                   | 1.538              | 1.539              | 1.562              | 1.562                | 2.379          | 1.523                     | 2.423          |

Table A.1 Continued

| XY   | $(X_{0.25}Y_{0.75})_2O_3$                    |                                     | $(X_{0.5}Y_{0.5})_2O_3$                      |  |  |  |  |                                    | $(X_{0.75}Y_{0.25})_2O_3$                    |                                    |
|------|--|-------------------------------------|--|--|--|--|--|------------------------------------|--|------------------------------------|
|      | PBE  | interp.<br>HSE                      | PBE <sup>1st</sup>                           | PBE <sup>2nd</sup>                           | PBE <sup>3rd</sup>                           | PBE <sup>4th</sup>                           | PBE <sup>aver.</sup>                         | interp.<br>HSE                     | PBE  | interp.<br>HSE                     |
|      | -2.410<br>34.868                             | -3.613                              | -2.689<br>1.745                              | -2.699<br>1.881                              | -2.701<br>2.014                              | -2.691<br>1.793                              | -2.695<br>1.858                              | -3.477                             | -2.490<br>2.247                              | -3.342                             |
| PrSc | 10.278<br>3.336<br>1.698<br>-1.639<br>10.833 | 10.232<br>6.062<br>2.966<br>-3.096  | 10.584<br>3.615<br>1.883<br>-1.732<br>22.632 | 10.592<br>3.684<br>1.825<br>-1.860<br>23.005 | 10.624<br>3.485<br>1.691<br>-1.794<br>22.627 | 10.569<br>3.762<br>1.905<br>-1.858<br>22.880 | 10.593<br>3.637<br>1.826<br>-1.811<br>22.786 | 10.548<br>5.919<br>2.801<br>-3.118 | 10.946<br>2.958<br>1.039<br>-1.920<br>25.034 | 10.864<br>5.775<br>2.636<br>-3.140 |
| PrSm | 11.07<br>3.784<br>1.546<br>-2.238<br>25.854  | 11.045<br>5.681<br>2.460<br>-3.221  | 11.145<br>3.734<br>1.517<br>-2.218<br>37.367 | 11.146<br>3.697<br>1.470<br>-2.228<br>37.582 | 11.141<br>3.681<br>1.449<br>-2.232<br>37.58  | 11.142<br>3.715<br>1.492<br>-2.224<br>37.492 | 11.144<br>3.707<br>1.482<br>-2.226<br>37.506 | 11.090<br>5.665<br>2.464<br>-3.201 | 11.217<br>3.601<br>1.379<br>-2.222<br>28.623 | 11.135<br>5.648<br>2.467<br>-3.182 |
| PrTb | 10.881<br>3.829<br>1.574<br>-2.255<br>0      | 10.851<br>5.803<br>2.481<br>-3.323  | 11.015<br>3.751<br>1.532<br>-2.219<br>0      | 11.017<br>3.694<br>1.453<br>-2.241<br>0      | 11.018<br>3.640<br>1.401<br>-2.240<br>0      | 11.011<br>3.732<br>1.498<br>-2.234<br>0      | 11.016<br>3.705<br>1.471<br>-2.234<br>0      | 10.961<br>5.746<br>2.478<br>-3.269 | 11.154<br>3.474<br>1.251<br>-2.224<br>0      | 11.071<br>5.689<br>2.474<br>-3.216 |
| PrTl | 10.949<br>0.303<br>-1.387<br>-1.689<br>0     | 10.870<br>1.732<br>-0.884<br>-2.616 | 11.049<br>0.777<br>-1.058<br>-1.835<br>0     | 11.074<br>0.881<br>-0.939<br>-1.820<br>0     | 11.067<br>0.878<br>-0.952<br>-1.83<br>0      | 11.048<br>0.833<br>-0.984<br>-1.817<br>0     | 11.060<br>0.843<br>-0.984<br>-1.826<br>0     | 10.973<br>3.032<br>0.235<br>-2.798 | 11.185<br>1.066<br>-1.007<br>-2.072<br>0     | 11.077<br>4.332<br>1.353<br>-2.980 |
| PrTm | 10.681<br>3.815<br>1.553<br>-2.263<br>12.351 | 10.649<br>5.917<br>2.445<br>-3.472  | 10.781<br>3.831<br>1.591<br>-2.240<br>23.942 | 10.785<br>3.742<br>1.467<br>-2.275<br>24.222 | 10.885<br>3.548<br>1.316<br>-2.233<br>23.919 | 10.870<br>3.714<br>1.487<br>-2.228<br>23.902 | 10.831<br>3.709<br>1.466<br>-2.244<br>23.996 | 10.826<br>5.822<br>2.454<br>-3.369 | 11.088<br>3.254<br>1.040<br>-2.214<br>26.220 | 11.003<br>5.727<br>2.462<br>-3.265 |
| PrV  | 10.031<br>0<br>1.488<br>1.521<br>9.815       | 9.743<br>3.199<br>2.404<br>-0.786   | 10.06<br>0<br>1.461<br>1.466<br>21.048       | 10.206<br>0.001<br>1.386<br>1.386<br>21.296  | 10.292<br>0<br>1.369<br>1.381<br>20.226      | 10.240<br>0<br>1.425<br>1.446<br>20.962      | 10.200<br>0.001<br>1.411<br>1.420<br>20.883  | 10.222<br>4.010<br>2.426<br>-1.578 | 10.710<br>0<br>1.131<br>1.131<br>21.864      | 10.701<br>4.821<br>2.449<br>-2.370 |
| PrY  | 10.847<br>3.932<br>1.722<br>-2.211           | 10.824<br>5.907<br>2.571<br>-3.337  | 10.997<br>3.796<br>1.609<br>-2.187           | 10.998<br>3.724<br>1.517<br>-2.208           | 10.999<br>3.670<br>1.464<br>-2.206           | 10.991<br>3.771<br>1.567<br>-2.204           | 10.997<br>3.741<br>1.540<br>-2.202           | 10.943<br>5.816<br>2.538<br>-3.278 | 11.143<br>3.479<br>1.274<br>-2.206           | 11.062<br>5.724<br>2.504<br>-3.220 |

Table A.1 Continued

| XY   | $(X_{0.25}Y_{0.75})_2O_3$ |                | $(X_{0.5}Y_{0.5})_2O_3$ |                    |                    |                    |                      |                | $(X_{0.75}Y_{0.25})_2O_3$ |                |
|------|---------------------------|----------------|-------------------------|--------------------|--------------------|--------------------|----------------------|----------------|---------------------------|----------------|
|      | PBE                       | interp.<br>HSE | PBE <sup>1st</sup>      | PBE <sup>2nd</sup> | PBE <sup>3rd</sup> | PBE <sup>4th</sup> | PBE <sup>aver.</sup> | interp.<br>HSE | PBE                       | interp.<br>HSE |
|      | 0                         |                | 0                       | 0                  | 0                  | 0                  | 0                    |                | 0                         |                |
| PrYb | 10.865                    | 10.811         | 11.02                   | 11.017             | 11.013             | 11.014             | 11.016               | 10.934         | 11.168                    | 11.057         |
|      | 4.040                     | 5.937          | 4.199                   | 4.096              | 4.091              | 4.139              | 4.132                | 5.835          | 3.817                     | 5.734          |
|      | 1.563                     | 2.336          | 1.592                   | 1.486              | 1.472              | 1.532              | 1.521                | 2.381          | 1.401                     | 2.426          |
|      | -2.478                    | -3.602         | -2.607                  | -2.610             | -2.620             | -2.607             | -2.611               | -3.455         | -2.417                    | -3.309         |
|      | 27.104                    |                | 38.771                  | 37.020             | 38.317             | 36.047             | 37.539               |                | 26.634                    | 0              |
| ScSm | 10.731                    | 10.729         | 10.471                  | 10.426             | 10.426             | 10.462             | 10.447               | 10.458         | 10.199                    | 10.187         |
|      | 3.337                     | 5.824          | 3.532                   | 3.818              | 3.829              | 3.725              | 3.726                | 5.951          | 3.449                     | 6.078          |
|      | 1.348                     | 2.626          | 1.747                   | 1.909              | 1.928              | 1.852              | 1.859                | 2.794          | 1.727                     | 2.963          |
|      | -1.989                    | -3.199         | -1.785                  | -1.910             | -1.902             | -1.874             | -1.868               | -3.157         | -1.722                    | -3.116         |
|      | 0                         |                | 0                       | 0                  | 0                  | 0                  | 0                    |                | 0                         |                |
| ScTb | 10.542                    | 10.535         | 10.339                  | 10.316             | 10.318             | 10.337             | 10.328               | 10.328         | 10.126                    | 10.122         |
|      | 3.653                     | 5.947          | 3.839                   | 3.958              | 3.925              | 3.945              | 3.917                | 6.033          | 3.561                     | 6.119          |
|      | 1.598                     | 2.646          | 1.955                   | 1.997              | 1.975              | 2.003              | 1.983                | 2.808          | 1.759                     | 2.969          |
|      | -2.056                    | -3.301         | -1.885                  | -1.961             | -1.951             | -1.943             | -1.935               | -3.225         | -1.802                    | -3.150         |
|      | 0                         |                | 0                       | 0                  | 0                  | 0                  | 0                    |                | 0                         |                |
| ScTl | 10.564                    | 10.554         | 10.356                  | 10.331             | 10.334             | 10.336             | 10.340               | 10.341         | 10.129                    | 10.128         |
|      | 0.514                     | 1.875          | 1.108                   | 0.967              | 0.935              | 1.045              | 1.014                | 3.318          | 1.616                     | 4.762          |
|      | -0.888                    | -0.719         | -0.360                  | -0.445             | -0.496             | -0.404             | -0.427               | 0.565          | -0.034                    | 1.848          |
|      | -1.402                    | -2.594         | -1.467                  | -1.412             | -1.431             | -1.448             | -1.440               | -2.754         | -1.65                     | -2.914         |
|      | 0                         |                | 0                       | 0                  | 0                  | 0                  | 0                    |                | 0                         |                |
| ScTm | 10.339                    | 10.333         | 10.201                  | 10.143             | 10.191             | 10.201             | 10.184               | 10.194         | 10.060                    | 10.055         |
|      | 3.946                     | 6.060          | 4.087                   | 2.790              | 4.039              | 4.128              | 3.761                | 6.108          | 3.676                     | 6.156          |
|      | 1.825                     | 2.610          | 2.148                   | 1.331              | 2.044              | 2.153              | 1.919                | 2.784          | 1.802                     | 2.958          |
|      | -2.121                    | -3.450         | -1.939                  | -1.460             | -1.995             | -1.976             | -1.843               | -3.325         | -1.875                    | -3.199         |
|      | 28.311                    |                | 37.053                  | 0                  | 36.956             | 37.541             | 27.888               |                | 23.230                    |                |
| ScV  | 9.456                     | 9.426          | 9.605                   | 9.619              | 9.638              | 9.622              | 9.621                | 9.589          | 9.781                     | 9.752          |
|      | 0                         | 3.342          | 0                       | 0                  | 0                  | 0.006              | 0.002                | 4.296          | 0                         | 5.251          |
|      | 1.542                     | 2.569          | 1.575                   | 1.486              | 1.385              | 1.43               | 1.469                | 2.756          | 1.475                     | 2.944          |
|      | 1.564                     | -0.764         | 1.660                   | 1.529              | 1.405              | 1.425              | 1.505                | -1.534         | 1.496                     | -2.304         |
|      | 0                         |                | 0                       | 0                  | 0                  | 0                  | 0                    |                | 0                         |                |
| ScY  | 10.512                    | 10.508         | 10.315                  | 10.297             | 10.300             | 10.315             | 10.307               | 10.310         | 10.114                    | 10.113         |
|      | 3.758                     | 6.051          | 3.938                   | 4.013              | 3.956              | 4.018              | 3.982                | 6.102          | 3.589                     | 6.153          |
|      | 1.708                     | 2.736          | 2.024                   | 2.039              | 1.998              | 2.065              | 2.032                | 2.868          | 1.777                     | 3.000          |
|      | -2.050                    | -3.315         | -1.914                  | -1.974             | -1.958             | -1.954             | -1.950               | -3.235         | -1.812                    | -3.154         |
|      | 0                         |                | 0                       | 0                  | 0                  | 0                  | 0                    |                | 0                         |                |

Table A.1 Continued

| XY   | $(X_{0.25}Y_{0.75})_2O_3$ |                | $(X_{0.5}Y_{0.5})_2O_3$ |                    |                    |                    |                      |                | $(X_{0.75}Y_{0.25})_2O_3$ |                |
|------|---------------------------|----------------|-------------------------|--------------------|--------------------|--------------------|----------------------|----------------|---------------------------|----------------|
|      | PBE                       | interp.<br>HSE | PBE <sup>1st</sup>      | PBE <sup>2nd</sup> | PBE <sup>3rd</sup> | PBE <sup>4th</sup> | PBE <sup>aver.</sup> | interp.<br>HSE | PBE                       | interp.<br>HSE |
| ScYb | 10.466                    | 10.494         | 10.275                  | 10.267             | 10.267             | 10.275             | 10.271               | 10.301         | 10.085                    | 10.108         |
|      | 4.581                     | 6.080          | 4.487                   | 4.676              | 4.691              | 4.616              | 4.618                | 6.122          | 3.702                     | 6.163          |
|      | 1.912                     | 2.501          | 2.275                   | 2.378              | 2.387              | 2.348              | 2.347                | 2.711          | 1.741                     | 2.921          |
|      | -2.670                    | -3.580         | -2.213                  | -2.298             | -2.304             | -2.269             | -2.271               | -3.411         | -1.961                    | -3.243         |
|      | 0.099                     |                | 0.090                   | 0.102              | 0.108              | 0.093              | 0.098                |                | 0.051                     |                |
| SmTb | 10.808                    | 10.806         | 10.872                  | 10.875             | 10.875             | 10.872             | 10.874               | 10.871         | 10.940                    | 10.936         |
|      | 3.910                     | 5.820          | 3.854                   | 3.829              | 3.809              | 3.840              | 3.833                | 5.779          | 3.736                     | 5.738          |
|      | 1.578                     | 2.478          | 1.547                   | 1.507              | 1.484              | 1.525              | 1.516                | 2.471          | 1.423                     | 2.464          |
|      | -2.333                    | -3.343         | -2.308                  | -2.323             | -2.326             | -2.315             | -2.318               | -3.309         | -2.314                    | -3.275         |
|      | 0                         |                | 0                       | 0                  | 0                  | 0                  | 0                    |                | 0                         |                |
| SmTl | 10.869                    | 10.825         | 10.907                  | 10.917             | 10.909             | 10.898             | 10.908               | 10.883         | 10.962                    | 10.942         |
|      | 0.369                     | 1.748          | 0.819                   | 0.869              | 0.869              | 0.852              | 0.853                | 3.064          | 1.187                     | 4.381          |
|      | -1.389                    | -0.888         | -1.076                  | -0.993             | -1.008             | -1.021             | -1.025               | 0.228          | -0.985                    | 1.342          |
|      | -1.757                    | -2.635         | -1.894                  | -1.862             | -1.877             | -1.872             | -1.877               | -2.837         | -2.172                    | -3.039         |
|      | 0                         |                | 0                       | 0                  | 0                  | 0                  | 0                    |                | 0                         |                |
| SmTm | 10.604                    | 10.604         | 10.655                  | 10.653             | 10.740             | 10.733             | 10.696               | 10.736         | 10.870                    | 10.868         |
|      | 3.930                     | 5.933          | 3.961                   | 3.895              | 3.752              | 3.843              | 3.863                | 5.854          | 3.578                     | 5.776          |
|      | 1.571                     | 2.442          | 1.614                   | 1.517              | 1.406              | 1.514              | 1.513                | 2.447          | 1.260                     | 2.452          |
|      | -2.360                    | -3.492         | -2.347                  | -2.378             | -2.346             | -2.329             | -2.350               | -3.408         | -2.319                    | -3.324         |
|      | 17.185                    |                | 30.119                  | 30.295             | 29.955             | 29.891             | 30.065               |                | 29.700                    |                |
| SmV  | 9.847                     | 9.698          | 10.069                  | 10.212             | 10.170             | 10.020             | 10.118               | 10.132         | 10.536                    | 10.566         |
|      | 0                         | 3.215          | 0                       | 0                  | 0                  | 0                  | 0                    | 4.042          | 0.003                     | 4.870          |
|      | 1.527                     | 2.401          | 1.536                   | 1.381              | 1.401              | 1.369              | 1.422                | 2.419          | 1.269                     | 2.438          |
|      | 1.556                     | -0.806         | 1.545                   | 1.406              | 1.420              | 1.406              | 1.445                | -1.618         | 1.267                     | -2.429         |
|      | 12.936                    |                | 25.318                  | 26.101             | 25.321             | 25.903             | 25.661               |                | 23.747                    |                |
| SmY  | 10.778                    | 10.779         | 10.852                  | 10.856             | 10.854             | 10.850             | 10.853               | 10.853         | 10.927                    | 10.927         |
|      | 4.009                     | 5.924          | 3.913                   | 3.876              | 3.855              | 3.900              | 3.886                | 5.848          | 3.761                     | 5.773          |
|      | 1.718                     | 2.568          | 1.635                   | 1.584              | 1.562              | 1.612              | 1.599                | 2.531          | 1.466                     | 2.494          |
|      | -2.292                    | -3.356         | -2.279                  | -2.292             | -2.293             | -2.288             | -2.288               | -3.318         | -2.295                    | -3.279         |
|      | 0                         |                | 0                       | 0                  | 0                  | 0                  | 0                    |                | 0                         |                |
| TmYb | 10.786                    | 10.766         | 10.875                  | 10.873             | 10.864             | 10.872             | 10.871               | 10.844         | 10.941                    | 10.922         |
|      | 3.954                     | 5.953          | 4.312                   | 4.268              | 4.276              | 4.281              | 4.285                | 5.868          | 4.056                     | 5.782          |
|      | 1.573                     | 2.332          | 1.592                   | 1.538              | 1.546              | 1.557              | 1.559                | 2.374          | 1.542                     | 2.415          |
|      | -2.381                    | -3.622         | -2.721                  | -2.730             | -2.730             | -2.724             | -2.727               | -3.495         | -2.514                    | -3.368         |
|      | 0.144                     |                | 1.216                   | 2.003              | 2.781              | 1.501              | 1.875                |                | 4.216                     |                |
| TbTl | 10.793                    | 10.76          | 10.776                  | 10.777             | 10.774             | 10.765             | 10.773               | 10.754         | 10.769                    | 10.748         |



Table A.1 Continued

| XY   | $(X_{0.25}Y_{0.75})_2O_3$ |                | $(X_{0.5}Y_{0.5})_2O_3$ |                    |                    |                    |                      |                | $(X_{0.75}Y_{0.25})_2O_3$ |                |
|------|---------------------------|----------------|-------------------------|--------------------|--------------------|--------------------|----------------------|----------------|---------------------------|----------------|
|      | PBE                       | interp.<br>HSE | PBE <sup>1st</sup>      | PBE <sup>2nd</sup> | PBE <sup>3rd</sup> | PBE <sup>4th</sup> | PBE <sup>aver.</sup> | interp.<br>HSE | PBE                       | interp.<br>HSE |
|      | 0.377                     | 1.789          | 0.860                   | 0.854              | 0.853              | 0.860              | 0.857                | 3.146          | 1.268                     | 4.503          |
|      | -1.421                    | -0.881         | -1.096                  | -1.056             | -1.075             | -1.067             | -1.074               | 0.241          | -0.967                    | 1.363          |
|      | -1.798                    | -2.669         | -1.955                  | -1.909             | -1.928             | -1.926             | -1.930               | -2.905         | -2.234                    | -3.141         |
|      | 0                         |                | 0                       | 0                  | 0                  | 0                  | 0                    |                | 0                         |                |
| TbTm | 10.543                    | 10.540         | 10.610                  | 10.520             | 10.613             | 10.609             | 10.588               | 10.607         | 10.680                    | 10.674         |
|      | 3.996                     | 5.974          | 3.962                   | 4.039              | 3.901              | 3.945              | 3.962                | 5.936          | 3.824                     | 5.898          |
|      | 1.559                     | 2.449          | 1.550                   | 1.567              | 1.465              | 1.524              | 1.527                | 2.460          | 1.405                     | 2.472          |
|      | -2.438                    | -3.526         | -2.412                  | -2.473             | -2.436             | -2.421             | -2.436               | -3.476         | -2.420                    | -3.426         |
|      | 9.380                     |                | 19.835                  | 20.078             | 19.882             | 19.859             | 19.914               |                | 26.962                    |                |
| TbV  | 9.709                     | 9.633          | 9.969                   | 9.903              | 10.047             | 9.926              | 9.962                | 10.002         | 10.396                    | 10.372         |
|      | 0                         | 3.256          | 0                       | 0                  | 0                  | 0                  | 0                    | 4.124          | 0                         | 4.992          |
|      | 1.555                     | 2.407          | 1.490                   | 1.412              | 1.415              | 1.389              | 1.427                | 2.433          | 1.320                     | 2.459          |
|      | 1.558                     | -0.840         | 1.542                   | 1.413              | 1.442              | 1.462              | 1.465                | -1.686         | 1.323                     | -2.531         |
|      | 6.950                     |                | 16.979                  | 17.598             | 17.302             | 17.421             | 17.325               |                | 22.394                    |                |
| TbY  | 10.717                    | 10.714         | 10.725                  | 10.728             | 10.726             | 10.725             | 10.726               | 10.723         | 10.733                    | 10.732         |
|      | 4.025                     | 5.965          | 3.983                   | 3.985              | 3.982              | 3.984              | 3.984                | 5.930          | 3.946                     | 5.895          |
|      | 1.675                     | 2.575          | 1.625                   | 1.626              | 1.627              | 1.625              | 1.626                | 2.545          | 1.581                     | 2.514          |
|      | -2.350                    | -3.390         | -2.358                  | -2.359             | -2.356             | -2.359             | -2.358               | -3.386         | -2.365                    | -3.381         |
|      | 32.703                    |                | 45.977                  | 46.829             | 3.113              | 46.405             | 35.581               |                | 2.515                     |                |
| TbYb | 10.717                    | 10.701         | 10.742                  | 10.737             | 10.734             | 10.735             | 10.737               | 10.714         | 10.741                    | 10.728         |
|      | 4.049                     | 5.994          | 4.390                   | 4.407              | 4.429              | 4.399              | 4.407                | 5.950          | 4.233                     | 5.905          |
|      | 1.549                     | 2.339          | 1.564                   | -1.526             | 1.584              | 1.561              | 0.796                | 2.387          | 1.627                     | 2.436          |
|      | -2.501                    | -3.656         | -2.827                  | -5.932             | -2.846             | -2.838             | -3.611               | -3.563         | -2.607                    | -3.470         |
|      | 9.565                     |                | 16.191                  | 16.309             | 16.451             | 16.230             | 16.295               |                | 16.660                    |                |
| TiTm | 10.558                    | 10.546         | 10.631                  | 10.526             | 10.643             | 10.63              | 10.608               | 10.619         | 10.719                    | 10.693         |
|      | 1.348                     | 4.616          | 0.796                   | 0.915              | 0.844              | 0.814              | 0.843                | 3.221          | 0.367                     | 1.826          |
|      | -0.948                    | 1.327          | -1.183                  | -1.081             | 1.363              | -1.169             | -0.518               | 0.218          | -1.464                    | -0.893         |
|      | -2.296                    | -3.290         | -1.979                  | -1.995             | 1.325              | -1.983             | -1.158               | -3.004         | -1.831                    | -2.719         |
|      | 8.282                     |                | 18.573                  | 18.620             | 18.480             | 18.560             | 18.558               |                | 27.376                    |                |
| TiV  | 10.609                    | 9.639          | 10.821                  | 11.096             | 12.23              | 11.542             | 11.423               | 10.015         | 10.481                    | 10.391         |
|      | 0                         | 1.899          | 1.271                   | 1.673              | 1.351              | 2.156              | 1.613                | 1.410          | 0                         | 0.921          |
|      | 1.319                     | 1.286          | 0.735                   | 1.338              | 1.236              | -0.048             | 0.816                | 0.190          | 0.422                     | -0.907         |
|      | 1.432                     | -0.604         | -0.537                  | -0.335             | -0.114             | -2.203             | -0.798               | -1.214         | 0.648                     | -1.824         |
|      | 14.005                    |                | 30.882                  | 31.554             | 33.159             | 32.632             | 32.057               |                | 29.766                    |                |
| TiY  | 10.735                    | 10.721         | 10.750                  | 10.743             | 10.755             | 10.748             | 10.749               | 10.736         | 10.781                    | 10.751         |
|      | 1.332                     | 4.607          | 0.856                   | 0.889              | 0.898              | 0.884              | 0.882                | 3.215          | 0.400                     | 1.823          |

Table A.1 Continued

| XY   | $(X_{0.25}Y_{0.75})_2O_3$ |                | $(X_{0.5}Y_{0.5})_2O_3$ |                    |                    |                    |                      |                | $(X_{0.75}Y_{0.25})_2O_3$ |                |
|------|---------------------------|----------------|-------------------------|--------------------|--------------------|--------------------|----------------------|----------------|---------------------------|----------------|
|      | PBE                       | interp.<br>HSE | PBE <sup>1st</sup>      | PBE <sup>2nd</sup> | PBE <sup>3rd</sup> | PBE <sup>4th</sup> | PBE <sup>aver.</sup> | interp.<br>HSE | PBE                       | interp.<br>HSE |
|      | -0.849                    | 1.453          | -1.038                  | -0.973             | 1.643              | -0.996             | -0.341               | 0.302          | -1.362                    | -0.851         |
|      | -2.180                    | -3.155         | -1.893                  | -1.862             | -2.396             | -1.879             | -2.008               | -2.914         | -1.761                    | -2.674         |
|      | 21.179                    |                | 32.609                  | 32.047             | 31.769             | 32.486             | 32.228               |                | 25.895                    |                |
| TlYb | 10.669                    | 10.707         | 10.686                  | 10.683             | 10.687             | 10.705             | 10.691               | 10.727         | 10.728                    | 10.747         |
|      | 2.247                     | 4.634          | 1.280                   | 1.377              | 1.383              | 1.343              | 1.346                | 3.235          | 0.458                     | 1.833          |
|      | -0.839                    | 1.217          | -1.273                  | -1.137             | -1.147             | -1.201             | -1.190               | 0.144          | -1.626                    | -0.930         |
|      | -3.086                    | -3.420         | -2.553                  | -2.514             | -2.530             | -2.543             | -2.535               | -3.091         | -2.084                    | -2.762         |
|      | 11.023                    |                | 19.303                  | 19.389             | 19.311             | 19.359             | 19.340               |                | 20.228                    |                |
| TmV  | 9.622                     | 9.566          | 9.881                   | 9.772              | 9.927              | 9.837              | 9.855                | 9.868          | 10.209                    | 10.170         |
|      | 0                         | 3.294          | 0                       | 0                  | 0.038              | 0                  | 0.010                | 4.200          | 0                         | 5.105          |
|      | 1.556                     | 2.395          | 1.531                   | 1.539              | -1.140             | 1.422              | 0.838                | 2.409          | 1.297                     | 2.423          |
|      | 1.599                     | -0.890         | 1.565                   | 1.574              | -1.983             | 1.494              | 0.663                | -1.785         | 1.305                     | -2.680         |
|      | 0                         |                | 0                       | 0                  | 0                  | 0                  | 0                    |                | 0                         |                |
| TmY  | 10.643                    | 10.647         | 10.595                  | 10.511             | 10.587             | 10.589             | 10.571               | 10.589         | 10.532                    | 10.531         |
|      | 3.948                     | 6.002          | 3.956                   | 4.054              | 4.038              | 3.992              | 4.010                | 6.005          | 4.040                     | 6.008          |
|      | 1.564                     | 2.563          | 1.543                   | 1.600              | -0.98              | 1.581              | 0.936                | 2.521          | 1.621                     | 2.479          |
|      | -2.384                    | -3.440         | -2.413                  | -2.454             | -1.878             | -2.411             | -2.289               | -3.485         | -2.420                    | -3.530         |
|      | 0                         |                | 0                       | 0.116              | 0                  | 0                  | 0.029                |                | 0                         |                |
| TmYb | 10.642                    | 10.634         | 10.590                  | 10.490             | 10.591             | 10.591             | 10.566               | 10.580         | 10.528                    | 10.526         |
|      | 3.963                     | 6.032          | 4.420                   | 4.545              | 4.545              | 4.456              | 4.492                | 6.025          | 4.332                     | 6.018          |
|      | 1.454                     | 2.327          | 1.477                   | 1.561              | 1.571              | 1.501              | 1.528                | 2.364          | 1.630                     | 2.400          |
|      | -2.509                    | -3.705         | -2.944                  | -2.985             | -2.975             | -2.955             | -2.965               | -3.662         | -2.702                    | -3.619         |
|      | 0.046                     |                | 0.052                   | 0.063              | 0.061              | 0.053              | 0.057                |                | 0.046                     |                |
| VY   | 10.372                    | 10.345         | 10.052                  | 9.877              | 9.902              | 10.059             | 9.973                | 9.984          | 9.693                     | 9.624          |
|      | 0                         | 5.096          | 0                       | 0                  | 0                  | 0                  | 0                    | 4.194          | 0                         | 3.291          |
|      | 1.341                     | 2.549          | 1.461                   | 1.410              | 1.403              | 1.423              | 1.425                | 2.493          | 1.558                     | 2.438          |
|      | 1.346                     | -2.545         | 1.484                   | 1.421              | 1.478              | 1.442              | 1.457                | -1.695         | 1.567                     | -0.845         |
|      | 0                         |                | 0                       | 0                  | 0                  | 0                  | 0                    |                | 0                         |                |
| VYb  | 10.140                    | 10.331         | 9.894                   | 9.848              | 9.743              | 9.881              | 9.842                | 9.975          | 9.612                     | 9.619          |
|      | 0                         | 5.126          | 0                       | 0                  | 0.015              | 0.006              | 0.006                | 4.213          | 0.008                     | 3.300          |
|      | 0.293                     | 2.313          | 1.317                   | 1.203              | 1.246              | 1.207              | 1.244                | 2.336          | 1.476                     | 2.359          |
|      | 0.387                     | -2.810         | 1.356                   | 1.276              | 1.231              | 1.201              | 1.266                | -1.872         | 1.468                     | -0.933         |
|      | 10.666                    |                | 7.064                   | 6.810              | 6.815              | 6.869              | 6.889                |                | 1.352                     |                |
| YYb  | 10.705                    | 10.692         | 10.718                  | 10.712             | 10.712             | 10.717             | 10.715               | 10.696         | 10.711                    | 10.701         |
|      | 4.132                     | 6.029          | 4.478                   | 4.501              | 4.531              | 4.474              | 4.496                | 6.019          | 4.367                     | 6.009          |
|      | 1.634                     | 2.369          | 1.710                   | 1.713              | 1.736              | 1.701              | 1.715                | 2.448          | 1.808                     | 2.526          |

Table A.1 Continued

| XY | $(\mathbf{X}_{0.25}\mathbf{Y}_{0.75})_2\mathbf{O}_3$ |                | $(\mathbf{X}_{0.5}\mathbf{Y}_{0.5})_2\mathbf{O}_3$ |                    |                    |                    |                      |                | $(\mathbf{X}_{0.75}\mathbf{Y}_{0.25})_2\mathbf{O}_3$ |                |
|----|--|----------------|--|--------------------|--------------------|--------------------|----------------------|----------------|--|----------------|
|    | PBE  | interp.<br>HSE | PBE <sup>1st</sup>                                 | PBE <sup>2nd</sup> | PBE <sup>3rd</sup> | PBE <sup>4th</sup> | PBE <sup>aver.</sup> | interp.<br>HSE | PBE  | interp.<br>HSE |
|    | -2.499   | -3.660         | -2.768   | -2.788             | -2.796             | -2.774             | -2.782               | -3.572         | -2.559   | -3.483         |
|    | 9.083  |                | 14.938   | 14.995             | 15.107             | 14.948             | 14.997               |                | 14.774   |                |



# Appendix B

## Supplementary information for Chapter 7

Table B.1: The calculated data for the *p*-type dopable ternary TCOs that have a band gap smaller than 2.5 eV. For each compound the HSE06 calculated band gaps (fundamental band gap  $E_g$ , first direct band gap  $E_g^d$ , second gap in the valence band  $E_{g,VB}^2$ ) are compared with the other available results (second row for each compound). The PBE calculated hole effective mass along symmetry directions ( $m_h^*$ ), average hole effective mass ( $m_h^{*avg}$ ), and enthalpy of formation  $\Delta H_f$  are also presented. (All energies are in eV, and all effective masses are in units of the free electron mass  $m_e$ )

| oxide   | $E_g$                          | $E_g^d$ | $E_{g,VB}^2$ | $m_h^*$  | $m_h^{*avg}$ | $\Delta H_f$ |
|---|--------------------------------|---------|--------------|--|--------------|--------------|
| Tb <sub>2</sub> Ti <sub>2</sub> S <sub>2</sub> O <sub>5</sub> | 1.81                           | 1.81    | 0.52         | 0.81 <sup>[001]</sup> , 0.86 <sup>[100]</sup>                            | 0.83         | -32.53       |
| BTi <sub>3</sub> O <sub>3</sub>                               | 1.96                           | 2.13    | 1.25         | 0.97 <sup>[100]</sup> , 0.63 <sup>[001]</sup>                            | 0.84         | -9.22        |
| Ca <sub>4</sub> As <sub>2</sub> O                             | 1.97<br>2.1 [147] <sup>b</sup> | 2.42    | 0.83         | 0.51 <sup>[100]</sup> , 0.97 <sup>[001]</sup>                            | 0.63         | -12.04       |
| DyZnPO  | 1.95                           | 2.41    | 0.71         | 0.22 <sup>[100]</sup> , 4.94 <sup>[001]</sup> §                          | 0.62         | -11.86       |
| Rb <sub>2</sub> Sn <sub>2</sub> O <sub>3</sub>                | 1.96<br>2.3 [147] <sup>b</sup> | 1.96    | 1.87         | 0.17 <sup>[100]</sup> , 0.31 <sup>[001]</sup> §                          | 0.21         | -10.38       |
| YZnPO   | 2.02                           | 2.07    | 0.72         | 0.23 <sup>[100]</sup> , 5.40 <sup>[001]</sup> §                          | 0.66         | -7.62        |
| MnWO <sub>4</sub>   | 2.11                           | 2.11    | 0.37         | ★  |              | -11.99       |
| CaNb <sub>2</sub> O <sub>4</sub>                              | 2.12                           | 2.34    | 0.31         | 0.59 <sup>[100]</sup> , 0.63 <sup>[010]</sup> ,<br>0.87 <sup>[001]</sup> | 0.69         | -18.49       |
| K <sub>2</sub> Sn <sub>2</sub> O <sub>3</sub>                 | 2.15<br>2.3 [147] <sup>b</sup> | 2.15    | 2.08         | 0.21   | 0.21         | -10.39       |
| NaNbO <sub>2</sub>  | 2.32<br>2.1 [147] <sup>b</sup> | 2.40    | 0.49         | 0.45 <sup>[100]</sup> , 1.16 <sup>[001]</sup>                            | 0.62         | -8.78        |
| LiNbO <sub>2</sub>  | 2.39                           | 2.39    | 0.46         | 0.41 <sup>[100]</sup> , 1.79 <sup>[001]</sup>                            | 0.67         | -9.51        |

| oxide | $E_g$ | $E_g^d$                | $E_{g,VB}^2$ | $m_h^{*\dagger}$ | $m_h^{*avg\dagger\dagger}$ | $\Delta H_f^\ddagger$ |
|-------|-------|------------------------|--------------|------------------|----------------------------|-----------------------|
|       |       | 2.0 [220] <sup>a</sup> |              |                  |                            |                       |

<sup>†</sup> For materials with a cubic structure, the effective mass is calculated along [100].

<sup>††</sup> Average hole effective mass is calculated using  $m^{*avg} = (m_1 m_2 m_3)^{1/3}$  where  $m_1$ ,  $m_2$ , and  $m_3$  is the hole effective mass along [100], [010], and [001], respectively.

<sup>§</sup> For materials with a rhombohedral structure, the effective mass is calculated for the corresponding hexagonal conventional cell.

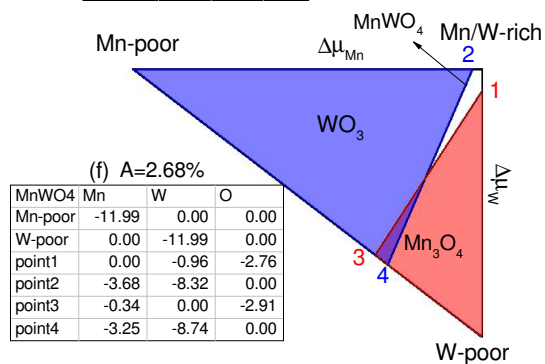
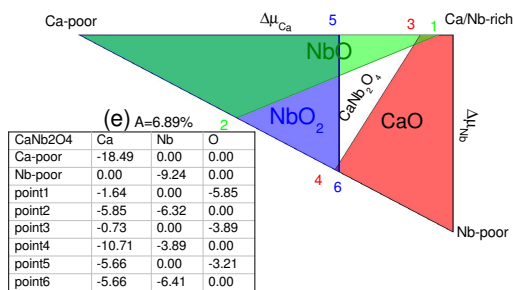
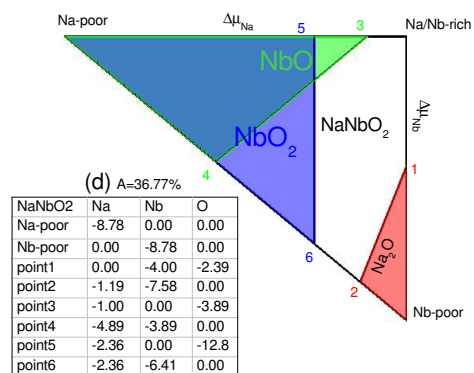
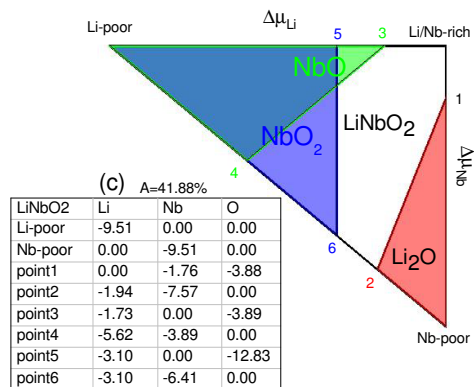
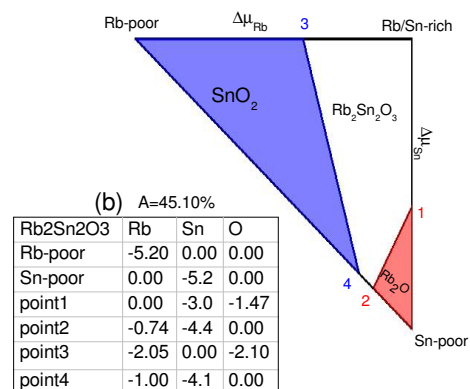
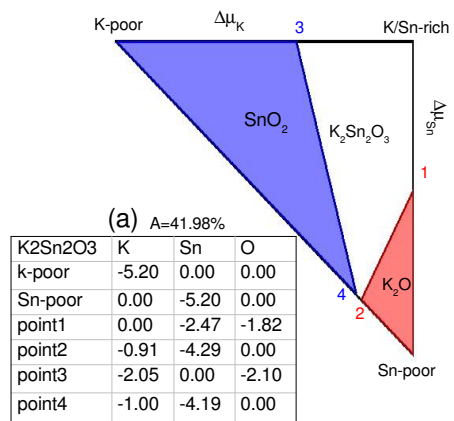
<sup>‡</sup>  $\Delta H_f$  is the formation energy of the compound with respect to the metal phase of the elements and oxygen molecules. It is calculated per formula unit of the studied compounds.

<sup>a</sup> Experimental results <sup>b</sup> Theoretical results

★ For this compound that is found metallic with PBE, the effective mass is not calculated.

Table B.2: HSE06 calculated magnetic moment per formula unit ( $\mu/f.u.$ ) of the oxides that have a non-zero total magnetic moment. The HSE06 values are also compared with the available corresponding values from the AFLOWLIB database. The values are in units of Bohr magneton  $\mu_B$ .

| oxide                              | $\mu/f.u.$<br>(HSE06) | $\mu/f.u.$<br>(AFLOWLIB) |
|------------------------------------|-----------------------|--------------------------|
| SrNiO <sub>2</sub>                 | 4.00                  | 4                        |
| Nd <sub>2</sub> SeO <sub>2</sub>   | 6.00                  | 6                        |
| Pr <sub>2</sub> SeO <sub>2</sub>   | 4.00                  | 4                        |
| Gd <sub>2</sub> SeO <sub>2</sub>   | 14.00                 | 14                       |
| Pr <sub>2</sub> SO <sub>2</sub>    | 4.00                  | 4                        |
| FeTeFO <sub>3</sub>                | 5.00                  | 5                        |
| KGdPdO <sub>3</sub>                | 7.00                  | 7                        |
| Bi <sub>2</sub> NdClO <sub>4</sub> | 3.00                  | 3                        |
| KNdPdO <sub>3</sub>                | 3.00                  | 3                        |
| MnWO <sub>4</sub>                  | 5.00                  | 5                        |
| MoNiSr <sub>2</sub> O <sub>6</sub> | 2.00                  | 2                        |
| NaVS <sub>2</sub> O <sub>8</sub>   | 2.00                  | 2                        |



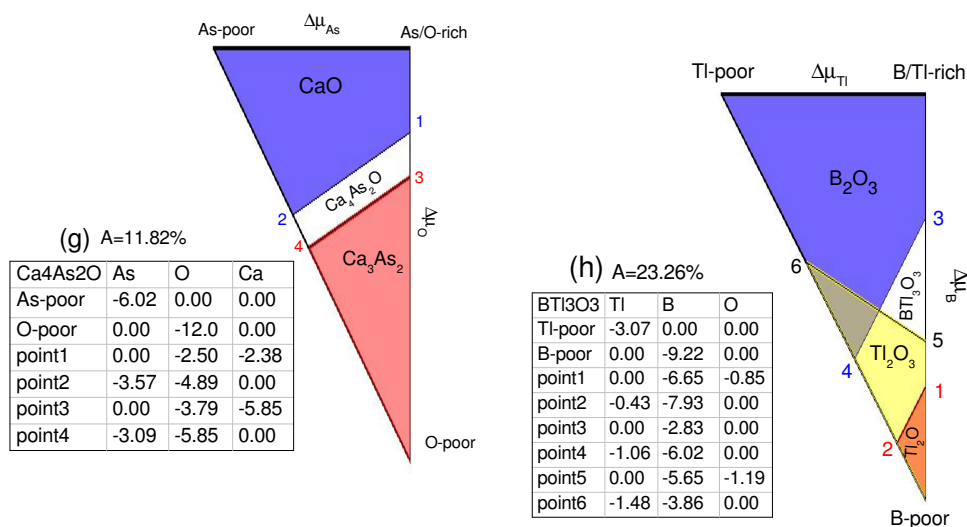


Figure B.1: Stability triangle of the *p*-type dopable ternary TCOs that have a band gap smaller than 2.5 eV. Each plot indicates the range of the chemical potentials for which the ternary oxide is stable against the formation of the competing phases<sup>a,b,c</sup>. For each compound, the chemical potential values (in eV) at the points delimiting the different stability areas are shown in the table next to the triangle. The value for 'A' above each table indicates the ratio of the ternary stability area to the total area of the triangle (in %).

CaNb<sub>2</sub>O<sub>4</sub>, and MnWO<sub>4</sub> are the compounds in the list of *p*-type dopable TCOs that have a stability area lower than our considered criterion (10%).

<sup>a</sup> All the binaries that may contribute in synthesis of a ternary are considered as competing phases.

<sup>b</sup> We ensure that the most common phase of each binary is considered as a competing phase (e.g. Tl<sub>2</sub>O<sub>3</sub> compared to Tl<sub>2</sub>O for BTl<sub>3</sub>O<sub>3</sub>) is considered as a competing phase.

<sup>c</sup> For clarity, we only show the binary oxide for which the stability area is not completely covered by that of other considered binary oxides.(e.g. the stability area of Tl<sub>2</sub>O is completely covered by that of Tl<sub>2</sub>O<sub>3</sub> in the case of BTl<sub>3</sub>O<sub>3</sub>.)



# Summary and outlook

The commercial interest in PVs as a reliable source of energy will further increase if the price decreases and the applications increase. This requires modifications in the structure and operations of PV cells. Finding new and cheap materials with specific properties for particular parts of the solar cell is one of the main goals. However, the high costs and time consuming synthesis procedures limit the experimental screening of hundreds or thousands of possible compounds to find new candidates. Fortunately, first principles computational methods are rapid, exact in results, and powerful in predictions. They can be used in high-throughput approaches to identify new possible materials for a particular part of the PV cell.

This thesis provides an accurate high-throughput calculation approach based on the density functional theory (DFT) formalism to study the optical properties and electronic structure of different materials that are part of a solar cell. **Chapter 1** presents an introduction to the structure of the solar cell by a discussion on the role of each part of the cell in its operation. It is followed in **Chapter 2** by a brief overview on the DFT formalism as an effective and accurate scheme to calculate the properties of materials.

The knowledge of a material's response to light is essential for predicting its optical properties. One can go one step further and benefit from such knowledge to design new materials with a particular optical behaviour for specific applications. **Chapter 3** introduces the linear optical response in semiconductors and some important quantities like plasma frequency, absorption edge, and refractive index. Such properties are calculated in **Chapter 3** for large band gap semiconductors and also in **Chapter 8** for small band gap semiconductors. In **Chapter 3** the DFT calculations are performed to investigate the optoelectronic properties of Al-doped MgO. We have studied the effect of the Al concentration on the structure, electronic and optical properties of Al-doped MgO. The results of our investigations show that the electronic properties of crystalline Al-doped MgO are rather robust against the doping level. Indeed, although the band gap, dielectric function, and related properties show quantitative changes upon changing the Al concentration, the changes are nearly monotonic. This implies that the electronic properties do not change qualitatively in a significant way. We have also compared the properties of the amorphous and crystalline phases for the highest considered Al concentration. We find a more significant change in the electronic properties

by the transition from the crystalline to the amorphous phase. The most important effect is the appearance of impurity levels deep in the band gap. There are several observable consequences of this. We mention, in particular, the important red shift of the optical absorption edge, due to these levels, and the related sudden drop of the band gap. A further consequence is an equally sudden jump upward of optical dielectric constant and of the refractive index. Thus, these effects can be considered as a further signature of the transition from the crystalline to the amorphous phase in these systems.

In **Chapter 4**, we have introduced our DFT based high-throughput approach to screen materials for a particular application. This approach is used throughout **Chapter 5** and **Chapter 7** of this thesis. Further we discuss the steps in our high-throughput infrastructure. The steps include data generation for the computations, handling the convergence problems in the electronic ground state calculations, storing the data in libraries and analysing the data to discover scientific trends between them. All these steps in a high-throughput project deal with a large number of input and output data. Therefore, these steps can only be completed using scripting tools. The chapter discusses further giving the details of these scripts and their role in each step of the high-throughput procedure.

**Chapter 5** presents a density-functional based computational high-throughput scheme to screen a class of oxides in order to find new TCO materials. The presented high-throughput method can be easily applied to different classes of materials. As an application, we replace In, partially or completely, in bixbyite  $\text{In}_2\text{O}_3$ . For this we screen all the binary oxides that can be found in the bixbyite structure, as well as ternaries arising from their alloying. This narrows the search to one crystal structure, and, at the same time, increases the likelihood of finding stable compounds. We consider ternaries with cation-cation alloying ratios of 25%, 50%, and 75%. We screen the electronic properties of 1541 bixbyite oxides, 23 binaries and 1518 ternaries. The screening criteria chosen are (i) a minimum band gap guaranteeing a reasonable transparency in the visible region, (ii) a minimum thermodynamic phase stability, and (iii) a positioning of an branching point energy (BPE) in the band gap indicating easy *n*- or *p*-type dopability. We show that this set of criteria can be efficiently used to screen the compounds in a large class of materials and that it has a good predictive power. Among the binaries, our calculations yield  $\text{V}_2\text{O}_3$ , a relatively simple system with a band gap of 2.4 eV, as an interesting possible *p*-type TCO. Our results indicate  $\text{Ga}_2\text{O}_3$  as an *n*-type candidate, besides  $\text{In}_2\text{O}_3$ . Among the ternaries, it is remarkable that most of the *n*-type candidates contain either Ga or In, while the *p*-type candidates all contain V. Focusing on the 50% alloys, a more robust short list of *n*-type candidates is produced by comparing the results of our screening approach with full HSE06 calculations. The promising candidates thus identified, most of them with a band gap larger than 3 eV, are given by  $(\text{A}_{0.5}\text{B}_{0.5})_2\text{O}_3$  with  $\text{AB}=(\text{DyIn}, \text{InLu}, \text{InSm}, \text{InTm})$ . Although  $(\text{In}_{0.5}\text{Pm}_{0.5})_2\text{O}_3$ , and  $(\text{Tl}_{0.5}\text{Yb}_{0.5})_2\text{O}_3$  are identified as *n*-type TCOs, we do not include them in the final list because Pm is radioactive, and Tl is toxic.

The results of our high-throughput calculation in **Chapter 6** show that the bixbyite  $\text{V}_2\text{O}_3$  could be a potential *p*-type TCO candidate. Therefore, in **Chapter 7** we have studied the *p*-type dopability of bixbyite  $\text{V}_2\text{O}_3$  within the DFT formalism. We first explain the defect calculation approach for semiconductors and specifically *p*-type oxides. We explain some important properties of defect studies like formation energies and transition levels. Finally we address specifically the prediction

of  $V_2O_3$  in the bixbyite structure as a novel *p*-type conductor.

We investigate the site preference of dopants in the bixbyite structure. Our DFT calculations show that, as in other bixbyite oxides, dopants with an atomic radius larger than the one of V prefer to sit on the b-site, rather than the d-site. We calculate the formation energies and charge transition levels of V and O vacancies as native defects, and of elements Mg, Y, and Sc substituting V as impurities. Our results show that  $Mg_V$  acts as a shallow acceptor, with a low formation energy. Furthermore, we found that oxygen vacancies are electrically neutral, and hence do not behave as hole-killing defects. Thus, we confirm that Mg-doped  $V_2O_3$  is a *p*-type conductor. We have also showed that  $V_V$  acts as a relatively shallow acceptor, with an activation energy of 0.14 eV. Thus, it may also lead to *p*-type conductivity. On the other hand, we found that substitutional Sc and Y ( $Sc_V$  and  $Y_V$ ) behave as deep donors.

**Chapter 7** applies our high-throughput approach to screen all binary, ternary, and quaternary oxides in order to identify potential low hole mass *p*-type TCOs. Our procedure consists of the following steps. We first screen all the binary, ternary and quaternary oxides in the AFLOWLIB database to identify those compounds that are reported to have a band gap larger than 2.5 eV, and a hole effective mass lower than  $1 m_e$ . We calculate the electronic structure of the thus identified compounds in order to determine their *p*-type dopability via the position of their BPE with respect to the band edges. We select the oxides for which the BPE level falls in the valence band or low in the band gap, within one-fourth of  $E_g$  above the VBM. Before proceeding, since the AFLOWLIB database does not provide theoretically accurate band gaps and in order to avoid investing resources on candidates that in fact have a low gap, we verify whether the band gaps of the materials found to be *p*-type dopable are indeed at least 2.5 eV wide. We determine the BPE by performing electronic structure calculations. We then determine the thermodynamic stability of the oxides that are *p*-type dopable and that are confirmed by our calculations to have a band gap of at least 2.5 eV. We identify the compounds  $La_2SeO_2$ ,  $Pr_2SeO_2$ ,  $Nd_2SeO_2$ ,  $Gd_2SeO_2$ , and  $FeTeFO_3$  as very good new *p*-type TCO candidates. These compounds have not been identified as such previously in the literature. With a direct band gap larger than 3.1 eV and an average hole effective mass lower than  $0.76 m_e$ , these materials have the potential of outperforming any of the currently used *p*-type TCO materials. In addition, the last four compounds are candidates to a quite unusual combination of *p*-type dopability, transparency, and magnetic order.

**Chapter 8** explains our approach to calculate the solar cell efficiency based on first-principles calculated properties. With the aim of identifying the possible absorber layers, we have studied the structure and optoelectronic properties of the Cu-based quaternary chalcogenides. Furthermore, we have used the spectroscopic limited maximum efficiency (SLME) metric to estimate the conversion efficiency of the studied solar cells and a comparison with the theoretical efficiency limit of Shockley-Queisser (SQ) is made. The effect of material composition on the optoelectronic properties and power conversion efficiency of the Cu-based solar cells are investigated. The results of our DFT calculations show that the optoelectronic properties of the studied Cu-based chalcogenides  $Cu_2-II-IV-VI_4$  strongly depend on the element VI in the material composition. The change of element VI has higher effect than changing element II, or IV in altering the characteristics of the studied chalcogenides. Replacement of the element VI by one from the same group that has a

higher atomic number decreases the plasma frequency and band gap and at the same time results in an increase in lattice parameters, and optical dielectric constant. There is a clear red shift in the absorption edge which is correlated with the decrease in the band gap. Further investigations on the compounds of interest show that besides the fundamental band gap that plays a main role in the efficiency of an absorber layer, its direct/indirect nature is an essential characteristic. The absorption coefficient is important to compare the efficiency of two compounds with the same band gap. In a case two compounds have the same band gap and therefore the same SQ efficiency limit, the one with higher absorptivity has higher efficiency and the absorber layer can be made thinner. The results of the calculations identify  $\text{Cu}_2\text{CdGeSe}_4$  and  $\text{Cu}_2\text{-II-SnS}_4$  with  $\text{II}=\text{Cd}$ , and  $\text{Zn}$  as high efficiency absorber layers.

In conclusion, this thesis presents the results of first-principles investigations of the optoelectronic properties of different classes of materials to be used in different parts of the solar cell. For each class of materials and each part of the solar cell, there are still many interesting systems to be explored. Moreover, the performed investigations in this thesis can be continued by further studies. In particular, the following topics can be considered for further investigation:

- The results of our high-throughput calculations identify a list of promising candidates for TCO applications. The natural step following this study is to search for suitable dopants, i.e. dopants that act as shallow donors or acceptors in the identified oxides. Furthermore, one must make sure that the doping energy levels are stable against the formation of native defects. Thus, further work is required to identify the impurities that will indeed convert these oxides in good *n*- or *p*-type TCOs. Regarding this point, the defect calculations for identified *n*- or *p*-type candidates have to be performed to find shallow donors or acceptors that can contribute in the conductivity.
- The results of our studies in **Chapter 8** show that the material composition changes the optoelectronic properties and efficiency of the studied semiconductors. CIGS has improved optoelectronic characteristics compared with its ternary parents, CIS and CGS, for solar cell applications. As a result, the alloying of the studied Cu-based compounds,  $\text{Cu}_2\text{-(II,II')-(IV,IV')-(VI,VI')}_4$  with  $\text{II}, \text{II}' = \{\text{Cd}, \text{Hg}, \text{and Zn}\}$ ,  $\text{IV}, \text{IV}' = \{\text{Sn}, \text{and Ge}\}$ , and  $\text{VI}, \text{VI}' = \{\text{S}, \text{Se}, \text{and Te}\}$  can have improved optoelectronic properties compared with their quaternary chalcogenide parents. The effect of the alloying on the characteristics of this class of compounds and also on the efficiency can be investigated.
- We have used the SLME metric to investigate the efficiency of the Cu-based absorber layers. In principle, it is possible to calculate this metric for other compounds. There is an intensive interest in the organometal perovskite compounds as high efficiency absorber layers. The original compound is  $\text{CH}_3\text{NH}_3\text{PbI}_3$  with almost 21% efficiency. The alloying makes it possible to have a huge number of organometal perovskite-like compounds,  $\text{CH}_3\text{NH}_3(\text{X}_n\text{X}'_{1-n})(\text{Y}_m\text{Y}'_{1-m})_3$  with  $\text{X}, \text{X}' = \{\text{Pb}, \text{and Sn}\}$  and  $\text{Y}, \text{Y}' = \{\text{I}, \text{Cl}, \text{and Br}\}$ . The existing theoretical studies are limited to a few of these compounds. Changing the electronic structure, optical properties, and efficiency of this class of materials with respect to the

material composition can be studied to identify new highly efficient organometal perovskite absorber layers.



# Samenvatting en Vooruitzicht

De commerciële interesse in fotonvoltaïsche cellen als een betrouwbare bron van energie zal verder groeien als de prijs verlaagt en het aantal toepassingen uitbreidt. Dit vereist aanpassingen in de structuur en werking van fotonvoltaïsche cellen. Het vinden van nieuwe en goedkope materialen met specifieke eigenschappen voor bepaalde delen van de zonnecel is een van de hoofddoelen. De hoge kostprijs en tijdrovende syntheseprocedures plaatsen echter een limiet op het aantal materialen dat experimenteel onderzocht kan worden. Gelukkig bieden first principles computationele methoden hier een oplossing. Door hun snelle productie van accurate resultaten en krachtige voorspellingen, kunnen ze gebruikt worden in een high-throughput aanpak om nieuwe mogelijke kandidaten te vinden voor een bepaald deel van de fotonvoltaïsche cel.

Deze thesis levert nauwkeurige high-throughput berekeningen, gebaseerd op het dichtheidsfunctionaaltheorie (DFT) formalisme, om de optische eigenschappen en elektronenstructuur van verscheidene materialen die deel uit maken van een zonnecel te bestuderen. **Hoofdstuk 1** presenteert een inleiding tot de structuur van de zonnecel, door elk onderdeel en zijn rol in de cel te bespreken. In **Hoofdstuk 2** wordt dit opgevolgd met een kort overzicht van het DFT formalisme als een effectieve en accurate methode om de eigenschappen van materialen te berekenen.

De kennis van de reactie van een materiaal op invallend licht is essentieel om haar optische eigenschappen te kunnen voorspellen. Het is mogelijk om nog een stap verder te gaan door deze kennis te gebruiken om nieuwe materialen te ontwikkelen met een bepaald optisch gedrag voor specifieke toepassingen. **Hoofdstuk 3** introduceert de lineaire optische respons in halfgeleiders en enkele belangrijke grootheden zoals de plasma frequentie, absorptierand en brekingsindex. Zulke eigenschappen worden berekend in **Hoofdstuk 3** voor halfgeleiders met een grote bandkloof, alsook in **Hoofdstuk 8** voor kleine bandkloof halfgeleiders. In **Hoofdstuk 3** worden de DFT berekeningen gebruikt om de optische en elektronische eigenschappen van Al-gedoteerd MgO te analyseren. We hebben hierbij de invloed van de Al concentratie op zowel de structuur als de opto-elektronische eigenschappen onderzocht. De resultaten van ons onderzoek tonen aan dat de elektronische eigenschappen van kristallijn Al-gedopeerd MgO tamelijk robuust zijn ten aanzien van de graad van dotering. Hoewel de bandkloof, de diëlektrische functie en de gerelateerde eigenschappen kwantitatieve veranderingen tonen bij variatie van de Al concentratie, zijn deze veran-

deringen bijna monotoon. Dit betekent dat de elektronische eigenschappen niet kwalitatief op een significante wijze veranderen. We hebben ook de eigenschappen van amorfe en kristallijne fases vergeleken voor de hoogste Al concentratie onder beschouwing. Hier vinden we een grotere verandering van de elektronische eigenschappen bij overgang van de kristallijne naar de amorfe fase. Het belangrijkste effect is de verschijning van onzuiverheidsniveaus diep in de bandkloof. Er zijn verscheidene observeerbare gevolgen hiervan. We vermelden in bijzonder de belangrijke roodverschuiving van de optische absorptierand, ten gevolge van deze tussenniveaus, en de gerelateerde plotse verkleining van de bandkloof. Een bijkomend gevolg is een even grote plotse stijging van de optische diëlektrische constante en van de brekingsindex. Deze effecten kunnen beschouwd worden als een verdere aanwijzing op de overgang van de kristallijne naar de amorfe fase in deze systemen.

In **Hoofdstuk 4** introduceren we onze DFT gebaseerde computationele high-throughput aanpak om materialen te onderzoeken voor een specifieke toepassing. Deze aanpak wordt gebruikt doorheen **Hoofdstuk 5** en **Hoofdstuk 7** van deze thesis. Verder bespreken we de stappen in onze high-throughput methodologie. De stappen omvatten de productie van gegevens voor de berekeningen, opslag van de gegevens in databanken en gegevensanalyse om wetenschappelijke trends te ontdekken. Al deze stappen in een high-throughput project gebruiken een grote hoeveelheid input- en outputgegevens. Daarom kunnen deze stappen enkel volbracht worden door gebruik van scripting tools. Het hoofdstuk gaat verder met het bespreken van deze scripts en hun rol in elke stap van de high-throughput procedure.

**Hoofdstuk 5** presenteert een dichtheidsfunctionaal gebaseerde computationele high-throughput methode voor een klasse van oxides te onderzoeken om nieuwe TCO materialen te vinden. De gepresenteerde high-throughput methode kan makkelijk worden toegepast op verschillende klassen van materialen. Als toepassing vervangen we in bixbyiet  $\text{In}_2\text{O}_3$  indium geheel of gedeeltelijk door andere elementen. Hiervoor onderzoeken we zowel alle binaire oxides die kunnen gevonden worden in de bixbyiet structuur, als ternaire structuren die voortkomen uit de legering. Dit beperkt onze zoektocht tot een kristalstructuur, en verhoogt tegelijkertijd de kans op het vinden van stabiele samenstellingen. We beschouwen ternaire structuren met kation-kation verhoudingen van 25%, 50%, en 75%. We onderzoeken de elektronische eigenschappen van 1541 bixbyiet oxides, waarvan 23 binaire en 1518 ternaire structuren. De gekozen onderzoekscriteria zijn (i) een minimale grootte van de bandkloof, die een redelijke transparantie garandeert in het zichtbare spectrum, (ii) een minimale thermodynamische fasestabiliteit en (iii) een vertakkingspuntenergie (VPE) in de bandkloof, welke wijst op een gemakkelijke mogelijkheid tot *n*- of *p*-type dotering. We tonen aan dat deze reeks criteria efficiënt kunnen gebruikt worden om samenstellingen te onderzoeken in een grote klasse van materialen, en dat hun voorspellingskracht goed is. Voor de binaire structuren geven onze berekeningen aan dat  $\text{V}_2\text{O}_3$ , een relatief eenvoudig systeem met een bandkloof van 2.4 eV, een interessante mogelijke *p*-type TCO kan leveren. Onze resultaten duiden  $\text{Ga}_2\text{O}_3$  aan als een *n*-type kandidaat, naast  $\text{In}_2\text{O}_3$ . Bij de ternaire structuren is het opvallend dat het meerendeel van de *n*-type kandidaten ofwel Ga of In bevatten, terwijl de *p*-type kandidaten allen V bevatten. Als we ons toespitsen op de 50% legeringen, vinden we een robuuste lijst van *n*-type kandidaten door de resultaten van onze screening te vergelijken met de volle HSE06 berekenin-



gen. Onder de veelbelovende kandidaten worden de materialen met een bandkloof groter dan 3 eV gegeven door  $(A_{0.5}B_{0.5})_2O_3$  met  $AB=(DyIn, InLu, InSm, \text{ and } InTm)$ . Hoewel  $(In_{0.5}Pm_{0.5})_2O_3$ , en  $(Tl_{0.5}Yb_{0.5})_2O_3$  geïdentificeerd worden als *n*-type TCO's, nemen we ze niet op in de uiteindelijke lijst omdat Pm radioactief en Tl toxisch is.

De resultaten van onze high-throughput berekening in **Hoofdstuk 6** tonen aan dat bixbyiet  $V_2O_3$  potentieel heeft als *p*-type TCO materiaal. Daarom hebben we in **Hoofdstuk 7** de *p*-type mogelijkheid tot dotering van bixbyiet  $V_2O_3$  onderzocht binnen het DFT formalisme. We leggen eerst de aanpak van de defectberekeningen uit voor halfgeleiders, specifiek voor de *p*-type oxides. We verduidelijken verder enkele belangrijke eigenschappen van het onderzoek van de defecten, zoals vormingsenergieën en overgangsniveaus. Uiteindelijk bespreken we specifiek de voorspelling van  $V_2O_3$  in de bixbyiet structuur als een nieuwe *p*-type geleider.

We onderzoeken ook de voorkeurslocatie voor het doteren van de bixbyiet structuur. Onze DFT berekeningen tonen aan dat, zoals bij andere bixbyiet oxides, doteringen met een atoomstraal groter dan die van V verkiezen om zich te vestigen op de b-site in vergelijking met de d-site. We berekenen de vormingsenergieën en overgangsniveaus van V en O vacatures als natuurlijke defecten, en van de elementen Mg, Y, en Sc wanneer ze V vervangen als onzuiverheid. Onze resultaten laten zien dat  $Mg_V$  zich gedraagt als een ondiepe acceptor, met een lage vormingsenergie. Verder vinden we dat O vacatures elektrisch neutraal zijn, en zich aldus niet gedragen als holte-vernietigende defecten. Daardoor kunnen we bevestigen dat Mg-gedoteerd  $V_2O_3$  een *p*-type geleider is. We hebben ook aangetoond dat  $V_V$  zich gedraagt als een relatief ondiepe acceptor, met een activatie energie van 0.14 eV. Hierdoor kan het defect ook leiden tot *p*-type geleiding. Daarnaast hebben we ontdekt dat substitutie door Sc en Y ( $Sc_V$  en  $Y_V$ ) defecten levert die zich gedragen als diepe donoren.

**Hoofdstuk 7** past onze high-throughput aanpak toe op alle binaire, ternaire en quaternaire oxides, met als opzet de *p*-type TCO's te identificeren met een lage holtemassa. Onze procedure bestaat uit de volgende stappen. We onderzoeken eerst alle binaire, ternaire en quaternaire oxides in de AFLOWLIB databank om de materialen te vinden welke een bandkloof hebben die groter is dan 2.5 eV, en een effectieve holtemassa lager dan  $1 m_e$ . We berekenen vervolgens de elektronische structuur van deze materialen om hun mogelijkheid tot *p*-type dotering te bepalen, gebruik makend van de positie van de VPE in vergelijking met de randen van de banden. We selecteren de oxides waarvoor het VPE niveau zich bevindt in de valentieband of laag in de bandkloof, d.w.z. binnen een vierde van  $E_g$  boven het valentieband maximum. Omdat de AFLOWLIB databank geen theoretisch nauwkeurige bandkloof voorziet, gaan we eerst na of de bandkloof van de gekozen materialen inderdaad minstens 2.5 eV groot is, om te vermijden dat we middelen investeren in kandidaten met een lage bandkloof. We bepalen de VPE aan de hand van onze elektronenstructuurberekeningen. Daarna onderzoeken we de thermische stabiliteit van de oxides die *p*-type halfgeleiders zijn en welke uit onze berekeningen een bandkloof hebben van ten minste 2.5 eV. We identificeren de materialen  $La_2SeO_2$ ,  $Pr_2SeO_2$ ,  $Nd_2SeO_2$ ,  $Gd_2SeO_2$ , en  $FeTeFO_3$  als zeer goede nieuwe TCO kandidaten. Deze samenstellingen zijn tot nu toe nog niet als dusdanig geïdentificeerd in de literatuur. Met een directe bandkloof groter dan 3.1 eV en een gemiddelde effectieve holtemassa lager dan  $0.76 m_e$  hebben deze materialen het potentieel om eender welk huidig *p*-type TCO materiaal te overtreffen. Daarnaast zijn de vier laatste samenstellingen kandidaten met een ongebruikelijke

combinatie van mogelijkheid tot *p*-type dotering, transparantie en magnetische orde.

**Hoofdstuk 8** legt onze aanpak uit voor de berekening van de zonnecel-efficiëntie gebaseerd op first-principles berekende eigenschappen. Met het oog op het identificeren van mogelijke materialen als absorptielaag hebben we de structuur en de opto-elektronische eigenschappen van de Cu-gebaseerde quaternaire chalcogeniden onderzocht. Verder hebben we de "spectroscopic limited maximum efficiency" (SLME) metriek gebruikt om de efficiëntie van de onderzochte zonnecellen te schatten, waarbij een vergelijking wordt gemaakt met de theoretische Shockley-Queisser (SQ) limiet. Het effect van de samenstelling van het materiaal op de opto-elektronische eigenschappen en de efficiëntie van de vermogensoverdracht van de Cu-gebaseerde zonnecellen wordt onderzocht. De resultaten van onze DFT berekeningen tonen aan dat de opto-elektronische eigenschappen van de onderzochte Cu-gebaseerde chalcogeniden  $\text{Cu}_2\text{-II-IV-VI}_4$  sterk afhankelijk zijn van het VI element in de samenstelling van het materiaal. Het vervangen van het VI element heeft een groter effect dan het vervanging van het II of IV element om de eigenschappen van de onderzochte chalcogeniden te veranderen. Substitutie van het VI element door een element uit dezelfde groep met een hoger atoomgetal verlaagt de plasmafrequentie en de bandkloof, en zorgt tegelijkertijd voor grotere rooster- en optische diëlektrische constanten. Er is een duidelijke roodverschuiving in de absorptierand, welke gecorreleerd is aan de verkleining van de bandkloof. Verder onderzoek van de materialen toont aan dat naast de grootte van de fundamentele bandkloof, welke een beduidende rol speelt in de efficiëntie van de absorptielaag, de indirect of directe natuur van de bandkloof een essentiële eigenschap is. De absorptiecoëfficiënt is belangrijk om de efficiëntie van twee materialen te vergelijken die een even grote bandkloof hebben. Wanneer twee materialen dezelfde bandkloof hebben, en dus dezelfde SQ limiet, heeft degene met een grotere absorptiviteit een grotere efficiëntie, waardoor de absorptielaag dunner gemaakt kan worden. De resultaten van de berekeningen identificeren  $\text{Cu}_2\text{CdGeSe}_4$  en  $\text{Cu}_2\text{-II-SnS}_4$ , met II=Cd en Zn, als absorptielagen met een hoge efficiëntie.

Deze thesis sluit af met het presenteren van de resultaten van het first-principles onderzoek van de opto-elektronische eigenschappen van de klassen van materialen die gebruikt worden in verschillende delen van de zonnecel. Voor elke klasse van materialen en elk deel van de zonnecel zijn er nog vele interessante systemen die kunnen bestudeerd worden. Bovendien kan het werk van deze thesis voortgezet worden in verder onderzoek. We vermelden specifiek de volgende onderwerpen:

- De resultaten van onze high-throughput berekeningen identificeren een lijst van veelbelovende kandidaten voor TCO toepassingen. Een logische volgende stap is het zoeken van geschikte doteringen, d.w.z. doteringen die zich gedragen als ondiepe donoren of acceptoren in de geïdentificeerde oxides. Verder moet men zeker zijn dat de energieniveaus van de dotering stabiel zijn ten opzichte van de vorming van defecten. Er is dus meer werk nodig om de onzuiverheden te vinden die deze oxides omvormen tot goede *n*- of *p*-type TCO's. Hiervoor moeten de defectberekeningen voor de geïdentificeerde *n*- of *p*-type kandidaten uitgevoerd worden om ondiepe donoren of acceptoren te vinden die kunnen bijdragen aan de geleiding.
- De resultaten van ons onderzoek in **Hoofdstuk 8** tonen aan dat de samenstelling van het

materiaal invloed heeft op de opto-elektronische kenmerken en de efficiëntie van de onderzochte halfgeleiders. CIGS heeft verbeterde opto-elektronische eigenschappen voor fotovoltaïsche toepassingen in vergelijking met de ternaire samenstellingen waarvan het afgeleid is: CIS en CGS. Daardoor kan een legering van de bestudeerde Cu-gebaseerde materialen  $\text{Cu}_2\text{-(II,II')-(IV,IV')-(VI,VI')}_4$ , met  $\text{II}, \text{II}' = \{\text{Cd}, \text{Hg}, \text{en Zn}\}$ ,  $\text{IV}, \text{IV}' = \{\text{Sn}, \text{en Ge}\}$ , en  $\text{VI}, \text{VI}' = \text{S}, \text{Se en Te}$  betere opto-elektronische eigenschappen hebben in vergelijking met de quaternaire chalcogeniden. Het effect van het legeren op de karakteristieken van deze klasse van materialen, alsook hun efficiëntie, kan nog verder onderzocht worden.

- We hebben de SLME metriek gebruikt om de efficiëntie te onderzoeken van de Cu-gebaseerde absorptielagen. In principe is het mogelijk om deze metriek te berekenen voor andere samenstellingen. Er is een grote interesse in de organometallische perovskiet materialen als absorptielagen met een hoge efficiëntie.

De originele samenstelling is  $\text{CH}_3\text{NH}_3\text{PbI}_3$ , welke een efficiëntie heeft van bijna 21%. Het legeren van dit materiaal geeft vele mogelijkheden voor organometallische perovskietachtige samenstellingen:  $\text{CH}_3\text{NH}_3(\text{X}_n\text{X}'_{1-n})(\text{Y}_m\text{Y}'_{1-m})_3$  met  $\text{X}, \text{X}' = \{\text{Pb}, \text{and Sn}\}$  en  $\text{Y}, \text{Y}' = \{\text{I}, \text{Cl}, \text{and Br}\}$ . De bestaande theoretische studies zijn beperkt tot een klein aantal van deze materialen. Veranderingen van de elektronenstructuur, optische eigenschappen en de efficiëntie van deze klasse van materialen ten opzichte van de samenstelling kunnen bestudeerd worden om nieuwe hoogefficiënte organometallische perovskieten te identificeren voor absorptielagen.



# Bibliography

- [1] *World Energy Resources 2013 Survey*. World Energy Council, London, 2013.
- [2] *International Energy Outlook 2013 With Projection to 2040*. US energy information administration, 2013.
- [3] B. Flynn, W. Wang, Chih hung Chang, and G. S. Herman. Microwave assisted synthesis of  $\text{Cu}_2\text{ZnSns}_4$  colloidal nanoparticle inks. *phys. status solidi a*, 209:2186, 2012.
- [4] D. K. Ferry. *Semiconductors: Bonds and Bands*. IOP Publishing, London, UK, 2013.
- [5] R. Das and S. Pandey. Comparison of optical properties of bulk and nano crystalline thin films of CdS using different precursors. *Int. J. Mat. Sci.*, 1:35, 2011.
- [6] P. P. Altermatt, A. Schenk, F. Geelhaar, and G. Heiser. Reassessment of the intrinsic carrier density in crystalline silicon in view of band-gap narrowing. *J. Appl. Phys.*, 93:1598, 2003.
- [7] A. B. Sproul and M. A. Green. Improved value for the silicon intrinsic carrier concentration from 275 to 375 K. *J. Appl. Phys.*, 70:846, 1991.
- [8] W. Shockley and H. J. Queisser. Detailed balance limit of efficiency of pn junction solar cells. *J. Appl. Phys.*, 32:510, 1961.
- [9] M. A. Green. Third generation photovoltaics: Ultra-high conversion efficiency at low cost. *Prog. Photovolt. Res. Appl.*, 9:123, 2001.
- [10] <http://www.solarbuzz.com/reports/pv-equipment-quarterly>. A guide to solar cell manufacturing and equipment trends.
- [11] M. Taguchi, A. Yano, S. Tohoda, K. Matsuyama, Y. Nakamura, T. Nishiwaki, K. Fujita, and E. Maruyama. 24.7% record efficiency HIT solar cell on thin silicon wafer. *IEEE J. Photovolt.*, 4:96, 2014.

- [12] H. J. Lewerenz and H. Jungblut. *Photovoltaik: Grundlagen und Anwendungen*. Springer-Verlag, Berlin, 1995.
- [13] J. Poortmans and V. Arkhipov. *Thin Film Solar Cells: Fabrication, Characterization and Applications*. John Wiley and Sons, U.S.A., 2006.
- [14] R. A. Street. *Hydrogenated Amorphous Silicon*. Cambridge University Press, Cambridge, UK, 1991.
- [15] D. E. Carlson and C. R. Wronski. Amorphous silicon solar cell. *Appl. Phys. Lett.*, 28:671, 1976.
- [16] P. Jackson, D. Hariskos, R. Wuerz, O. Kiowski, A. Bauer, T. M. Friedlmeier, and M. Powalla. Properties of Cu(In,Ga)Se<sub>2</sub> solar cells with new record efficiencies up to 21.7%. *Phys. Status Solidi RRL*, 9:28, 2015.
- [17] D. Neamen. *Semiconductor Device Physics: Basic Principles*. McGraw-Hill, New York, 4 edition, 2012.
- [18] J. Emsley. *Nature's building blocks: an A-Z guide to the elements*. Oxford University Press, Oxford, UK, 2001.
- [19] A. Tanaka. Toxicity of indium arsenide, gallium arsenide, and aluminium gallium arsenide. *Toxicol. Appl. Pharm.*, 198:405, 2004.
- [20] S. M. Sze and K. Ng. Kwok. *Physics of Semiconductor Devices*. John Wiley and Son, New Jersey, 3 edition, 2007.
- [21] P. Wurfel. *Physics of Solar Cells: From Principles to New Concepts*. Wiley-VCH Verlag GmbH and Co. KGaA, Weinheim, Germany, 2005.
- [22] *Handbook of Photovoltaic Science and Engineering*. John Wiley and Sons, Chichester, UK, 2003. edited by A. Luque and S. Hegedus.
- [23] R. U. Ayres and L. W. Ayres. *A Handbook of Industrial Ecology*. Edward Elgar Publishing, Cheltenham, UK, 2002.
- [24] V. Fthenakis and K. Zweibel. CdTe PV: Real and Perceived EHS Risks. *NREL/CP*, 520:33561, May 2003.
- [25] T. Tinoco, C. Rincón, M. Quintero, and G. S. Pérez. Phase diagram and optical energy gaps for CIGS alloys. *Phys. Status Solidi a*, 124:427, 1991.
- [26] P. Jackson, D. Hariskos, E. Lotter, S. Paetel, R. Wuerz, R. Menner, W. Wischmann, and M. Powalla. New world record efficiency for Cu(In, Ga)Se<sub>2</sub> thin-film solar cells beyond 20%. *Prog. Photovolt. Res. Appl.*, 19:894, 2011.

- [27] A. Chirila, S. Buecheler, F. Pianezzi, P. Bloesch, C. Gretener, A. R. Uhl, C. Fella, L. Kranz, J. Perrenoud, S. Seyrling, R. Verma, S. Nishiwaki, Y. E. Romanyuk, G. Bilger, and A. N. Tiwari. Highly efficient Cu(In, Ga)Se<sub>2</sub> solar cells grown on flexible polymer films. *Nature Mater.*, 10:857, 2011.
- [28] H. Katagiri, K. Saitoh, T. Washio, H. Shinohara, T. Kurumadani, and S. Miyajima. Development of thin film solar cell based on Cu<sub>2</sub>ZnSnS<sub>4</sub> thin films. *Sol. Energ. Mat. Sol. C.*, 65:141, 2001.
- [29] W. Wang, M. T. Winkler, O. Gunawan, T. Gokmen, T. K. Todorov, Y. Zhu, and D. B. Mitzi. Device characteristics of CZTSSe thin-film solar cells with 12.6% efficiency. *Adv Energy Mater.*, 4:13101465, 2014.
- [30] A. Polman and H. A. Atwater. Photonic design principles for ultrahigh-efficiency photovoltaics. *Nature Mat.*, 11:174, 2012.
- [31] <http://www.nrel.gov/ncpv/>.
- [32] R. M. Martin. *Electronic Structure: Basic Theory and Practical Methods*. Cambridge University Press, UK, 2004.
- [33] M. Born and J. R. Oppenheimer. Zur quantentheorie der molekeln. *Ann Physik*, 84:457, 1927.
- [34] D. R. Hartree. The wave mechanics of an atom with a non-coulomb central field. part I - theory and methods. *Proc. Cam. Phil. Soc.*, 24:89, 1928.
- [35] D. R. Hartree. The wave mechanics of an atom with a non-coulomb central field. part II - theory and methods. *Proc. Cam. Phil. Soc.*, 24:111, 1928.
- [36] D. R. Hartree. The wave mechanics of an atom with a non-coulomb central field. part III - theory and methods. *Proc. Cam. Phil. Soc.*, 24:426, 1928.
- [37] J. C. Slater. The theory of complex spectra. *Phys. Rev.*, 34:1293, 1929.
- [38] C. Møller and M. S. Plesset. Note on an approximation treatment for many-electron systems. *Phys. Rev.*, 46:618, Oct 1934.
- [39] C. D. Sherrill and H. F. Schaefer. The configuration interaction method: Advances in highly correlated approaches. *Advances in Quantum Chemistry*, 43:143, 1999.
- [40] H. Kümmel. Origins of the coupled cluster method. *Theoretica chimica acta*, 80:81, 1991.
- [41] D. Ceperley, G. V. Chester, and M. H. Kalos. Monte carlo simulation of a many-fermion study. *Phys. Rev. B*, 16:3081, 1977.

- [42] P. Hohenberg and W. Kohn. Inhomogenous electron gas. *Phys. Rev.*, 136:B684, 1964.
- [43] M. Levy. Universal variational functionals of electron densities, first order density matrices, and natural spin-orbitals and solutions of the v-representability problem. *Proc. Natl. Acad. Sci.*, 76:606265, 1979.
- [44] E. H. Lieb. Density functionals for coulomb systems. *Int. J. Quantum Chem.*, 24:24377, 1983.
- [45] W. Kohn and L. J. Sham. Self-consistent equations including exchange and correlation effects. *Phys. Rev.*, 140:A1133, 1965.
- [46] J. C. Slater. A simplification of the Hartree-Fock method. *Phys. Rev.*, 81:385, 1951.
- [47] P. A. M. Dirac. Note on Exchange Phenomena in the Thomas Atom. *Proceedings of the Cambridge Philosophical Society*, 26:376385, 1930.
- [48] D. M. Ceperley and B. J. Alder. Ground state of the electron gas by a stochastic method. *Phys. Rev. Lett.*, 45:566, 1980.
- [49] J. P. Perdew and Y. Wang. accurate and simple analytic representation of the electron-gas correlation energy. *Phys. Rev. B*, 45:13244, 1992.
- [50] J. P. Perdew. Density functional theory and the band gap problem. *International Journal of Quantum Chemistry*, 30:451, 1986.
- [51] J. P. Perdew, K. Burke, and M. Ernzerhof. Generalized gradient approximation made simple. *Phys. Rev. Lett.*, 77:3865, 1996.
- [52] A. D. Becke. Density-functional exchange-energy approximation with correct asymptotic behavior. *Phys. Rev. A*, 38:3098, 1988.
- [53] C. Lee, W. Yang, and R. G. Parr. Development of the colic-salvetti correlation-energy formula into a functional of the electron density. *Phys. Rev. B*, 37:785, 1988.
- [54] D. C. Patton, D. V. Porezag, and M. R. Pederson. Simplified generalized-gradient approximation and anharmonicity: Benchmark calculations on molecules. *Phys. Rev. B*, 55:7454, 1997.
- [55] J. E. Jaffe, Z. Lin, and A. C. Hess. Gaussian-basis LDA and GGA calculations for alkali-metal equations of state. *Phys. Rev. B*, 57:11834, 1998.
- [56] J. Heyd, G. E. Scuseria, and M. Ernzerhof. Hybrid functionals based on a screened coulomb potential. *J. Chem. Phys.*, 118(18):8207, 2003.



- [57] A. V. Krukau, O. A. Vydrov, A. F. Izmaylov, and G. E. Scuseria. Influence of the exchange screening parameter on the performance of screened hybrid functionals. *J. Chem. Phys.*, 125:224106, 2006.
- [58] J. Paier, M. Marsman, K. Hummer, G. Kresse, I. C. Gerber, and J. G. Angyan. Screened hybrid density functionals applied to solids. *J. Chem. Phys.*, 124:154709, 2006.
- [59] S. Y. Savrasov and G. Kotliar. Linear response calculations of lattice dynamics in strongly correlated systems. *Phys. Rev. Lett.*, 90:056401, 2003.
- [60] B. I. Min, H. J. F. Jansen, T. Oguchi, and A. J. Freeman. Total-energy local-density studies of the  $\alpha - \gamma$  phase transition in Ce. *Phys. Rev. B*, 34:369, 1986.
- [61] F. L. Tang, Z. X. Zhu, H. T. Xue, W. J. Lu, Y. D. Feng, Z. M. Wang, and Y. Wang. Optical properties of Al-doped CuInSe<sub>2</sub> from the first principle calculation. *Physica B*, 407:4814, 2012.
- [62] F. Ch. Wan, F. L. Tang, Z. X. Zhu, H. T. Xue, W. J. Lu, Y. D. Feng, and Z. Y. Rui. First-principles investigation of the optical properties of CuIn(S<sub>x</sub>Se<sub>1-x</sub>)<sub>2</sub>. *Mat. Sci. Semicon. Proc.*, 16:1422, 2013.
- [63] J. Heyd, J. E. Peralta, G. E. Scuseria, and R. L. Martin. Energy band gaps and lattice parameters evaluated with the heyd-scuseria-ernzerhof screened hybrid functional. *J. Chem. Phys.*, 123:174101, 2006.
- [64] F. Tran and P. Blaha. Accurate band gaps of semiconductors and insulators with a semilocal exchange-correlation potential. *Phys. Rev. Lett.*, 102:226401, 2009.
- [65] A. Janotti and C. G. Van de Walle. LDA+U and hybrid functional calculations for defects in ZnO, SnO<sub>2</sub>, and TiO<sub>2</sub>. *Phys. Status Solidi. B*, 248:799, 2011.
- [66] H. D. Monkhorst and J. D. Pack. Special points for brillonin-zone integrations. *Phys. Rev. B*, 13:5188, 1976.
- [67] J. C. Slater. An augmented plane wave method for the periodic potential problem. *Phys. Rev.*, 92:3, 1953.
- [68] P. E. Blöchl. Projector augmented-wave method. *Phys. Rev. B*, 50(24):17953, 1994.
- [69] Z. Bodrog and A. Gali. The spin-spin zero-field splitting tensor in the projector-augmented-wave method. *J. Phys.: Condens. Matter*, 26:015305, 2014.
- [70] G. Kresse and J. Furthmüller. Efficiency of ab-initio total energy calculations for metals and semiconductors using a plane-wave basis set. *Comput. Mater. Scienc*, 6:15, 1996.

- [71] S. Maekawa, T. Tohyama, S. E. Barnes, S. Ishihara, W. Koshibae, and G. Khaliullin. *Physics of Transition Metal Oxides*. Springer-Verlag, Berlin, 2004.
- [72] D. C. Harris. Durable 3-5 mm transmitting infrared window materials. *Infr. Phys. Technol.*, 39:185, 1998.
- [73] J. P. Beouf. Plasma display panels: physics, recent developments and key issues. *J. Phys. D: Appl. Phys.*, 36:R53, 2003.
- [74] M. M. Tardío, R. Ramírez, R. González, and Y. Chen. *p*-type semiconducting properties in lithium-doped MgO single crystals. *Phys. Rev. B*, 66:134202, 2002.
- [75] M. Pesci, F. Gallino, C. Di Valentin, and G. Pacchioni. Nature of defect states in nitrogen-doped MgO. *J. Phys. Chem. C*, 114:1350, 2010.
- [76] F. Stavale, N. Nilius, and H. J. Freund. Cathodoluminescence of near-surface centres in Cr-doped MgO (001) thin films probed by scanning tunnelling microscopy. *New J. Phys.*, 14:033006, 2012.
- [77] V. Georgieva, M. Saraiva, N. Jehanathan, O. I. Lebelev, D. Depla, and A. Bogaerts. Compositional effects on the growth of films. *J. Phys. D: Appl. Phys.*, 42:065107, 2009.
- [78] M. Saraiva, H. Chen, W. P. Leroy, S. Mahieu, N. Jehanathan, O. Lebedev, V. Georgieva, R. Persoons, and D. Depla. Sputter-deposited Mg-Al-O thin films: linking molecular dynamics simulations to experiments. *Plasma Process. Polym.*, 6:5751, 2009.
- [79] M. Saraiva, V. Georgieva, S. Mahieu, K. Van Aeken, A. Bogaerts, and D. Depla. Compositional effects on the growth of Mg(M)O films. *J. Appl. Phys.*, 107:034902, 2010.
- [80] V. Georgieva, I. T. Todorov, and A. Bogaerts. Molecular dynamics simulation of oxide thin film growth: Importance of the inter-atomic interaction potential. *Chem. Phys. Lett.*, 485:315, 2010.
- [81] E. Runge and E. K. U. Gross. Density-Functional Theory for Time-Dependent Systems. *Phys. Rev. Lett.*, 52:997, 1984.
- [82] H. Ehrenreich and M. H. Cohen. Self-consistent field approach to the many-electron problem. *Phys. Rev.*, 115:786, 1959.
- [83] S. L. Adler. Quantum Theory of the Dielectric Constant in Real Solids. *Phys. Rev.*, 126:413, 1962.
- [84] M. Gajdoš, K. Hummer, G. Kresse, J. Furthmüller, and F. Bechstedt. Linear optical properties in the projector-augmented wave methodology. *Phys. Rev. B*, 73:045112, 2006.

- [85] V. Lucarini, J. J. Saarinen, K. E. Peiponen, and E. M. Vartiainen. *Kramers-Kronig Relations in Optical Materials Research*. Springer-Verlag, Berlin Heidelberg, 2005.
- [86] M. Bass. *HANDBOOK OF OPTICS: optical properties of materials, nonlinear optics, quantum optics: Vol. IV*. McGraw-Hill Companies, US, 3rd edition, 2010. edited by M. Bass and G. Li and E. W. Van Stryland.
- [87] J. Tauc. Optical properties and electronic structure of amorphous Ge and Si. *Materials Research Bulletin*, 3:37, 1968.
- [88] F. Urbach. The long-wavelength edge of photographic sensitivity and of the electronic absorption of solids. *Phys. Rev.*, 92:1324, 1953.
- [89] J. S. Toll. Causality and the dispersion relation: Logical foundations. *Phys. Rev.*, 104:1760, 1965.
- [90] D. Y. Smith. Comments on the dispersion relations for the complex refractive index of circularly and elliptically polarized light. *J. Opt. Soc. Am.*, 66:454, 1976.
- [91] G. Kresse and J. Hafner. Ab initio molecular dynamics for liquid metals. *Phys. Rev. B*, 47(1):R558, 1993.
- [92] G. Kresse and J. Joubert. From ultrasoft pseudopotentials to the projector augmented-wave method. *Phys. Rev. B*, 59(3):1758, 1999.
- [93] U. Schönberger and F. Aryasetiawan. Bulk and surface electronic structures of MgO. *Phys. Rev. B*, 52:8788, 1995.
- [94] S. K. Yadav, T. Sadowski, and R. Ramprasad. Density functional theory study of ZnX (X = O, S, Se, Te) under uniaxial strain. *Phys. Rev. B*, 81:144120, 2010.
- [95] L. Dong, S. K. Yadav, R. Ramprasad, and S. P. Alpay. Band gap tuning in gan through equibiaxial in-plane strains. *Appl. Phys. Lett.*, 96:202106, 2010.
- [96] N. W. Ashcroft and N. D. Mermin. *Solid State Physics*. Saunders College, Fort Worth, 1976.
- [97] K. Morigaki. *Physics of Amorphous Semiconductors*. Imperial college press, London, UK, 1999.
- [98] G. A. N. Connell. *Amorphous Semiconductors*. Springer, Berlin, m. h. brodsky edition, 1979.
- [99] J. T. Titantah and D. Lamoén. Determination of the electron effective band mass in amorphous carbon from density-functional theory calculations. *Phys. Rev. B*, 70:033101, 2004.
- [100] B. A. Andersson. Materials availability for large-scale thin-film photovoltaics. *Progress in Photovoltaics: Research and Applications*, 8:61, 2000.

- [101] A. Klein, C. Körber, A. Wachau, F. Säuberlich, Y. Gassenbauer, S. P. Harvey, D. E. Proffit, and T. O. Mason. Transparent conducting oxides for photovoltaics: Manipulation of fermi level, work function and energy band alignment. *materials*, 3:4892–4914, 2010.
- [102] T. W. Eagar. Bringing new materials to market. *Technology Review*, 98:42, 1995.
- [103] R. Potyrailo and E. Amis. *High-Throughput Analysis: A Tool for Combinatorial Materials Science*. Springer, 2003.
- [104] D. de Fontaine. *Cluster Approach to Order-Disorder Transformations in Alloys and in Solid State Physics*. Wiley, New York, 1994. edited by H. Ehrenreich and D. Turnbull.
- [105] R. O. Jones and R. O. Gunnarson. The density functional formalism, its applications and prospects. *Rev. Mod. Phys.*, 61:689, 1989.
- [106] E. G. Lewars. *Computational Chemistry: Introduction to the Theory and Applications of Molecular and Quantum Mechanics*. Kluwer, Boston, 2003.
- [107] Y. Wang, S. Shang, L. Q. Chen, , and Z. K. Liu. Density functional theory-based database development and CALPHAD automation. *JOM*, 65:1533, 2013.
- [108] D. Morgan, G. Ceder, and S. Curtarolo. High-throughput and data mining with ab initio methods. *Meas. Sci. Technol.*, 16:296, 2005.
- [109] K. Rajan. Materials informatics. *Materials Today*, 8:38, 2005.
- [110] S. Curtarolo, D. Morgan, K. Persson, J. Rodgers, and G. Ceder. Predicting crystal structures with data mining of quantum calculations. *Phys. Rev. Lett.*, 91:135503, 2003.
- [111] S. Curtarolo, D. Morgan, and G. Ceder. Accuracy of ab initio methods in predicting the crystal structures of metals: review of 80 binary alloys. *Calphad*, 29:163, 2005.
- [112] C. C. Fischer, K. J. Tibbetts, D. Morgan, and G. Ceder. Predicting crystal structure by merging data mining with quantum mechanics. *Nature Mater.*, 5:641, 2006.
- [113] X. D. Xiang, X. Sun, G. Briceno, Y. Lou, K. A. Wang, H. Chang, W. G. Wallace-Freedman, S.-W. Chen, and P. G. Schultz. A combinatorial approach to materials discovery. *Science*, 268:1738, 1995.
- [114] Y. M. Chiang, D. R. Sadoway, M. K. Aydinol, Y. I. Jang, B. Huang, and G. Ceder. A combinatorial approach to materials discovery. *Nature*, 392:694, 1998.
- [115] G. H. Jóhannesson, T. Bligaard, A. V. Ruban, H. L. Skriver, K. W. Jacobsen, and J. K. Nørskov. Combined electronic structure and evolutionary search approach to materials design. *Phys. Rev. Lett.*, 88:255506–1:5, 2002.

- [116] D. P. Stucke and V. H. Crespi. Predictions of new crystalline states for assemblies of nanoparticles: Perovskite analogues and 3-D arrays of self-assembled nanowires. *Nano Lett.*, 3:1183, 2003.
- [117] M. L. Cohen. Predicting new materials and their properties. *Solid State Communications*, 107:589, 1998.
- [118] G. K. H. Madsen. Automated search for new thermoelectric materials: The case of LiZnSb. *J. Am. Chem. Soc.*, 128:12140, 2006.
- [119] H. Koinuma and I. Takeuchi. Combinatorial solid-state chemistry of inorganic materials. *Nature Mater.*, 3:429, 2004.
- [120] T. R. Boussie, G. M. Diamond, C. Goh, K. A. Hall, A. M. LaPointe, M. Leclerc, C. Lund, V. Murphy, J. A. W. Shoemaker, U. Tracht, H. Turner, J. Zhang, T. Uno, R. K. Rosn, and J. C. Stevens. A fully integrated high-throughput screening methodology for the discovery of new polyolefin catalysts: Discovery of a new class of high temperature single-site group (IV) copolymerization catalysts. *J. Am. Chem. Soc.*, 125:4306, 2003.
- [121] J. Hafner, C. Wolverton, and G. Ceder. Toward computational materials design: The impact of density functional theory on materials research. *MRS Bull.*, 31:659, 2006.
- [122] K. Kang, Y. S. Meng, J. Bréger, C. P. Grey, and G. Ceder. Electrodes with high power and high capacity for rechargeable lithium batteries. *Science*, 311:977, 2006.
- [123] A. N. Kolmogorov, M. Calandra, and S. Curtarolo. Thermodynamic stabilities of ternary metal borides: An ab initio guide for synthesizing layered superconductors. *Phys. Rev. B*, 78:094520–1:9, 2008.
- [124] J. L. Spivack, J. N. Cawse, D. W. Whisenhunt, B. F. Johnson, K. V. Shalyaev, J. Male, E. J. Pressman, J. Y. Ofori, G. L. Soloveichik, B. P. Patel, T. L. Chuck, D. J. Smith, T. M. Jordan, M. R. Brennan, R. J. Kilmer, and E. D. Williams. Combinatorial discovery of metal co-catalysts for the carbonylation of phenol. *Appl. Catal. A*, 254:5, 2003.
- [125] R. A. Potyrailo, B. J. Chisholm, W. G. Morris, J. N. Cawse, W. P. Flanagan, L. Hassib, C. A. Molaison, K. Ezbiasky, G. Medford, and H. Reitz. Development of combinatorial chemistry methods for coatings: High-throughput adhesion evaluation and scale-up of combinatorial leads. *J. Comput. Chem.*, 5:472, 2003.
- [126] R. A. Potyrailo and I. Takeuchi. Combinatorial and high-throughput materials research. *Meas. Sci. Technol.*, 16:1, 2005.
- [127] S. Curtarolo, W. Setyawan, G. L. W. Hart, M. Jahnatek, R. V. Chepulskii, R. H. Taylor, S. Wang, J. Xue, K. Yang, O. Levy, M. Mehl, H. T. Stokes, D. O. Demchenko, and D. Morgan. Aflow: An automatic framework for high-throughput materials discovery. *Comp. Mat. Sci.*, 58:218, 2012.

- [128] <http://icsd.fiz-karlsruhe.de/icsd>. Inorganic Crystal Structure Database.
- [129] G. Bergerhoff, R. Hundt, R. Sievers, and I. Brown. The inorganic crystal structure data base. *J. Chem. Inf. Model.*, 23:66, 1983.
- [130] G. Ceder, D. Morgan, C. Fischer, K. Tibbetts, and S. Curtarolo. Data-mining-driven quantum mechanics for the prediction of structure. *MRS Bull.*, 31:981, 2006.
- [131] G. Hautier, C. C. Fischer, A. Jain, T. Mueller, and G. Ceder. Finding nature’s missing ternary oxide compounds using machine learning and density functional theory. *Chem. Mater.*, 22:3762, 2010.
- [132] E. R. Davidson. *Methods in Computational Molecular Physics*. Eds. Plenum, New York, 1983. edited by G. H. F. Dierckson, S. Wilson.
- [133] D. Wood and A. Zunger. A new method for diagonalising large matrices. *Journal of Physics A: Mathematical and General*, 18:1343, 1985.
- [134] P. Pulay. Convergence acceleration of iterative sequences. the case of SCD iteration. *Chemical Physics Letters*, 73:393, 1980.
- [135] G. Kresse, M. Marsman, and J. Furthmüller. <http://cms.mpi.univie.ac.at/vasp/vasp/vasp.html>. VASP the GUIDE 2010.
- [136] G. Kresse and J. Furthmüller. Efficient iterative schemes for ab initio total-energy calculations using a plane-wave basis set. *Phys. Rev. B*, 54:11169, 1996.
- [137] P. B. Blöchl, O. Jepsen, and O. Andersen. Improved tetrahedron method for brillouin-zone integrations. *Phys. Rev. B*, 49:16223, 1994.
- [138] [www.sybase.com](http://www.sybase.com).
- [139] [www.oracle.com](http://www.oracle.com).
- [140] E. F. Codd. *The relational model for database management*. Addison-Wesley Longman Publishing Co., Boston, 1990.
- [141] R. G. Gordon. Criteria for choosing transparent conductors. *MRS Bull.*, 25:52, 2000.
- [142] E. Fortunato, D. Ginley, H. Hosono, and D. C. Paine. Transparent conducting oxides for photovoltaics. *MRS Bulletin*, 32(3):242, 2007.
- [143] Y. Wu, P. Lazic, G. Hautier, K. Persson, and G. Ceder. First principles high throughput screening of oxynitrides for water-splitting photocatalysts. *Energy Environ. Sci.*, 6(1):157, 2013.

- [144] S. Curtarolo, G. L. W. Hart, M. B. Nardelli, N. Mingo, S. Sanvito, and O. Levy. The high-throughput highway to computational materials design. *Nature Mater.*, 12(3):191, 2013.
- [145] K. Yang, W. Setyawan, S. Wang, M. B. Nardelli, and S. Curtarolo. A search model for topological insulators with high-throughput robustness descriptors. *Nature Mater.*, 11(7):614, 2012.
- [146] R. Armiento, B. Kozinsky, M. Fornari, and G. Ceder. Screening for high-performance piezoelectrics using high-throughput density functional theory. *Phys. Rev. B*, 84(1):014103, 2011.
- [147] G. Hautier, A. Miglio, G. Ceder, G. M. Rignanese, and X. Gonze. Identification and design principles of low hole effective mass *p*-type transparent conducting oxides. *Nature Commun.*, 4:2292, 2013.
- [148] G. Kresse and J. Hafner. Norm-conserving and ultrasoft pseudopotentials for first-row and transition elements. *J. Phys. Cond. Matt.*, 6(40):8245, 1994.
- [149] H. Xiao, J. Tahir-Kheli, and W. A. Goddard. Accurate band gaps for semiconductors from density functional theory. *J. Phys. Chem. Lett.*, 2(3):212, 2011.
- [150] A. Walsh, J. L. F. Da Silva, S. Wei, C. Körber, A. Klein, L. F. J. Piper, A. De Masi, K. E. Smith, G. Panaccione, P. Torelli, D. J. Payne, A. Bourlange, and R. G. Egdell. Nature of the band gap of  $\text{In}_2\text{O}_3$  revealed by first-principles calculations and X-ray spectroscopy. *Phys. Rev. Lett.*, 100:167402, 2008.
- [151] K. L. Chopra, S. Major, and D. K. Pandya. Transparent conductors—a status review. *Thin Solid Films*, 102(1):1, 1983.
- [152] K. A. Johnson and N. W. Ashcroft. Corrections to density-functional theory band gaps. *Phys. Rev. B*, 58(23):15548, 1998.
- [153] C. S. Wang and W. E. Pickett. Density-functional theory of excitation spectra of semiconductors: Application to Si. *Phys. Rev. Lett.*, 51(7):597, 1983.
- [154] T. M. Henderson, J. Paier, and G. E. Scuseria. Accurate treatment of solids with the HSE screened hybrid. *Phys. Status Solidi B*, 248(4):767, 2011.
- [155] A. Schleife, F. Fuchs, C. Rödl, J. Furthmüller, and F. Bechstedt. Branch-point energies and band discontinuities of III-nitrides and III-II-oxides from quasiparticle band-structure calculations. *Appl. Phys. Lett.*, 94(1):012104, 2009.
- [156] P. Deák, B. Aradi, and T. Frauenheim. Band lineup and charge carrier separation in mixed rutile-anatase systems. *J. Phys. Chem. C*, 115(8):3443, 2011.
- [157] B. Höffling, A. Schleife, F. Fuchs, C. Rödl, and F. Bechstedt. Band lineup between silicon and transparent conducting oxides. *Appl. Phys. Lett.*, 97:032116, 2010.

- [158] S. H. Wei. Overcoming the doping bottleneck in semiconductors. *Comput. Mater. Sci.*, 30:337, 2004.
- [159] A. Walsh, Y. Yan, M. M. Al-Jassim, and S. H. Wei. Electronic, energetic, and chemical effects of intrinsic defects and Fe-doping of  $\text{CoAl}_2\text{O}_4$ : A DFT+U study. *J. Chem. Phys.*, 112:12044, 2008.
- [160] Y. Bréard, H. Fjellvåg, and B. Hauback. Investigation of bixbyite type scandium oxides involving a magnetic cation:  $\text{Sc}_{2-x}\text{Fe}_x\text{O}_3$  ( $0 \leq x \leq 1$ ). *Solid State Commun.*, 151:223, 2011.
- [161] H. H. Tippins. Absorption edge spectrum of scandium oxide. *J. Phys. Chem. Solids*, 27:1069, 1966.
- [162] J. R. Rustad. Density functional calculations of the enthalpies of formation of rare-earth orthophosphates. *Am. Mineral.*, 97:791, 2012.
- [163] D. R. Lide. *Handbook of Chemistry and Physics*. CRC Press, Boca Raton, 84 edition, 2004.
- [164] D. Weber, A. Stork, S. Nakhal, C. Wessel, C. Reimann, W. Hermes, A. Müller, T. Ressler, R. Pöttgen, T. Bredow, R. Dronskowski, and M. Lerch. Bixbyite-type  $\text{V}_2\text{O}_3$ -a metastable polymorph of vanadium sesquioxide. *Inorg. Chem.*, 50:6762, 2011.
- [165] A. Bergerud, R. Buonsanti, J. L. Jordan-Sweet, and D. J. Milliron. Synthesis and phase stability of metastable bixbyite  $\text{V}_2\text{O}_3$  colloidal nanocrystals. *Chem. Mater.*, 25:3172, 2013.
- [166] C. M. Julien, M. Massot, and C. Poinignon. Lattice vibrations of manganese oxides part I. periodic structures. *Spectrochim. Acta Mol. Biomol.*, 60:689, 2004.
- [167] L. Ben-Dor, E. Fischbein, and Z. Kalman. Concerning the  $\beta$  phase of iron (III) oxide. *Acta Cryst. B*, 32(2):667, 1976.
- [168] S. Yoshioka, H. Hayashi, A. Kuwabara, F. Oba, K. Matsunaga, and I. Tanaka. Structures and energetics of  $\text{Ga}_2\text{O}_3$  polymorphs. *J. Phys. Cond. Matt.*, 19:346211, 2007.
- [169] Ž. Antić, R. Krsmanović, M. Wojtowicz, E. Zych, B. Bártoová, and M. D. Dramićanin. Preparation, structural and spectroscopic studies of  $(\text{Y}_x\text{Lu}_{1-x})_2\text{O}_3 : \text{Eu}^{3+}$  nanopowders. *Opt. Mater.*, 32:1612, 2010.
- [170] P. W. Peacock and J. Robertson. Band offsets and schottky barrier heights of high dielectric constant oxides. *J. Appl. Phys.*, 92:4712, 2002.
- [171] G. Wilk and R. M. Wallace. Alternative gate dielectrics for microelectronics. *MRS Bulletin*, 27(3):186, 2002.



- [172] L. Marsella and V. Fiorentini. Structure and stability of rare-earth and transition-metal oxides. *Phys. Rev. B*, 69:172103, 2004.
- [173] A. Bourlange, D. J. Payne, R. G. Egdell, J. S. Foord, P. P. Edwards, M. O. Jones, A. Schertel, P. J. Dobson, and J. L. Hutchison. Growth of  $\text{In}_2\text{O}_3$  (100) on Y-stabilized  $\text{ZrO}_2$  (100) by O-plasma assisted molecular beam epitaxy. *Appl. Phys. Lett.*, 92(9):092117, 2008.
- [174] P. D. C. King, T. D. Veal, F. Fuchs, Ch. Y. Wang, D. J. Payne, A. Bourlange, H. Zhang, G. R. Bell, V. Cimalla, O. Ambacher, R. G. Egdell, F. Bechstedt, and C. F. McConville. Band gap, electronic structure, and surface electron accumulation of cubic and rhombohedral  $\text{In}_2\text{O}_3$ . *Phys. Rev. B*, 79:205211, 2009.
- [175] I. Tanaka, K. Tatsumi, M. Nakano, and H. Adachi. First-principles calculations of anion vacancies in oxides and nitrides. *J. Am. Ceram. Soc.*, 85:68, 2002.
- [176] S. Lany and A. Zunger. Comment on "intrinsic  $n$ -type behavior in transparent conducting oxides: A comparative hybrid-functional study of  $\text{In}_2\text{O}_3$ ,  $\text{SnO}_2$ , and  $\text{ZnO}$ ". *Phys. Rev. Lett.*, 106(6):069601, 2011.
- [177] G. y. Adachi and N. Imanaka. The binary rare earth oxides. *Chem. Rev.*, 98(4):1479, 1998.
- [178] A. F. Andreeva, I. Ya. Gilman, and Zh. Prikl. *Spectrosc.*, 28:895, 1978.
- [179] H. Jiang, R. I. Gomez-Abal, P. Rinke, and M. Scheffler. Localized and itinerant states in lanthanide oxides united by  $\text{GW@LDA+U}$ . *Phys. Rev. Lett.*, 102:126403, 2009.
- [180] W. B. White. *Appl. Spectrosc.*, 21:167, 1967.
- [181] G. Concas, J. K. Dewhurst, A. Sanna, S. Sharma, and S. Massidda. Anisotropic exchange interaction between nonmagnetic europium cations in  $\text{Eu}_2\text{O}_3$ . *Phys. Rev. B*, 84:014427, 2011.
- [182] M. Badylevich, S. Shamuilia, V. V. Afanas'ev, and A. Stesmans. Investigation of the electronic structure at interfaces of crystalline and amorphous  $\text{Gd}_2\text{O}_3$  thin layers with silicon substrates of different orientations. *App. Phys. Lett.*, 90:252101, 2007.
- [183] A. I. Shelykh, A. V. Prokofiev, and B. T. Melekh. *Fiz. Tverd. Tela (St. Petersburg)*, 38:427, 1996.
- [184] A. W. Carbonari, J. Mestnik-Filho, R. N. Attili, M. Morales, and R. N. Saxena. Electric field gradient in bixbyite rare-earth oxides  $\text{R}_2\text{O}_3$  ( $\text{R} = \text{Tl}, \text{Eu}, \text{Lu}, \text{Tm}$ ) measured by perturbed angular correlation. *Hyperfine Interact.*, 120:475, 1999.
- [185] A. B. Kehoe, D. O. Scanlon, and G. W. Watson. Nature of the band gap of  $\text{Tl}_2\text{O}_3$ . *Phys. Rev. B*, 83:233202, 2011.

- [186] A. Matsumoto, Y. Koyama, and I. Tanaka. Structures and energetics of  $\text{Bi}_2\text{O}_3$  polymorphs in a defective fluorite family derived by systematic first principles lattice dynamics calculations. *Phys. Rev. B*, 81:094117, 2010.
- [187] P. Reunchan, X. Zhou, S. Limpijumnong, A. Janotti, and C. G. Van de Walle. Vacancy defects in indium oxide: An ab-initio study. *Current Appl. Phys.*, 11(3):S296, 2011.
- [188] J. B. Varley, J. R. Weber, A. Janotti, and C. G. Van de Walle. Oxygen vacancies and donor impurities in  $\beta\text{-Ga}_2\text{O}_3$ . *Appl. Phys. Lett.*, 97:142106, 2010.
- [189] K. Held, G. Keller, V. Eyert, D. Vollhardt, and V. I. Anisimov. Mott-hubbard metal-insulator transition in paramagnetic  $\text{V}_2\text{O}_3$ : An LDA+DMFT (QMC) study. *Phys. Rev. Lett.*, 86(23):5345, 2001.
- [190] G. A. Thomas, D. H. Rapkine, S. A. Carter, A. J. Millis, T. F. Rosenbaum, P. Metcalf, and J. M. Honig. Observation of the gap and kinetic energy in a correlated insulator. *Phys. Rev. Lett.*, 73(11):1529, 1994.
- [191] C. Wessel, C. Reimann, A. Müller, D. Weber, M. Lerch, T. Ressler, T. Bredow, and R. Dronskowski. Electronic structure and thermodynamics of  $\text{V}_2\text{O}_3$  polymorphs. *J. Comput. Chem.*, 33(26):2102, 2012.
- [192] L. Vegard. Die konstitution der mischkristalle und die raumfallung der atome. *Z. Phys. B*, 5(1):17, 1921.
- [193] J. Robertson and S. J. Clark. Limits to doping in oxides. *Phys. Rev. B*, 83(7):075205, 2011.
- [194] N. Sarmadian, R. Saniz, B. Partoens, D. Lamoén, K. Volety, G. Huyberegts, , and J. Paul. High throughput first-principles calculations of bixbyite oxides for tco applications. *Phys. Chem. Chem. Phys.*, 16:17724, 2014.
- [195] A. Tanaka. Theory on electronic structure and phase transitions in  $\text{V}_2\text{O}_3$ . *Physica B*, 329:753, 2003.
- [196] M. Wu, X. Lin, Y. Wang, L. Wang, W. Guo, D. Qi, X. Peng, A. Hagfeldt, M. Grätzel, and T. Ma. Economical Pt-free catalysts for counter electrodes of dye-sensitized solar cells. *J. Am. Chem. Soc.*, 134:3419, 2012.
- [197] A. Julbe, D. Farrusseng, and C. Guizard. Synthesis and characterisation of a vanadium-based 'chemical valve' membrane. *Sep. Purif. Technol.*, 25:11, 2001.
- [198] M. N. Amini, R. Saniz, D. Lamoén, and B. Partoens. Hydrogen impurities and native defects in  $\text{CdO}$ . *J. Appl. Phys.*, 110:063521, 2011.
- [199] F. Hanic, M. Hartmanová, G. G. Knab, A. A. Urusovskaya, and K. S. Bagdasarov. Real structure of undoped  $\text{Y}_2\text{O}_3$  single crystals. *Acta Cryst. B*, 40(2):76, 1984.

- [200] A. Alkauskas, P. Deák, J. Neugebauer, A. Pasquarello, and C. G. Van de Walle. *Advanced Calculations for Defects in Materials: Electronic Structure Methods*. Wiley-VCH, Weinheim, Germany, 2011.
- [201] C. R. Stanek, K. J. McClellan, and B. P. Uberuaga. Determining the site preference of trivalent dopants in bixbyite sesquioxides by atomic-scale simulations. *K. E. Sickafus Phys. Rev. B*, 75:134101, 2007.
- [202] J. E. Coulter, E. Manousakis, and A. Gali. Limitations of the hybrid functional approach to electronic structure of transition metal oxides. *Phys. Rev. B*, 88:041107, 2013.
- [203] W. Li, C. F. J. Walther, A. Kuc, and T. Heine. Density functional theory and beyond for band-gap screening: Performance for transition-metal oxides and dichalcogenides. *J. Chem. Theory Comput.*, 9:2950, 2013.
- [204] P. Y. Yu and M. Cardona. *Fundamentals of Semiconductors*. Springer-Verlag, Berlin, 2010.
- [205] J. C. Slater. Atomic radii in crystals. *J. Chem. Phys.*, 41:3199, 1964.
- [206] A. Stadler. Transparent conducting oxides-an up-to-date review. *Materials*, 5:661, 2012.
- [207] D. Ginley, B. Roy, A. Ode, C. Warmsingh, Y. Yoshida, Ph. Parilla, Ch. Teplin, T. Kaydanova, A. Miedaner, C. Curtis, A. Martinson, T. Coutts, D. Readey, H. Hosono, and J. Perkins. Non-vacuum and PLD growth of next generation tco materials. *Thin Solid Films*, 445:193, 2003.
- [208] Y. Guo, S. J. Clark, and J. Robertson. Calculation of metallic and insulating phases of  $V_2O_3$  by hybrid density functionals. *J. Chem. Phys.*, 140:054702, 2013.
- [209] E. Fortunato, P. Barquinha, and R. Martins. Oxide semiconductor thin-film transistors: A review of recent advances. *Adv. Mater.*, 24:2945, 2012.
- [210] C. G. Granqvist. Transparent conductors as solar energy materials: A panoramic review. *Sol. Energ. Mat. Sol. C.*, 91:1529, 2007.
- [211] K. Ellmer. Past achievements and future challenges in the development of optically transparent electrodes. *Nature Photon.*, 6:809, 2012.
- [212] D. O. Scanlon, K. G. Godinho, B. J. Morgan, and G. W. Watson. Understanding conductivity anomalies in Cu-I-based delafossite transparent conducting oxides: Theoretical insights. *J. Chem. Phys.*, 132:024707, 2010.
- [213] A. Schleife, F. Fuchs, C. Rödl, J. Furthmüller, and F. Bechstedt. Band-structure and optical-transition parameters of wurtzite MgO, ZnO, and CdO from quasiparticle calculations. *Phys. Status Solidi B* 246, 9:2150, 2009.

- [214] A. N. Sokolov, S. Atahan-Evrenk, R. Mondal, H. B. Akkerman, R. S. Sánchez-Carrera, S. Granados-Focil, J. Schrier, S. C. B. Mannsfeld, A. P. Zoombelt, Z. Bao, and A. Aspuru-Guzik. From computational discovery to experimental characterization of a high hole mobility organic crystal. *Nature Commun.*, 2:437, 2011.
- [215] W. Setyawan and S. Curtarolo. High-throughput electronic band structure calculations: Challenges and tools. *Comp. Mat. Sci.*, 49:299, 2010.
- [216] S. Curtarolo, W. Setyawan, S. Wang, J. Xue, K. Yang, R. H. Taylor, L. J. Nelson, G. L. W. Hart, S. Sanvito, M. Buongiorno-Nardelli N. Mingo, and O. Levy. Aflowlib.org: a distributed materials properties repository from high-throughput ab initio calculations. *Comp. Mat. Sci.*, 58:227, 2012.
- [217] <http://www.fiz-karlsruhe.de/icsd.html>.
- [218] A. Jain, G. Hautier, Ch. J. Moore, S. P. Ong, Ch. C. Fischer, T. Mueller, K. A. Persson, and G. Ceder. A high-throughput infrastructure for density functional theory calculations. *Comp. Mat. Sci.*, 50:2295, 2011.
- [219] W. Setyawan, R. M. Gaume, S. Lam, R. S. Feigelson, and S. Curtarolo. High-throughput combinatorial database of electronic band structures for inorganic scintillator materials. *ACS Comb. Sci.*, 13:382, 2011.
- [220] W. E. Henderson, W. L. Calley, A. G. Carver, H. Chen, and W. A. Doolittle. A versatile metal-halide vapor chemistry for the epitaxial growth of metallic, insulating and semiconducting films. *J. Cryst. Growth*, 324:134, 2011.
- [221] H. Lincke, R. Glaum, V. Dittrich, M. Tegel, D. Johrendt, W. Holmes, M. H. Möller, T. Nilges, and R. Pöttgen. Magnetic, optical, and electronic properties of the phosphide oxides REZnPO (RE=Y, La–Nd, Sm, Gd, Dy, Ho). *Z. Anorg. Allg. Chem.*, 634:1339, 2008.
- [222] C. Persson, Y. J. Zhao, S. Lany, and A. Zunger. *n*-type doping of CuInSe<sub>2</sub> and CuGaSe<sub>2</sub>. *Phys. Rev. B*, 72:035211, 2005.
- [223] D. Segev and S. H. Wei. Structure-driven electronic and optical properties of transparent conducting oxides. *Phys. Rev. B*, 71:125129, 2005.
- [224] M. Baghaie Yazdi, M. L. Goyallon, T. Bitsch, A. Kastner, M. Schlott, and L. Alff. Transparent magnetic oxide thin films of Fe<sub>3</sub>O<sub>4</sub> on glass. *Thin Solid Films*, 519:2531, 2011.
- [225] X. Zhou, F. Lin, W. Shi, and A. Liu. Structural, electrical, optical and magnetic properties of *p*-type Cu(Cr<sub>1-x</sub>Mn<sub>x</sub>)O<sub>2</sub> thin films prepared by pulsed laser deposition. *J. Alloys Compd.*, 614:221, 2014.
- [226] T. Shimada, T. Ueda, J. Wang, and T. Kitamura. Hybrid Hartree-Fock density functional study of charged point defects in ferroelectric PbTiO<sub>3</sub>. *Phys. Rev. B*, 87:174111, 2013.

- [227] J. B. Varley, V. Lordi, A. Miglio, and G. Hautier. Electronic structure and defect properties of  $\text{B}_6\text{O}$  from hybrid functional and many-body perturbation theory calculations: A possible ambipolar transparent conductor. *Phys. Rev. B*, 90:045205, 2014.
- [228] K. L. Chopra, P. D. Paulson, and V. Dutta. Thin-film solar cells: An overview. *Prog. Photovolt. Res. Appl.*, 12:69, 2004.
- [229] M. A. Contreras, B. Egaas, K. Ramanathan, J. Hiltner, A. Swartzlander, F. Hasoon, and R. Noufi. Progress toward 20% efficiency in  $\text{Cu}(\text{In,Ga})\text{Se}_2$  polycrystalline thin-film solar cells. *Prog. Photovolt. Res. Appl.*, 7:311, 1999.
- [230] M. A. Contreras, K. Ramanathan, J. A. Shama, F. Hasoon, D. L. Young, B. Egass, and R. Noufi. Diode characteristics in state-of-the-art  $\text{ZnO}/\text{CdS}/\text{Cu}(\text{In}_{1-x}\text{Ga}_x)\text{Se}_2$  solar cells. *Prog. Photovolt. Res. Appl.*, 13:209, 2005.
- [231] J. J. Scragg, P. J. Dale, and L. M. Peter. Towards sustainable materials for solar energy conversion: Preparation and photoelectrochemical characterization of  $\text{Cu}_2\text{ZnSnS}_4$ . *Electrochem. Commun.*, 10:639, 2008.
- [232] S. Chen, X. G. Gong, A. Walsh, and S. H. Wei. Crystal and electronic band structure of  $\text{Cu}_2\text{ZnSnX}_4$  ( $\text{X} = \text{S}$  and  $\text{Se}$ ) photovoltaic absorbers: First-principles insights. *Appl. Phys. Lett.*, 94:041903, 2009.
- [233] S. Chen, X. G. Gong, A. Walsh, and S. H. Wei. Electronic structure and stability of quaternary chalcogenide semiconductors derived from cation cross-substitution of II-VI and I-III-VI<sub>2</sub> compounds. *Phys. Rev. B*, 79:165211, 2009.
- [234] J. Paier, R. Asahi, A. Nagoya, and G. Kresse.  $\text{Cu}_2\text{ZnSnS}_4$  as a potential photovoltaic material: A hybrid Hartree-Fock density functional theory study. *Phys. Rev. B*, 79:115126, 2009.
- [235] C. H. L. Goodman. The prediction of semiconducting properties in inorganic compounds. *J. Phys. Chem. Solids*, 6:305, 1958.
- [236] B. R. Pamplin. Super-cell structure of semiconductors. *Nature*, 188:136, 1960.
- [237] B. R. Pamplin. A systematic method of deriving new semiconducting compounds by structural analogy. *J. Phys. Chem. Solids*, 25:675, 1964.
- [238] H. Katagiri, K. Jimbo, S. Yamada, T. Kamimura, W. S. Maw, T. Fukano, T. Ito, and T. Motohiro. Enhanced conversion efficiencies of  $\text{Cu}_2\text{ZnSnS}_4$ -based thin film solar cells by using preferential etching technique. *Appl. Phys. Express*, 1:041201, 2008.
- [239] S. Schorr, G. Wagner, M. Tovar, and D. Sheptyakov. Comparative studies of the structure and microstructure of  $\text{Zn}_{2x}(\text{Cu}^{\text{III}})_{1-x}\text{X}_2$  semiconductors ( $\text{b}^{\text{III}} = \text{Ga, In}$ ;  $\text{X} = \text{S, Se, Te}$ ). *Mater. Res. Soc. Symp. Proc.*, 1012:Y03, 2007.

- [240] O. V. Parasyuk, I. D. Olekseyuk, and L. V. Piskach. X-ray powder diffraction refinement of  $\text{Cu}_2\text{ZnGeTe}_4$  structure and phase diagram of the  $\text{Cu}_2\text{GeTe}_3$ -ZnTe system. *J. Alloy. Compd.*, 397:169, 2005.
- [241] H. Matsushita, T. Maeda, A. Katsui, and T. Takizawa. Thermal analysis and synthesis from the melts of Cu-based quaternary compounds  $\text{Cu-III-IV-VI}_4$  and  $\text{Cu}_2\text{II-IV-VI}_4$  (II = Zn, Cd; III = Ga, In; IV = Ge, Sn; VI = Se). *J. Cryst. Growth*, 208:416, 2000.
- [242] Y. Z. Zhu, G. D. Chen, H. Ye, A. Walsh, C. Y. Moon, and S. H. Wei. Electronic structure and phase stability of MgO, ZnO, CdO, and related ternary alloys. *Phys. Rev. B*, 77:245209, 2008.
- [243] O. M. Madelung. *Semiconductors: Data Handbook*. Springer, New York, 3 edition, 2004.
- [244] O. V. Parasyuk, L. D. Gulay, Y. E. Romanyuk, and L. V. Piskach. Phase diagram of the  $\text{Cu}_2\text{GeSe}_3$ -ZnSe system and crystal structure of the  $\text{Cu}_2\text{ZnGeSe}$  compound. *J. Alloys Compd.*, 329:202, 2001.
- [245] D. B. Mitzi, O. Gunawan, T. K. Todorov, K. Wang, and S. Guha. The path towards a high-performance solution-processed kesterite solar cell. *Sol. Energy Mater. Sol. Cells*, 95:1421, 2011.
- [246] T. K. Todorov, J. Tang, S. Bag, O. Gunawan, T. Gokmen, Y. Zhu, and D. B. Mitzi. Beyond 11% efficiency: Characteristics of state-of-the-art  $\text{Cu}_2\text{ZnSn}(\text{S,Se})_4$  solar cells. *Adv. Energy Mater.*, 3:34, 2013.
- [247] D. Barkhouse, O. Gunawan, T. Gokmen, T. Todorov, and D. Mitzi. Device characteristics of a 10.1% hydrazine-processed  $\text{Cu}_2\text{ZnSn}(\text{Se,S})_4$  solar cell. *Prog. Photovolt. Res. Appl.*, 20:6, 2012.
- [248] M. Altosaar, J. Raudoja, K. Timmo, M. Danilson, M. Grossberg, J. Krustok, and E. Mellikov.  $\text{Cu}_2\text{Zn}_{1-x}\text{Cd}_x\text{Sn}(\text{Se}_{1-y}\text{S}_y)_4$  solid solutions as absorber materials for solar cells. *Phys. Status Solidi A*, 205:167, 2008.
- [249] S. Siebentritt. Why are kesterite solar cells not 20% efficient? *Thin Solid Films*, 535:1, 2013.
- [250] L. Yu and A. Zunger. Identification of potential photovoltaic absorbers based on first-principles spectroscopic screening of materials. *Phys. Rev. Lett.*, 108:068701, 2012.
- [251] M. R. Green. *Solar Cells: Operating Principles, Technology, and System Applications*. Prentice Hall, U.S.A., 1981.
- [252] R. Williams. Becquerel Photovoltaic Effect in Binary Compounds. *J. Chem. Phys.*, 32:1505, 1960.

- [253] F. A. Lindholm and J. G. Fossum. Application of the superposition principle to solar-cell analysis. *E. L. Burgess. IEEE Trans. Electron Devices.*, 26:165, 1979.
- [254] B. S. Richards. Enhancing the performance of silicon solar cells via the application of passive luminescence conversion layers. *Sol. Energ. Mat. Sol. C.*, 90:2329, 2006.
- [255] B. Jalali. Physics and technology forefronts: Silicon lasers. *Am. Phys. Soc.*, 15:3, 2006.
- [256] S. Schorr. The crystal structure of kesterite type compounds: A neutron and x-ray diffraction study. *Sol. Energy Mater. Sol. Cells*, 95:1482, 2011.
- [257] I. D. Olekseyuk, L. D. Gulay, I. V. Dydchak, L. V. Piskach, O. V. Parasyuk, and O. V. Marchuk. Single crystal preparation and crystal structure of the  $\text{Cu}_2\text{Zn/Cd,Hg/SnSe}_4$  compounds. *J. Allo. Comp.*, 340:141, 2002.
- [258] M. L. Liu, I. W. Chen, F. Q. Huang, and L. D. Chen. Improved thermoelectric properties of Cu-doped quaternary chalcogenides of  $\text{Cu}_2\text{CdSnSe}_4$ . *Adv. Mater.*, 21:3808, 2009.
- [259] B. Adolph, J. Furthmüller, and F. Bechstedt. Optical properties of semiconductors using projector-augmented waves. *Phys. Rev. B*, 63:125108, 2001.
- [260] D. Chen and N. M. Ravindra. Electronic and optical properties of  $\text{Cu}_2\text{ZnGeX}_4$  ( $X = \text{S, Se}$  and  $\text{Te}$ ) quaternary semiconductors. *J. Alloy. Compd.*, 579:468, 2013.
- [261] P. U. Bhaskar, G. S. Babu, Y. B. K. Kumar, and V. S. Raja. Preparation and characterization of co-evaporated  $\text{Cu}_2\text{ZnGeSe}_4$  thin films. *Thin Solid Films*, 534:249, 2013.
- [262] H. Zhao and C. Persson. Optical properties of  $\text{Cu(In,Ga)Se}_2$  and  $\text{Cu}_2\text{ZnSn(S,Se)}_4$ . *Thin Solid Films*, 519:7508, 2011.
- [263] H. Shen, X. D. Jiang, S. Wang, Y. Fu, C. Zhou, and L. S. Li. Facile preparation of metal telluride nanocrystals using di-n-octylphosphine oxide (DOPO) as an air-stable and less toxic alternative to the common tri-alkylphosphines. *J. Mater. Chem.*, 22:25050, 2012.
- [264] M. L. Liu, F. Q. Huang, L. D. Chen, , and I. Chen. A wide-band-gap  $p$ -type thermoelectric material based on quaternary chalcogenides of  $\text{Cu}_2\text{ZnSnQ}_4$  ( $Q = \text{S, Se}$ ). *Appl. Phys. Lett.*, 94:202103, 2009.
- [265] J. L. Jambor and A. C. Roberts. New mineral names. *Am. Mineral.*, 84:1464, 1999.
- [266] L. V. Piskach, O. V. Parasyuk, and Ya. E. Romanyuk. The phase equilibria in the quasi-binary  $\text{Cu}_2\text{GeS}_3/\text{Se}_3/-\text{CdS/Se/}$  systems. *J. Allo. Comp.*, 299:227, 2000.
- [267] W. Schafer and R. Nitsche. *Z. Kristallogr.*, 145:356, 1977.
- [268] H. Guan, J. Zhao, X. Wang, and F. Yu.  $\text{Cu}_2\text{CdSnS}_4$  thin film prepared by a simple solution method. *Chalcogenide Lett.*, 10:367, 2013.

- [269] M. Ibáñez, D. Cadavid, R. Zamani, V. I. Roca N. G. Castelló, W. Li, A. Fairbrother, J. D. Prades, A. Shavel, J. Arbiol, A. P. Rodríguez, J. R. Morante, and A. Cabot. Composition control and thermoelectric properties of quaternary chalcogenide nanocrystals: The case of stannite  $\text{Cu}_2\text{CdSnSe}_4$ . *Chem. Mater.*, 24:562–570, 2012.
- [270] H. Haueseler, F. W. Ohrendorf, and M. Himmrich. *Z. Naturforsch. B*, 46:1049, 1991.
- [271] Yu. K. Kabalov, T. L. Evstigneeva, and E. M. Spiridonov. *Krystallographiya*, 43:21, 1998.
- [272] W. Li, M. Ibáñez, R. Zamani, N. G. Castelló, S. Gorsse, D. Cadavid, J. D. Prades, J. Arbiol, and A. Cabot.  $\text{Cu}_2\text{HgSnSe}_4$  nanoparticles: synthesis and thermoelectric properties. *Cryst. Eng. Comm*, 15:8966, 2013.
- [273] D. Li, X. Zhang, Z. Zhu, H. Zhang, and F. Ling. Ab initio calculations of structural, electronic, and optical properties of  $\text{Cu}_2\text{HgSnSe}_4$ . *Solid State Sci.*, 14:890, 2012.



# Curriculum Vitae

Name     **Nasrin Sarmadian**  
Born      16/09/1983, Tehran, Iran  
Contact   U 317, Condensed matter theory (CMT) group  
            University of Antwerp, Groenenborgerlaan 171  
            B-2020, Antwerp, Belgium  
Email     [nasrin.sarmadian@uantwerpen.be](mailto:nasrin.sarmadian@uantwerpen.be)  
            [nasrin.sarmadian@gmail.com](mailto:nasrin.sarmadian@gmail.com)  
Phone     +32-488-276270

## Education

2010-2015     **PhD** Physics, Physics Department, University of Antwerp, Belgium.  
2004-2007     **MSc** Solid State physics, Physics Department, Urmia University, Urmia, Iran.  
2000-2004     **BCs** Physics, Physics Department, Kashan University, Kashan, Iran.

## Teaching Experiences

Lecturer             General Physics (Mechanics, Electromagnetism, and Thermodynamics)  
                          2007-2010, Azad university of Saveh, Iran  
Assistant instructor   Mechanics, Electromagnetism and Thermodynamics Lab  
                          2007-2010, Azad university of Saveh, Iran  
Teaching assistant    Quantum Mechanics  
                          2006-2007, Physics Department, Urmia University, Iran

### **Computer Skills**

- DFT Package: VASP, ABINIT
- Operating systems: Windows, Linux
- Programming languages: Python, Fortran
- Mathematical software: MATLAB, Mathematica
- Packages: Office, Latex, Origin, Visual Studio

### **Professional Training**

|               |  |
|---------------|--|
| Winter School | School on Computational Modeling of Materials<br>2-3 December 2010; University of Antwerp, Belgium |
| Winter School | Hands on tutorial on electronic structure computations<br>14-18 January 2013; ICTP, Trieste, Italy |
| Spring school | Computational Tools for Materials Science<br>13-17 April 2015; Gent University, Belgium            |

### **List of Publications:**

- N. Sarmadian, R. Saniz, D. Lamoen, and B. Partoens, *Influence of Al concentration on the opto-electronic properties of Al-doped MgO*, Phys. Rev. B. **86**, 205129 (2012).
- N. Sarmadian, R. Saniz, B. Partoens, D. Lamoen, K. Volety, G. Huyberegts, and J. Paul, *High Throughput First-Principles Calculations of Bixbyite Oxides for TCO Applications* J. Phys. Chem. Chem. Phys. **16**, 17724(2014).
- N. Sarmadian, R. Saniz, B. Partoens, and D. Lamoen, *Ab initio study of shallow acceptors in bixbyite  $V_2O_3$* , J. Appl. Phys. **117**, 015703 (2014).
- N. Sarmadian, R. Saniz, B. Partoens, and D. Lamoen, *Identification of p-type TCOs based on high-throughput first-principles calculations (submitted)*.

### **Conference Presentations**

|                 |   |
|-----------------|---|
| Poster          | 8th conference on Condensed matter Physics<br>Ferdowsi University of Mashad, Mashhad, Iran, February 2006   |
| Poster          | 16th International Workshop on Computational Physics and Materials Science:<br>Total Energy and Force Methods, 10-12 January 2013, ICTP, Trieste, Italy |
| Oral            | General Scientific Meeting of Belgian Physical Society<br>22 May 2013, Université Catholique de Louvain, Louvain la Nouvelle, Belgium                   |
| Poster/Oral     | International Workshop on high throughput materials development:<br>when Time-to-Market matters, 11-12 June 2013, Gent, Belgium                         |
| Poster          | 12th E-MRS Fall Meeting<br>16-20 September 2013, Warsaw University of Technology, Poland  |
| Poster          | General Scientific Meeting of Belgian Physical Society<br>28 May 2014, University of Louvain, Louvain, Belgium  |
| Oral (accepted) | International Workshop on high throughput materials development:<br>Bridging the gap between lab and market, 2-4 June 2015, Gent, Belgium               |

### **Research Interests**

- Optical and electronic properties of materials using ab-initio calculations
- Optoelectronic properties of Nano-scales materials
- High-throughput screening of materials using computational methods

### **Languages**

Persian(Native), English(Fluent), and French(Average)

### **Awards**

- Award of top MSc student, Physics department of Urmia University, Urmia, Iran (2007).